

# Network Structural Perturbation and its Applications for Controlling Misinformation Diffusion

Guest Editors: Wei Wang, Luxing Yang, and Chenquan Gan





---

**Network Structural Perturbation and its  
Applications for Controlling Misinformation  
Diffusion**

**Network Structural Perturbation  
and its Applications for Controlling  
Misinformation Diffusion**

Guest Editors: Wei Wang, Luxing Yang, and  
Chenquan Gan



---




Copyright © 2022 Hindawi Limited. All rights reserved.

This is a special issue published in "Security and Communication Networks." All articles are open access articles distributed under the Creative Commons Attribution License, which permits unrestricted use, distribution, and reproduction in any medium, provided the original work is properly cited.

# Chief Editor

Roberto Di Pietro, Saudi Arabia

## Associate Editors

Jiankun Hu , Australia  
Emanuele Maiorana , Italy  
David Megias , Spain  
Zheng Yan , China

## Academic Editors




Saed Saleh Al Rabae , United Arab Emirates  
Shadab Alam, Saudi Arabia  
Goutham Reddy Alavalapati , USA  
Jehad Ali , Republic of Korea  
Jehad Ali, Saint Vincent and the Grenadines  
Benjamin Aziz , United Kingdom  
Taimur Bakhshi , United Kingdom  
Spiridon Bakiras , Qatar  
Musa Balta, Turkey  
Jin Wook Byun , Republic of Korea  
Bruno Carpentieri , Italy  
Luigi Catuogno , Italy  
Ricardo Chaves , Portugal  
Chien-Ming Chen , China  
Tom Chen , United Kingdom  
Stelvio Cimato , Italy  
Vincenzo Conti , Italy  
Luigi Coppolino , Italy  
Salvatore D'Antonio , Italy  
Juhriyansyah Dalle, Indonesia  
Alfredo De Santis, Italy  
Angel M. Del Rey , Spain  
Roberto Di Pietro , France  
Wenxiu Ding , China  
Nicola Dragoni , Denmark  
Wei Feng , China  
Carmen Fernandez-Gago, Spain  
AnMin Fu , China  
Clemente Galdi , Italy  
Dimitrios Geneiatakis , Italy  
Muhammad A. Gondal , Oman  
Francesco Gringoli , Italy  
Biao Han , China  
Jinguang Han , China  
Khizar Hayat, Oman  
Azeem Irshad, Pakistan

M.A. Jabbar , India  
Minho Jo , Republic of Korea  
Arijit Karati , Taiwan  
ASM Kayes , Australia  
Farrukh Aslam Khan , Saudi Arabia  
Fazlullah Khan , Pakistan  
Kiseon Kim , Republic of Korea  
Mehmet Zeki Konyar, Turkey  
Sanjeev Kumar, USA  
Hyun Kwon, Republic of Korea  
Maryline Laurent , France  
Jegatha Deborah Lazarus , India  
Huaizhi Li , USA  
Jiguo Li , China  
Xueqin Liang, Finland  
Zhe Liu, Canada  
Guangchi Liu , USA  
Flavio Lombardi , Italy  
Yang Lu, China  
Vincente Martin, Spain  
Weizhi Meng , Denmark  
Andrea Michienzi , Italy  
Laura Mongioi , Italy  
Raul Monroy , Mexico  
Naghme Moradpoor , United Kingdom  
Leonardo Mostarda , Italy  
Mohamed Nassar , Lebanon  
Qiang Ni, United Kingdom  
Mahmood Niazi , Saudi Arabia  
Vincent O. Nyangaresi, Kenya  
Lu Ou , China  
Hyun-A Park, Republic of Korea  
A. Peinado , Spain  
Gerardo Pelosi , Italy  
Gregorio Martinez Perez , Spain  
Pedro Peris-Lopez , Spain  
Carla Ràfols, Germany  
Francesco Regazzoni, Switzerland  
Abdalhossein Rezai , Iran  
Helena Rifà-Pous , Spain  
Arun Kumar Sangaiah, India  
Nadeem Sarwar, Pakistan  
Neetesh Saxena, United Kingdom  
Savio Sciancalepore , The Netherlands

De Rosal Ignatius Moses Setiadi ,  
Indonesia  
Wenbo Shi, China  
Ghanshyam Singh , South Africa  
Vasco Soares, Portugal  
Salvatore Sorce , Italy  
Abdulhamit Subasi, Saudi Arabia  
Zhiyuan Tan , United Kingdom  
Keke Tang , China  
Je Sen Teh , Australia  
Bohui Wang, China  
Guojun Wang, China  
Jinwei Wang , China  
Qichun Wang , China  
Hu Xiong , China  
Chang Xu , China  
Xuehu Yan , China  
Anjia Yang , China  
Jiachen Yang , China  
Yu Yao , China  
Yinghui Ye, China  
Kuo-Hui Yeh , Taiwan  
Yong Yu , China  
Xiaohui Yuan , USA  
Sherali Zeadally, USA  
Leo Y. Zhang, Australia  
Tao Zhang, China  
Youwen Zhu , China  
Zhengyu Zhu , China


# Contents

## **DEDGCN: Dual Evolving Dynamic Graph Convolutional Network**

Fengzhe Zhong , Yan Liu , Lian Liu, Guangsheng Zhang, and Shunran Duan 

Research Article (11 pages), Article ID 6945397, Volume 2022 (2022)

## **Adaptive Alleviation for Popularity Bias in Recommender Systems with Knowledge Graph**

Feng Wei, Shuyu Chen , Jie Jin, Shuai Zhang, Hongwei Zhou, and Yingbo Wu


Research Article (9 pages), Article ID 4264489, Volume 2022 (2022)

## **LGBM-CBFS: A Heuristic Feature Sampling Method Based on Tree Ensembles**

Yu Zhou , Hui Li , and Mei Chen 




Research Article (8 pages), Article ID 5156086, Volume 2022 (2022)

## **Enhancing Personalized Recommendation by Transductive Support Vector Machine and Active Learning**

Xibin Wang , Yunji Li, Jing Chen, and Jianfeng Yang




Research Article (10 pages), Article ID 1705527, Volume 2022 (2022)

## **A Network Sampling Strategy Inspired by Epidemic Spreading**

Qiang Dong , En-Yu Yu , and Wen-Jun Li 




Research Article (7 pages), Article ID 7003265, Volume 2022 (2022)

## **Dynamical Behavior of Hybrid Propagation of Computer Viruses**

Qingyi Zhu , Pingfan Xiang, Xuhang Luo , and Chenquan Gan 




Research Article (15 pages), Article ID 2576685, Volume 2022 (2022)

## **A Novel Tripartite Evolutionary Game Model for Misinformation Propagation in Social Networks**

Xianyong Li , Qizhi Li , Yajun Du , Yongquan Fan, Xiaoliang Chen, Fashan Shen, and Yunxia Xu




Research Article (13 pages), Article ID 1136144, Volume 2022 (2022)

## **Lag Secure Consensus for Second-Order Nonlinear Multiagent Systems with Event-Triggered Control Strategy under DoS Attacks**

Qi Han , Ao Zhang , Tengfei Weng, Yan Xie, Liping Feng , Guorong Chen, and Yuan Tian




Research Article (12 pages), Article ID 4451304, Volume 2022 (2022)

## **Containing Misinformation Spread: A Collaborative Resource Allocation Strategy for Knowledge Popularization and Expert Education**

Linhong Li , Kaifan Huang , and Xiaofan Yang 


Research Article (14 pages), Article ID 4510694, Volume 2022 (2022)

## **Spread of Misinformation in Social Networks: Analysis Based on Weibo Tweets**

Han Luo , Meng Cai , and Ying Cui 

Research Article (23 pages), Article ID 7999760, Volume 2021 (2021)

## **Controlling Virus Spread Using an Intermittent Quarantine Strategy on Multiplex Networks**

Xingguo Li, Xiaoping Luo, and Yiwu Wang 

Research Article (9 pages), Article ID 8643873, Volume 2021 (2021)

## Research Article

# DEDGCN: Dual Evolving Dynamic Graph Convolutional Network

Fengzhe Zhong <sup>1</sup>, Yan Liu <sup>1</sup>, Lian Liu,<sup>2</sup> Guangsheng Zhang,<sup>2</sup> and Shunran Duan <sup>1</sup>

<sup>1</sup>Henan Key Laboratory of Cyberspace Situation Awareness, Zhengzhou, Henan 450001, China

<sup>2</sup>Investigation Technology Center PLCCM, Beijing 100000, China

Correspondence should be addressed to Yan Liu; [ms\\_liuyan@aliyun.com](mailto:ms_liuyan@aliyun.com)

Received 25 November 2021; Accepted 18 April 2022; Published 10 May 2022

Academic Editor: Wei Wang

Copyright © 2022 Fengzhe Zhong et al. This is an open access article distributed under the Creative Commons Attribution License, which permits unrestricted use, distribution, and reproduction in any medium, provided the original work is properly cited.

With the wide application of graph data in many fields, the research of graph representation learning technology has become the focus of scholars' attention. Especially, dynamic graph representation learning is an important part of solving the problem of change graph in reality. On the one hand, most dynamic graph representation methods focus either on graph structure changes or node embedding changes, ignoring the internal relationship. On the other hand, most dynamic graph neural networks require learn node embeddings from specific tasks, resulting in poor universality of node embeddings and cannot be used in unsupervised tasks. Hence, Dual Evolving Dynamic Graph Convolutional Network (DEDGCN) was proposed to solve the above problems. DEDGCN uses the recurrent neural network to push the evolvement of GCN and nodes, from which it can extract the structural features of dynamic graph and learns the stability features of nodes, respectively, forming an adaptive dynamic graph convolution network. DEDGCN can be classified as unsupervised graph convolutional network. Thus, it is capable of training the unlabeled dynamic graph, it has more extensive application scenarios, and the calculated node embedding has strong generality. We evaluate our proposed method on experimental data in three tasks which are node classification, edge classification, and link prediction. In the classification task, facing the graph with large scale, complex connection relationship, and uncertain change rule, the F1 value of node classification task obtained by DEDGCN reaches 77%, and the F1 value of edge classification task reaches more than 90%. The results show that DEDGCN is effective in capturing graph features, and the effect of DEDGCN is much higher than other baseline methods, which proves the importance of capturing node stability features in dynamic graph representation learning. At the same time, the ability of DEDGCN in unsupervised tasks is further verified by using clustering and anomaly detection tasks, which proves that DEDGCN learning network embedding is widely used.

## 1. Introduction

There are many graph data in complex practical systems [1], such as social platforms, financial investment platforms, e-commerce platforms, etc. Because of various shapes and complex connection relationships, the graph is more difficult to represent than other data types of data. This also makes graph representation the key of application graph data. Graph representation is also called graph embedding (GE). At present, mature methods mainly include DeepWalk [2] and Node2vec [3] based on a random walk, GraRep [4] and HOPE [5] based on matrix decomposition, Struc2vec [6] and LINE [7] based on graph structure characteristics, SDNE [8] and DRNE [9] based on neural network, graph neural network [10], etc.

These methods are mostly applied in static graph. In practical application, graph does not remain unchanged but constantly changes over time, for example, making new friends in the relationship network, increasing and decreasing devices in the topology network, and iterating commodities in the e-commerce network. These graphs have time attributes. Static network representation learning technology cannot capture the time characteristics of dynamic graphs, and cannot learn and update the changes of nodes and the relationship between nodes, which makes the learning results of graph representation lack authenticity and dynamics.

Graph Convolution Networks [11] (GCN) have a simple structure, low complexity, fewer training times, and a good learning effect. As the basis of graph representation, it is



applied by many models. GCN cannot capture the change features in dynamic graph, but the Recursive Neural Network (RNN) can extract these features by processing change sequence information with time relation. In other words, the combination of GCN and RNN can effectively process dynamic graph. GCRN [12], RgCNN [13], etc., input the structural features of graph data captured by GCN into RNN, learn the timing relationship of nodes, and obtain the time features. These methods separate the structural features of graph from the time features, ignoring the internal connection. Moreover, the single GCN model is unable to capture dynamic structural features adaptively. EvolveGCN [14] uses RNN to evolve the parameters of the GCN so that the GCN can adaptively adjust according to the shape of graph at different times to extract the structural features with time characteristics. In addition, the graph shows periodic changes in many cases, such as significant differences in the communication relationship between employees in enterprises on working days and rest days. Employees are closely connected on weekdays and sparsely connected on rest days. However, the essential attributes of employees have not changed, when mapped to the graph representation, although nodes do not appear, they still maintain their original properties and characteristics, which is the stability of nodes. EvolveGCN lacks cognition of node stability and learning of node inherent attributes. The essence of GCN is supervised learning, which requires labeled data and is difficult to apply to tasks such as clustering and community discovery, making the model poor in universality.

Through the above analysis, we summarized the challenges faced by dynamic graph representation learning: the first problem is the stability of nodes. When capturing the dynamically changing graph structure features, the embedding of nodes is entirely influenced by the graph structure. Still, the attributes of nodes themselves determine the nature of nodes, and this nature does not change significantly with time under normal circumstances, which is the stability feature of nodes. Maintaining the stability of nodes in the graph structure with dynamically changing protrusions is a significant challenge. The second problem is the problem of unlabeled graph data training. The node embedding features obtained by supervised learning are suitable for specific tasks, and the universality is poor. When faced with unsupervised tasks such as clustering and anomaly detection, node embedding cannot be directly applied. Given these two problems, in this paper, a dual evolution dynamic graph convolutional neural network, DEDGCN, is proposed. Firstly, the stability characteristics of nodes are learned through the node evolution module. Secondly, the loss function is calculated by using the stability characteristics of nodes, and the unsupervised dynamic graph representation model is constructed while modifying the network architecture.

The following are the main contributions of this paper:

- (i) We propose a dual evolution model. Based on EvolveGCN, a node evolution module is added to form a dual evolution model. While capturing the structural characteristics of a dynamic graph, the

stability characteristics of nodes are learned. The GCN network architecture is jointly revised from graph structure and nodes to build an adaptive dynamic graph convolution model.

- (ii) We build an unsupervised GCN model. We use the node stability of the dynamic graph and the prediction ability of the node evolution module to construct the loss function independent of the data label. Without relying on specific data label and tasks, DEDGCN is an unsupervised dynamic graph convolutional network. We can apply DEDGCN to a broader range of tasks.

Architecture: Section 2 describes the related work, relevant concepts are given in Section 3, solutions to the problems are put forward in Section 4, an experimental evaluation of our methods is presented in Section 5, and Section 6 provides a summary.

## 2. Related Work

The purpose of graph representation learning technology is to obtain low-dimensional dense vectors of nodes and apply them to downstream tasks such as node classification, link prediction, network reconfiguration, community discovery, network data visualization, etc. [15]. At present, most graph representation learning methods are mainly aimed at static graph. When faced with dynamic graph data, these methods cannot capture the changing characteristics of the graph, resulting in unsatisfactory results in the application process. The essence of dynamic graph data and static graph is the same; so, many dynamic graph representations often evolve from the static model.

At the earliest stage, node embedding was generated by decomposing the Laplace and adjacency matrix of graph data, called Graph Factorization (GF). The most typical examples are GraRep [4], HOPE [5], etc. These algorithms use matrix decomposition to calculate eigenvalues and eigenvectors to represent node embedding. The key of graph decomposition technology is to obtain eigenvalues and eigenvectors which directly determine the quality of node embedding. In dynamic graph data, to reduce algorithm complexity, the evolution of eigenvalues and eigenvectors is carried out to update node embedding, the most typical of which is DHPE [16]. In addition, another direct factor that determines the quality of node embedding is the node itself. TIMERS [17] decomposes the adjacency matrix of the initial time graph and updates the node embedding in the subsequent time graph. After each update, the loss value represented by the graph is calculated. When the loss value exceeds the threshold, the time graph is matrix decomposed again. However, with the increase of graph scale, matrix decomposition becomes more and more difficult, and the node representation generated by matrix decomposition is challenging to explain. This problem makes applying the graph representation learning method based on matrix decomposition to large-scale graph challenging.

Dynamic graph has many structural characteristics, and many scholars use them to reconstruct the generation

probability of graphs to calculate node embedding. For example, DyREP [18] used the relational evolution and social evolution in dynamic graph to initially describe the characteristics of nodes, periodic changes of nodes, and the influence of external nodes on embedding from the perspectives of local embedding propagation, self-propagation, and external factor driving. Then, DyREP used the probability of node emergence to reconstruct data and calculate node embedding. Zhou et al. [19] adopted the triadic closure process, combined with social isomorphism and temporal smoothness, to construct the loss function and reconstruct the graph to obtain node embedding. These methods all belong to the transductive method. Whenever new graph data come, it is necessary to retrain the model to obtain node embeddings. The process is high in complexity, long in time, and inefficient.

With the appearance of Graph Neural Network (GNN), graph embedding technology has entered a new stage of development, especially GCN, which realizes the end-to-end learning of graphs of any size and shape. GCN has a good effect in node classification, link prediction, and other tasks, and has the advantages of simple structure, few parameters, strong ability to extract graph features, and suitability for large-scale graph. At present, many graph embedding technologies are based on GCN, learning the timing information of nodes themselves and capturing the time characteristics of graph data. For example, GCRN [12] combines GCN with RNN, captures the timing information of graph through input node embeddings into RNN. Similar ideas include WD-GCN/CD-GCN [20], RgCNN [13], and so on. However, these methods only start from the dynamic changes of the nodes themselves, ignoring the graph structure's constant changes. The learned structure features are fixed and single, and the adaptability to frequently changing graphs is poor. To make the model adapt to the shift of graph, Addgraph [21] uses an attention mechanism to aggregate GCN parameters in the past period to generate current GCN network parameters. EvolveGCN [14] also aims at the ever-changing graph structure problem. With the help of RNN to evolve GCN, a dynamic GCN model is built, which ensures that the model can learn the changing graph structure adaptively. However, the nature of GCN is still a kind of supervised learning, which cannot extract the structure and dynamic features of unlabeled data, leading to the failure of community division, clustering, anomaly detection, and other tasks.

The most common method for learning unsupervised graph is the dynamic autoencoder network, which utilizes the symmetry between encoder and decoder to generate highly nonlinear node embedding. For dynamic graph, DynGEM [22] increases the number and width of layers of encoder and decoder according to the graph size each time, which ensures the adaptive change of the model. At the same time, using the first-order approximation and second-order approximation of nodes, the loss values of local structure and global structure of graph are calculated to construct the loss function and train the network. Dyngraph2vec [23] replaces the neurons of the self-encoder with long-term and short-term memory cells (LSTM). It takes the historical neighbor information of the nodes

multiple times as input so that the model can capture time characteristics. Dyngraph2vec constructs the loss function in the way of prediction, inputs multiple historical graph into the network, predicts the graph structure of the next time, compares it with the real graph structure, and forms the loss function. The autoencoder network includes multi-layer encoders and decoders, and there are many parameters in the training process, limiting its application in large-scale graph.

The dynamic network representation learning technologies involved are summarized in Table 1 according to the learning methods to facilitate further research in the future.

### 3. Relevant Concepts

In this section, we formally define the basic concepts and related issues of dynamic graph representation learning.

*Definition 1.* (Static Graph)  $G = (V, E)$  is composed of a group of nodes  $V = \{v_1, \dots, v_N\}$  and the connection relationship (called edge)  $E \in \{(v_i, v_j) | (v_i, v_j) \in V \times V\}$  between nodes, where  $N$  represents the number of nodes.  $A$  represents the adjacency matrix of a graph with the size of  $N \times N$ , where if  $e_{ij} \in E$ , then  $A_{ij} = 1$ , otherwise  $A_{ij} = 0$ . If the graph is undirected,  $A$  is a symmetric matrix.

*Definition 2.* (Dynamic Graph) A series of static graphs that change continuously constitute a dynamic graph, denoted by  $\mathcal{G} = \{G_1, G_2, \dots, G_t, \dots\}$ , where each  $G_t = (V_t, E_t)$  is called a snapshot.  $t$  represents the serial number of snapshots,  $V_t$  represents the set of nodes under the  $t$  snapshot,  $E_t$  represents the set under the  $t$  snapshot, and  $A_t$  means the adjacency matrix of the graph of the  $t$  snapshot.

*Definition 3.* (Graph Representation Learning) For a given graph  $G = (V, E)$ , graph representation learning is defined as mapping the nodes into the vector space of  $d$  ( $d \ll |V|$ ) dimension by function  $f: V \rightarrow X \in \mathbb{R}^d$ .

Generally speaking, we define the problems related to our work as follows.

*Problem:* (Dynamic Graph Representation Learning) For a given  $\mathcal{G} = \{G_1, G_2, \dots, G_T\}$ , the dynamic graph representation learning is defined as mapping nodes in snapshot  $t$  into  $d$ -dimensional vector space by function  $f_t: V_t \rightarrow X_t \in \mathbb{R}^d$ , and the  $f_t$  can capture the following characteristics:

- (i) Similarity characteristics of structure. The Euclidean distance between  $x_t^i$  and  $x_t^j$  is small if  $i$  and  $j$  are neighbors.
- (ii) Stability characteristics of nodes. The Euclidean distance between  $V_t$  and  $V_{t+1}$  is small if graph evolves normally.

### 4. Methodology

This section puts forward a dual evolving dynamic graph convolution network, DEDGCN, whose framework is provided in Figure 1. DEDGCN mainly includes GCN

TABLE 1: A summary of dynamic network embedding methods.

Method	Learning techniques	Supervised	Unsupervised
DHPE [16]	Matrix decomposition, embedded update		✓
TIMERS [17]	Matrix decomposition, embedded update		✓
DyREP [18]	Dynamic network structure characteristics		✓
DynamicTriad [19]	Dynamic network structure characteristics		✓
GCRN [12]	Splicing GCN and RNN	✓	
WD-GCN/CD-GCN [20]	Splicing GCN and RNN	✓	
RgCNN [13]	Splicing GCN and RNN	✓	
Addgraph [21]	Attentional mechanism evolves GCN	✓	
EvolveGCN [14]	RNN evolves GCN	✓	
DynGEM [22]	Scalable autoencoder network		✓
Dyngraph2vec [23]	LSTM evolves autoencoder network		✓

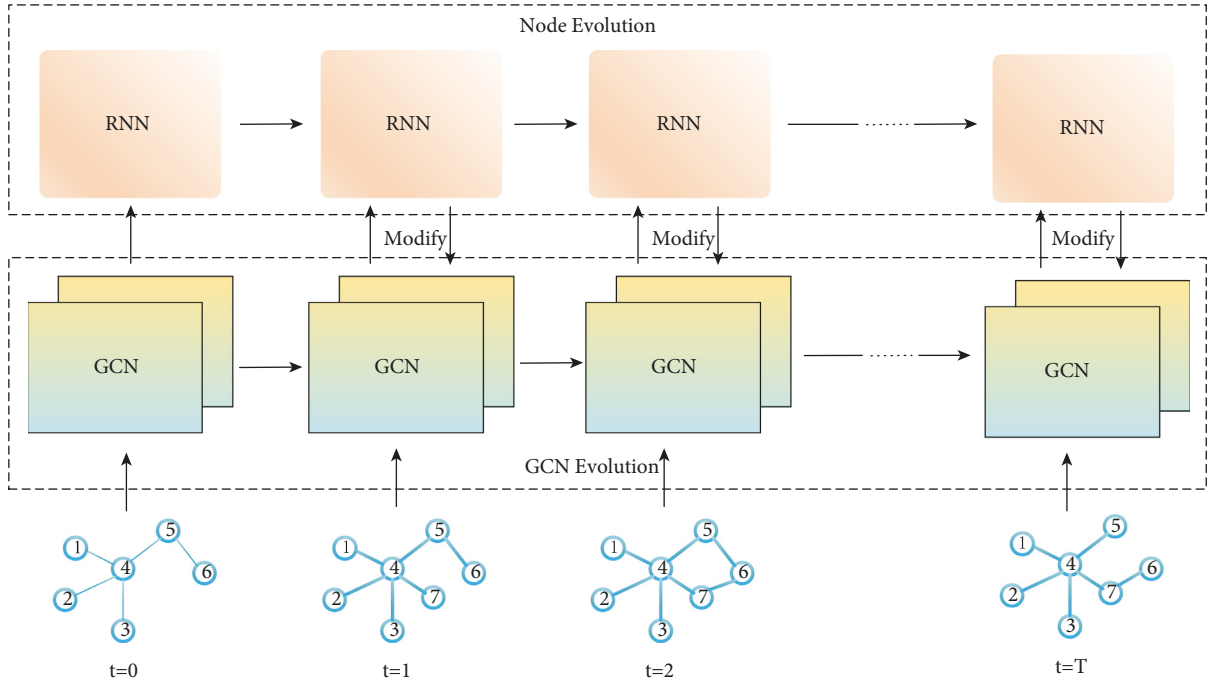


FIGURE 1: The framework of DEDGCN. DEDGCN consists of two parts: the upper Node Evolution learning the stability characteristics of nodes and the lower GCN evolution learning dynamic structure characteristics of graphs. They work together to modify GCN and build an unsupervised graph convolutional network framework.

evolution and node evolution. The graphs' dynamic structure characteristics and node stability characteristics are learned, respectively, to build an adaptive unsupervised dynamic graph convolutional network.

In the part of GCN evolution, we learn from the evolution process of GCN by EvolveGCN and use RNN to capture the morphological change rule of GCN in historical snapshots to generate the GCN network needed by the current snapshot. GCN parameters are the key to building a GCN model. Using RNN to evolve GCN parameters can quickly correct the GCN to capture changing graph structure features.

In node evolution, we mainly consider the stability characteristics of nodes. The attributes of nodes themselves are stable during the normal development of graph and will not change significantly. The change process with time contains a lot of temporal information, which can reflect the fluctuation of its attributes. By capturing the temporal

information, we can predict the changes of nodes and get the stability characteristics of nodes. Similarly, we use RNN to learn the timing information of nodes, extract the attributes of nodes themselves, and ensure the stable generation of node embedding with time. We modify the GCN by constructing the loss function and feeding back the stability characteristics of nodes to the GCN.

The loss function mainly comprises node embedding generated by the GCN and node embedding predicted by RNN. RNN can predict the embedding of nodes at the next moment by learning the timing information of nodes. In vector space, the predicted value should be as close as possible to the generated value of GCN to ensure the authenticity of the learned timing information. In addition, the stability of nodes also makes the embedding of nodes in adjacent snapshots not change significantly, and the generated values calculated by GCN should be close to each other. Therefore, we use the gap

between the predicted value and the generated value of GCN and the distance of node embedding between adjacent snapshots to construct the loss function in order to provide constant feedback and correct the GCN. Ensure that the node embedding generated by the GCN can have the node stability characteristics in the predicted value. At the same time, the loss function of DEDGCN does not depend on data labels, forming an unsupervised dynamic graph convolution network. The number of nodes in each moment graph changes with time in the dynamic graph, and they are not precisely the same. To describe snapshots conveniently, we use  $N$  to indicate the number of nodes in each snapshot.

**4.1. GCN Evolution.** We use the GCN to extract the structural features of graph. GCN contains multiple graph convolution layers, which can aggregate multi-layer neighbor features and capture structure features. For  $G_t = (V_t, E_t)$ , the propagation rules among the graph convolution layers are as follows:

$$H_t^{(l+1)} = \sigma(\tilde{A}_t \cdot H_t^{(l)} \cdot W_t^{(l)}),$$

$$\tilde{A}_t = D_t^{-\frac{1}{2}} A_t' D_t^{-\frac{1}{2}}, A_t' = A_t + I. \quad (1)$$

Here,  $H_t^{(l)}$  represents the calculation result of the snapshot  $t$  after the  $l$ -th graph convolution layer.  $\tilde{A}_t$  is defined as the regularized form of the adjacency matrix  $A_t$  of the snapshot  $t$ .  $A_t'$  is the self-connection matrix of snapshot  $t$ .  $D$  is the degree matrix,  $D_{ii} = \sum_j A_{ij}'$ , and  $W_t^{(l)}$  represents the parameters of the  $l$ -th graph convolution layer at  $t$ .  $\sigma(\cdot)$  refers to the activation function, such as ReLU, sigmoid, etc.

To enable GCN to capture the structural features of dynamic graphs adaptively, we use EvolveGCN as a reference for evolving the parameters of GCN, and modify the architecture of GCN to adaptively obtain to the changing graph. At present, the commonly RNN cell is Long-Short Term Memory [24] (called LSTM), which consists of an input gate, a forget gate, and an output gate, which can selectively capture the information of time series, save the key and forget the redundant content. For the parameter evolution of GCN, we choose LSTM as the memory cell, and the process is shown in Figure 2. We input the GCN parameter  $W_{t-1}^{(l)}$  of  $l$ -th layer at  $t-1$  into LSTM, and get GCN parameter  $W_t^{(l)}$  of  $l$ -th layer at  $t$ .

The calculation method of GCN parameter evolution is as follows:

$$W_t^{(l)} = \text{LSTM}(W_{t-1}^{(l)}),$$

$$i_t = \text{sigmoid}(U^{(i)} W_{t-1}^{(l)} + B^{(i)}),$$

$$f_t = \text{sigmoid}(U^{(f)} W_{t-1}^{(l)} + B^{(f)}),$$

$$o_t = \text{sigmoid}(U^{(o)} W_{t-1}^{(l)} + B^{(o)}),$$

$$\tilde{c}_t = \tanh(U^{(c)} W_{t-1}^{(l)} + B^{(c)}),$$

$$c_t = f_t \circ c_{t-1} + i_t \circ \tilde{c}_t,$$

$$W_t^{(l)} = o_t \circ \tanh(c_t). \quad (2)$$

In the process of GCN parameter evolution, LSTM constantly learns the changing rules of GCN parameters in

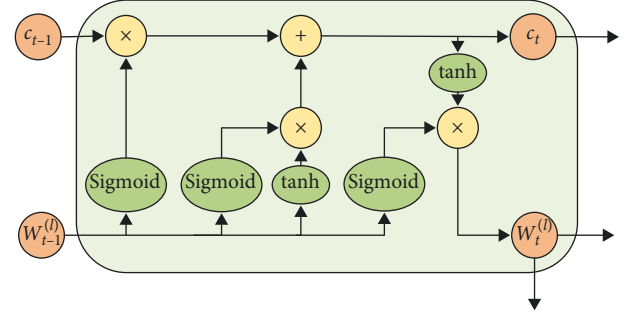


FIGURE 2: The process of GCN evolution.

continuous snapshots. Memory cells are updated continuously, and new GCN parameters are continually predicted so that the GCN can adaptively modify the shelf shape with the change of graph to capture the dynamic structural features effectively.

**4.2. Node Evolution.** LSTM has an excellent ability to capture timing information. We use LSTM to learn the behavior of nodes in continuous snapshots, extract the stability characteristics of nodes, and predict the state of nodes in the next snapshot. Here, we use LSTM to evolve nodes, and the evolution process of nodes is shown in Figure 3.

We input the embedded  $\{X_{t-w+1}, X_{t-w+2}, \dots, X_t\}$  calculated by GCN in continuous snapshots into LSTM and get predicted embedding  $P_{t+1}$  at time  $t+1$ .  $w$  represents the window size of LSTM and  $P_t$  indicates node embedding at the predicted time  $t$ . The calculation method is shown in the following formula.

$$P_{t+1} = \text{LSTM}(X_t, P_t),$$

$$i_{t+1} = \text{sigmoid}(W^{(i)} X_t + U^{(i)} P_t + B^{(i)}),$$

$$f_{t+1} = \text{sigmoid}(W^{(f)} X_t + U^{(f)} P_t + B^{(f)}),$$

$$o_{t+1} = \text{sigmoid}(W^{(o)} X_t + U^{(o)} P_t + B^{(o)}), \quad (3)$$

$$\tilde{c}_{t+1} = \tanh(W^{(c)} X_t + U^{(c)} P_t + B^{(c)}),$$

$$c_{t+1} = f_{t+1} \circ c_t + i_{t+1} \circ \tilde{c}_{t+1},$$

$$P_{t+1} = o_{t+1} \circ \tanh(c_{t+1}).$$

By learning the node state during the window  $w$ , the predicted node embedding includes the attribute characteristics of the node itself and the stability characteristics in the changing process. We spread the attributes of nodes into the GCN in the form of the loss function and further modified the GCN network structure.

**4.3. Construction of Loss Function.** We use the node embedding generated by GCN and the node evolution results to construct the loss function and modify the GCN model. Let us go into the details below.

In the normal changes of dynamic networks, the characteristics of nodes will not change drastically. In dynamic graph

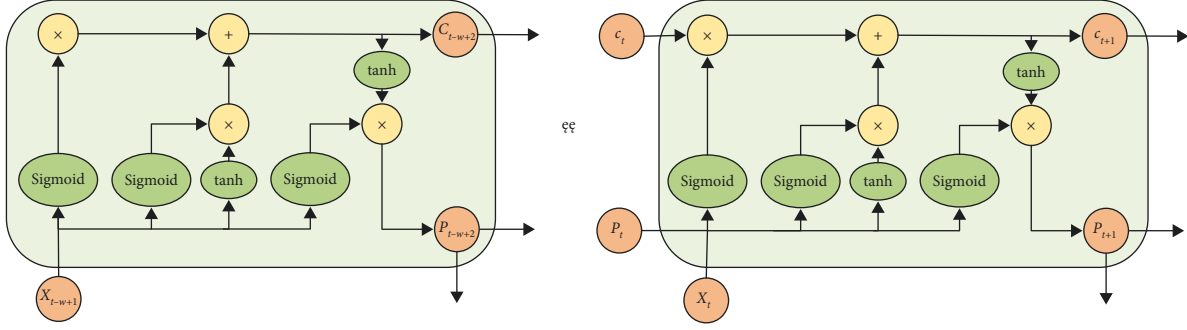


FIGURE 3: The process of Node Evolution.

networks with frequent increase or decrease of nodes, the inherent characteristics of nodes will not change enormously, which denotes the stability of the nodes. The property of nodes transformed into vector space shows that the embedding similarity between adjacent snapshots is higher. Therefore, we can express it by calculating the embedding similarity of adjacent snapshot nodes, and the calculation method is shown in the following formula:

$$\mathcal{L}_1 = \sum_{i=1}^N 1 - \text{similarity}(x_{t-1}^i, x_t^i). \quad (4)$$

In formula (4),  $x_t^i$  indicates the node embedding generated by GCN by node  $i$  at time  $t$ , and *similarity* represents cosine similarity function.

In the process of node evolution, LSTM is used to predict node embedding, and the expected embedding value of the node at the next moment is obtained. When the predicted value is consistent with the generated value of GCN, the GCN model can acquire the ability to extract the stability features of nodes. The same is true for the ability to extract the structural characteristics of nodes. We calculate the similarity between the predicted value and the GCN-generated value to keep their consistency. The calculation method is as shown in formula (5), where  $p_t^i$  represents the node embedding expected by LSTM for node  $i$  at time  $t$ .

$$\mathcal{L}_2 = \sum_{i=1}^N 1 - \text{similarity}(p_t^i, x_t^i). \quad (5)$$

In addition, to prevent the overfitting phenomenon in the training process, we add the weight attenuation function to the loss function to reduce the parameter weight as shown in formula (6), where  $w$  represents the GCN parameter.

$$\mathcal{L}_3 = \frac{\lambda \sum_w \|w\|_2^2}{2N}. \quad (6)$$

The final loss function is defined as follows:

$$\text{loss} = \mathcal{L}_1 + \mathcal{L}_2 + \mathcal{L}_3, \quad (7)$$

## 5. Experiments

**5.1. Dataset.** We experiment with our method DEDGCN on publicly available basic datasets. The datasets are described below.

Elliptic [25] is a bitcoin transaction graph in which nodes represent transactions and edges represent bitcoin flows between transactions. The types of nodes in this graph can be divided into two categories: legal and illegal, so we use this dataset for experiments of node classification and node clustering tasks.

Bitcoin alpha is a platform for trading in bitcoin, which uses the trading behaviors among users to form a graph. Members of the platform rate other members on a scale of F02D 10 to +10, which indicates the trust level of each member. According to the user's trust score, we divide the score into two categories: trustworthy and untrustworthy. The transaction behaviors among users are built into a dynamic network. The nodes represent users, and edges represent transactions between users. In scoring each user's transaction process, users are given the label of trust or distrust. For Bitcoin alpha, we carry out the edge classification task and link prediction task.

Reddit Hyperlink is a graph composed by extracting the link relationships in Reddit posts. Each link relationship contains the time and the source post's emotion (positive or negative) to the target post. We performed edge classification on this dataset to predict the emotional relationships that existed between unlinked posts.

UCI is a graph composed of private information sent by UC-Irvine on the campus social platforms. Users can search for other people on this social platform and then send conversations according to the profile information. The edge represents a piece of private information sent by user  $u$  to user  $v$  at time  $t$ . We predict the links of this dataset to capture the possible contacts of users at the next moment.

AS network is a graph composed of connections between autonomous systems. Nodes represent autonomous systems, while edges represent connectivity between autonomous systems. We make the link prediction task on this graph to predict the connection relationship of the network at the next moment.

Myanmar network refers to the network composed of autonomous systems applied by Myanmar. Nodes represent autonomous systems belonging to Myanmar, and edges represent the connectivity relationship between autonomous systems. Through the continuous monitoring of the network in the Myanmar autonomous system, the abnormal behavior of the network can be warned, and a reference can be provided for maintaining the regular operation of the network.

The basic information of these data is shown in Table 2. According to the characteristics of different datasets, we divide them into snapshots at different time intervals and apply them to different tasks.

**5.2. Baseline.** We will compare DEDGCN with the following five basic methods.

**Methods 1:** GCN is a static graph convolution neural network, which cannot extract dynamic features. We fuse all snapshots to form static graph, and compare the importance of time features. At the same time, GCN is a network structure feature extractor in DEDGCN, which is tested as a module unit of DEDGCN.

**Method 2:** GCN-GRU is a method of generating node embedding with fixed GCN and evolving node timing relationship with GRU. This method can be regarded as a node embedding module and tested as a unit module of DEDGCN.

**Method 3:** DynGEM is a dynamic unsupervised network representation learning method based on deep autoencoder model. DynGEM carries out adaptive learning for graph at different times through the evolution of the parameters of the deep autoencoder model, so as to ensure the learning of network structural features and spontaneously capture the relationship characteristics between graph at different times, so as to make the network embedding results at different times continuous.

**Method 4:** Dyngraph2vec is a dynamic unsupervised node representation method that integrates the deep autoencoder model, LSTM, and MLP networks. Neurons in the deep autoencoder model are replaced by short and long memory cells to construct a deep autocoding model with memory function. According to the different combination modes of the three networks, dyngraph2vec includes three versions, namely, dyngraph2vecAE, dyngraph2vecRNN, and dyngraph2vecAERNN. Dyngraph2vecAE and DynGEM are similar in architecture, so the second and third methods are used for comparison.

**Method 5:** EvolveGCN is similar to GCN-GRU, which uses RNN to evolve GCN parameters and learn the time series relationship of models. This method is regarded as a GCN parameter evolution module and tested as a DEDGCN unit module.

**5.3. Metric.** The evaluation methods used in this paper include F1 value and MAP. The calculation of these two evaluation methods is introduced in detail below.

First of all, we need to make the following definitions:

**True positive (TP):** the number of samples where the predicted and actual values are positive.

**True negatives (TN):** the number of samples where the predicted value is positive and the actual value is negative.

**False positives (FP):** the number of samples where the predicted value is negative and the actual value is positive.

**False negatives (FN):** the number of samples where the predicted and actual values are negative.

Through the above four definitions, we can calculate the precision and recall of the prediction results, and the formula is as follows:

$$\text{precision} = \frac{TP}{TP + FP} \quad (8)$$

$$\text{recall} = \frac{TP}{TP + FN}$$

F1 value is the harmonic average of accuracy rate and recall rate, which can objectively reflect the validity of prediction. The calculation formula is as follows:

$$F1 = 2 \frac{\text{precision} \times \text{recall}}{\text{precision} + \text{recall}} \quad (9)$$

AP refers to the integral of the PR (precision-recall) curve, the average precision of all recall values between 0 and 1. The formula is as follows:

$$AP = \sum_{i=1}^N \text{precision}(i) \Delta \text{recall}(i). \quad (10)$$

MAP refers to the average of all kinds of AP, and the calculation formula is as follows.  $K$  indicates the number of categories of AP.

$$\text{MAP} = \frac{1}{K} \sum_{i=1}^K AP_i. \quad (11)$$

**5.4. Task.** In this paper, we prove the effectiveness of our proposed DEDGCN through four tasks: node classification, edge classification, link prediction, and anomaly detection.

**5.4.1. Node Classification.** Predict the types of unlabeled nodes by learning the characteristics of labeled nodes. In this section, the probability of node embedding is calculated by the feedforward neural network and softmax function to judge the node type  $u$  at time  $t$ . For node classification, we use the F1 value to measure the effectiveness of the method.

**5.4.2. Edge Classification.** Predict the types of unlabeled edges by learning the features of labeled edges. In this paper, the probability of edge embedding is calculated by feedforward neural network and softmax function to judge the edge type at time  $t$ . The embedding is obtained by aggregating node  $u$  and node  $v$  representation. The aggregation method adopts the Hadamard product. The measurement method of edge classification adopts the F1 value.

**5.4.3. Link Prediction.** Whether the edge at time  $t + 1$  exists or not is predicted by embedding of node  $u$  and node  $v$  before time  $t + 1$ . We aggregate node  $u$  and node  $v$ , and then use MLP to obtain the existence probability of edges. For link prediction, we use MAP to measure the effectiveness of the results.

TABLE 2: Basic information of experimental data.

Dataset	# Nodes	# Edges	# Snapshots	Tasks
Elliptic	230769	234355	49	Node classification and clustering
Bitcoin alpha	3783	24186	136	Link prediction, edge classification
Reddit hyperlink network	55863	858490	174	Edge classification
UCI	1899	59835	192	Link prediction
AS network	6474	13895	100	Link prediction
Myanmar	209	48857	75	Anomaly detection

5.4.4. *Anomaly Detection.* Through the representation of node embedding in the continuous snapshot, the normal state of the node at the next moment is predicted, and the expected value is compared with the actual value of the node to judge whether the node is abnormal.

### 5.5. Details

- (1) For any dataset, we use a one-hot node-degree as the input feature of the model.
- (2) For all GCN, we set the number of graph convolution layers to 2; For all MLP used in classification tasks, we set the depth to 2, and the softmax function calculates the classification probability. For classification tasks and link prediction tasks, the loss function of MLP adopts cross-entropy.
- (3) We use fixed-size dimension to represent nodes for any dataset, and the value is 100.
- (4) For the weight attenuation coefficient, we set its size to 0.01.
- (5) We divide the data into training set and test set according to the ratio of 8 : 2

### 5.6. Results and Analysis

5.6.1. *Node Classification.* We apply Elliptic to the node classification task. For GCN parameters and node embedding evolution, we all adopt a time window size of 5. Meanwhile, GCN, GCN-GRU, EvloveGCN, and DEDGCN constitute unit test experiments to verify the effectiveness of different modules of DEDGCN in node classification tasks, respectively. The experimental results are shown in Figure 4.

As we can see from Figure 4, DEDGCN performs node classification tasks in Elliptic dataset, and its F1 value is much higher than that of GCN, GCN-GRU, and EvloveGCN. GCN is not effective in the dynamic graph representation learning, and the F1 value is only 47% in node classification tasks, which shows that the graph structure changes have a great impact on the generation of node embedding in the dynamic evolution process. The lack of time leads to a lot of old information in the graph, much noise in structural features, and poor effect in practical tasks of node embedding application. However, the two versions of EvloveGCN, version H and version O, are not effective in node classification of Elliptic dataset, especially in version H, the F1 value of node classification is 44%. To sum up, the attributes of nodes on Elliptic are relatively stable, and it is

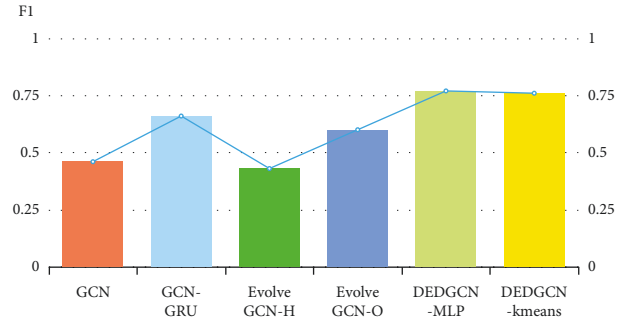


FIGURE 4: F1 value of Elliptic in the node classification task.

difficult to convert between legal nodes and illegal nodes. GCN-GRU model and DEDGCN model proposed in this section can evolve nodes, extract inherent features of nodes, and maintain the stability of nodes. F1 values are higher than EvloveGCN, which shows the importance of node stability features in the process of snapshot evolution. In addition, the F1 value of DEDGCN using MLP for supervised classification reaches 77%. Besides supervised classification, K-means clustering algorithm is used for unsupervised classification of node types, and the effect is only 1% lower than that of supervised method. This also proves that DEDGCN learning node embedding is suitable for unsupervised clustering tasks.

5.6.2. *Edge Classification.* We apply Bitcoin Alpha and Reddit Hyperlink Network datasets to edge classification task. For GCN parameters and node embedding evolution, we both adopt a time window size of 5. At the same time, GCN, GCN-GRU, EvloveGCN, and DEDGCN constitute unit test experiments to verify the effectiveness of different modules of DEDGCN in the edge classification task, respectively. The experimental results are shown in Figure 5.

As shown in Figure 5, in the edge classification task, the F1 value of DEDGCN classification reaches 93% on Bitcoin Alpha and 90% on Reddit Hyperlink Network dataset, and the classification effect is far better than that of module unit classification. The F1 value of EvloveGCN for edge classification is higher than that of GCN and GCN-GRU. In dynamic graph, nodes rely on edges to form a network, and edges are an important component of the graph, and the characteristics of edges depend on the network structure. In EvloveGCN and DEDGCN, relying on GCN parameter evolution module, dynamic network structure characteristics can be captured, while GCN and GCN-GRU can only

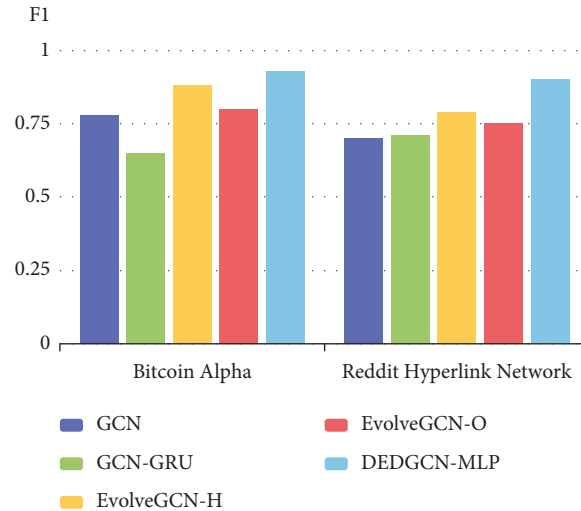


FIGURE 5: F1 value of Reddit hyperlink and Bitcoin Alpha in the edge classification task.

extract fixed network structure characteristics, but have no updating ability. The learned network embedding contains a lot of old information, which cannot reflect the current state of the graph, and has poor effect in edge classification tasks.

Combining the experimental results of node classification and edge classification tasks, DEDGCN has different advantages in different tasks. In node classification task, the stability feature captured by node embedding evolution module helps to improve the node classification effect. In edge classification task, the dynamic network structure feature captured by GCN parameter evolution module helps to improve the edge classification effect. Compared with GCN, GCN-GRU, and EvolveGCN, the F1 value of DEDGCN is higher than that of the unit module, which shows the importance of GCN parameter evolution module and node embedding evolution module in DEDGCN. DEDGCN is an integral part of dynamic graph representation learning.

**5.6.3. Link Prediction.** We conducted link prediction experiments on Bitcoin Alpha, UCI, and AS Network datasets, respectively, and the results are shown in Table 2.

From Table 3, we can see that the MAP values of DEDGCN are higher than those of other methods, and remain above 0.15, which has a good effect on the link prediction task. MAP value is the comprehensive embodiment of accuracy and recall rate and can reflect the global performance index of the algorithm. Bitcoin Alpha, UCI, and AS Network belong to three different types of graph data: transaction network, social network, and device network. DEDGCN has stable MAP values on different graph types, which also directly shows that DEDGCN can be applied to most graph data and has better robustness.

**5.6.4. Anomaly Detection.** We use the global BGP routing path information (including the AS relationship to which BGP belongs) collected by route views to build a global

dynamic AS relationship network in two hours. Due to the huge number of AS globally, we selected Myanmar’s AS network as the research object to verify DEDGCN’s ability in anomaly detection tasks.

First of all, we learn the evolution law of the normal AS network through DEDGCN. Then, the AS network to be detected is input into the trained model to obtain the node embedding and node evolution results of the AS network. Finally, the similarity of node embedding and node evolution results is calculated to determine when the network anomaly occurs.

Here, we use the cosine similarity method to calculate the similarity between each node’s embedding and evolution result. This similarity is also called the normal value in anomaly detection. To determine whether anomalies occur at time  $t$ , we take the average similarity of all nodes in the AS network at time  $t$  as the normal value of the network at time  $t$ . In the process of continuous monitoring, when the network is abnormal, the normal value of the network will appear to “steep drop.” At this time, we can judge the time when the AS network is abnormal.

Taking Myanmar as an example, we collected Myanmar’s AS network from January to February 2021, divided snapshots in two-hour units, and used DEDGCN for monitoring. The monitoring results are shown in Figure 6.

It can be clearly seen from Figure 6 that from 0:00 on February 1, 2021, the score of Myanmar’s AS network has experienced a “steep drop,” indicating that there is a problem with the Myanmar network at this time. Through Wikipedia verification, it can be known on February 1, 2021, the Myanmar military took over the government. To complete social control and control speech, it cut off the Internet and communications in major cities, resulting in large-scale network outages across the country. This also verified DEDGCN’s ability in anomaly detection tasks.



TABLE 3: The MAP value on the link prediction task.

	DynGEM	Dyngraph 2vecAE	Dyngraph 2vecAERNN	GCN-GRU	Evolve GCN-H	Evolve GCN-O	DEDGCN
Bitcoin alpha	0.0525	0.0507	0.1100	0.0001	0.0049	0.0036	0.1668
UCI	0.0209	0.0044	0.0205	0.0114	0.0126	0.0270	0.1584
AS network	0.0529	0.0331	0.0711	0.0713	0.1534	0.1139	0.1691

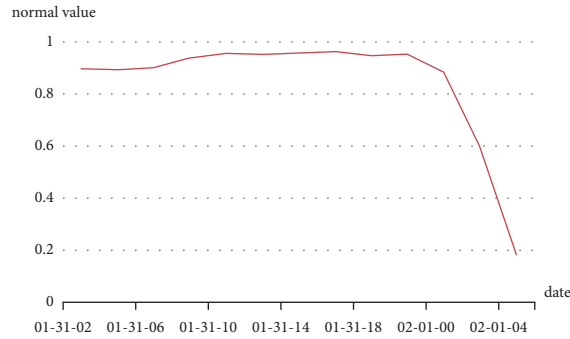


FIGURE 6: Monitoring of the AS network in Myanmar.

## 6. Conclusions

Through the performance of node classification, edge classification, link prediction, and anomaly detection tasks, the effect of our proposed method DEDGCN has been proved. Based on the experimental results, we discussed the applicable task scenarios of GCN-RNN based on node evolution and EvolveGCN based on parameter evolution. DEDGCN, which combines the advantages of node evolution and parameter evolution, makes the extracted node features dynamic while retaining the inherent stability characteristics of the node and has achieved good results in various tasks, which proves the broad application of the DEDGCN method. In addition, DEDGCN is an unsupervised graph representation model. We use unsupervised clustering methods to determine the type of nodes in the node classification task for experimental data. Its effect is only 1% lower than the effect of supervised classification. In the network anomaly detection task for realistic graph data, DEDGCN can perceive the time when the network anomaly occurs, which also shows the effectiveness of DEDGCN in unsupervised tasks.

## Data Availability

Elliptic dataset can be obtained from <https://www.kaggle.com/elliptico/elliptic-data-set>. Bitcoin alpha dataset can be obtained from <http://snap.stanford.edu/data/soc-sign-bitcoin-alpha.html>. Reddit Hyperlink dataset can be obtained from <http://snap.stanford.edu/data/soc-RedditHyperlinks.html>. UCI dataset can be obtained from <http://konect.cc/networks/opsahl-ucsocial/>. AS network dataset can be obtained from <http://snap.stanford.edu/data/as-733.html>. Myanmar Network dataset is constructed by extracting global BGP path which can be obtained from <http://archive.routeviews.org/>. The wiki address for the February 1, 2021 events in Myanmar can be obtained from [https://en.wikipedia.org/wiki/2021\\_Myanmar\\_coup\\_d%27%C3%A9tat](https://en.wikipedia.org/wiki/2021_Myanmar_coup_d%27%C3%A9tat).

## Conflicts of Interest

The authors declare that there are no conflicts of interest regarding the publication of this paper.

## Acknowledgments

This work was supported by the National Natural Science Foundation of China (No.U1804263) and the Zhongyuan Science and Technology Innovation Leading Talent Project (No. 214200510019).

## References

- [1] X. Guotong, Z. Ming, and L. Jianxin, "Dynamic network embedding survey," p. 5, 2021, <https://arxiv/abs.org/2103.15447>.
- [2] B. Perozzi, A. Rami, and S. Steven, "Deepwalk: online learning of social representations," in *Proceedings of the Twentyth ACM SIGKDD international conference on Knowledge discovery and data mining*, pp. 701–710, New York NY USA, August 2014.
- [3] A. Grover and J. Leskovec, "node2vec: scalable feature learning for networks," in *Proceedings of the 22nd ACM SIGKDD international conference on Knowledge discovery and data mining*, pp. 855–864, San Francisco CA USA, August 2016.
- [4] S. Cao, W. Lu, and Q. Xu, "Grarep: learning graph representations with global structural information," in *Proceedings of the 24th ACM international on conference on information and knowledge management*, pp. 891–900, Melbourne Australia, October 2015.
- [5] M. Ou, P. Cui, and J. Pei, "Asymmetric transitivity preserving graph embedding," in *Proceedings of the 22nd ACM SIGKDD international conference on Knowledge discovery and data mining*, pp. 1105–1114, San Francisco CA USA, August 2016.
- [6] L. F. R. Ribeiro, P. H. P. Saverese, and D. R. Figueiredo, "struc2vec: learning node representations from structural identity," in *Proceedings of the 23rd ACM SIGKDD international conference on knowledge discovery and data mining*, pp. 385–394, Halifax Canada, August 2017.
- [7] T. Jian, Q. Meng, W. Mingzhe, Z. Ming, Y. Jun, and M. Qiaozhu, "Line: large-scale information network embedding," in *Proceedings of the 24th international conference on world wide web*, pp. 1067–1077, Florence Italy, May 2015.
- [8] D. Wang, P. Cui, and W. Zhu, "Structural deep network embedding," in *Proceedings of the 22nd ACM SIGKDD international conference on Knowledge discovery and data mining*, pp. 1225–1234, San Francisco CA USA, August 2016.
- [9] K. Tu, P. Cui, X. Wang, P. S. Yu, and W. Zhu, "Deep recursive network emberegular equivalence," in *Proceedings of the 24th ACM SIGKDD International Conference on Knowledge Discovery & Data Mining*, pp. 2357–2366, London UK, August 2018.
- [10] Z. Wu, S. Pan, F. Chen, and G. C. P. S. Long, "A comprehensive survey on graph neural networks," *IEEE Transactions*

- on *Neural Networks and Learning Systems*, vol. 32, no. 1, pp. 4–24, 2021.
- [11] T. N. Kipf and M. Welling, “Semi-supervised classification with graph convolutional networks,” 2016, <https://arxiv.org/abs/1609.02907>.
  - [12] Y. Seo, M. Defferrard, P. Vandergheynst, and X. Bresson, “Structured sequence modeling with graph convolutional recurrent networks,” in *Proceedings of the International Conference on Neural Information Processing*, pp. 362–373, Springer, Siem Reap, Cambodia, December 2018.
  - [13] A. Narayan and P. H. ON Roe, “Learning graph dynamics using deep neural networks,” *IFAC-PapersOnLine*, vol. 51, no. 2, pp. 433–438, 2018.
  - [14] A. Pareja, G. Domeniconi, J. Chen, and T. T. H. T. T. C. Ma, “EvolveGCN: evolving graph convolutional networks for dynamic graphs,” in *Proceedings of the AAAI Conference on Artificial Intelligence*, vol. 34, no. 4, pp. 5363–5370, New York, NY, USA, February 2020.
  - [15] L. H. William, Y. Rex, and L. Jure, “Representation Learning on Graphs: Methods and Applications,” 2017, <https://arxiv.org/abs/1709.05584>.
  - [16] D. Zhu, P. Cui, Z. Zhang, and J. W. Pei, “High-order proximity preserved embedding for dynamic networks,” *IEEE Transactions on Knowledge and Data Engineering*, vol. 30, no. 11, p. 1, 2018.
  - [17] Z. Zhang, P. Cui, and J. Pei, “Timers: error-bounded svd restart on dynamic networks,” in *Proceedings of the AAAI Conference on Artificial Intelligence*, vol. 32, no. 1, New Orleans, LA, USA, 2018.
  - [18] R. Trivedi, M. Farajtabar, P. Biswal, and H. Zha, “Dyrep: learning representations over dynamic graphs,” in *Proceedings of the International Conference on Learning Representations*, p. 28, New Orleans, NO, USA, May 2019.
  - [19] L. Zhou, Y. Yang, and X. Ren, “Dynamic network embedding by modeling triadic closure process,” in *Proceedings of the AAAI Conference on Artificial Intelligence*, vol. 32, no. 1, New Orleans, LA, USA, 2018.
  - [20] F. Manessi, A. Rozza, and M. Manzo, “Dynamic Graph Convolutional Networks,” *Pattern Recognition*, 2019, <https://arxiv.org/abs/1704.06199>.
  - [21] L. Zheng, Z. Li, and J. Li, “AddGraph: anomaly detection in dynamic graph using attention-based temporal GCN,” in *Proceedings of the Twenty-Eighth International Joint Conference on Artificial Intelligence*, pp. 4419–4425, Macao, August 2019.
  - [22] P. Goyal, “Dyngem: Deep Embedding Method for Dynamic Graphs,” 2018, <https://arxiv.org/abs/1805.11273>.
  - [23] P. Goyal, S. R. Chhetri, and A. Canedo, “dyngraph2vec: Capturing Network Dynamics Using Dynamic Graph Representation Learning,” *Knowledge-Based Systems*, vol. 187, 2020.
  - [24] M. Sundermeyer, R. Schlüter, and H. Ney, “LSTM neural networks for language modelling,” in *Proceedings of the Thirteenth annual conference of the international speech communication association*, Portland, OR, USA, September 2012.
  - [25] M. Weber, G. Domeniconi, and J. Chen, “Anti-money laundering in bitcoin: experimenting with graph convolutional networks for financial forensics,” in *Proceedings of the KDD '19 Workshop on Anomaly Detection in Finance*, Anchorage, AK, USA, 2019.

## Research Article

# Adaptive Alleviation for Popularity Bias in Recommender Systems with Knowledge Graph

Feng Wei,<sup>1</sup> Shuyu Chen ,<sup>1</sup> Jie Jin,<sup>2</sup> Shuai Zhang,<sup>1</sup> Hongwei Zhou,<sup>1</sup> and Yingbo Wu<sup>1</sup>

<sup>1</sup>School of Big Data and Software Engineering, Chongqing University, Chongqing 400044, China

<sup>2</sup>Science and Technology Innovation Department, China Telecom, Chongqing Branch, Chongqing, China

Correspondence should be addressed to Shuyu Chen; [sychen@cqu.edu.cn](mailto:sychen@cqu.edu.cn)

Received 15 November 2021; Accepted 16 February 2022; Published 7 April 2022

Academic Editor: Chenquan Gan

Copyright © 2022 Feng Wei et al. This is an open access article distributed under the Creative Commons Attribution License, which permits unrestricted use, distribution, and reproduction in any medium, provided the original work is properly cited.

Recommender systems are known to suffer from the popularity bias problem: popular items are recommended frequently, and nonpopular ones rarely, if at all. Prior studies focused on tackling this issue by increasing the number of recommended nonpopular (long-tail) items. However, these methods ignore the users' personal popularity preferences and increase the exposure rate of the nonpopular items indiscriminately, which may hurt the user experience because different users have diverse interests in popularity. In this work, we propose a novel debias framework with knowledge graph (AWING), which adaptively alleviates popularity bias from the users' perspective. Concretely, we explore fine-grained preferences (including popularity preference) behind a user-item interaction by using the heterogeneous graph transformer over the knowledge graph embedded with popularity nodes and endow the preferences with explicit semantics. Based on this idea, we can manipulate how much popularity preference affects recommendation results and improves the exposure rate of nonpopular items while considering the popularity preferences of different users. Experiments on public datasets show that the proposed method AWING can effectively alleviate popularity bias and ensure the user experience at the same time. The case study further demonstrates the feasibility of AWING on the explainable recommendation task.

## 1. Introduction

In the age of the Internet, users can enjoy a variety of services on various electronic platforms. However, as the number of users continues to increase, the problem of information overload becomes more serious, which makes users cannot effectively search for the content they want. Recommendation system is an effective method to solve such problems [1]. Among these, collaborative filtering, as one of the most successful methods of recommendation system, can predict the rating of a certain user for an item and generate a recommendation list by using the preference of a certain user group [2]. So, accurately characterizing users' interests lives at the heart of an effective recommender system [3], which is challenging, however. There are even some studies aiming at hindering the system in its efforts to accurately profile users for their privacy [4]. One barrier to the effectiveness of capturing users' representation is the problem

of popularity bias: collaborative filtering recommenders typically emphasize popular items much more than nonpopular ones [5], which makes popular items to be rated higher than their ideal values so that they may be recommended to some users who are actually not interested in those items. Figure 1 illustrates the long-tail phenomenon in the well-known LastFM [6]. The vertical line separates the top 20% of items by popularity, and these items cumulatively have many more ratings than the 80% long-tail items to the right. Similar distributions can be found in other systems as well. After being trained on such long-tailed data, the models inherit this bias and, in many cases, expand it by over-recommending the popular items. As a result, they will be rated by more users and this goes on again and again; the rich gets richer and the poor gets poorer.

Although popular items often get good recommendation, recommending them to users is sometimes not meaningful because these items are likely well-known. In

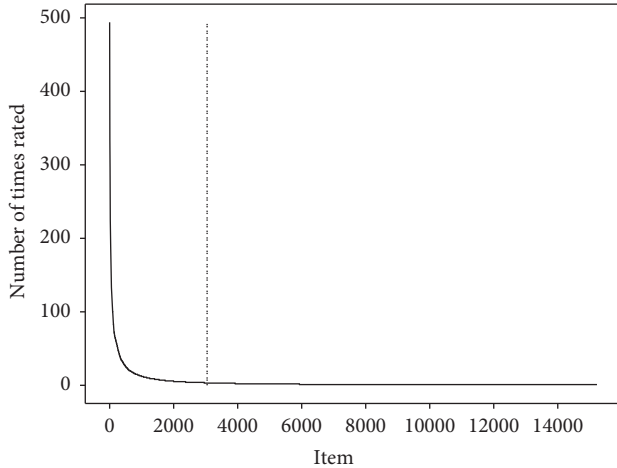


FIGURE 1: Item popularity in LastFM.

other words, recommending serendipitous items from the nonpopular items is ordinarily considered valuable to users [7], as these are items that users are less likely to know about. Therefore, recommender systems should explore a balance between popular and nonpopular items. Previous studies have mainly focused on increasing the number of recommended nonpopular (long-tail) items. Jones introduces a reweighting method to improve performance on small community detection [8]. Then, some studies [9, 10] introduce a regularization term to correct popularity bias. Besides, a few methods [11] utilize propensity score to decrease the ratio of popular items. However, these methods increase the exposure rate of the nonpopular items indiscriminately, largely ignoring the user’s interest in popularity, which may hurt the user experience [12].

In this paper, we propose an adaptive framework to alleviate popularity bias from the users’ perspective, named AWING (Adaptive Alleviation for Popularity Bias with Knowledge Graph). The key idea is that a user typically has multiple preferences (or reasons), driving him to consume different items. Based on this idea, we can capture users’ popularity preferences and remove a percentage of popularity preferences (lower a ratio of weight in popularity preferences) based on their profiles with a knowledge graph for these users who are not interested in popular items. The knowledge graph is a practical approach to represent large-scale information from multiple domains [13]. To describe a knowledge graph, we can use nodes in the graph as entities and edges as relations between entities, which follows the resource description framework (RDF) standard [14]. Of course, to capture users’ multiple preferences on items, the content feature information is important and helpful; some studies also utilize it to optimize the learning model [15]. However, disentangling these preferences is challenging and has not been well explored. Specifically, we face two key challenges: (1) although knowledge graph can provide rich information to learn these preferences, it lacks knowledge of popularity bias; (2) different users have diverse interests in popular items; how to adaptively eliminate popularity bias according to personal taste is another challenge. To cope

with these two challenges, we design AWING with two stages: identifying fine-grained preferences behind a user-item interaction and generating recommendation results that match the user’s interest in popular items. AWING mainly includes the following four components: (1) a component which constructs knowledge graph embedded with popularity nodes; (2) a component which models fine-grained user preferences; (3) a component which learns the representations of the users, items, and fine-grained preferences based on a heterogeneous graph transformer model; (4) a component which generates personalized recommendation list with removing popularity preference personally. Among these components, components (1–3) deal with challenge (1), while the component (4) deals with challenge (2).

The contributions of this work are summarized as follows:

- (i) To the best of our knowledge, we are the first to introduce knowledge graph embedded with popularity nodes in heterogeneous graph to alleviate popularity bias
- (ii) We propose a flexible framework AWING to alleviate popularity bias from the users’ perspective, which uses fine-grained preferences to profile user-item relationships over the knowledge graph and then remove a percentage of popularity preference for different users
- (iii) We conduct extensive experiments on two public datasets to demonstrate the effectiveness of the proposed model for alleviating popularity bias and the case study shows the feasibility of our model on the explainable recommendation task

## 2. The Proposed Model

In this section, we first introduce the notions and definitions used throughout this paper, and then we show how popularity nodes are embedded in knowledge graph and how to model fine-grained preferences of users. After that, we present how to develop the heterogeneous graph transformer [16] module of the proposed AWING on the synthetic graph. Finally, we use the trained AWING to estimate whether a user will adopt an item considering the fine-grained preferences.

### 2.1. Preliminary

Interaction data: given a list of user-item interactions  $Y = \{(u, i)\}$ , we use implicit feedback as the protocol so that each pair  $(u, i)$  implies the user  $u \in U$  consumes the item  $i \in I$ . An additional relation `interact_with` is introduced to explicitly present the user-item relationship and convert a  $(u, i)$  pair to the  $(u, \text{interact\_with}, i)$  triplet. As such, the user-item interactions can be seamlessly combined with KG.

Knowledge graph (KG): KG is a directed graph composed of subject – property – object triple facts. Each

triplet denotes a relationship  $r$  from head entity  $s$  to tail entity  $t$ , formally defined by  $(s, r, t)$ , where  $s$  and  $t$  are entities, and  $r$  is a relation. With the mappings between items and KG entities (also includes items), KG can profile items and offer complementary information to the interaction data.

**Heterogeneous graph (HG):** formally, a heterogeneous graph is defined as a directed graph  $G = (V, E, A, R)$  where each node  $v \in V$  and each edge  $e \in E$  are associated with their type mapping functions  $\tau(v): V \rightarrow A$  and  $\phi(e): E \rightarrow R$ .  $A$  and  $R$  donate the sets of node types and edge types, respectively.

**Task description:** given the interaction data  $Y$  and the KG  $G$ , our task is to learn a function that can predict how likely a user would select an item while further alleviating popularity bias.

*Definition 1.* Popularity: we define the number of times an item rated by all users as its popularity.

*Definition 2.* Popular item: an item is a popular item if its popularity is in the top 20% of all items.

*Definition 3.* Niche user (N) [12]: a user is a niche user if she/he is in the bottom 20% regarding the ratio of popular items in her/his profile. For these users, more than half of their profile consists of nonpopular (long-tail) items.

*Definition 4.* Blockbuster-focused user (B) [12]: a user is a blockbuster-focused user if she/he is in the top 20% regarding the ratio of popular items in her/his profile. These users, on average, have most popular items in their profile.

*Definition 5.* Diverse user (D) [12]: a user is a diverse user if she/he is neither a niche user nor a blockbuster-focused user.

**2.2. The Architecture of AWING.** We now present the proposed AWING. As illustrated in Figure 2, it consists of four key components: (1) KG embedded with popularity nodes, which inserts popularity nodes into KG to enrich the relations of KG; (2) fine-grained user preferences modeling, which uses multiple preferences to profile user-item relationships and aligns each preference with the relation in knowledge graph embed with popularity nodes; (3) heterogeneous graph transformer, which fully models heterogeneity to maintain dedicated representations for different types of nodes and edges in the heterogeneous graph; (4) model prediction, which uses the mutual attention to predict how likely the user would adopt the item under each preference.

**2.2.1. KG Embedded with Popularity Nodes.** We first divide the items into  $K$  groups according to their popularity. Next, we create  $K$  popularity nodes, termed  $pn_i, i \in \{1, \dots, K\}$ , representing these groups and connecting items to their corresponding nodes. In this way, a new relation,

$(i, \text{popularity}, pn)$ , is introduced to KG, which integrates popularity information into the knowledge graph. There also exists other relations and entities (come from the attributes of items) in KG. As shown in Figure 2, we denote the new graph as KGEPN (KG embedded with popularity nodes).

**2.2.2. Fine-Grained User Preferences Graph.** We aim to capture the intuition that multiple preferences influence the behaviors of users. Here, we frame the preference as the reason for users' choices of items, reflecting the commonality of all users' behaviors. Taking music recommendation as an example, possible preferences are diverse considerations on music attributes, such as artist, genre, or popularity mentioned above. Such intuition motivates us to model user-item relations at the granularity of preferences. Assuming  $P$  as the set of preferences shared by all users and  $n$  as the number of types in the set  $P$ , we can slice a uniform user-item relation into the  $n$  preferences and decompose each  $(u, \text{interact\_with}, i)$  triple into  $\{(u, p, i) \mid p \in P\}$ , as illustrated in Figure 2, termed preference graph (PG for short). Since the preferences are expressed as latent vectors that are vague to deeper understanding, we set the number of preferences as that of relations in KGEPN and transfer the information on the relation in KGEPN to the preferences. Concretely, we utilize the Euclidean norm to align the preferences embeddings  $p$  (between users and items) and relations embeddings  $r$  (between items and entities) in KGEPN:

$$L_{\text{align}} = \sum_{p \in P} \|p - r\|_2^2. \quad (1)$$

**2.2.3. Heterogeneous Graph Transformer.** After we get PG and KGEPN mentioned above, we combined them into a new heterogeneous graph (HG); we developed heterogeneous graph transformer (HGT for short) on the HG. HGT aims to aggregate information from the neighbors of target node  $t$ . Such a process can be decomposed into two parts: message computation and message aggregation. We denote the output of the  $(l)$ -th HGT layer as  $H(l)$  and the depth of HGT as  $L$ .

The message computation part incorporates the message matrix,  $W_{\phi(e)}^{\text{MSG}}$ , to alleviate the distribution differences of nodes and edges of different types. Based on a source node  $s$  and an edge  $e$ , HGT calculates the message passed by  $s$  on  $e$  by

$$\text{Message}(s, e, t) = M_{\tau(s)}(H^{(l-1)}[s]) \cdot W_{\phi(e)}^{\text{MSG}}, \quad (2)$$

where  $M_{\tau(s)}$  is a unique linear projection for node type  $\tau(s)$ .

In message aggregation part, HGT first calculates the heterogeneous mutual attention between source node  $s$  and target node  $t$  to control the influences of  $s$  on  $t$ . The attention mechanism was first proposed by the Google team to classify images [17]. Now, it is widely used in graph neural networks in recommender system [18]. HGT utilizes a unique linear projection ( $Q_{\tau(t)}$  or  $K_{\tau(s)}$ ) for each type of node and a distinct edge-based matrix  $W_{\phi(e)}^{\text{ATT}} \in \mathbb{R}^{d \times d}$  for each edge type

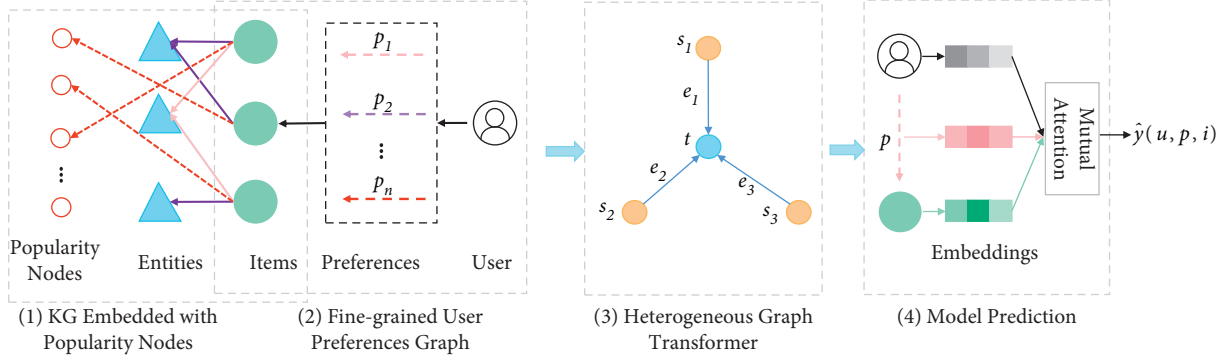


FIGURE 2: The overall architecture of AWING. Different colored arrows indicate different preferences and relations. It is best viewed in color.

$\phi(e)$  to model the distribution differences maximally;  $d$  is the size of dimension in the head of attention mechanism. The model can capture different semantic relations even between the same node type pairs, e.g., multiple preferences between

the same user-item pair as mentioned above. Specifically, we calculate the heterogeneous mutual attention for each edge  $(s, e, t)$  by

$$\text{Attention}(s, e, t) = \underset{\forall s \in N(t)}{\text{softmax}} \left( \frac{K_{\tau(s)}(H^{(l-1)}[s]) \cdot W_{\phi(e)}^{\text{ATT}} \cdot Q_{\tau(t)}(H^{(l-1)}[t])}{\sqrt{d}} \right), \quad (3)$$

where  $N(t)$  denotes the one-hop neighbors of node  $t$ .

Next, HGT uses the attention vector as the weight to average the corresponding messages from the source nodes and get the updated vector  $\tilde{H}^{(l)}[t]$  as

$$H^{(l)}[t] = \sum_{s \in N(t)} (\text{Attention}(s, e, t) \cdot \text{Message}(s, e, t)). \quad (4)$$

We opt for the pairwise BPR loss to train HGT. Specifically, we encourage the score between node  $s$  and node  $t$  to be higher than the score between node  $s$  and random node  $t'$ :

$$L_{\text{BPR}} = \sum_{(s,e,t) \in \text{HG}} \sum_{(s,e,t') \in \text{HG}'} -\ln \sigma(\hat{y}(s, e, t) - \hat{y}(s, e, t')), \quad (5)$$

$$\hat{y}(s, e, t) = \frac{K_{\tau(s)}(H^{(L)}[s]) \cdot W_{\phi(e)}^{\text{ATT}} \cdot Q_{\tau(t)}(H^{(L)}[t])}{\sqrt{d}}.$$

By combining the aligning loss and BPR loss, we minimize the following objective function to learn the model parameter:

$$L_{\text{HGT}} = L_{\text{BPR}} + \alpha L_{\text{align}} + \lambda \|\Theta\|_2^2, \quad (6)$$

where  $\Theta$  is the set of model parameters and  $\alpha$  and  $\lambda$  are two hyperparameters to control the aligning loss and  $L_2$  regularization term, respectively.

**2.2.4. Model Prediction.** Benefiting from the individual edge-based matrix for each edge type, we can quantify the user's preference at a finer granularity. Specifically, as is exhibited in Figure 2, given final representations of user  $u$  and item  $i$ , for each preference, we calculate the corresponding score between  $u$  and  $i$  by

$$\hat{y}(u, p, i) = \frac{K_{\tau(i)}(H^{(L)}[i]) \cdot W_{\phi(p)}^{\text{ATT}} \cdot Q_{\tau(u)}(H^{(L)}[u])}{\sqrt{d}}. \quad (7)$$

Then, we sum these different scores up as the probability of  $u$  adopting  $i$ :

$$\hat{y}_{ui} = \sum_{p \in P} \hat{y}(u, p, i). \quad (8)$$

In addition, we can combine multiple preferences as needed. To alleviate popularity bias, we remove a percentage of popularity preference for every user. Concretely, we design a weight  $w$  to manipulate how much popularity preference affects recommendation results:

$$\hat{y}_{ui/\text{adaptive}} = \sum_{p \in P} \hat{y}(u, p, i) - w \cdot \hat{y}(u, \text{popularity}, i), \quad (9)$$

where  $w = 1 - RP(u)$  and  $RP(u)$  is the ratio of popular items in the profile of user  $u$ . If a user is very interested in popular items, we will hardly remove her popularity preference, which can guarantee user experience.

### 3. Experiments

We provide empirical results to demonstrate the effectiveness of our proposed AWING. The experiments are designed to answer the following research questions (RQ):

- (i) RQ1: how does AWING perform, compared to the state-of-the-art recommender models? Mainly, can AWING effectively alleviate popularity bias?
- (ii) RQ2: how does the key hyperparameter  $K$  affect the recommendation performance?
- (iii) RQ3: can AWING provide insights on user preferences and give an intuitive impression of explainability?

#### 3.1. Experimental Settings

**3.1.1. Datasets.** To evaluate the effectiveness of AWING, we utilize two benchmark datasets: LastFM and DBbook-2014, which are publicly accessible and vary in terms of domain, size, and sparsity.

- (i) LastFM: the dataset is the collection of listening records. The songs, which interacted with the current user only once, are treated as negative feedback. Because these songs may be mislicked by the user and are not helpful for improving the recommendation performance, to ensure the quality of the dataset, we use the 5-core setting, i.e., retaining users and items with at least five interactions.
- (ii) DBbook-2014 [19]: the dataset consists of users and their binary feedback (1 for likes and 0 otherwise). Similarly, we use the 5-core setting to ensure that each user and item have at least five interactions.

Besides the user-item interactions, we need to construct item knowledge for each dataset. For LastFM and DBbook-2014, we follow the way in [20] to map items into freebase entities. We summarize the statistics of the two datasets in Table 1. We randomly select 80% of items associated with each user to constitute the training set and use all the remaining as the test set. The experiments are conducted with five-fold cross-validation for ten times, and the average results are reported.

**3.1.2. Evaluation Metrics.** Apart from a relevance-based metric (Recall@N) and a ranking-based metric (NDCG@N), we choose three metrics to measure the popularity bias.

- (i) DGAP [12]: the group average popularity (GAP ( $g$ )) metric measures the average popularity of items in the profiles of users in a particular group  $g$  or their

recommendation lists. Furthermore, the change in GAP ( $\Delta$  GAP) is the amount of unwanted popularity in the recommendations imposed by the algorithms to each group:

$$\Delta \text{GAP}(g) = \frac{\text{GAP}(g)_r - \text{GAP}(g)_p}{\text{GAP}(g)_p},$$

$$\text{GAP}(g)_p = \frac{\sum_{u \in g} \sum_{i \in P_u} \phi(i) / |P_u|}{|g|}, \quad (10)$$

$$\text{GAP}(g)_r = \frac{\sum_{u \in g} \sum_{i \in R_u} \phi(i) / |R_u|}{|g|},$$

where  $g$  is the group of users (in our case, it is either  $N$ ,  $D$ , or  $B$ ),  $\phi(\cdot)$  is the popularity of a specific item,  $P_u$  is the list of items in the profile of user  $u$ , and  $R_u$  is the list of items in the recommendation result of user  $u$ .

- (ii) APT@N [9]: the average percentage of tail items (APT) quantifies the ratio of nonpopular items in the recommendation lists:

$$\text{APT@N} = \frac{1}{|U|} \sum_{u \in U} \frac{|R_u \cap I^{up}|}{N}. \quad (11)$$

- (iii) AD@N [21]: aggregate diversity (AD) counts the total number of different items that have been recommended to at least one user:

$$A D@N = \frac{|\cup_{u \in U} R_u @N|}{|I|}. \quad (12)$$

**3.1.3. Comparison Method.** We compare our proposed AWING with the following baselines:

- (i) BPRMF [22] is a classical CF method that only uses the user-item ratings for the recommendation, assuming that users tend to assign higher ranks to observed items.
- (ii) BPRMF [23] is a GCN-based general recommendation model that leverages the user-item proximity to learn node representations and generate recommendations, which is reported as the state-of-the-art method.
- (iii) KTUP [24] employs TransH on user-item interactions and KG triplets simultaneously to learn user preference and perform KG completion.
- (iv) IPS-CN [25] adds normalization, which also achieved lower variance than plain IPS, at the expense of introducing a small amount of bias.
- (v) ESAM [10] regards popular and nonpopular items as the source and target domains, respectively, and introduces three regularization terms for transferring the knowledge from these well-trained popular items to the long-tail items.

TABLE 1: Statistics of the datasets.

		LastFM	DBbook-2014
User-item interactions	#Users	7,457	5,576
	#Items	15,226	2,680
	#Interactions	303,917	65,961
	#Sparsity	0.27%	0.44%
Knowledge 1 graph	#Entities	35,952	13,882
	#Relations	9	13
	#Triplets	464,567	334,511

**3.1.4. Implementation Details.** We implement our AWING model in PyTorch. We use AdamW [26] to train the model, where the initial learning rate is 0.001. In addition, we use 256 as the hidden dimension throughout the neural networks, and the batch size is fixed as 1024. As for other hyperparameters, we conduct a grid to confirm the optimal settings. More specifically, the coefficients of additional constraints (i.e., aligning loss and L2 regularization)  $\alpha$  and  $\lambda$  are searched in  $\{10^{-5}, 10^{-4}, \dots, 10^{-1}\}$  and the number  $L$  of HGT layers is tuned in  $\{1, 2, 3\}$ . Finally, we set  $\alpha = 10^{-2}$ ,  $\lambda = 10^{-3}$ , and  $L = 2$  in our experiments.

**3.2. Overall Performance Comparison (RQ1).** Table 2 shows the best recommendation performance of all models on two datasets. In particular, AWING-APS is the variant of AWING which removes a percentage of popularity preference when recommended. In addition, the bold numbers indicate the best in each row and the *underlined* values indicate the second best. We can draw the following conclusions from the table.

Firstly, the BPRMF model, the most basic model, has the worst performance on two datasets and has serious popularity bias. Although LightGCN performs better than BPRMF, its APT value is also meager, showing that the popularity bias is ubiquitous in recommender systems.

Next, the performance of the KG-aware baseline, KTUP, is better than LightGCN and BPRMF on all metrics, which demonstrates that the introduction of KG is beneficial not only for the recommendation but also for alleviating popularity bias. Nevertheless, the improvement of APT and GAP is not enough.

Besides, compared with the three models above, IPS-CN and ESAM improve a lot on APT, but they do not keep the ratio of popular and nonpopular items according to their profiles, which may hurt the user experience.

Finally, our proposed method AWING which outperforms all the compared baselines on both datasets in terms of recall and NDCG, which indicates that identifying fine-grained preferences is helpful for the recommendation. Moreover, our proposed method AWING-APS performs best among all models in the light of  $\Delta$  GAP, AD, and APT, which verifies the significance of removing popularity preference to alleviate popularity bias. Especially, AWING-APS has a shallow value of  $\Delta$  GAP. In other words, AWING-APS keeps a similar ratio of popular and nonpopular items, which guarantees the user experience well. It should be noted that although AWING-APS sacrifices a small amount

of recall and NDCG, this is negligible compared to IPS-CN and ESAM.

We can also find that, in the two datasets, the former dataset is sparser. The proposed model performs worse than the latter in the metrics of ranking task (Recall@N and NDCG@N) for the recommendation. However, for most metrics to measure the popularity bias, e.g., AD and APT, the improvement on the LastFM is greater than the DBbook-2014.

**3.3. Parameter Sensitivity Analysis (RQ2).** In this section, we investigate the impact of the number of popularity nodes  $K$  for popularity bias. In this experiment, we tune  $K$  in the range of  $[2, 13]$  with a step of 1 to report the corresponding performance. From Figure 3, we observe that AWING-APS achieves the best performance when  $K = 6$  and 7 on two datasets, respectively. This is because a too small  $K$  does not have enough capacity to distinguish the different degrees of popularity, while a too-large  $K$  causes sparse data in each group and adversely suffers from overfitting.

**3.4. Case Study (RQ3).** An important benefit of attention recommender system is the explainability of the results [27]. In the same way, benefiting from the HGT, we can infer the fine-grained user preferences on the target item. Towards this end, we present an example of LastFM to give an intuitive impression of our explainability. We randomly selected one user, u306, and two relevant music m749 and m1364 (from the test, unseen in the training phase). Figure 4 shows the visualization of the example. AWING searches for the most influential preference based on the attention scores (cf. (7)). Thus, it explains this behavior as user u306 selects music m749 since it matches her interest in the featured artist. Similarly, we can infer that u306 chooses m1364 just because of its popularity.

## 4. Related Work

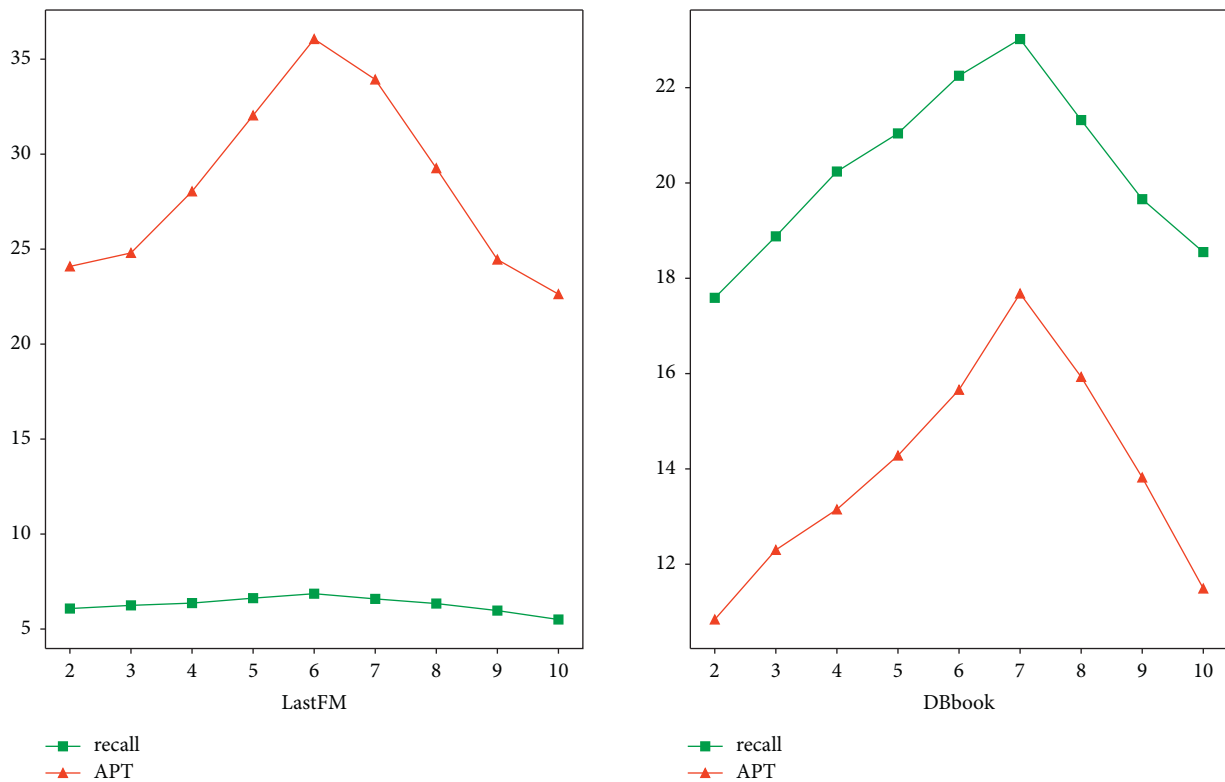
In recent years, with the development of recommender systems, more and more attention has been paid to the fairness of recommender systems. Popularity bias is one of the critical factors affecting its fairness. The problem of popularity bias and the challenges it creates for the recommender systems has been well studied by other researchers [5, 28]. Authors in the mentioned works have mainly explored the overall accuracy of the recommendations in the presence of long-tail distribution in rating data.



TABLE 2: Performance comparison of different recommendation models.

Dataset	Metric	BPRMF	LightGCN	KTUP	IPS-CN	ESAM	AWING	AWING-APS
LastFM (@10,%)	Recall	5.17	5.82	6.75	6.49	5.64	<b>7.31</b>	6.86
	NDCG	5.39	5.48	6.04	5.32	5.59	<b>6.94</b>	5.89
	$\Delta$ GAP (N)	92.67	80.49	60.83	38.13	25.84	59.08	<b>5.21</b>
	$\Delta$ GAP (D)	95.71	87.25	57.39	53.04	31.82	64.26	<b>7.56</b>
	$\Delta$ GAP (B)	87.52	82.98	68.52	-60.49	-55.25	63.94	<b>-4.81</b>
	AD	5.62	12.07	17.61	16.47	18.15	16.24	<b>24.28</b>
	APT	1.56	3.76	14.79	23.59	25.33	14.66	<b>36.06</b>
DBbook (@10,%)	Recall	17.23	20.45	23.15	19.45	18.92	<b>24.62</b>	23.02
	NDCG	18.86	22.67	25.92	22.62	21.53	<b>27.62</b>	25.27
	$\Delta$ GAP (N)	88.77	94.14	53.32	25.96	27.71	55.62	<b>2.18</b>
	$\Delta$ GAP (D)	85.48	83.46	61.28	35.09	32.89	62.52	<b>8.03</b>
	$\Delta$ GAP (B)	75.49	79.71	43.76	-34.28	-43.27	42.24	<b>-5.33</b>
	AD	9.58	11.26	14.36	17.33	17.61	15.38	<b>19.78</b>
	APT	2.91	5.51	7.95	12.06	13.17	12.27	<b>17.68</b>

The bold numbers indicate the best in each row and the underlined values indicate the second best.

FIGURE 3: Performance impact of  $K$ .

Moreover, some other researchers have proposed algorithms that can control this bias and give more chances for non-popular items to be recommended [9, 29, 30]. Gruson et al. [25] and Joachims et al. [11] use IPS (Inverse Propensity Score) to eliminate popularity bias by reweighting each instance according to item popularity. Besides, Abdollahpouri et al. [9] provide a regularization term to control popularity bias. Recently, Chen et al. [10] address this problem from domain adaptation, regarding popular and nonpopular items as the source and target domains. In this work, however, we focus on alleviating popularity bias from

the perspective of users. That is, we want to take into account the personal interest in popular and nonpopular items.

The recommendation system based on knowledge graph has attracted extensive attention of researchers now. This method can not only improve the accuracy of the recommendation system but also provide explanations for the recommendation results. Zhang et al. [31] proposed CKE with three-information sources: structural information, textual information, and visual information, which shows the structure information of the knowledge graph can enhance the semantic information of the item embedding.

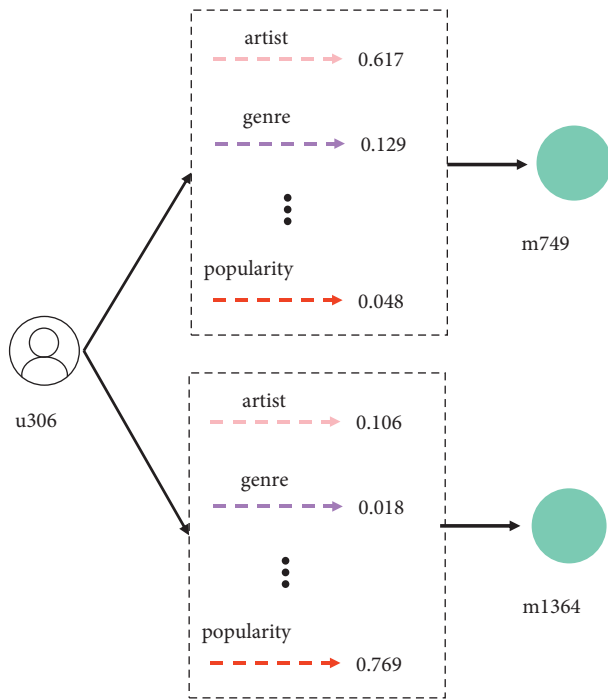


FIGURE 4: Real example from LastFM.

Wang et al. [32] used KGAT to obtain the item representations and propagate them on the user-item interaction graph with the graph attention mechanism. Huang et al. [33] constructed multiple metapaths from users to entities on the interaction and knowledge graph to obtain user representation. Tu et al. [34] proposed KCAN, which uses the knowledge graph to help automatically distill the knowledge graph into the target-specific subgraph and get the refined node representations. They all did not consider introducing knowledge graph embedded with popularity nodes.

## 5. Conclusion

This paper aims to utilize KG embedded with popularity nodes to alleviate popularity bias by identifying the fine-grained preferences of users. Our method first constructs a heterogeneous graph that combines KG, preference graph, and popularity nodes. Secondly, we use heterogeneous graph transformer over the heterogeneous graph while aligning fine-grained preferences with the relations in KG to learn the user/item/preference embeddings and the parameters of the mutual attention. Finally, according to the user's interest in popular items, we adaptively remove popularity preference to eliminate popularity bias. In the future, a valuable direction is to consider the dynamic change of popularity, instead of keeping the popularity constant.

## Data Availability

The datasets generated during and/or analyzed during the current study are available from the corresponding author on reasonable request.

## Conflicts of Interest

The authors declare that there are no conflicts of interest regarding the publication of the manuscript.

## Acknowledgments

This work was supported in part by the National Key Research and Development Project under grant 2019YFB1706101, National Natural Science Foundation under grant 72161005, and research program of Chongqing Technology Innovation and Application Development under grant CSTC2019jcx-zdztzxX0031.

## References

- [1] G. Adomavicius and A. Tuzhilin, "Toward the next generation of recommender systems: a survey of the state-of-the-art and possible extensions," *IEEE Transactions on Knowledge and Data Engineering*, IEEE, vol. 17, no. 6, pp. 734–749, 2005.
- [2] X. Su and M. k. Taghi, "A survey of collaborative filtering techniques," *Advances in Artificial Intelligence*, vol. 2009, Article ID 421425, 19 pages, 2009.
- [3] M. Jamali and M. Ester, "A matrix factorization technique with trust propagation for recommendation in social networks," in *Proceedings of the Fourth ACM Conference on Recommender Systems*, pp. 135–142, ACM, Barcelona, Spain, September 2010.
- [4] W. Wang, S. Wang, and J. Huang, "Privacy Preservation for Friend-Recommendation Applications," *Security and Communication Networks*, vol. 2018, Article ID 1265352, 11 pages, 2018.
- [5] Y. J. Park and A. Tuzhilin, "The long tail of recommender systems and how to leverage it," in *Proceedings of the ACM Conference on Recommender Systems, Recsys*, October 2008.
- [6] HetRec2011, <https://grouplens.org/datasets/hetrec-2011>, 2011.
- [7] G. Shani and A. Gunawardana, *Evaluating Recommendation Systems. Recommender Systems Handbook* Springer, Boston, MA, USA, 2011.
- [8] I. Jones, R. Wang, J. Han, and H. Liu, "Community Cores: Removing Size Bias from Community Detection," in *Proceedings of the Tenth International AAAI Conference on Web and Social Media*, AAAI press, Cologne, Germany, May 2016.
- [9] H. Abdollahpouri, R. Burke, and B. Mobasher, "Controlling popularity bias in learning-to-rank recommendation," in *Proceedings of the Eleventh ACM Conference on Recommender Systems*, pp. 42–46, ACM, Como Italy, August 2017.
- [10] Z. Chen, R. Xiao, C. Li, G. Ye, G. Sun, and H. E. Deng, "Discriminative domain adaptation with non-displayed items to improve long-tail performance," in *Proceedings of the 43rd International ACM SIGIR Conference on Research and Development in Information Retrieval*, pp. 579–588, SIGIR, NY, United States, July 2020.
- [11] T. Joachims, A. Swaminathan, and T. Schnabel, "Unbiased learning-to-rank with biased feedback," in *Proceedings of the Tenth ACM International Conference on Web Search and Data Mining*, pp. 781–789, WSDM, NY, United States, February 2017.
- [12] H. Abdollahpouri, M. Mansoury, and R. Burke, "The Unfairness of Popularity Bias in Recommendation," 2019, <https://arxiv.org/abs/1907.13286>.

- [13] L. Ehrlinger and W. Wolfram, "Towards a definition of knowledge graphs," *SEMANTiCS (Posters, Demos, SuCCESS)*, vol. 48, pp. 1–4, 2016.
- [14] J. M. Gomez-Perez, J. Z. Pan, G. Vetere, and H. Wu, "Enterprise knowledge graph: an introduction, Exploiting linked data and knowledge graphs in large organisations," *Exploiting Linked Data and Knowledge Graphs in Large Organisations*, Springer, New York, NY, USA, pp. 1–14, 2017.
- [15] O. Tal and Y. Liu, "A Joint Deep Recommendation Framework for Location-Based Social Networks," *Complexity*, vol. 2019, Article ID 2926749, 2 pages, 2019.
- [16] Z. Hu, Y. Dong, K. Wang, and Y. Sun, "Heterogeneous graph transformer," in *Proceedings of the Web Conference 2020*, pp. 2704–2710, WWW, Taipei, Taiwan, April 2020.
- [17] V. Mnih, N. Heess, and A. Graves, "Recurrent models of visual attention," in *Proceedings of the Advances in Neural Information Processing Systems*, NIPS, San Francisco, CA, USA, December 2014.
- [18] P. Veličković, G. Cucurull, and A. Casanova, "Graph Attention Networks," 2017, <https://arxiv.org/abs/1710.10903>.
- [19] 2014 <http://challenges.2014.eswc-conferences.org>.
- [20] X. Zhao, G. He, H. Dou, J. Huang, S. Ouyang, and J. Wen, "KB4Rec: A Dataset for Linking Knowledge Bases with Recommender Systems," 2018, <https://arxiv.org/pdf/1807.11141.pdf>.
- [21] G. Adomavicius and Y. YoungOk Kwon, "Improving aggregate recommendation diversity using ranking-based techniques," *IEEE Transactions on Knowledge and Data Engineering*, vol. 24, no. 5, pp. 896–911, 2012.
- [22] S. Rendle, C. Freudenthaler, Z. Gantner, and L. Schmidt-Thieme, "Bpr: bayesian personalized ranking from implicit feedback," in *Proceedings of the 25th Conference on Uncertainty in Artificial Intelligence*, pp. 452–461, AUAI Press, Quebec, Canada, June 2009.
- [23] X. He, K. Deng, X. Wang, Y. Li, Y. Zhang, and M. Wang, "LightGCN: Simplifying and Powering Graph Convolution Network for recommendation," 2020, <https://arxiv.org/abs/2002.02126>.
- [24] Y. Cao, X. Wang, X. He, and Z. Hu, "Tat-Seng Chua. Unifying knowledge graph learning and recommendation: towards a better understanding of user preferences," in *Proceedings of the Web Conference*, pp. 151–161, WWW, San Francisco, CA, USA, May 2019.
- [25] A. Gruson, P. Chandar, C. Charbuillet et al., "Offline evaluation to make decisions about playlist recommendation algorithms," in *Proceedings of the 12th ACM International Conference on Web Search and Data Mining*, pp. 420–428, WSDM, Melbourne, Australia, February, 2019.
- [26] I. Loshchilov and F. Hutter, "Decoupled weight decay regularization," in *proceedings of the 7th International Conference on Learning Representations*, ICLR, New Orleans, LA, USA, May 2019.
- [27] J. Bastings and F. Katja, "The elephant in the interpretability room: why use attention as explanation when we have saliency methods?," 2020, <https://arxiv.org/abs/2010.05607>.
- [28] E. Brynjolfsson, Y. J. Hu, and M. D. Smith, "From Niches to Riches: Anatomy of the Long Tail," *Social Science Electronic Publishing*, vol. 47, 2006.
- [29] H. Abdollahpouri, R. Burke, and B. Mobasher, "Managing popularity bias in recommender systems with personalized re-ranking," in *Proceedings of the Florida AI Research Symposium*, pp. 413–418, FLAIRS, Beach Resort in Sarasota, FL, US, May, 2019.
- [30] T. Kamishima, S. Akaho, H. Asoh, and J. Sakuma, "Correcting popularity bias by enhancing recommendation neutrality," in *Proceedings of the 8th ACM Conference on Recommender Systems*, RecSys, Silicon Valley, CA, USA, October 2014.
- [31] F. Zhang, N. J. Yuan, and D. Lian, "Collaborative knowledge base embedding for recommender systems," in *Proceedings of the 22nd ACM SIGKDD International Conference on Knowledge Discovery and Data Mining*, pp. 353–362, SIGKDD, San Francisco, CA, USA, 1 August 2016.
- [32] X. Wang, X. He, and Y. Cao, "Kgat: knowledge graph attention network for recommendation," in *Proceedings of the 25th ACM SIGKDD International Conference on Knowledge Discovery Data Mining*, pp. 950–958, SIGKDD, Anchorage, AK, USA, July 2019.
- [33] R. Huang, C. Han, and L. Cui, "Entity-aware collaborative relation network with knowledge graph for recommendation," in *Proceedings of the 30th ACM International Conference on Information Knowledge Management*, pp. 3098–3102, ACM, Queensland, Australia, October 2021.
- [34] K. Tu, P. Cui, D. Wang et al., "Conditional graph attention networks for distilling and refining knowledge graphs in recommendation," in *Proceedings of the 30th ACM International Conference on Information Knowledge Management*, pp. 1834–1843, ACM, Queensland, Australia, October 2021.

## Research Article

# LGBM-CBFS: A Heuristic Feature Sampling Method Based on Tree Ensembles

Yu Zhou , Hui Li , and Mei Chen 

*College of Computer Science and Technology, Guizhou University, Guiyang, China*

Correspondence should be addressed to Hui Li; [cse.huili@gzu.edu.cn](mailto:cse.huili@gzu.edu.cn)

Received 26 November 2021; Accepted 14 February 2022; Published 16 March 2022

Academic Editor: Chenquan Gan

Copyright © 2022 Yu Zhou et al. This is an open access article distributed under the Creative Commons Attribution License, which permits unrestricted use, distribution, and reproduction in any medium, provided the original work is properly cited.

Gradient boosting decision tree (GBDT) is widely used because of its state-of-art performance in academia, industry, and data science competitions. The efficiency of the model is limited by the overwhelming training cost with the surge of data. A common solution is data reduction by sampling on training data. Current popular implementations of GBDT such as XGBoost and LightGBM both supports cut the search space by using only a random subset of features without any prior knowledge, which is ineffective and may lead the model fail to converge when sampling on a high-dimensional feature space with a small sampling rate assigned. To mitigate this problem, we proposed a heuristic sampling algorithm LGBM-CBFS, which samples features based on an available prior knowledge named “importance scores” to improve the performance and the effectiveness of GBDT. Experimental results indicate that LGBM-CBFS obtains a higher level of model accuracy than uniform sampling without introducing unacceptable time cost in the sparse high-dimensional scenarios.

## 1. Introduction

Gradient boosting decision tree [1] achieves state-of-the-art performance in machine learning and data mining applications ranging from classification, regression to ranking. The rapid growth of data volume leads to expensive training cost. The major computation cost of training the GBDT model comes from building a decision tree in each gradient boosting round, in which finding the optimal split point results in the most time-consuming operation because it requires scanning entire training data for each feature. Recently, two open-source projects XGBoost [2] and LightGBM [3] have been widely used for their superiority in machine learning and data analytic applications, which exploit histogram-based data partitioning to accelerate decision tree building. However, both of them still suffer from performance degradation in large-scale learning tasks at a limited time and economic cost.

To alleviate this problem, sampling techniques are commonly used to reduce the data size by obtaining a random subset from the input dataset with both row-oriented and column-oriented perspectives. Current sampling research includes static

sampling and adaptive sampling techniques. The former one draws samples based on a preset sample size determined prior to the start of sampling, which encounters the difficulty of determining an appropriate sample size. Chernoff-Hoeffding bounds [4, 5] have been widely used to test whether the number of samples seen so far is sufficient to assure estimation accuracy and confidence. Nevertheless, a static sampling scheme tends to overestimate the sample size due to the worst situation considered at the beginning of sampling, which is rare in practical applications [6]. Adaptive sampling [7–9] is proposed to address this situation by picking samples in an online fashion, and its stopping condition depends on the number of observations, namely, random samples seen so far. There are some studies [10, 11] that seek a tighter bound on sufficient sample size without jeopardizing accuracy and confidence. Compared to static sampling, adaptive sampling can approximate input datasets well with a lower sample size which achieves better scalability of learning algorithms. Nevertheless, sampling randomly on a high-dimensional dataset with a quite small sample size often makes the model hard to converge in an adaptive sampling scheme since most features involved in the training set are sparse.

Currently, the representative open-source implementations of GBDT such as XGBoost and LightGBM used uniform sampling to choose a subset of features. It is a simple and effective way to reduce the dimensions of feature space with a low time consumption. Nevertheless, there are no prior insights taken into account in the sampling process in this sampling scheme. Uniform sampling with a small sample size tends to be underperforming in sparse scenarios since there is little information that can be learned. Scores-based nonuniform sampling [12, 13] will obtain further performance improvement by picking a representative subset of features according to a metric that indicates the importance of the features. However, it will bring additional time costs due to the calculation of scores introduced.

To address the aforementioned issues, in this paper, we devised a sampling method named LGBM-GBFS to choose features based on an available prior ‘‘importance score,’’ which reveals the contribution of every single feature to information gain in GBDT, meanwhile, and heavily reduced the computational cost bringing by building scores. Then, the features with high scores will be kept in the training set. The features with low scores will be discarded at random with a certain probability to cut the feature space. We integrate our LGBM-GBFS algorithm into LightGBM and conduct a series of experiments to verify the correctness and effectiveness of the approach. The experimental results show that our algorithm significantly improved the effectiveness when sampling features on high-dimensional sparse data, and it works better than uniform sampling without additional heavy computational cost.

## 2. Related Work

In this section, we present a brief review of gradient boosting and elaborate the related work of feature sampling for ensemble learning.

*2.1. Review of GBDT.* Gradient boosting tree is an ensemble learning method that takes decision tree as its base learner. It is proposed first by Friedman in [1] and is increasingly adopted as a crucial solution in data analytics with the advent of more efficient implementations. XGBoost and LightGBM are two well-known GBDT implementations that achieve outstanding performance in learning applications like ranking as well as classification. Both of them exploit histogram-based algorithms to find the optimal split point and employ many engineering or theoretical optimizations to improve the efficiency and scalability. For instance, XGBoost uses the second-order Taylor expansion as an approximation for the objective function in the general setting and introduces a well-designed regularization term to make the objective easy to parallelize.

In XGBoost, for a given dataset with  $n$  instances and  $m$  features  $D = \{(x_i, y_i)\}_1^n (x_i \in \mathbb{R}^m, y_i \in \mathbb{R})$ , the general regularized objective is given by

$$Obj = \sum_{i=1}^n l(y_i, \hat{y}_i) + \sum_k \Omega(f_k), f_k \in F \quad (1)$$

where  $\Omega(f) = \gamma T + (1/2)\lambda \sum_{j=1}^T \omega_j^2$  is the regularization term, in which  $T$  and  $\omega$  are the number of leaves and leaf weights of one single decision tree.  $l$  is the conventional loss function for tree boosting.  $F$  is the functional space of regression trees.  $k$  is the number of decision trees we build. The tree boosting method in XGBoost rewrites the loss function by applying forward stagewise additive modeling. Then take Taylor expansion of the objective which is given by  $Obj^{(t)} = \sum_{j=1}^T [G_j \omega_j + (1/2)(H_j + \lambda)\omega_j^2] + \gamma T$ , where  $G_j = \sum_{i \in I_j} g_i$ ,  $H_j = \sum_{i \in I_j} h_i$ . Here,  $I_j$  is the instance set in leaf  $j$ .  $g_i$  and  $h_i$  are first- and second-order gradient statistics on  $l$ . With this, the optimal  $j$ -th leaf weight and objective function value can be calculated by

$$\omega_j^* = -\frac{G_j}{H_j + \lambda}, Obj^* = -\frac{1}{2} \sum_{j=1}^T \frac{G_j^2}{H_j + \lambda} + \gamma T. \quad (2)$$

The loss reduction of objective for each split is given by the following equation:

$$Gain = \frac{1}{2} \left[ \frac{G_L^2}{H_L + \lambda} + \frac{G_R^2}{H_R + \lambda} - \frac{(G_L + G_R)^2}{H_L + H_R + \lambda} \right] - \gamma, \quad (3)$$

where  $G_L$  and  $G_R$  are the sum of the first-order gradient statistics of the instances on the left and right nodes after splitting.  $H_L$  and  $H_R$  are the sum of the second-order gradient statistics after splitting. The regularization coefficient  $\gamma$  indicates the complexity cost of additional leaf nodes added.

The feature importance score is obtained by (3) when taking the best split solution, which is used as a measure of the importance of a feature.

In order to conduct further optimization based on the work of XGBoost, LightGBM proposed GOSS (gradient-based one-side sampling) to choose a subset of the instances by keeping those instances with gradients greater than a preset threshold and sampling on the rest of the instances randomly. GOSS works better than uniform sampling from an accuracy perspective since more under-trained instances with a potentially greater contribution are involved in training data. Moreover, LightGBM proposed EFB (exclusive feature bundling) to convert data with quite sparse feature space into a dense form by bundling those features rarely taking nonzero values simultaneously together. Both GOSS and EFB give over 20x speedup of the conventional training process and achieve nearly the same accuracy.

To take advantage of the efficiency of LightGBM, we extend it to support the proposal sampling algorithm in this paper and conduct experiments based on the modification version. More details of the modifications are introduced in section 3.2.

*2.2. Sampling Schemes in Ensemble Learning.* Sampling is an effective technique widely used to improve the generalization and scalability in large-scale machine learning. Many researches related to sampling in ensemble learning are proposed in recent years. SGB (stochastic gradient boosting) [14] trains the base learner on a subset sampled uniformly from input data in a static way, which requires the sample

ratio is known in advance. This approach is also supported by XGBoost and LightGBM. Watanabe proposed an adaptive sampling scheme MadaBoost [6] to dynamically adjust sample size in the training progress by using theoretical bounds like Chernoff-Hoeffding bound [4, 15]. MadaBoost achieves a higher accuracy with data of the same size as the static sampling method. Inspired by the works in MadaBoost, a new adaptive sampling scheme [10] proposed by Jianhua Chen et al. recently achieves a tighter bound of sample size by using Massart’s inequality. Empirically, feature sampling outperforms row sampling in preventing overfitting. It is as well as used to reduce the search space in tree ensembles to improve training speed when finding the best split. Off-the-shelf feature sampling schemes fall into four general categories: uniform sampling, reweight-based sampling, score-based sampling, and bandit-based sampling. Uniform sampling is the simplest one that chooses columns with equal probability with taking no prior into account. It is the default and unique column sampling strategy in XGBoost, LightGBM, RandomForest [16], [17, 18]. Reweight-based sampling first trains base learners on a random subset of the data instances in the first iteration and then chooses columns in terms of the suitable weight like classification error [17] in the previous iteration. The score-based strategy [19–22] introduces an importance sampling distribution to sample the features. Bandit-based sampling chooses columns by making a tradeoff between those with large past rewards and those never selected in every boosting round.

Uniform sampling has been widely used due to its simplicity and low computational cost. But it accepts important features with quite a low probability in high-dimension feature space. Moreover, it comes with a penalty in prediction accuracy due to taking no prior information into account. The latter three sampling schemes all construct an “importance score” for each feature of the input dataset to measure the impact of the corresponding feature on the model output. Then perform biased random sampling based on the scores in previous step. Schemes (2), (3), and (4) can improve the test accuracy effectively but require more computation cost due to the extra step of score construction.

In this paper, instead of constructing a new importance score, we select features by using the gain information of GBDT formulated by (3) to avoid additional calculation. We propose a column subsampling algorithm LGBM-CBFS, which chooses columns by filtering out those over-trained to obtain better efficiency. And we implement it into LightGBM with a minor modification. The extensive experimental results show our sampling algorithm obtained better accuracy than uniform sampling with acceptable overheads.

### 3. Contribution-Based Feature Sampling Algorithm

In this section, we train GBDT models on various datasets with different distributions and sparsity to study their differences with importance scores. And then, we implement

our contribution-based feature sampling algorithm named LGBM-CBFS based on our analysis.

*3.1. Importance Scores in High-Dimensional Data.* Importance scores of each feature in GBDT indicate how much a feature contributes to the model output. In order to observe the difference in scores among the features of the training set, we build GBDT models on four publicly available data sets (real-sim, news20, kdda, and higgs) and details are described in Table 1, and we use a pie chart to depict the final contribution of each feature in an intuitive way. Features are automatically named in terms of their index in the input array of the charts. The GBDT model calculates importance scores by first adding up the value a feature split point improving the performance measure for a decision tree, then averaging across all the trees in the model. The more a feature is important, the higher it scores. Figure 1 shows the ratio of different feature scores to the total, which is sorted in descending order before plotting. We can see a few features contribute a lot at the overall level in real-sim, news20, and kdda, and there are relatively small differences in higgs.

We classify features into two categories that refer to as key features and valid features according to the effect on model output. Valid features represent features whose importance score is greater than 0. Key features represent features ranking in 80% of scores. The number of features, valid features, and key features is shown in Table 2. In the case of News20, the dataset consists of 50K features, of which 1090 features have scores greater than 0. And 79 of the 1090 features provide 80% of the total importance scores. Moreover, the number of valid features accounted for 2.18%, 3.8%, and 0.0058% of the total number of features in news20, real-sim, and kdda, respectively. The number of key features accounted for about 16.4%, 7.65%, and 17% of the number of valid features in news20, real-sim, and kdda, respectively. It can be seen that valid features have a lower proportion in high-dimensional sparse data, which means a low sampling probability of key features.

We plot the cumulative contributions of key features for every dataset in Figure 2 to show the change of importance scores at each boosting round. From Figure 2, we can observe that the ranking of certain features varies little during the training process. It means the importance of features from the current iteration to the next iteration is relatively stable. Besides, we can conclude that the features with high scores in the current iteration may have more impact on model output in the next iteration.

Here, we assume that features are independent of each other. When training the GBDT models on a high-dimensional sparse data set, the characteristics of importance scores could be summarized as follows:

- (1) There is a considerable difference among the features in sparse data. Only a few features (valid features) play an important role in contributing to the information gain, in which the proportion of key features, that contribute most of the overall level, is quite small.

TABLE 1: Experimental datasets.

Dataset	#Data	#Features	Description
Gamma Norm Poisson Uniform	100K	500	Dense
Higgs News20 Real-sim Kdda	10.5 M 6K 72309 8407752	28 5K 20958 20216830	Sparse

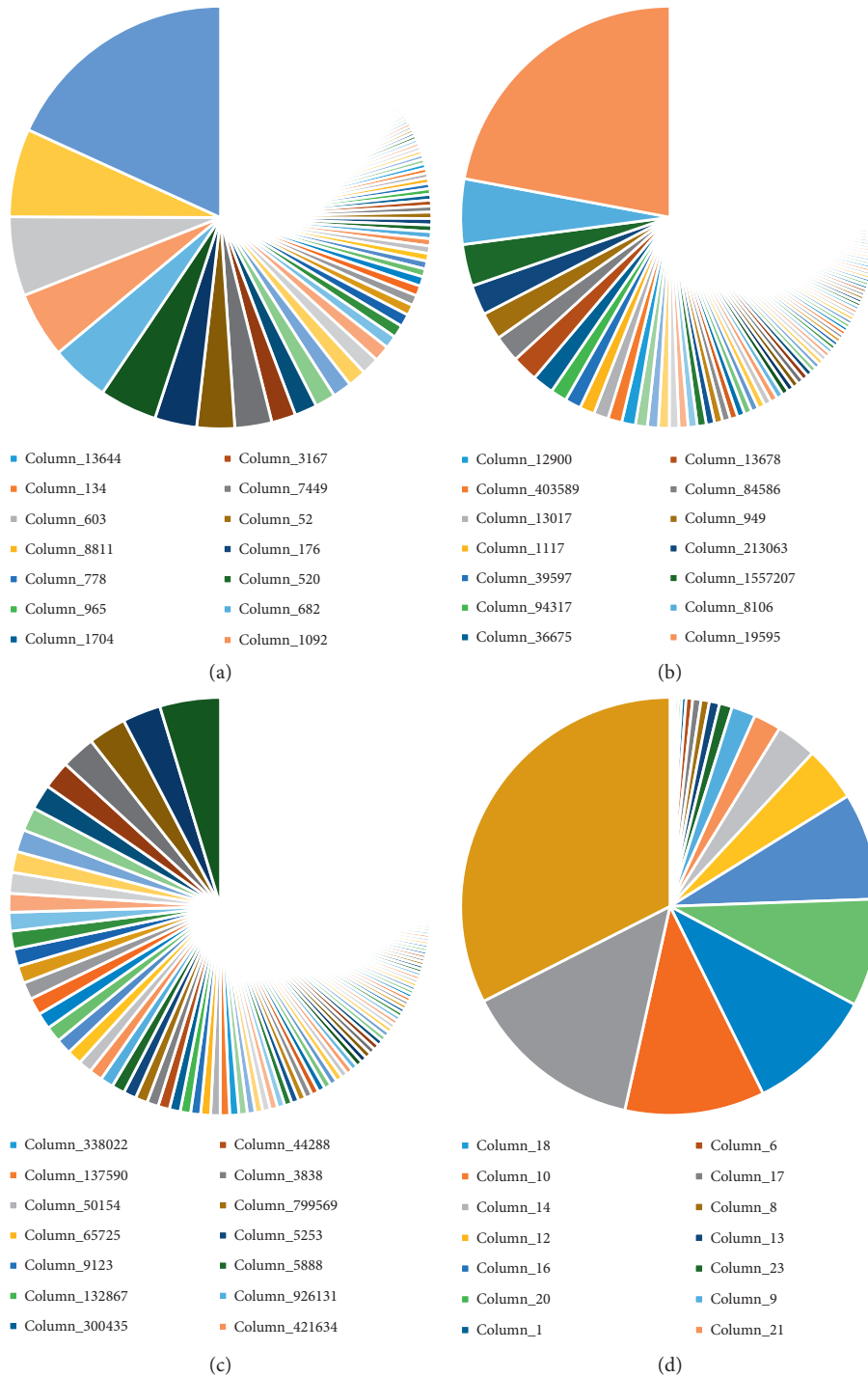


FIGURE 1: The proportion of importance scores (gain). (a) Real-sim. (b) News20. (c) kdda. (d) higgs.

TABLE 2: The number of different types of features.

Dataset	#Features	#valid_features	#key_features
Higgs	28	22	6
News20	50K	1090	179
Real-sim	20958	797	61
Kdda	20216830	1170	199

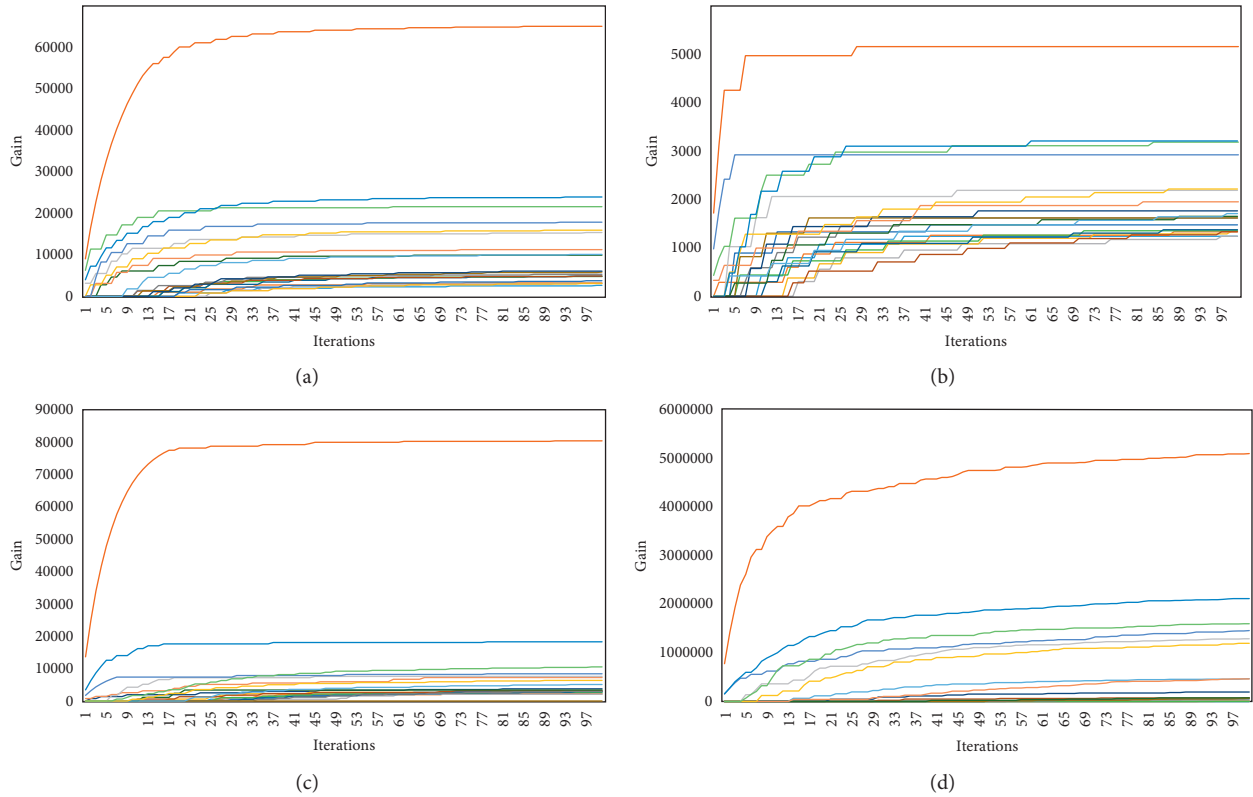


FIGURE 2: Accumulated values of importance score in the training process. (a) Real-sim. (b) News20. (c) higgs. (d) kdda.

- (2) There are little differences in cumulative contribution to the information gain of each feature, but the contribution of a particular feature in a single iteration generally decreases as the number of iterations increases.
- (3) In GBDT, key features are sampled at random with the same quite small probability, when high-dimensional sparse data are fed into the training program and a small sampling rate is given. That is why uniform sampling does not work in this case.

In summary, we can choose features based on the cumulative contribution, which is the importance scores of the features at one single iteration. It improves the effectiveness of the training process by keeping the key features are sampled into the training set.

### 3.2. LGBM-CBFS: LightGBM with Contribution-Based Feature Sampling.

In this subsection, we devised a contribution-based feature sampling algorithm named LGBM-CBFS

and integrate it into LightGBM. The details of the algorithm and the modifications made to LightGBM will be described.

The pseudocode of LGBM-CBFS is illustrated in Algorithm 1. Three inputs are fed into the function `selectTopN`. The first parameter `featImportances` denotes the importance scores of valid features at one boosting iteration. The second parameter `validIndices` represents the position indices of valid features, which has the same size with `featImportances`. The last parameter `featCount` describes the number of features added to the final training set. At the beginning of the algorithm, we sort the features based on importance scores in descending order (line 3). Then, calculating the number of features with high scores needs to be retained in the result set `idxSelect` (line 4, 5). The built-in parameter `feature_fraction` indicates the feature sampling rate.  $p$  is the value of the parameter `remain_feature_ratio` that indicates the proportion of high-score features we keep. Here, we take an empirical value of 0.5 for `remain_feature_ratio`. Not only possible significant features but also randomness is kept during the sampling process. After this process, according to the value obtained



```

Algorithm SelectTopN
Input: featImportances//the vector containing importance scores of valid features
Input: validFeatIndices//the vector containing position indices of valid features
Input: featCount//the number of valid features
(1)  $i dx$   $Selecte d \leftarrow$  //the result set
(2) //sort features based on scores
(3)  $sorte dI dx \leftarrow$  Sort(validFeatIndices, featImportances)
(4)  $importantFeatNum \leftarrow$  validFeatIndices.size()*feature_fraction*, p
(5)  $importantFeatNum \leftarrow$  Min(importantFeatNum, featCount)
(6)  $i dx$   $Selecte d \leftarrow$  The first importantFeatNum elements in  $sorte dI dx$ 
(7)  $samplingNum \leftarrow$  featCount - nonRan dC nt
(8)  $ran dI dx \leftarrow$  rand.get(sorte dI dx -  $i dx$   $Selecte d$ , samplingNum)
(9)  $i dx$   $Selecte d \leftarrow$   $i dx$   $Selecte d \cup samplingNum$ 
(10) Return  $i dx$   $Selecte d$ 

```

ALGORITHM 1: Contribution-based feature sampling algorithm.

in the previous step, the corresponding feature indices are included in result set (line 6). Finally, we sample uniformly from the rest of the features and merge them into  $i dx$   $Selecte d$  as a final result (line 7,8,9).

To make our algorithm is easy to use, we make some necessary modifications to LightGBM. Two parameters *feature\_sampling\_method* and *remain\_feature\_ratio* are added to source file config.h which is defined in the *include* module and contains descriptions of all parameters in LightGBM. Our sampling algorithm is enabled when *feature\_sampling\_method* set as LGBM-CBFS. User can determine how many features with high scores will be kept by setting the value of *remain\_feature\_ratio*. We define an interface for LGBM-CBFS by implement it in a new source file *feature\_sampling.cpp* of boosting module. The calling code is added before building a decision tree at one iteration, which is added to *gbdt.cpp*. Now that only a few lines in LightGBM were modified to provide an accessible interface to users.

## 4. Experiments

In this section, we compare LGBM-CBFS with the built-in feature sampling algorithm in LightGBM from an accuracy and speed perspective. The datasets used in our experiments comprise four artificial datasets generated by MATLAB and four publicly available datasets. The number of data instances and features are shown in Table 1. All experiments run on a single computer with two quad core i7-4790 CPUs and 16G memories.

**4.1. Accuracy Evaluation.** All of the artificial datasets in our experiments consist of 500 features and 100K instances exported by a 100K-by-500 matrix in MATLAB. We generate dataset Gamma from the gamma distribution with shape parameter in 2 and scale parameter in 500. Dataset Norm is generated from the normal distribution with mean parameter in 0 and deviation parameter in 500. We generate Poisson datasets from the Poisson distribution specified by the rate parameter  $\lambda = 2$ . A 100K-by-500 matrix of uniformly distributed random

numbers is generated between 0 and 1000. Our experimental datasets cover different distribution and sparsity and list in Table 1 in detail.

To verify the correctness and effectiveness of LGBM-CBFS, we train three GBDT models, respectively, by specifying different sampling strategies on real-sim and kdda datasets and recording their binary error and AUC as performance metrics at every boosting iteration. Our experimental results are depicted in Figure 3, in which we use LGBM, and the orange line denotes the performance of the model trained with all features. LGBM\_FS and the green line denote the performance of the model built on features sampling by built-in strategy in LightGBM, which is picking a subset of features uniformly at random. LGBM-CBFS and the pink line denote the performance of the model trained on features sampling by using the proposed approach in every boosting round.

In our experiments, a small sampling rate is assigned to evaluate the performance of our algorithm. We set the sampling rate to 0.05% in our experiment. The results in Figure 3 can be summarized as follows: (1) LGBM-CBFS performs better than LGBM\_FS in the first few iterations when taking AUC or binary error as performance metrics, but it gradually approaches LGBM\_FS during the subsequent training process. (2) LGBM-CBFS has a significant effect on model output at the beginning of the training process, but the effect has decreased as the number of iterations increases. (3) LGBM\_FS leads the model to fail to converge (in the case of kdda) when sampling on high-dimensional sparse data with few key features due to quite a small probability assigned. In summary, we can learn from these experiments that, LGBM-CBFS outperforms the built-in strategy in LightGBM (uniform sampling), and it continuously improves the model quality during the training process.

**4.2. Efficiency Evaluation.** In this subsection, we report the experimental results with respect to efficiency upon all datasets. The average time cost (1e-3 seconds) for training one iteration on sparse datasets is shown in Figure 4. We set

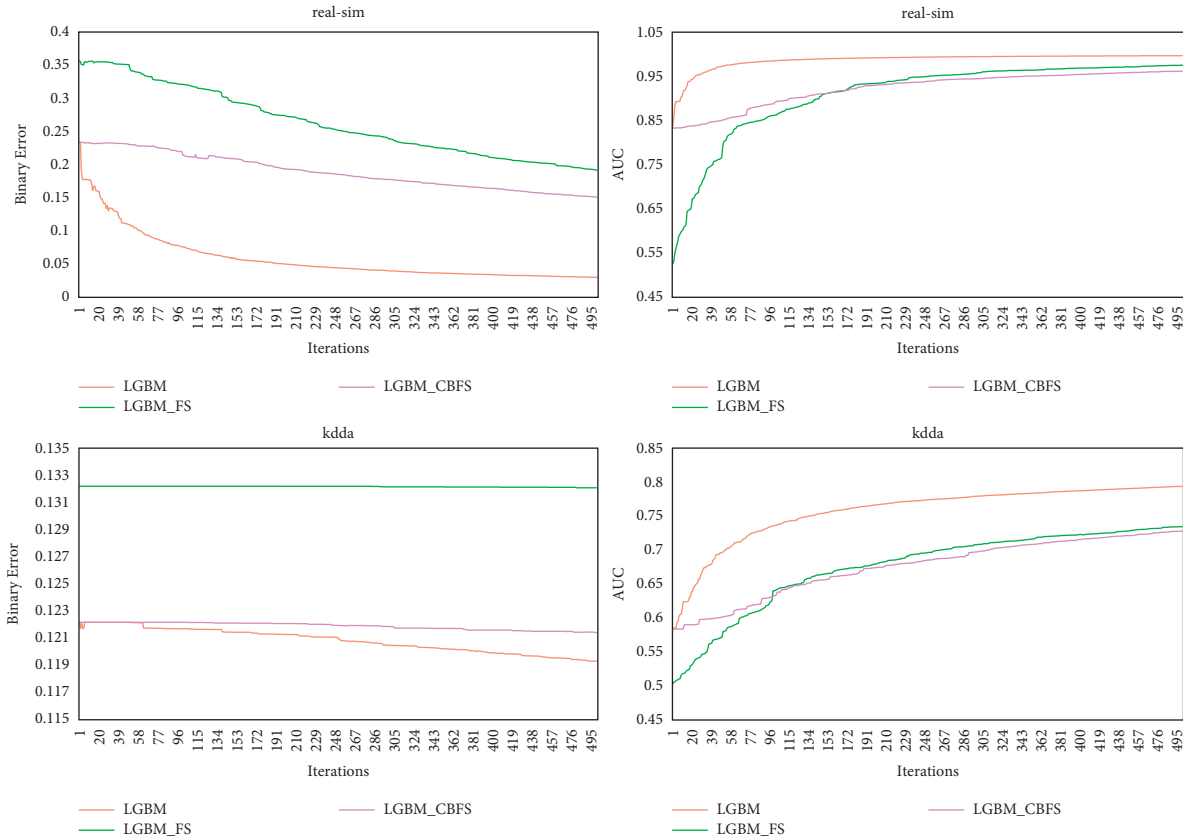


FIGURE 3: Iteration-accuracy curve.

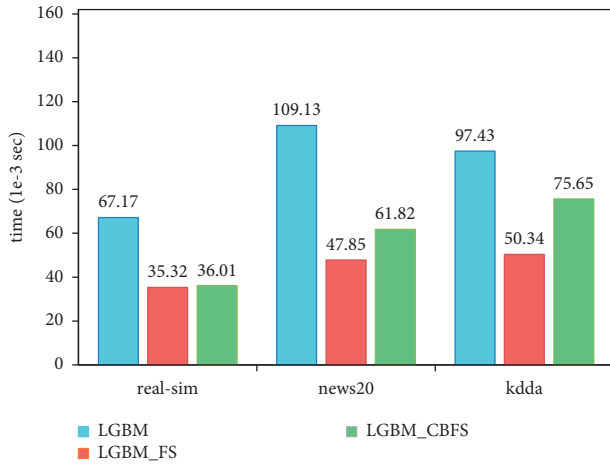


FIGURE 4: The average time cost for one iteration (sparse data).

0.05% as the value of the sampling ratio. From the results, both LGBM\_FS and LGBM-CBFS have accelerated the training process. LGBM-CBFS takes additional memory and computation cost because of the extra sort operation on features. It leads to more time overheads of training than LGBM\_FS.

We use four artificial datasets described in section 3.1 in our experiments to evaluate the training speed on dense datasets. We set 10% as the value of the sampling

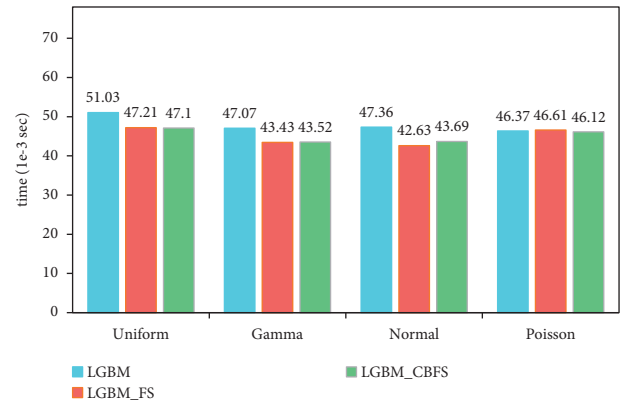


FIGURE 5: The average time cost for one iteration (dense data).

ratio. The experimental results in Figure 5 show that LGBM-CBFS and LGBM\_FS slightly improve the computational efficiency in most situations. And there is no significant difference between LGBM-CBFS and LGBM\_FS in time overheads.

In general, all these evaluations from accuracy and speed perspectives demonstrate that LGBM-CBFS could cut down the risk of training failure triggered by using a small sampling ratio; meanwhile, it often leads to higher accuracy in a high-dimensional sparse scenario.

## 5. Conclusions

In a real application context, training a GBDT model over a large-scale dataset is time-consuming. A natural idea to solve this issue is that sampling on input dataset to reduce data size, but it may lead model fail to converge in high-dimensional scenarios when using uniform sampling in LightGBM. In order to address this problem, we devised a heuristic feature sampling algorithm named LGBM-CBFS and implement it into LightGBM. Benefit from the strategy that chooses a representative subset of features based on the native importance scores of GBDT, LGBM-CBFS can heavily reduce excessive computation costs. We conduct a series of experiments and compare the proposed LGBM-CBFS algorithm with the built-in feature sampling algorithm in LightGBM. The experimental results show that LGBM-CBFS significantly improved the training effectiveness of GBDT over sparse data with high-dimensional features, meanwhile, without introducing additional computation overheads. In the future, we will explore potential optimization solutions of our sampling strategy for dense dataset scenarios.

## Data Availability

The data are available on request by contacting the corresponding author (cse.HuiLi@gzu.edu.cn).

## Conflicts of Interest

The authors declare that they have no conflicts of interest.

## Acknowledgments

This work was partially supported by the National Natural Science Foundation of China (62162010, 62162011, and 72161005) and Research Projects of the Science and Technology Plan of Guizhou Province (no. [2021]449).

## References

- [1] J. H. Friedman, "Greedy function approximation: a gradient boosting machine," *Annals of Statistics*, vol. 29, no. 5, pp. 1189–1232, 2001.
- [2] T. Chen and C. Guestrin, "XGBoost: a scalable tree boosting system," in *Proceedings of the 22nd ACM SIGKDD International Conference on Knowledge Discovery and Data Mining*, pp. 785–794, New York, NY, United States, 2016.
- [3] G. Ke, Q. Meng, T. Finley et al., "A highly efficient gradient boosting decision tree," in *Proceedings of the 31st International Conference on Neural Information Processing Systems*, pp. 3146–3154, Red Hook, NY, United States, 2017.
- [4] H. Chernoff, "A measure of asymptotic efficiency for tests of a hypothesis based on the sum of observations," *The Annals of Mathematical Statistics*, vol. 23, no. 4, pp. 493–507, 1952.
- [5] W. Hoeding, "Probability inequalities for sums of bounded random variables," *Journal of the American Statistical Association*, vol. 58, no. 301, pp. 13–30, 1963.
- [6] O. Watanabe, "Sequential sampling techniques for algorithmic learning theory," *Theoretical Computer Science*, vol. 348, no. 1, pp. 3–14, 2005.
- [7] C. Domingo, R. Gavaldà, and O. Watanabe, *Adaptive Sampling Methods for Scaling up Knowledge Discovery Algorithms*, pp. 131–152, Discovery Science, 1999.
- [8] C. Domingo, R. Gavaldà, and O. Watanabe, "Adaptive sampling methods for scaling up knowledge discovery algorithms," *Data Mining and Knowledge Discovery*, vol. 6, no. 2, pp. 131–152, 2002.
- [9] O. Watanabe, *Simple Sampling Techniques for Discovery Science*, Technical Report, 2000.
- [10] J. Chen and X. Chen, *A New Method for Adaptive Sequential Sampling for Learning and Parameter Estimation*, pp. 220–229, Foundations of Intelligent Systems-international Symposium Springer-Verlag, 2011.
- [11] J. Chen, "Scalable ensemble learning by adaptive sampling," in *Proceedings of the International Conference on Machine Learning and Applications*, vol. 1, pp. 622–625, Edinburgh, Scotland, 2012.
- [12] P. Drineas, M. W. Mahoney, and S. Muthukrishnan, "Relative-error CUR matrix decompositions," *SIAM Journal on Matrix Analysis and Applications*, vol. 30, no. 2, pp. 844–881, 2007.
- [13] A. Kyriklidis and A. Zouzias, "Non-uniform feature sampling for decision tree ensembles," in *Proceedings of the IEEE International Conference on Acoustics, Speech and Signal Processing*, pp. 4548–4552, Florence, Italy, 4–9 May 2014.
- [14] J. H. Friedman, "Stochastic gradient boosting," *Computational Statistics & Data Analysis*, vol. 38, no. 2, pp. 367–378, 2002.
- [15] W. Hoefding, "Probability inequalities for sums of bounded random variables," *Journal of the American Statistical Association*, vol. 58, no. 301, pp. 13–30, 1963.
- [16] L. Breiman, "Random forests," *Machine Learning*, vol. 45, no. 1, pp. 5–32, 2001.
- [17] R. E. Schapire, "The boosting approach to machine learning: an overview," *Nonlinear Estimation and Classification*, vol. 171, pp. 149–171, 2003.
- [18] Z. Kalal, J. Matas, and K. Mikolajczyk, "Weighted sampling for large-scale boosting," in *Proceedings of the British Machine Vision Conference*, pp. 1–10, Leeds, UK, 2008.
- [19] A. Ahmed El and M. W. Mahoney, *Fast Randomized Kernel Methods with Statistical Guarantees*, ArXiv <http://abs/1411.0306>, 2014.
- [20] P. Drineas, M. M. Ismail, M. W. Mahoney, and D. P. Woodruff, "Fast approximation of matrix coherence and statistical leverage," *Journal of Machine Learning Research*, vol. 13, pp. 3475–3506, 2011.
- [21] A. Rudi, D. Calandriello, L. Carratino, and L. Rosasco, "On fast leverage score sampling and optimal learning," in *Proceedings of the NeurIPS*, pp. 5677–5687, Montréal, Canada, 2018.
- [22] D. Teng and S. Dasgupta, "Lifelong learning via online leverage score sampling," in *Proceedings of the Adaptive & Multitask Learning Workshop*, Long Beach, CA, USA, 2019.

## Research Article

# Enhancing Personalized Recommendation by Transductive Support Vector Machine and Active Learning

Xibin Wang <sup>1,2,3</sup> Yunji Li,<sup>1</sup> Jing Chen,<sup>4</sup> and Jianfeng Yang<sup>1,2</sup>

<sup>1</sup>School of Data Science, Guizhou Institute of Technology, Guiyang 550003, Guizhou, China

<sup>2</sup>Special Key Laboratory of Artificial Intelligence and Intelligent Control of Guizhou Province, Guiyang 550003, Guizhou, China

<sup>3</sup>Key Laboratory of Electric Power Big Data of Guizhou Province, Guiyang 550003, Guizhou, China

<sup>4</sup>College of Information Engineering, Guizhou University of Traditional Chinese Medicine, Guiyang 550025, Guizhou, China

Correspondence should be addressed to Xibin Wang; [binxiwang@git.edu.cn](mailto:binxiwang@git.edu.cn)

Received 26 November 2021; Revised 24 January 2022; Accepted 17 February 2022; Published 9 March 2022

Academic Editor: Chenquan Gan

Copyright © 2022 Xibin Wang et al. This is an open access article distributed under the Creative Commons Attribution License, which permits unrestricted use, distribution, and reproduction in any medium, provided the original work is properly cited.

As an important component of information service networks, personalized recommendation technology provides users with better options and enables them to obtain information anytime and anywhere. Collaborative filtering (CF) is a successful and widely used form of this technology. However, the traditional CF recommendation algorithm is ineffective in environments with frequent entry of new users and high levels of data sparsity. For new users in the system, few or no scores, labels, or other such information is available, leading to the user cold start problem. Simultaneously, data sparsity leads to the selection of unreasonable neighbors, which reduces the recommendation accuracy. In addition, the traditional CF recommendation algorithm ignores the inherent connections between users' preferences and their basic information (such as demographics). Users with similar demographic information are likely to have similar preferences, which can serve as a good basis for finding neighbors. To address the aforementioned problems, we propose a recommendation model that combines active learning (AL) and a semi-supervised transductive support vector machine (TSVM). To enable neighbors to be found quickly and accurately, similar users are clustered together on the basis of their basic information. Then, the TSVM-based classifier is trained on each cluster. To improve the quality of sample labeling and thus the classifier performance, an active learning method based on the distance strategy and a multiclassifier voting mechanism is implemented. Finally, the TSVM-based recommendation model is trained on the labeled samples. The extensive experiments conducted using a real data set from MovieLens demonstrate that the proposed model effectively alleviates the aforementioned cold start and data sparsity problems.

## 1. Introduction

Information technology and the Internet have developed rapidly, and numerous online forums and e-commerce, social, and consulting service platforms have been established, resulting in the availability of a huge amount of information. However, obtaining effective information can be challenging due to information overload. Recommendation systems can address such problems [1, 2], in which a preference model between users and items is developed by acquiring users' behavior characteristics or preferences, predicting their preferences for unknown or unselected items, and generating a recommendation list. A recommendation algorithm is central to this type of system as it

determines the recommendation effect and quality. Current personalized recommendation algorithms include content-based, collaborative filtering (CF), model-based, and hybrid recommendation algorithms [3–6]. Of these, the CF recommendation algorithm is one of the most successful and widely used algorithms. It has the advantages of not relying on the feature information of the item and not being constrained by content analysis technology and thus represents a major development in theoretical and practical terms. However, it requires continuous improvement due to the limitations of cold start (many users with little or no historical data) and data sparsity (limited user-item rating information or few items rated by multiple users) [7, 8].

The user cold start problem occurs when there are few or no scores, labels, or other information about new users in the system. The recommendation function of the system is even more important for such new users. Reference [9] shows that the loyalty of users to the system depends on whether and when the system provides effective personalized services. Users will have a greater reliance on the system and thus improve user loyalty if the recommendation function can be implemented for new users as early as possible. Thus, solving this cold start problem is necessary to improve the quality and efficiency of recommendation systems.

A common solution to the problem of new users is to use non-personalized recommendations; however, a lack of personal information means that the system must accumulate a certain level of data before it can provide recommendations. Another solution is to use user registration information as the basis for recommendations, but the resulting recommendations are likely to be coarse as the information is often limited. A more effective solution entails the use of active inquiry-based models that acquire the required knowledge through communicating with users and therefore provide rapid and accurate results.

The goal of a recommendation system is to satisfy users by providing appropriate recommendations by learning the users' preferences from their operations, which can be achieved through active learning. Active learning should therefore be integrated into recommendation systems [10]. The notion of the highest predicted score in [11] involves predicting the scores of unlabeled items, and the item with the highest predicted score may be the user's favorite item. The notion of the lowest predicted score in [12] is similar, in which the item with the lowest predicted score is selected and the user identifies the least preferred items with a score. An active learning algorithm is proposed in [13] based on matrix decomposition, which selects the sample with the lowest predicted score for users to choose. Reference [14] uses the aspect model to predict the probability that a target user  $u$  belonging to an interest group  $z$  will give a score  $r$  to a specific item  $i$ , where the user is a combination of multiple interest groups.

Data sparsity has also become a major problem for recommendation systems as it results in unreasonable neighbors being selected by the target user, which reduces the accuracy of the recommendations [15]. This issue can be addressed using a clustering algorithm to improve the recommendation accuracy. For example, [16] proposes a novel and scalable CCCF method, which improves the performance of CF methods via user-item co-clustering. Users and items are clustered into several subgroups, and each includes a set of like-minded users and a set of items they share an interest in. A hybrid approach is proposed by [17], which combines a content-based approach with CF under a unified model called co-clustering with augmented matrices (CCAMs). This method is based on information-theoretic co-clustering but further considers augmented data matrices, including user profiles and item descriptions. Reference [4] proposes a novel recommendation model based on a time correlation coefficient and an improved

K-means with cuckoo search. The clustering method can cluster similar users together for further quick and accurate recommendations. The novel method of [18] applies clustering algorithms to the latent vectors of users and items, which can capture the interests that are common to the clusters of users and of items in a latent space. Some scholars have used matrix factorization (MF) techniques and singular value decomposition to solve this problem. For example, [19] proposes neural variational matrix factorization, which is a novel deep generative model that incorporates side information (features) of both users and items to effectively capture the corresponding latent representations to generate more accurate CF recommendations. To alleviate the effects of data sparsity, [20] proposes a framework that involves two efficient matrix factorizations, a dynamic single-element-based CF integrating manifold regularization (DSMMF) and a dynamic single-element-based Tikhonov graph regularization nonnegative MF (DSTNMF). A novel imputation-based recommendation method is proposed by [21] to solve the problem of data sparsity in SVD-based methods.

Building upon these studies, we propose a new personalized recommendation model in which active learning is integrated with semi-supervised learning and apply the cluster analysis method to solve the cold start and data sparsity problems. Users with similar rating patterns generally have similar interest preferences in recommendation systems and can be classified together on the basis of their item ratings. Thus, the basic information of new users (e.g., registration and demographic information) can determine the user group they belong to, and the system can accordingly provide more accurate item recommendations, to some extent solving the cold start problem. Semi-supervised learning and active learning methods can then be used to label the users' item preferences, which not only alleviate the data sparsity problem but also solve the cold start problem.

Our study makes four main contributions to the literature. First, we use cluster analysis due to the sparsity of a new user's query list, through which we can classify new users and obtain more reliable preference information, thus solving the problem of cold start.

Second, the label information of user-item association data, i.e., rating information expressed by users about items, is scarce, so we use the semi-supervised transductive support vector machine (TSVM) as the benchmark classifier, together with an active learning strategy based on distance, to label the association data.

Third, the quality of data is considered in active learning and fewer but higher quality items are selected for inquiring users, which address the problems of cold start and data sparsity. Specific inquiry information such as item scores can also be selected in active learning, which can supplement the scarce data for interest-related aspects, thus helping to ensure that the interest model is comprehensive.

Finally, as active learning does not rely on any similarity between users or items, the recommendations are not limited to similar modules, which expands the choices presented to users along with their cognitive domains and better portrays user preferences.

## 2. Semi-Supervised Transductive Support Vector Machine

Joachims et al. propose a transductive support vector machine learning algorithm (TSVM), which is the same as the traditional SVM learning method for binary classification problems, especially suitable for small sample training sets [22, 23]. In the TSVM training process, the test data (unlabeled sample) set is also considered together, and then, the classification error of the test data set is minimized. In other words, TSVM tries to assign different labels to unlabeled samples and find the classification hyperplane with the largest interval on all samples.

The principle of TSVM algorithm is as follows [24]:

Given a set of independently and identically distributed labeled training samples:

$$\begin{aligned} D_l &= \{(x_1, y_1), \dots, (x_l, y_l)\} \in R^n \times R, \\ i &= 1, \dots, l, \\ y_i &= \{-1, +1\}. \end{aligned} \quad (1)$$

Another set of unlabeled samples from the same distribution is as follows:

$$D_u = \{x_{l+1}, \dots, x_{l+u}\}. \quad (2)$$

The learning objective of TSVM is to predict the unlabeled samples in  $D_u$  and give the prediction labels, so that

$$\begin{aligned} &\min(y_1, \dots, y_n, w, b, \xi_1, \dots, \xi_l, \xi_{l+1}, \dots, \xi_{l+u}) \\ &\frac{1}{2} \|w\|^2 + C_1 \sum_{i=1}^l \xi_i + C_2 \sum_{i=l+1}^{l+u} \xi_j \end{aligned} \quad (3)$$

$$\text{s.t.} : \forall_{i=1}^l : y_i [w \cdot x_i + b] \geq 1 - \xi_i; \xi_i \geq 0$$

$$\forall_{i=l+1}^{l+u} : y_j [w \cdot x_j + b] \geq 1 - \xi_j; \xi_j \geq 0,$$

where  $(w, b)$  determines a classification hyperplane;  $\xi_i$  ( $i = 1, 2, \dots, l$ ) is the slack variable of labeled samples;  $\xi_j$  ( $j = l+1, l+2, \dots, l+u$ ) is the slack variable of unlabeled samples;  $C_1$  and  $C_2$  are the impact factors of labeled and unlabeled samples specified by the user; and  $C_2 \xi_j$  is the ‘‘influence term’’ of the unlabeled sample  $x_j$  in the objective function.

The training process of TSVM algorithm is as follows [25]:

Step 1: set parameters  $C_1$  and  $C_2$ , train labeled samples by inductive learning, and get an initial classifier. Set the estimated number  $N$  of positive samples in unlabeled samples.

Step 2: use the initial classifier to calculate the value of the decision function for all unlabeled samples. Label the first  $N$  unlabeled samples with large value of decision function as positive samples, and label the remaining unlabeled samples as negative samples. Set  $C_{\text{temp}}$  as a temporary impact factor.

Step 3: retrain the SVM model on all the labeled samples. For the newly generated classifier, according to the principle of reducing the objective function (3) as much as possible, exchange the labels of each pair of samples until there are no samples that meet the exchange conditions; otherwise, repeat the process.

Step 4: increase the value of  $C_{\text{temp}}$  uniformly, and return to Step 3. When  $C_{\text{temp}} \geq C_2$ , terminate the algorithm and return the labels of all unlabeled samples.

## 3. Active Learning

Aiming at the shortcoming of supervised learning that a large number of labeled samples must be used to construct a learner, active learning is proposed. In particular, in the case of a very large amount of data, the cost of labeling each sample will be very high [26]. The goal of active learning is to obtain a higher classification accuracy rate when the training data are limited and then these samples are labeled, which can not only reduce the training cost but also improve the classification effect of the learner.

Generally, the process of active learning includes two steps: establishing a basic classifier and selecting appropriate samples, where the basic classifier is obtained using supervised learning algorithm to learn and train on the labeled sample set; the process of sample selection is to select the samples with the largest value from the unlabeled sample set based on a certain sample selection strategy, then label them by domain experts or users, and add the labeled samples into the training set. Repeating the above two steps can gradually improve the performance of the classifier until the termination condition is met.

According to the different problem scenarios and unlabeled sample selection ways, active learning strategies can be divided into three types: membership query synthesis, stream-based selective sampling, and pool-based sampling [27]. Their differences are shown in Figure 1.

In the active learning strategy, it is mainly to determine which unlabeled sample has the largest amount of information or the most uncertain to be inquiry, and this inquiry strategy is the focus of research. Reference [28] proposes a new semi-supervised learning framework, which combines the active learning of the Gaussian random field with harmonic function, and selects unlabeled samples based on the value of the energy function. In [29], a combination of active learning and semi-supervised learning is proposed for sequence labeling, which can greatly reduce the cost of manual labeling. It only labels unlabeled samples with high uncertainty, and other sequences and subsequences are automatically labeled.

## 4. Sample Labeling Method Based on Distance Measurement and a Multiclassifier Voting Decision

4.1. *TSVM Algorithm Analysis.* We identified the following shortcomings in the TSVM algorithm through our analysis:

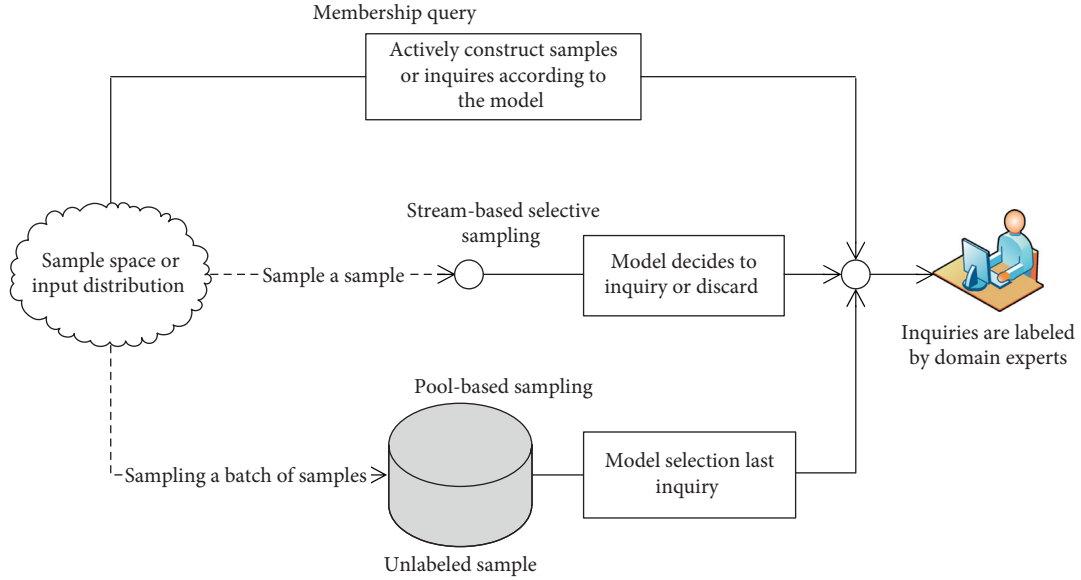


FIGURE 1: Three main active learning scenarios.

- (1) If there are  $u$  unlabeled samples, then to achieve an accurate solution to the problem, all possible classification results for the sample sets must be searched for, that is,  $2^u$  results, which belongs to a typical NP problem. If the unlabeled sample  $u$  is relatively small, the solution of this algorithm is completely possible. However, when the unlabeled sample  $u$  is large, it is almost impossible to find its exact solution, so it must be solved using labeled samples and various approximate optimization algorithms.
- (2) The algorithm labels samples in pairs and selects those samples most likely to be support vectors in the boundary area for labeling each time, and the labeling speed is very slow.

Thus, to solve the above problems, we propose an active learning method that combines multiclassifier voting and collaborative training when labeling samples. The advantages of this method are as follows:

- (1) The algorithm does not simply rely on the classification results of a single classifier to determine the samples to be labeled but trains multiple classifiers and uses the voting results of all of the classifiers to determine the samples to be labeled, which can improve the accuracy of labeling.
- (2) When training multiple classifiers, the training set must be divided into multiple sub-training sets, and how these are divided determines the performance of the trained classifier. We use the clustering algorithm to divide the training set, which considers all of the geometric and spatial distribution characteristics of the labeled samples. A proportion of samples are then extracted according to the clustering results and the size of each cluster to construct a new training set and train the classifier, which can effectively improve its performance.

- (3) In every iteration, each training set is small, so the training time cost of each classifier is relatively low.
- (4) We train the obtained labeled samples and the previously labeled samples to obtain the final classifier, which improves not only the training speed of the classifier but also its performance.

**4.2. Sample Labeling Based on Distance Strategy and Multiclassifier Voting.** We apply the multiclassifier collaborative voting mechanism to label unlabeled samples, which improves the training speed of TSVM and the labeling accuracy of samples. The time complexity of the iterative training is reduced, and multiple classifiers use a voting mechanism to determine the class label of samples, thus improving the labeling accuracy in each iteration.

Figure 2 illustrates the multiclassifier voting decision labeling process. We divide the entire sample set into the labeled sample set  $L$  and an unlabeled sample set  $U$ . First, we cluster the labeled sample set and extract a specific number of samples from each cluster according to a specific proportion to form  $k$  ( $k$  is odd and greater than 1) subsample sets as the training sets, which guarantees that each training set is different. Second,  $k$  initial classifiers  $C_1, C_2, \dots, C_k$  are trained based on  $k$  training sets, following which we use these  $k$  classifiers to predict each unlabeled sample and obtain the output  $f_1, f_2, \dots, f_k$ . Third, we label unlabeled samples and decide whether to iterate further based on the termination conditions. Four key problems must be solved in this process:

- (1) Using the clustering algorithm to distinguish the training samples
- (2) Selecting the samples to be labeled
- (3) Adding the labeled samples to the corresponding classifier and using them in further iterative training

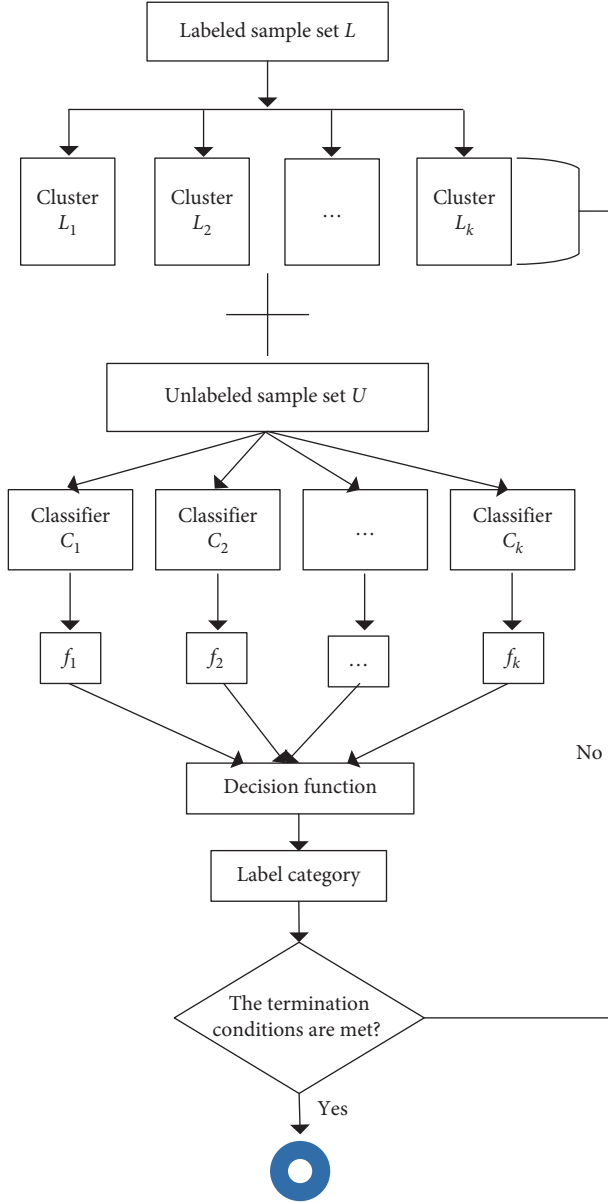


FIGURE 2: Framework of multiclassifier voting decision labeling.

## (4) Determining the iteration termination conditions

**4.2.1. Training Set Division Based on the Clustering Algorithm.** The basic principles of training set division are as follows: first, the sample distribution in each training set and the differences between the training sample sets ensure that the output result of each set is reasonable; second, the difference between the training sets ensures the reliability of the voting results of multiple classifiers. The clustering method is used to construct the training set to ensure that the differences among the initial classifiers are as large as possible.  $k$  clusters are formed through cluster analysis, which is as similar as possible within the cluster and as dissimilar as possible between clusters. Samples are then randomly selected from each cluster in a specific proportion to form each training set.

We use the K-means clustering algorithm to cluster the initial training set. The specific steps are as follows:

Step 1: suppose the labeled sample set is  $L = \{x_1, x_2, \dots, x_l\}$ , the number of clusters is  $K$ , the iteration round is  $r$ , and the initial value is 0; then, the initial  $K$  cluster centers are set as  $(C_1^r, C_2^r, \dots, C_K^r)$ .

Step 2: assume that the set corresponding to the  $i$ -class sample is  $L_i^r$ . For any sample  $x_j, j = 1, \dots, l$ , if the distance between  $x_j$  and the cluster center  $C_j^r$  is the shortest, as shown in equation (4), then the sample  $x_j$  is added to the  $L_j^r$  class.

$$\|x_j - C_j^r\| \leq \|x_j - C_k^r\|, \quad k = 1, 2, \dots, K. \quad (4)$$

Step 3: recalculate  $K$  cluster centers as follows:

$$C_i^r = \frac{1}{o_i} \sum_{x_j \in L_i^r} x_j, \quad i = 1, 2, \dots, K, \quad (5)$$

where  $o_i \in L_i^r$ .

Step 4: define the clustering criterion function and calculate the clustering error as follows:

$$E(t) = \sum_{i=1}^K \sum_{x_j \in L_i^r} \|x_j - C_i^r\|. \quad (6)$$

Step 5: determine whether the stop condition is met. If  $|E(t-1) - E(t)|$  is less than the preset error value, the final clusters and cluster centers are  $L_i = L_i^r, C_i = C_i^r, i = 1, 2, \dots, K$ ; otherwise,  $r = r + 1$  is set, and go to Step 2.

**4.2.2. Sample Labeling Strategy Based on Distance Strategy and the Multiclassifier Voting Mechanism.** The size of the data set of the training samples is considered when selecting the samples to be labeled. Common labeling methods include the boundary-based sample method (e.g., pairwise sample labeling in TSVM), which has high labeling accuracy but very low labeling speed, and the region-based labeling method, which can simultaneously label multiple samples and thus has a high labeling speed but may have low labeling accuracy. We propose a multiclassifier voting decision labeling method that selects samples for labeling that belong to more than  $m$  classifier boundary regions at the same time; i.e., the minority is subordinate to the majority. If  $m$  samples meet equation (8), they are labeled as positive, and if  $m$  samples meet equation (9), they are labeled as negative.

Assuming that the classification hyperplane is  $f(x)$  and the unlabeled sample set is  $U = \{x_{l+1}, x_{l+2}, \dots, x_{l+u}\}$ , the distance from the sample  $x_i$  to the classification hyperplane is expressed as follows:

$$d(x_i) = \frac{|\omega^T x_i + b|}{\|\omega\|} = \frac{y(\omega^T x_i + b)}{\|\omega\|} = \frac{yf(x_i)}{\|\omega\|}, \quad (7)$$

$$i = l + 1, \dots, l + u.$$



We select unlabeled samples that are most likely to be support vectors for labeling and increase the labeling speed using a compromise between the pairwise labeling and region labeling methods to label the unlabeled samples. In each iteration process, unlabeled samples meeting the first  $p$  maximum of equation (8) are selected and labeled as positive, while those meeting the first  $q$  minimum values of equation (9) are then selected and labeled as negative.

$$\max(f(x_i)), \text{ s.t. } \frac{\omega^T x_i + b}{\|\omega\|} \geq d(x_i), \quad i = l + 1, \dots, l + u. \quad (8)$$

$$\min(f(x_i)), \text{ s.t. } \frac{\omega^T x_i + b}{\|\omega\|} \leq -d(x_i), \quad i = l + 1, \dots, l + u, \quad (9)$$

where the values of  $p$  and  $q$  determine the number of samples labeled in each iteration, i.e., the learning speed of transductive learning. When  $p$  and  $q$  equal 1, we apply the pairwise labeling method. When  $p$  and  $q$  are greater than 1,  $p$  or  $q$  samples in the boundary region of the optimal classification hyperplane are labeled in each iteration, and their values can be tuned according to the actual application scenario.

**4.2.3. Adding Labeled Samples to the Corresponding Classifier.** After the samples are labeled, they must be added to the training set for iteration if the stop condition of the algorithm is not met. Instead of adding the samples to all training sets, they are added to those corresponding to classifiers whose output class labels are consistent. For example, if the output results of the five classifiers  $A$ ,  $B$ ,  $C$ ,  $D$ , and  $E$  are positive class, positive class, positive class, positive class, and negative class, respectively, then adding samples to the training set corresponding to training classifier  $E$  is obviously inappropriate. In addition, if the output results of two classifiers  $A$  and  $B$  meet equation (8) and if the output result of  $A$  is 0.05 and  $B$  is 0.95, then the probability of  $A$  labeling the sample correctly is relatively low compared with  $B$ . Thus, the difference in training and the accuracy of the sample labeling can be guaranteed by adding the labeled samples to the training set corresponding to the classifier whose labeled class is consistent with the output result and whose output value is the largest.

**4.2.4. Termination Conditions.** If in the process of sample labeling and model training the currently labeled sample class is inconsistent with the previously labeled class, then the labeled class must be reset; that is, the sample must be relabeled. The approach in this case is to take the sample as an unlabeled sample again and delete it from the corresponding training set and proceed to the next iteration. If there are no samples that need to be reset in the iteration and there are no unlabeled samples that meet the labeling condition, then the iteration is stopped.

## 5. Improved TSVM Algorithm Based on Active Learning

The TSVM algorithm is based on multiclassifier collaborative labeling and is designed by combining the TSVM algorithm and the proposed multiclassifier voting decision labeling. The specific steps of Algorithm 1 are as follows:

## 6. Experiment Evaluation

### 6.1. Experimental Data Set and Experimental Setting

**6.1.1. Data Description.** We select the MovieLens data set for the experiment, which comprises movie rating data collected by the GroupLens team of the University of Minnesota. Movies are recommended based on users' scores (1–5) [30]. Four levels of data are provided: 100,000 scores, 1 million scores, 10 million scores, and 20 million scores. We select the first data set of 100,000 real scores for 1682 movies submitted by 943 users, with a sparsity of 94.3%, and a rating range of [1, 5]. The higher the score, the more the user likes that movie. Each user in the data set has rated at least 20 movies. We regard a movie with a score of 3–5 as one liked by the user and is thus labeled as +1 and one with a score of 1–2 as disliked (labeled as -1).

**6.1.2. Experimental Setting.** The experimental environment of this study is a computer configured with Intel Core i5 1.6 GHZ, 8 G memory, and Windows 10 operating system, and the simulation software is MATLAB 2015b.

In the experiment, we set the parameters, for example, the number of clusters  $k$ , of the proposed algorithm through experiments, and all the experimental results are the average results of 5 experiments.

**6.1.3. Evaluation Metrics.** We use precision and F score to evaluate the performance of the recommendation model. The specific calculation methods are as follows.

Suppose  $n$  items are recommended for user  $u$ , denoted as  $R(u)$ . The set of items that user  $u$  likes on the test set is  $T(u)$ . Then, the accuracy and recall are defined as follows:

$$\text{precision} = \frac{\sum_u |R(u) \cap T(u)|}{\sum_u |T(u)|}, \quad (10)$$

$$\text{recall} = \frac{\sum_u |R(u) \cap T(u)|}{\sum_u |R(u)|}.$$

Accuracy and recall are a pair of mutually exclusive indicators that are typically combined, and the F score is used to measure the recommendation quality. The higher the F score, the higher the quality.

$$\text{F score} = \frac{2 \times \text{precision} \times \text{recall}}{\text{precision} + \text{recall}}. \quad (11)$$

**Input:** Labeled sample set  $L$ ; unlabeled sample set  $U$ ; the number of classifiers  $k$ .

**Output:** The final classifier TSVM.

**Step 1:** Apply the K-means algorithm to cluster the labeled sample set  $L$ , and extract samples from each cluster according to a specific proportion to form  $k$  sub-training sets, which are denoted as  $L_1, L_2, \dots, L_k$ .

**Step 2:** Utilize the SVM algorithm to train  $k$  training subsets to obtain  $k$  initial classifiers:  $C_1, C_2, \dots, C_k$ .

**Step 3:** Input unlabeled samples into  $C_1, C_2, \dots, C_k$ , and obtain  $k$  output results:  $f_1^i, f_2^i, \dots, f_k^i$ .

**Step 4:** For any unlabeled sample  $x_j$ , if the classification results of a  $k$  classifier meet equation (8), then label it as a positive class; if the classification results of a  $k$  classifier meet equation (9), then label it as a negative class.

**Step 5:** If the currently labeled class of  $x_j$  is inconsistent with the previously labeled class, cancel the labeling and delete it from the corresponding training set. If the currently labeled class is consistent with the previous and  $\max(f(x_j^i)), j = 1, 2, \dots, k$  is inconsistent, then add the sample to  $L_j$ . If the sample is not labeled in the early stage, then find  $j$  that meets  $\max(f(x_j^i)), j = 1, 2, \dots, k$ , and add the sample to  $L_j$ ; otherwise, stop the iteration and go to **Step 8**.

**Step 6:** Repeat steps 4 and 5 until all unlabeled samples are labeled.

**Step 7:** Train the new training subset and obtain the new classifiers  $C_{1\text{new}}, C_{2\text{new}}, \dots, C_{k\text{new}}$ . If the sub-training sets of the previous and current iterations remain unchanged, the corresponding training should continue to use the classifier from the previous iteration; then, go to **Step 3**.

**Step 8:** Combine each training subset to form the final training set, and retrain the sample set to obtain the final classifier.

ALGORITHM 1: TSVM algorithm based on distance strategy and multiclassifier collaborative labeling (DCTSVM).

## 6.2. Experimental Results

**6.2.1. Role of Clustering in Solving the Cold Start Problem for New Users.** We assess the performance of the clustering algorithm in alleviating the cold start of new users and compare it with the performance of the following algorithms: user-based collaborative filtering (UserCF) algorithm, cluster-based UserCF algorithm (CUserCF), TSVM algorithm based on the distance metric, proposed multiclassifier voting decision mechanism (DCBTSVM), TSVM algorithm based on the distance metric, and multiclassifier voting decision mechanism without cluster analysis (ALTSVM). Figure 3 presents the performance of these reference algorithms, in terms of their recommendation accuracy, with a different number of clusters.

These results show that the clustering algorithm improves the performance of the recommendation model. By analyzing the characteristics of the data set, the model automatically selects neighbors and excavates the potential association relationship of users (i.e., it looks for users that are highly similar), thus helping new users find their own user groups quickly and alleviating the problem of reduced recommendation accuracy due to user cold start. Owing to the use of cluster analysis, the recommendation accuracy of the CUserCF algorithm is better than that of UserCF. Similarly, the recommendation accuracy of DCBTSVM is better than that of ALTSVM.

In the classification-based recommendation system, the number of samples (user-item) in each cluster gradually decreases as the number of clusters  $k$  increases, while the number of classifiers trained (equal to the number of clusters  $k$ ) using the active learning classification model gradually increases. As the number of samples in each cluster decreases, the ability of the trained model to generalize also changes. When  $k = 30$ , the recommendation accuracy begins to decline, as the labeling of unlabeled samples by all classifiers is inaccurate; this may be related to model overfitting.

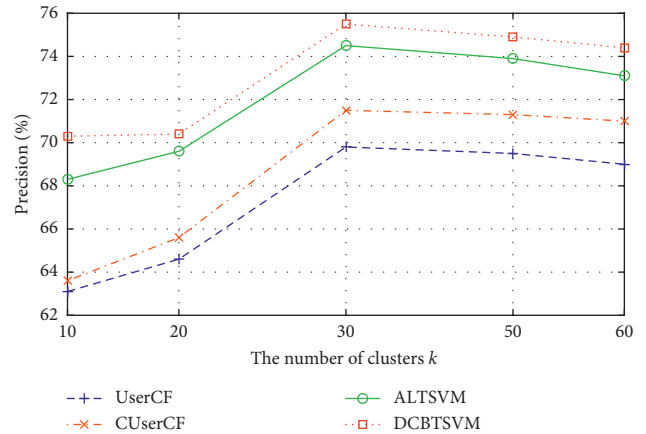


FIGURE 3: Recommended accuracy of four algorithms with a different number of clusters.

A high level of accuracy (i.e., precision) and the ability to identify as many items of user interest as possible (i.e., recall) are key factors characterizing the performance of a recommendation model. The F score is an important indicator of these abilities. Figure 4 shows that the proposed DCBTSVM method has better F score than the other three methods. The scores are highest when  $k = 30$  and when the proportion of training samples accounts for 60% of the whole training sample set.

**6.2.2. Active Learning Strategy for Solving Data Sparsity and User Cold Start Problems.** To better simulate real online user situations, we divide the users into the MovieLens data set into two groups. We select one group of users and their rated movie data for the initial training set and no longer regard them as new users. Users in the other group are regarded as new users, and their rated movie data are divided into two subgroups. Each user randomly reserves 20 movie scores for

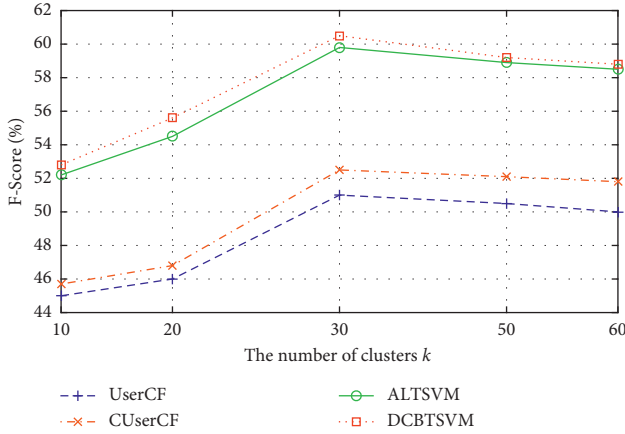


FIGURE 4: F scores of four algorithms with a different number of clusters.

the final test set, and the other subgroup is used as an unlabeled sample set. We assume that users can rate any movie. Each time the movie samples are selected from the unlabeled sample set to be labeled, and they are added into the training set to retrain the model.

On the basis of the aforementioned experimental results, the number of clusters  $k$  is first set to 30 and then to 40. Figures 5 and 6 show the performance change trend of the proposed DCBTSVM recommendation model as the sample label proportion increases from 20% to 60%. In each iteration, the DCBTSVM model uses the designed active learning strategy to inquire and label unlabeled movie samples. Then, the labeled samples are put into the training set as labeled samples, and the model is retrained, to iterate continuously until the termination condition.

Figures 5 and 6 reveal that the performance of the proposed recommendation algorithm improves as the sample label proportion increases. First, when the number of clusters  $k = 30$ , the recommendation performance is better than that when  $k = 40$ . When clustering according to user characteristics,  $k = 30$  case yields a wider range of user interests and preferences. For new users, the accuracy rate of being correctly classified into one of the classes is slightly higher; thus, the samples labeled by active learning appear to better reflect the real interests of the users. Second, the preferences of users (both new and old) are better labeled as the proportion of labeled samples increases, thus supplementing the scarce data and making the interest model more effective.

It is worth noting that the active learning strategy does not label all unlabeled samples, but labels that are the most valuable and as few as possible. On the one hand, it can not only reduce the labeling cost of samples; on the other hand, it can reduce the time complexity of model training.

**6.2.3. Comparison with Other Methods.** To verify the effectiveness of the DCBTSVM algorithm, we compare its precision and F score with that of SVM, TSVM, ALTSVM, and UserCF-based models (Figures 7 and 8), where SVM algorithm only uses the labeled samples and performs well in

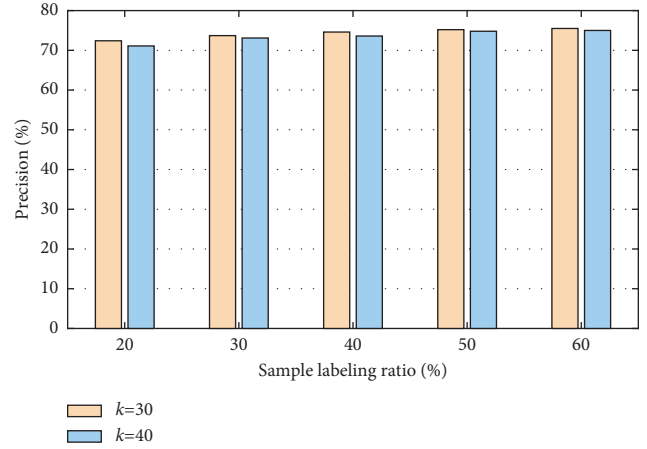


FIGURE 5: Recommendation accuracy of the DCBTSVM algorithm with different sample labeling ratios when  $k = 30$  and  $k = 40$ , respectively.

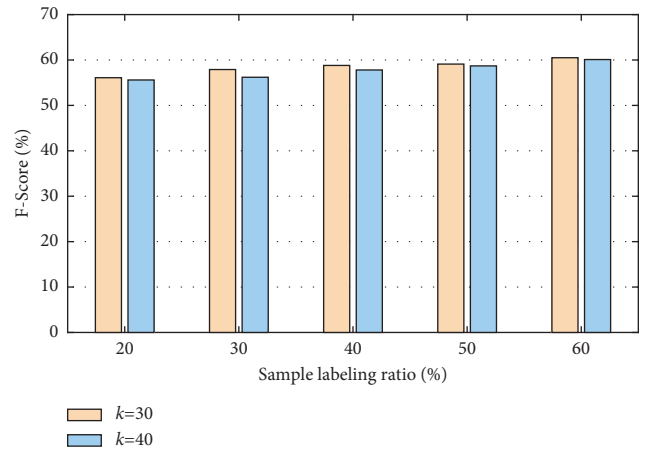


FIGURE 6: F scores of the DCBTSVM algorithm when  $k = 30$  and  $k = 40$  with different sample labeling ratios.

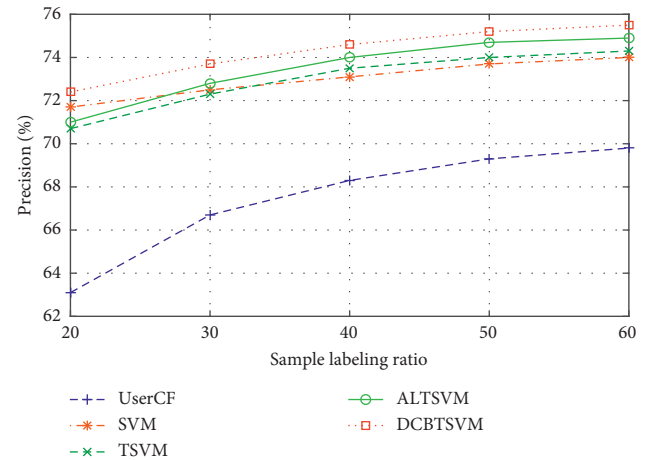


FIGURE 7: Recommendation accuracy of five algorithms with different sample labeling ratios.

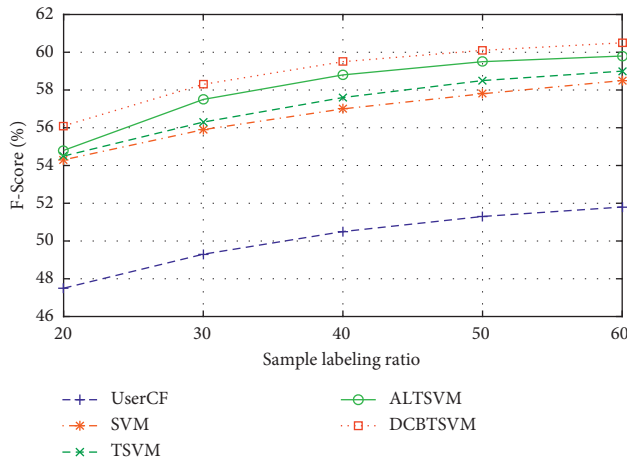


FIGURE 8: F scores of five algorithms with different sample labeling ratios.

the case of a sufficient number of labeled samples, but the performance will be degraded when the labeled samples are scarce; ALTSVM is the DCBTSVM algorithm without the clustering analysis.

From Figures 7 and 8, it can be found that the precision and F score of the DCBTSVM model are better than those of other recommendation algorithms. Its level of precision and F score also increases with the number of labeled samples, due to the implementation of the active learning strategy. First, the model selects fewer but higher quality samples for labeling, which compensates for the scarce data and enriches the interest model. Second, as it does not rely on the similarity between users or items, the recommendations are not limited to similar modules, and therefore, user choices and cognitive domains can be expanded and their preferences better described. Third, the integration of active learning and semi-supervised learning compensates for the shortcomings of both methods while amplifying their advantages, thus improving the quality of sample labeling. Therefore, the practical value of the method proposed in this study is evident.

## 7. Conclusion

We propose a novel model-based collaborative filtering algorithm that combines active learning and the semi-supervised transductive support vector machine, which we term DCBTSVM. We use the clustering method to cluster similar users together, thereby alleviating the cold start problem of new users. The sample labeling method design is based on distance measurement and the use of a multiclassifier voting decision to label unlabeled “user-item” association data, thus solving the problems of cold start and data sparsity. The resulting DCBTSVM-based recommendation model is effective and offers personalized and high-quality recommendations. Experimental results obtained using MovieLens data demonstrate that the proposed model provides efficient and accurate recommendations.

## Data Availability

The data set used in the experiment of this study is a public data set, which can be freely obtained by researchers. For details, the following website can be reversed: <https://grouplens.org/datasets/movielens/>.

## Conflicts of Interest

The authors declare no conflicts of interest.

## Acknowledgments

This work was partially supported by the National Natural Science Foundation of China (grant nos. 72161005, 71901078, and 71964009), Technology Foundation of Guizhou Province (grant nos. QianKeHeJiChu[2020]1Y269 and [2018]1068), High-Level Talent Project of Guizhou Institute of Technology (grant no. XJGC20190929), and Special Key Laboratory of Artificial Intelligence and Intelligent Control of Guizhou Province (grant no. KY[2020]001).

## References

- [1] S. Zhang, L. Yao, A. Sun, and Y. Tay, “Deep learning based recommender system: a survey and new perspectives,” *ACM Computing Surveys*, vol. 52, no. 1, pp. 1–38, 2019.
- [2] J. Bu, X. Shen, B. Xu, C. Chen, X. He, and D. Cai, “Improving collaborative recommendation via user-item subgroups,” *IEEE Transactions on Knowledge and Data Engineering*, vol. 28, no. 9, pp. 2363–2375, 2016.
- [3] Y. Shi, M. Larson, and A. Hanjalic, “Collaborative filtering beyond the user-item matrix,” *ACM Computing Surveys*, vol. 47, no. 1, pp. 1–45, 2014.
- [4] Z. Cui, X. Xu, F. Xue et al., “Personalized recommendation system based on collaborative filtering for IoT scenarios,” *IEEE Transactions on Services Computing*, vol. 13, no. 4, pp. 685–695, 2020.
- [5] A. Da’u, N. Salim, I. Rabiou, and A. Osman, “Recommendation system exploiting aspect-based opinion mining with deep learning method,” *Information Sciences*, vol. 512, pp. 1279–1292, 2020.
- [6] M. Li, Y. Li, W. Lou, and L. Chen, “A hybrid recommendation system for Q&A documents,” *Expert Systems with Applications*, vol. 144, Article ID 113088, 2020.
- [7] W. Zhang and J. Wang, “A collective bayesian Poisson factorization model for cold-start local event recommendation,” in *Proceedings of the 21th ACM SIGKDD International Conference on Knowledge Discovery and Data Mining*, pp. 1455–1464, Sydney NSW Australia, August 2015.
- [8] L. Wang, Y. Liu, and J. Wu, “Research on financial advertisement personalised recommendation method based on customer segmentation,” *International Journal of Wireless and Mobile Computing*, vol. 14, no. 1, pp. 97–101, 2018.
- [9] Z. Hu and Y. Hu, “Research on collaborative filtering recommendation bottleneck problem,” *Wireless Internet Technology*, vol. 9, no. 46, pp. 100–101, 2016.
- [10] N. Rubens, M. Elahi, M. Sugiyama, and D. Kaplan, “Active learning in recommender systems,” *Recommender Systems Handbook*, Springer, Boston, MA, USA, pp. 809–846, 2015.
- [11] M. Elahi, F. Ricci, and N. Rubens, “Active learning strategies for rating elicitation in collaborative filtering: a system-wide

- perspective,” *ACM Transactions on Intelligent Systems & Technology*, vol. 5, no. 1, pp. 1–33, 2014.
- [12] M. Elahi, V. Reppas, and F. Ricci, “Rating elicitation strategies for collaborative filtering,” in *Proceedings of the International Conference on Electronic Commerce and Web Technologies*, pp. 160–171, Toulouse, France, 29 August 2011.
- [13] R. Karimi, C. Freudenthaler, A. Nanopoulos, and L. Schmidt-Thieme, “Non-myopic active learning for recommender systems based on matrix factorization,” in *Proceedings of the 2011 IEEE International Conference on Information Reuse & Integration*, pp. 299–303, Nevada, USA, 3 August 2011.
- [14] A. M. Rashid, I. Albert, D. Cosley, and S. K. Lam, “Getting to know you: learning new user preferences in recommender systems,” in *Proceedings of the 7th International Conference on Intelligent User Interfaces*, pp. 127–134, San Francisco, CA, USA, 13 January 2002.
- [15] Y. Song, L. Zhang, and C. L. Giles, “Automatic tag recommendation algorithms for social recommender systems,” *ACM Transactions on the Web*, vol. 5, no. 1, pp. 1–31, 2011.
- [16] M. Li, L. Wen, and F. Chen, “A novel Collaborative Filtering recommendation approach based on Soft Co-Clustering,” *Physica A: Statistical Mechanics and Its Applications*, vol. 561, Article ID 125140, 2021.
- [17] M.-L. Wu, C.-H. Chang, and R.-Z. Liu, “Integrating content-based filtering with collaborative filtering using co-clustering with augmented matrices,” *Expert Systems with Applications*, vol. 41, no. 6, pp. 2754–2761, 2014.
- [18] N. Mirbakhsh and C. X. Ling, “Leveraging clustering to improve collaborative filtering,” *Information Systems Frontiers*, vol. 20, no. 1, pp. 111–124, 2018.
- [19] T. Xiao and H. Shen, “Neural variational matrix factorization for collaborative filtering in recommendation systems,” *Applied Intelligence*, vol. 49, no. 10, pp. 3558–3569, 2019.
- [20] Y. Li, D. Wang, H. He, L. Jiao, and Y. Xue, “Mining intrinsic information by matrix factorization-based approaches for collaborative filtering in recommender systems,” *Neurocomputing*, vol. 249, pp. 48–63, 2017.
- [21] X. Yuan, L. Han, S. Qian, G. Xu, and H. Yan, “Singular value decomposition based recommendation using imputed data,” *Knowledge-Based Systems*, vol. 163, pp. 485–494, 2019.
- [22] T. Joachims, “Transductive inference for text classification using support vector machines,” in *Proceedings of the 16th International Conference on Machine Learning*, pp. 200–209, San Francisco CA, 27 June 1999.
- [23] T. Joachims, “Transductive support vector machines,” *Semi-Supervised Learning*, pp. 105–118, MIT Press, Cambridge, MA, 2006.
- [24] T. Joachims, *Learning to Classify Text Using Support Vector machines*, Springer Science & Business Media, Berlin, Germany, 2002.
- [25] X. Wang, Z. Dai, H. Li, and J. Yang, “A new collaborative filtering recommendation method based on transductive SVM and active learning,” *Discrete Dynamics in Nature and Society*, vol. 2020, Article ID 6480273, 15 pages, 2020.
- [26] S. Cassel, F. Howar, B. Jonsson, and B. Steffen, “Active learning for extended finite state machines,” *Formal Aspects of Computing*, vol. 28, no. 2, pp. 233–263, 2016.
- [27] M. Sharma and M. Bilgic, “Evidence-based uncertainty sampling for active learning,” *Data Mining and Knowledge Discovery*, vol. 31, no. 1, pp. 164–202, 2017.
- [28] X. Zhu, J. Lafferty, and Z. Ghahramani, “Combining active learning and semi-supervised learning using Gaussian fields and harmonic functions,” in *Proceedings of the ICML 2003 Workshop on the Continuum from Labeled to Unlabeled Data in Machine Learning and Data Mining*, pp. 58–65, Washington, DC, USA, March 2003.
- [29] H. Hassanzadeh and M. Keyvanpour, “A two-phase hybrid of semi-supervised and active learning approach for sequence labeling,” *Intelligent Data Analysis*, vol. 17, no. 2, pp. 251–270, 2013.
- [30] GroupLens. MovieLensdatasets[EB/OL]. <https://grouplens.org/datasets/movielens.2016-11-03/2021-08-10>.

## Research Article

# A Network Sampling Strategy Inspired by Epidemic Spreading

Qiang Dong <sup>1</sup>, En-Yu Yu <sup>1</sup>, and Wen-Jun Li <sup>2</sup>

<sup>1</sup>School of Computer Science and Engineering, University of Electronic Science and Technology of China, Chengdu 611731, China

<sup>2</sup>School of Software and Services Outsourcing, Suzhou Vocational Institute of Industrial Technology, Suzhou 215004, China

Correspondence should be addressed to Qiang Dong; [dongq@uestc.edu.cn](mailto:dongq@uestc.edu.cn)

Received 3 November 2021; Accepted 31 December 2021; Published 28 February 2022

Academic Editor: Wei Wang

Copyright © 2022 Qiang Dong et al. This is an open access article distributed under the Creative Commons Attribution License, which permits unrestricted use, distribution, and reproduction in any medium, provided the original work is properly cited.

Nowadays, network sampling has become an indispensable premise and foundation for large-scale network analysis, and its effectiveness determines to a large extent the reliability and practicability of the subsequent network analysis results. In this paper, we propose a network sampling algorithm inspired by an epidemic spreading model named the contact process. The contact process is similar to the random walk process but different from it in two key points. First, at each time step, a randomly selected sampled node rather than the latest sampled node is responsible for recruiting a new node from its neighborhood. Second, the responsible node recruits one of its neighbor nodes with a probability inversely proportional to the degree of this neighbor node, instead of equal probability. Experiments on nine indiscriminately selected real-world networks show that our proposed sampling algorithm has a significant advantage in preserving two basic network properties, the degree distributions and clustering coefficient distributions of original networks, compared with seven classical sampling methods.

## 1. Introduction

In recent decades, the rapid development of storage technology has allowed online social network (OSN) providers to deposit almost all user-generated information every day. The analysis of OSNs is receiving remarkable research attention from both the academic and industrial communities. However, in some scenarios, some access restrictions are imposed on the network such that it is hard or infeasible for people to study the whole network. In other scenarios, the network is, however, available but too large to be stored and analyzed in a reasonable amount of memory and time. In the face of these problems, network sampling techniques have emerged to help us effectively and efficiently study and analyze real-world networks. The concept of network sampling can be simply described as follows. Given a network  $G = (V, E)$  and the sampling ratio  $\rho$ , where  $0 < \rho \ll 1$ , the primary goal of network sampling is to construct a representative subnetwork  $G_S = (V_S, E_S)$  which preserves the most important properties of the original network, where  $V_S \subset V$ ,  $E_S \subset E$ , and  $|V_S| = \rho * |V| = N_S$ .

Nowadays, network sampling has become an indispensable premise and foundation for large-scale network

analysis, and its effectiveness determines to a large extent the reliability and practicability of the subsequent network analysis results. Besides, network sampling also has a wide spectrum of applications, e.g., surveying hidden population in sociology, visualizing social graph, scaling down Internet AS graph, and graph sparsification [1].

A large number of sampling techniques have been proposed in the past few decades, designed for various purposes and for preserving different network properties [2]. These sampling techniques can be categorized into two groups: random selection and network exploration techniques. In the first group, nodes or links are recruited in the sample uniformly at random or proportional to some particular characteristic like degree or PageRank values [3]. In the second group, the sample network starts from a randomly selected seed node and is expanded following the local connections of previously sampled nodes.

Leskovec and Faloutsos [4] show that, among the typical network sampling methods, random walk (RW) and forest fire (FF) sampling methods have the best overall performance. Recently, Blagus et al. [3] empirically compared 11 representative network sampling methods on 12 real-world networks and concluded that breadth-first search (BFS) and

random walk with subgraph induction (RWI) sampling methods show the best overall performance in preserving the degree and clustering coefficient distribution of original networks. Next, we will briefly review these sampling methods, which will be used as comparing counterparts of our proposed algorithm.

Random walk (RW), forest fire (FF), and breadth-first search (BFS) are somewhat similar to each other. Initially, the sampled node set  $V_S$  and edge set  $E_S$  are both empty. At the first step, a randomly selected node is added into  $V_S$ . At each following step, for every node  $u$  added into  $V_S$  at the previous step,  $j$  randomly selected neighbor nodes of  $u$ , say  $v_1, v_2, \dots, v_j$ , are added into  $V_S$ , and the corresponding edges  $(u, v_1), (u, v_2), \dots, (u, v_j)$  are added into  $E_S$ . For RW,  $j = 1$ ; for FF,  $j$  follows a geometric distribution with mean value  $p/(1 - p)$ , where we set  $p$  to be 0.7 as suggested in [4]; for BFS,  $j = k_u$ , where  $k_u$  is the degree of node  $u$ . This step repeats until the sampling size is reached; that is,  $|V_S| = \rho * |V|$ . Another key different point is that the random walk is memoryless and a visited node has a probability of being visited again in the future, while the forest fire and breadth-first search never include the repeated nodes.

Besides the abovementioned methods, Metropolis–Hastings random walk (MHRW) is demonstrated to be a well-performed sampling method in the literature [5, 6]. It achieves a uniform distribution of sampled nodes by the following transition probability:

$$p_{u,v}^{MH} = \begin{cases} \min\left\{\frac{1}{k_u}, \frac{1}{k_v}\right\}, & \text{if } v \text{ is a neighbor of } u, \\ 1 - \sum_{w \neq u} p_{u,w}^{MH}, & \text{if } u = v, \\ 0, & \text{otherwise.} \end{cases} \quad (1)$$

Blagus et al. [3] proposed analyzing the sampling methods with subgraph induction, where the final sample network is constructed from a generated sample and all the existing edges between any two nodes of this sample. They empirically show that RW, FF, and MHRW with subgraph induction, named RWI, FFI, and MHRWI, improve the performance of the corresponding methods without subgraph induction. Therefore, RWI, FFI, and MHRWI are also used as baseline algorithms in this paper.

In this paper, we propose a network sampling algorithm inspired by an epidemic spreading model, the contact process, and thus, it is called contact process sampling (CPS). It is similar to RW but has two key different points. First, at each time step, a randomly selected sampled node rather than the latest sampled node is responsible for recruiting a new node from its neighborhood. Second, a sampled node chooses one of its neighbor nodes with a probability inversely proportional to the degree of this neighbor node, instead of an equal probability.

The rest of this paper is organized as follows. Section 2 describes the contact process and introduces the CPS algorithm. Section 3 compares the sampling quality of CPS

with the aforementioned well-performed sampling methods. Section 4 concludes the whole work and makes some remarks.

## 2. Proposed Model

The contact process, which was first proposed as a susceptible-infected-susceptible (SIS) model for epidemic spreading, has found wide applications in science and engineering [7]. A general contact process on a network is described as follows. Initially, a set of nodes are infected by a virus (or carry a piece of information), and other nodes on the network are susceptible (not infected). At each time step, an infected node is chosen at random, say node  $u$ . With probability  $p$ , the virus on node  $u$  dies, and node  $u$  becomes susceptible again; with probability  $1 - p$ , the virus on node  $u$  selects one neighbor of  $u$  to contact, say  $v$ . If  $v$  is already infected, nothing happens; if  $v$  is susceptible, it gets infected.

In such a contact process, the fraction of infected nodes on a given network in an ultimately steady state is dependent on two critical factors: the aforementioned death rate  $p$  and the contact probability  $W(k)$ , which is the probability that an infected node chooses a neighbor node of degree  $k$  to contact. Yang et al. [7] proved that, when  $p$  is smaller than the threshold value, if the contact probability  $W(k)$  takes the form of  $W(k) \sim k^\beta$ , the fraction of infected nodes in the ultimately steady state is maximized when  $\beta = -1$ .

In this paper, we propose a network sampling algorithm named contact process sampling (CPS), which employs a process analogous to the contact process across the network. In order to get a sample network of  $N_S$  nodes as soon as possible, we eliminate the effect of the death rate  $p$  from our CPS model by setting it to be 0. To ensure the connectedness of a sample network, the CPS algorithm starts from only one node.

The CPS algorithm is presented by Algorithm 1. Initially, a randomly chosen node is recruited into the sample set. At each time step, a sampled node is chosen at random, say node  $u$ . Following the conclusion of Yang et al., node  $u$  chooses a neighbor node  $v$  to recruit into the sample set with probability  $p_{u,v} = k_v^{-1} / \sum_{w \in \Gamma_u} k_w^{-1}$ , where  $k_v$  is the degree of node  $v$  and  $\Gamma_u$  represents the set of  $u$ 's neighbor nodes. This recruitment step repeats until the sample set contains  $N_S$  distinct nodes. Then, we construct the final sample network with these sampled nodes and the links which connect any two of these sampled nodes in the original network.

## 3. Performance Evaluation

**3.1. Datasets.** Nine indiscriminately selected real-world networks from KONECT [8] are employed to test the performance of sampling models. They are all undirected and unweighted networks, and their basic statistics are presented in Table 1. The fill of a network is the proportion of edges to the total number of possible edges. The global clustering coefficient is defined as the probability that two incident edges are completed by a third edge to form a triangle. Assortativity is defined as the Pearson correlation coefficient between the degrees of connected nodes. For

```

Input: an undirect and unweighted graph  $G = (V, E)$ ; the sample ratio  $\rho$ , where  $0 < \rho < 1$ ;
Output: a sample graph  $G_S = (V_S, E_S)$ , where  $V_S \subseteq V$ ,  $E_S \subseteq E$  and  $|V_S| = \rho * |V|$ ;
(1) Randomly select one node  $u_0 \in V$ , and let  $V_S = \{u_0\}$  and  $E_S = \emptyset$ ;
(2) while  $|V_S| = \rho * |V|$  do
(3) Randomly select one node  $v$  from  $V_S$ ;
(4) Select one node  $w$  from the neighborhood of  $v$ , with probability inversely proportional to the degree of  $w$ ;
(5)  $V_S = V_S \cup \{w\}$ ;
(6) end while
(7) for  $(x, y) \in E$  do
(8) if  $x \in V_S$  and  $y \in V_S$  then
(9)  $E_S = E_S \cup \{(x, y)\}$ ;
(10) end if
(11) end for
(12) return  $G_S = (V_S, E_S)$ ;

```

ALGORITHM 1: Contact process sampling.

TABLE 1: Basic statistics of real-world networks used in this paper.

Network	Category	Nodes	Edges	Fill	Avg. degree	Global clust. (%)	Assortativity
PowerGrid	Infrastructure	4941	6594	$5.40 \times 10^{-4}$	2.669	10.30	0.003 46
Amazon	Miscellaneous	334 863	925 872	$1.65 \times 10^{-5}$	5.530	20.50	-0.05882
WordNet	Lexical	146 005	656 999	$6.16 \times 10^{-5}$	9.000	9.58	-0.06233
AstroPh	Coauthorship	18 771	198 050	$1.12 \times 10^{-3}$	21.102	31.80	0.205 13
Livemocha	Social	104 103	2193 083	$4.05 \times 10^{-4}$	42.133	1.41	-0.14677
Gowalla	Social	196 591	950 327	$4.92 \times 10^{-5}$	9.668	2.35	-0.02926
Brightkite	Social	58 228	214 078	$1.26 \times 10^{-4}$	7.353	11.10	0.010 82
Douban	Social	154 908	327 162	$2.73 \times 10^{-5}$	4.224	1.04	-0.18033
Flickr	Miscellaneous	105 938	2316 948	$4.13 \times 10^{-4}$	43.742	40.20	0.246 85

other characteristics of these networks, the reader is referred to KONECT [8].

In this paper, we consider the sample ratio ranging from 0.2% to 20% of original networks (by step of 0.2% in 0.2% ~ 1% and 2% in 2% ~ 20%) as suggested in [3]. For each network, we perform 30 realizations of each sampling technique and each sample ratio. For each run of the exploration techniques, the sample starts from a randomly selected new seed node.

**3.2. Evaluation Measures.** For the evaluation of sampling algorithms, two well-known and widely used network statistics are used to measure the representativeness of the sampled network. They are degree distribution (DD) as a global statistical property and clustering coefficient distribution (CCD) as a local statistical property. The DD of a network refers to the probability distribution of degrees of all nodes in the network [9] and is represented by the fraction  $p_k$  of nodes of degree  $k$ ,  $k > 0$ . The clustering coefficient of a node in a network is the proportion of that node's neighbors that are connected, and the CCD of a network refers to the probability distribution of the clustering coefficient of all nodes in the network [10].

We compare the DD and CCD of the sample network and the original network by the Kolmogorov–Smirnov D-statistic (KSD). KSD is used to measure the agreement of

two cumulative distribution functions [11]: original distribution  $F_1$  and estimated distribution  $F_2$ . It is defined as  $KSD = \max_x \{|F_1(x) - F_2(x)|\}$ , where  $x$  is over the range of the random variable. Clearly, it is a value between 0 and 1. The closer it is to zero, the higher is the similarity between the two distributions. Note that KSD does not address the issue of the scaling but rather compares the shape of the (normalized) distribution [4].

**3.3. Algorithm Comparison.** The comparison of sampling techniques based on degree distribution is shown in Figure 1. We can see that, in most datasets, the techniques without subgraph induction (RW, FF, and MHRW) perform significantly different from other methods. This group of techniques approximates the degree distribution of the original networks with a larger deviation than others (except for PowerGrid and Douban). Therefore, this observation reinforces the conclusion of Blagus et al. [3] that the techniques with induction improve the performance of the corresponding techniques without it.

As for the performance of techniques with subgraph induction, the nine datasets can be categorized into two groups. In the first group of datasets (PowerGrid, Amazon, WordNet, AstroPh, and Livemocha), the techniques with subgraph induction perform similarly to each other, and our proposed CPS algorithm is the best in three datasets



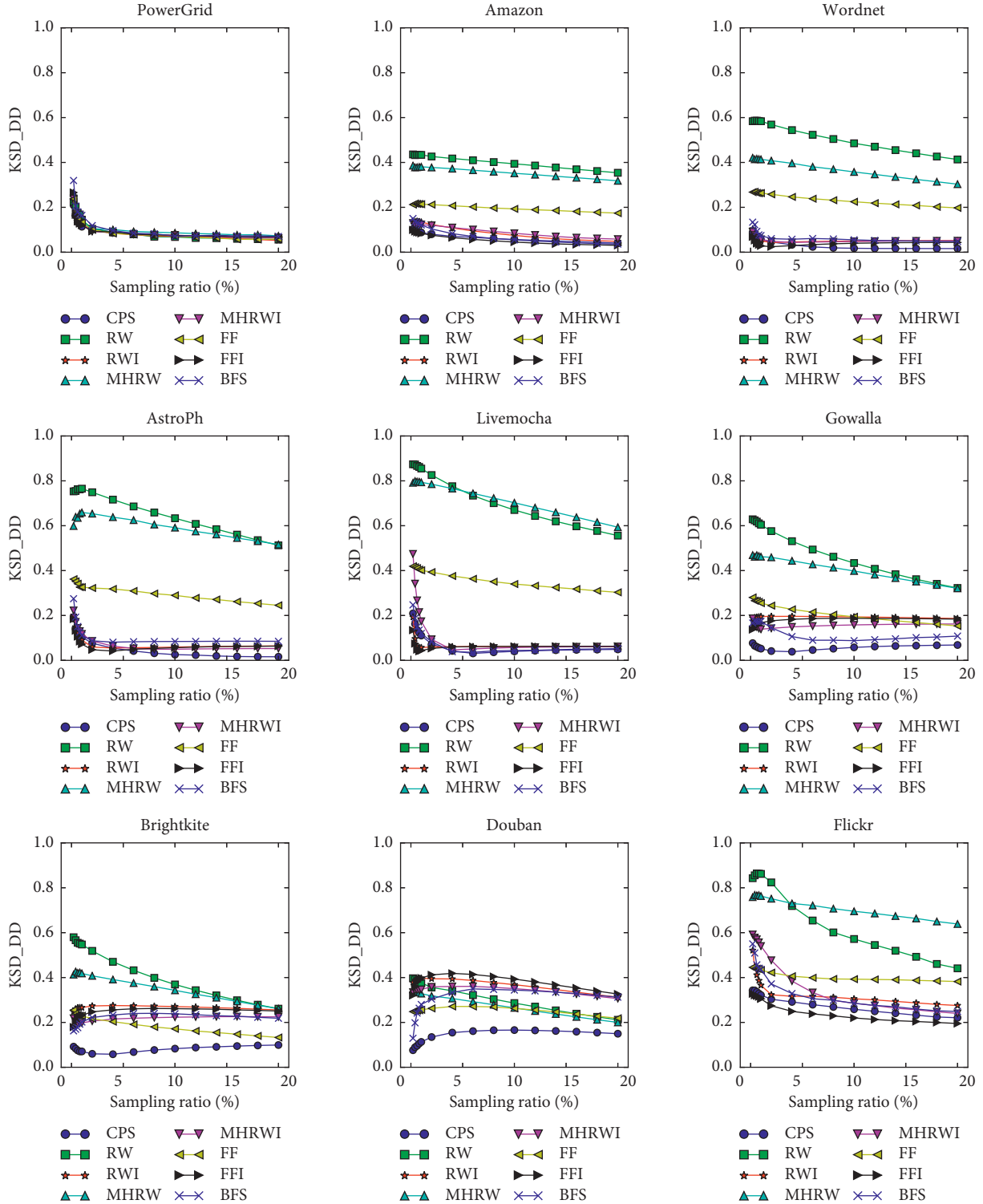


FIGURE 1: Comparison of sampling techniques based on degree distribution.

(WordNet, AstroPh, and Livemocha) and has a negligible difference from the best ones in the other two datasets. In the second group of datasets (Gowalla, Brightkite, Douban, and Flickr), the techniques with subgraph induction perform greatly different from each other. Our proposed CPS algorithm shows a significant advantage in three datasets

(Gowalla, Brightkite, and Douban) and is the second-best in Flickr. In general, our proposed CPS algorithm is the best performing technique in preserving the degree distribution of the original networks.

The comparison of sampling techniques based on clustering coefficient distribution is shown in Figure 2. Similarly

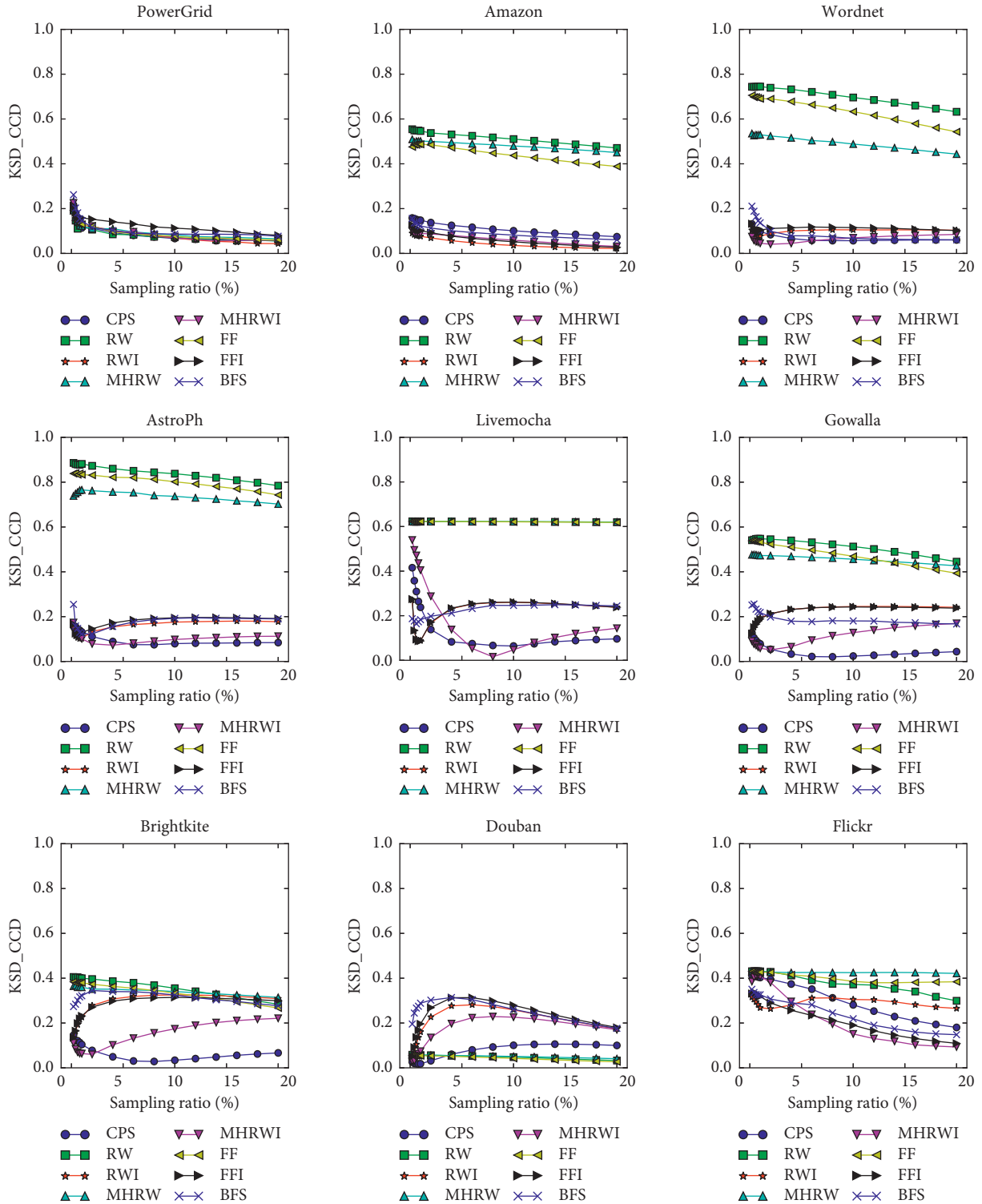


FIGURE 2: Comparison of sampling techniques based on clustering coefficient distribution.

to that of degree distribution, the techniques with subgraph induction perform better than the corresponding techniques without subgraph induction in most datasets (except for PowerGrid and Douban). The three techniques without subgraph induction, RW, FF, and MHRW, unless otherwise specified, are excluded from our following discussion.

The five techniques with subgraph induction have a similar declining shape of KSD plot in 3 datasets, PowerGrid, Amazon, and Flickr, where the CPS algorithm is comparable to other techniques. In contrast, in the other 6 networks, the KSD plots of RWI, FFI, and BFS algorithms begin to increase with the growth of sampling ratio, except for BFS in

TABLE 2: The D-statistics of degree distributions of 8 sampling algorithms on 9 real-world datasets, where the sampling ratio is 10%.

Network	RW	RWI	FF	FFI	MHRW	MHRWI	BFS	CPS
PowerGrid	<b>0.068</b>	0.071	0.075	0.075	0.086	0.077	0.072	0.072
Amazon	0.394	0.075	0.193	<b>0.045</b>	0.352	0.084	0.055	0.057
WordNet	0.485	0.050	0.225	0.040	0.358	0.048	0.055	<b>0.018</b>
AstroPh	0.633	0.059	0.290	0.056	0.591	0.050	0.084	<b>0.026</b>
Livemocha	0.670	0.062	0.340	0.062	0.702	0.057	0.044	<b>0.040</b>
Gowalla	0.434	0.194	0.194	0.188	0.398	0.158	0.088	<b>0.058</b>
Brightkite	0.369	0.271	0.171	0.261	0.343	0.223	0.238	<b>0.083</b>
Douban	0.286	0.368	0.263	0.393	0.265	0.351	0.344	<b>0.166</b>
Flickr	0.572	0.305	0.393	<b>0.220</b>	0.695	0.285	0.285	0.258

TABLE 3: The D-statistics of clustering coefficient distributions of 8 sampling algorithms on 9 real-world datasets, where the sampling ratio is 10%.

Network	RW	RWI	FF	FFI	MHRW	MHRWI	BFS	CPS
PowerGrid	0.072	0.069	0.076	0.113	0.082	0.070	0.086	<b>0.067</b>
Amazon	0.510	<b>0.036</b>	0.437	0.052	0.479	0.059	0.082	0.101
WordNet	0.696	0.105	0.633	0.115	0.488	0.070	0.067	<b>0.057</b>
AstroPh	0.838	0.176	0.802	0.195	0.737	0.098	0.192	<b>0.079</b>
Livemocha	0.622	0.261	0.621	0.261	0.621	<b>0.047</b>	0.246	0.064
Gowalla	0.513	0.245	0.469	0.243	0.456	0.129	0.181	<b>0.024</b>
Brightkite	0.355	0.326	0.334	0.314	0.340	0.174	0.325	<b>0.034</b>
Douban	0.048	0.259	<b>0.042</b>	0.279	0.051	0.226	0.261	0.101
Flickr	0.372	0.305	0.386	0.190	0.425	<b>0.151</b>	0.220	0.281

WordNet and Gowalla. Fortunately, the KSD plots of the CPS algorithm are always declining in these 6 networks, and the KSD values are very small compared with those of the RWI, FFI, and BFS algorithms. The performance of MHRWI is intermediate between that of CPS and those of RWI, FFI, and BFS, where the KSD value is closer to the former, and the shape of the KSD plot is similar to the latter. In general, the CPS algorithm has the best overall performance in preserving the clustering coefficient distribution of the original networks.

To quantitatively demonstrate the superiority of CPS to other methods, Tables 2 and 3 present the KSD values of DD and CCD produced by 8 sampling techniques on 9 datasets when the sampling ratio is 10% as suggested in [3], where the best and second best values for every dataset are highlighted in bold type. For DD, the CPS algorithm is the best in 6 out of 9 datasets, and for CCD, the CPS algorithm is the best in 5 out of 9 datasets. Other than CPS, no algorithm is ranked in the first position in more than 2 datasets, whether DD or CCD or both. Recall that the nine real-world network datasets are indiscriminately selected from KONECT [8]. We conclude that the CPS algorithm has a significant advantage in preserving degree distributions and clustering coefficient distributions of original networks.

#### 4. Concluding Remarks

In this paper, we proposed a network sampling strategy inspired by the contact process and empirically validated its superior performance in preserving two important structural properties of original networks. Although it is a little similar to random walk sampling, two key different

operations from RW make it produce better sample network than RW and several typical RW-variant sampling methods.

There is much work that remains to be done in the future. First of all, test of the CPS algorithm in preserving other properties of the original network would be useful to show possible limits of its applicability. Second, one should also investigate the characteristics of some datasets, typically Douban, where the sampling methods without subgraph induction perform better than the ones with subgraph induction. Finally, but not the least, the function approximation of a sample network is worthy of exploration. For example, the comparison of the epidemic spreading process on sample and original networks may be the topic of our next work [12].

#### Data Availability

The readers can access all the 9 datasets supporting the conclusions of the study from <http://konect.cc/>, and the details are listed as follows: PowerGrid, <http://konect.cc/networks/opsahl-powergrid/>; Amazon, <http://konect.cc/networks/com-amazon/>; WordNet, <http://konect.cc/networks/wordnet-words/>; AstroPh, <http://konect.cc/networks/ca-AstroPh/>; Livemocha, <http://konect.cc/networks/livemocha/>; Gowalla, [http://konect.cc/networks/loc-gowalla\\_edges/](http://konect.cc/networks/loc-gowalla_edges/); Brightkite, [http://konect.cc/networks/loc-brightkite\\_edges/](http://konect.cc/networks/loc-brightkite_edges/); Douban, <http://konect.cc/networks/douban/>; and Flickr, <http://konect.cc/networks/flickrEdges/>

#### Conflicts of Interest

The authors declare that they have no conflicts of interest.

## References

- [1] P. Hu and W. C. Lau, "A survey and taxonomy of graph sampling," 2013, <https://arxiv.org/abs/1308.5865>.
- [2] D. D. Heckathorn and C. J. Cameron, "Network sampling: from snowball and multiplicity to respondent-driven sampling," *Annual Review of Sociology*, vol. 43, no. 1, pp. 9.1–9.19, 2017.
- [3] N. Blagus, L. Šubelj, and M. Bajec, "Empirical comparison of network sampling: h," *Physica A: Statistical Mechanics and Its Applications*, vol. 477, pp. 136–148, 2017.
- [4] J. Leskovec and C. Faloutsos, "Sampling from large graphs," in *Proceedings of the 20th ACM SIGKDD International Conference on Knowledge Discovery and Data Mining*, pp. 631–636, Seoul, South Korea, May 2006.
- [5] M. Gjoka, M. Kurant, C. T. Butts, and A. Markopoulou, "Walking in facebook: a case study of unbiased sampling of OSNs," in *Proceedings of the 2010 IEEE INFOCOM*, pp. 1–9, IEEE, San Diego, CA, USA, March 2010.
- [6] A. H. Rasti, M. Torkjazi, R. Rejaie, N. Duffield, W. Willinger, and D. Stutzbach, "Respondent-driven sampling for characterizing unstructured overlays," in *Proceedings of the INFOCOM 2009*, pp. 2701–2705, IEEE, Rio de Janeiro, Brazil, April 2009.
- [7] R. Yang, T. Zhou, Y. B. Xie, Y. C. Lai, and B. H. Wang, "Optimal contact process on complex networks," *Physical review. E, Statistical, nonlinear, and soft matter physics*, vol. 78, no. 6, Article ID 066109, 2008.
- [8] J. Kunegis, "KONECT-the koblenz network collection," in *Proceedings of the 22nd international conference on World Wide Web companion*, pp. 1343–1350, Rio de Janeiro, Brazil, May 2013.
- [9] A. L. Barabasi and R. Albert, "Emergence of scaling in random networks," *Science (New York, N.Y.)*, vol. 286, no. 5439, pp. 509–512, 1999.
- [10] D. J. Watts and S. H. Strogatz, "Collective dynamics of 'small-world' networks," *Nature*, vol. 393, no. 6684, pp. 440–442, 1998.
- [11] N. K. Ahmed, J. Neville, and R. Kompella, "Network sampling: from static to streaming graphs," *ACM Transactions on Knowledge Discovery from Data*, vol. 8, no. 2, pp. 1–56, 2013.
- [12] Z. S. Jalali, A. Rezvanian, and M. R. Meybodi, "Social network sampling using spanning trees," *International Journal of Modern Physics C*, vol. 27, no. 5, Article ID 1650052, 2016.

## Research Article

# Dynamical Behavior of Hybrid Propagation of Computer Viruses

Qingyi Zhu <sup>1,2</sup>, Pingfan Xiang,<sup>2</sup> Xuhang Luo <sup>1</sup>, and Chenquan Gan <sup>3</sup>

<sup>1</sup>School of Cyber Security and Information Law, Chongqing University of Posts and Telecommunications, Chongqing 400065, China

<sup>2</sup>School of Computer Science and Technology, Chongqing University of Posts and Telecommunications, Chongqing 400065, China

<sup>3</sup>School of Communication and Information Engineering, Chongqing University of Posts and Telecommunications, Chongqing 400065, China

Correspondence should be addressed to Chenquan Gan; gcq2010ccqu@163.com

Received 3 November 2021; Revised 1 January 2022; Accepted 12 January 2022; Published 9 February 2022

Academic Editor: Mamoun Alazab

Copyright © 2022 Qingyi Zhu et al. This is an open access article distributed under the Creative Commons Attribution License, which permits unrestricted use, distribution, and reproduction in any medium, provided the original work is properly cited.

Considering the horizontal and vertical propagation of computer viruses over the Internet, this article proposes a hybrid susceptible-latent-breaking-recovered-susceptible (SLBRS) model. Through mathematical analysis of the model, two equilibria (virus-free and virose equilibria) and their global stabilities are both proved depending on the basic reproduction number  $R_0$ , which is affected by the vertical propagation of infected computers. Moreover, the feasibility of the obtained results is verified by numerical simulations. Finally, the dependence of  $R_0$  on system parameters and the parameters affecting the stability level of infected computers are both analyzed.

## 1. Introduction

Computer virus is a malevolent network code designed to disseminate from one device to another [1]. Even minor computer virus can wreak havoc on a system performance, consume computer memory, and cause frequent computer crashes. With all the technological advances of the 21st century, computer virus grew at a breakneck rate. Mail viruses and macroviruses that rely on the Internet to spread have emerged in large numbers. Due to the characteristics of fast-spreading, strong concealment, and great destructiveness of computer viruses, the work of anticomputer virus becomes very difficult [2], which has brought immeasurable losses to people. At the beginning of the twenty-first century, email was an important way for computer viruses to spread. The Medsa virus and the love letter virus spread rapidly around the world via email. In 2017, the WannaCry ransomware quickly infected extensive computers in a short period, causing incalculable damage [3]. On April 12, 2021, KrebsSecurity, an international information network security media, reported that hackers were selling the personal details of tens of millions of users of ParkMobile, a North American mobile parking application, on a Russian-

language cybercrime forum along with screenshots of the data [4]. Later, Code Red and Nimda virus appeared one after another. These two viruses used a combination of mail transmission and active attack on server vulnerabilities, creating a new way of virus transmission and greatly increasing the speed of virus transmission in the network. Owing to the enormous harm brought by the malevolent virus attack, it is urgent to study the spreading behavior of viruses among network nodes and propose effective prevention and control strategies.

Seeing the resemblance between computer viruses and biological viruses, many researchers use epidemiological models to study the spread of network viruses. In the twentieth century, the author introduced the susceptibility-infection-susceptibility (SIS) model in the field of network viruses [5]. Thereafter, the susceptible-exposed-infected (SEI) model was proposed by introducing latency bins. Xie [6] proposed the SEI model by considering the effect of heterogeneity of email networks on virus propagation. On this basis, increasingly popular models are being used and studied in the field of virus transmission, for example, susceptible-infected-recovered (SIR) models [7–9], susceptible-infected-recovered-susceptible (SIRS) models [10–13],

susceptible-exposed-infected-recovered (SEIR) models [14–17], susceptible-exposed-infected-recovered-susceptible (SEIRS) models [18–21], susceptible-exposed-infected-quarantined-vaccinated (SEIQV) models [22, 23], and susceptible-exposed-infected-quarantined-recovered-susceptible (SEIQRS) models [24–26]. To explicitly compare the individual characteristics of computer virus propagation models, we have made tabular discussions in Table 1.

Based on the direction of computer virus transmission, network viruses can be divided into horizontal transmission and vertical transmission. Horizontal spreading refers to the copying and spreading of malicious programs through the spreading medium between nodes. Specifically, after a network virus infects a computer, it infects other computers associated with it through emails, web browsing, disk media, and mobile media. After these infected computers become new sources of infection, they can infect other computers associated with them in the same way as described above. Vertical transmission refers to the virus attacking the main server, making it a source of infection, and then passing it from the main server to any node. For example, Code Red and Nimda viruses actively attack server vulnerabilities through vertical transmission.

Generally speaking, in real life, once a computer is infected, it is immediately infectious. However, preceding scholars did not notice this difference between computer viruses and biological viruses, and they believed that latent computers are not infectious. The author [33] first noticed this deficiency of the previous computer virus model and proposed the susceptible-latent-breaking-susceptible (SLBS) model that was more consistent with the actual situation in 2012, and then proposed a series of improved models. Subsequently, a four-compartment model called the primitive SLBRS model was proposed by Yang [34]. By studying the safety tendency of a virus system based on security entropy, Tang proposed a new application scenario SLBRS computer virus model [32]. However, these models always focus on the horizontal propagation behavior of computer viruses.

In a computer network, some computer viruses may be transmitted vertically from the master server to any node, such as worms [35]. On the Internet, we have to pay attention to the influence of vertical transmission of computer virus on uninfected new nodes, but the literature on the vertical analysis of computer virus transmission behavior is not extensive. Considering some computer viruses may be vertical transmission from the main server to any node, Kumar [35] proposed the worms in the computer network SEIRS model of vertical transmission. However, this model ignores the fact that computer viruses might be infectious during both the latent and outbreak phases.

Given the vertical spread of computer viruses and the fact that latent computers are still infectious, a new SLBRS model is introduced to discuss the spread of network viruses in both horizontal and vertical directions from a

macroperspective. Admittedly, this model is more sophisticated and reasonable than previous models, with the rapid growth of master servers. We deeply study the dynamics of this model. Qualitative analysis of the model has obtained the virus-free equilibrium and the virose equilibrium. Global stability of the SLBRS model is verified by using the global geometric method. In addition, numerical experiments illustrate the feasibility of the theoretical results, and the parameters of the system are discussed and analyzed.

The rest of this article is organized as follows: In Section 2, we describe the SLBRS model with vertical propagation. In Section 3, we confirm a globally asymptotically stable virus-free equilibrium, and the virose equilibrium is obtained. In Section 4, we perform detailed numerical calculations to verify the local and global stability of the virose equilibrium. In Section 5, the influence of system parameters on  $R_0$  is discussed. In Section 6, we present the numerical simulation results. Finally, Section 7 summarizes this article.

## 2. Mathematical Model Expression

In the SLBRS model with vertical propagation, the networked computers are defined as four types: susceptible nodes ( $S$ ), latent nodes ( $L$ ), breaking-out nodes ( $B$ ), and recovering nodes ( $R$ ).

Let  $S$ ,  $L$ ,  $B$ , and  $R$  represent the proportion of the number of nodes in each of the above four categories among all nodes at a certain time, so we have

$$S + L + B + R = 1. \quad (1)$$

Figure 1 shows the transformation process of nodes in various states, and parameters used in the model are given in Table 2. The basic terms and assumptions given are used for the rest of this article.

### 2.1. Model Assumptions.

- (1) Once newly added nodes are infected, they become contagious
- (2) Within the network, nodes are connected to each other
- (3) At some point, the bilinear infection rate of  $S$  nodes becoming  $L$  nodes is  $\beta S(L + B)$
- (4) Since the probabilities that the descendants of  $L$  and  $B$  nodes are  $L$  nodes are  $p$  and  $q$ , respectively, satisfying  $0 \leq p \leq 1$ ,  $0 \leq q \leq 1$ , the probability that the newly accessed computers are  $S$  nodes is  $\xi - p\xi L - q\xi B$

2.2. Model Expression. Based on the previous description and assumptions, the state transition differential system of the model is

TABLE 1: Individual characteristics and stability of computer virus propagation models.

Contributors	Model	Characteristics	Stability	
			Virus-free equilibrium stability	Virose equilibrium stability
Essouifi et al. [27]	SIR-SIS	Two-degree networks and stochastic method	n/a	Locally asymptotically stable
Upadhyay et al. [28]	SVEIR	Nonlinear incident rate	Locally and globally asymptotically stable	Locally and globally asymptotically stable
Yang et al. [29]	SEIR-KS	Hopf bifurcation	n/a	Locally asymptotically stable
Anibal et al. [30]	SEIR-KS	Periodic environment	n/a	n/a
Zdemir et al. [31]	SEIR-KS	The kill signals	Locally asymptotically stable	Locally asymptotically stable
Tang et al. [32]	SLBRS	Safety entropy	n/a	Globally asymptotically stable
This work	SLBRS	Vertical transmission	Locally and globally asymptotically stable	Locally and globally asymptotically stable

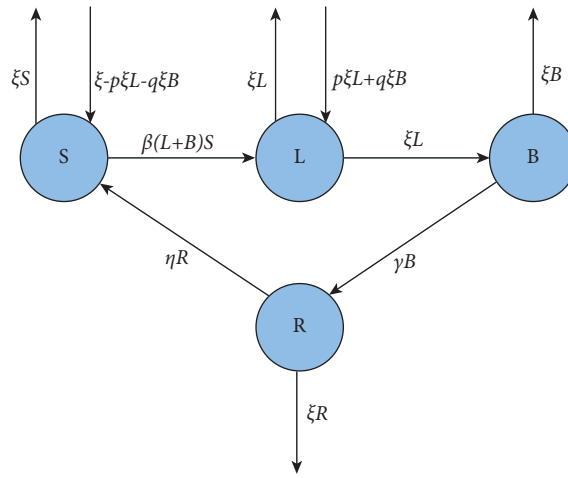


FIGURE 1: Migration blueprint of the SLBRS model.

TABLE 2: Parameters involved in the model.

Parameters	Description
$\xi$	The ratio of computers connected to the Internet.
$\beta$	The ratio at which each $S$ computer becomes $L$ computer by contact with either $L$ computer or $B$ computer.
$\varepsilon$	The rate at which $B$ computers are cured.
$\gamma$	The rate at which $B$ computers are cured.
$\eta$	The rate at which $R$ computers lose immunity.
$p$	The rate at which the descendants of the $L$ computers become the $S$ computers.
$q$	The rate at which the descendants of the $B$ computer become the $S$ computers.

$$\left\{ \begin{array}{l} \frac{dS}{dt} = \xi - \beta S(L+B) + \eta R - p\xi L - q\xi B - \xi S, \\ \frac{dL}{dt} = \beta S(L+B) - \varepsilon L + p\xi L + q\xi B - \xi L, \\ \frac{dB}{dt} = \varepsilon L - \gamma B - \xi B, \\ \frac{dR}{dt} = \gamma B - \eta R - \xi R. \end{array} \right. \quad (2)$$

Based on the above theoretical analysis, we know that  $R = 1 - S - L - B$ , and differential equations of system (2) state can be converted into

$$\left\{ \begin{array}{l} \frac{dS}{dt} = \xi - \beta S(L+B) + \eta(1-S-L-B) - p\xi L - q\xi B - \xi S, \\ \frac{dL}{dt} = \beta S(L+B) - \varepsilon L + p\xi L + q\xi B - \xi L, \\ \frac{dB}{dt} = \varepsilon L - \gamma B - \xi B. \end{array} \right. \quad (3)$$

The initial states of all kinds of computers in system (3), respectively, satisfy:  $L(0) \geq 0$ ,  $S(0) \geq 0$ , and  $B(0) \geq 0$ . The initial value belongs to the positive invariant set:

$$\Psi = \{(S, L, B): S + L + B \leq 1, S \geq 0, L \geq 0, B \geq 0\}. \quad (4)$$

The basic regeneration number is the threshold at which a disease tends to die out or persist. We calculated the basic reproductive number is as follows:

$$R_0 = \frac{\beta(\xi + \gamma + \epsilon) + (\xi + \gamma)p\xi + \epsilon q\xi}{(\xi + \gamma)(\epsilon + \xi)}. \quad (5)$$

For one thing, from the above description, the virus-free equilibrium is calculated as  $E_0 = (S_0, L_0, B_0) = (1, 0, 0)$ . In addition, data analysis of system (3) was performed to determine the unique endemic equilibrium point  $E^* = (S^*, L^*, B^*)$ . Specific results are as follows:

$$\begin{aligned} S^* &= \frac{(\xi + \gamma)(\epsilon + \xi) - (\xi + \gamma)p\xi - \epsilon q\xi}{\beta(\xi + \gamma + \epsilon)}, \\ L^* &= \frac{(\xi + \gamma)^2(\xi + \eta)(\epsilon + \xi)(R_0 - 1)}{(\xi + \gamma + \epsilon)[(\xi + \gamma)(\xi + \eta) + (\xi + \eta + \gamma)\epsilon]}, \\ B^* &= \frac{\epsilon(\xi + \gamma)(\xi + \eta)(\epsilon + \xi)(R_0 - 1)}{(\xi + \gamma + \epsilon)[(\xi + \gamma)(\xi + \eta) + (\xi + \eta + \gamma)\epsilon]}. \end{aligned} \quad (6)$$

$$(\lambda + \eta + \xi) \left[ \lambda^2 + \lambda(\gamma + \xi - \beta + \epsilon + \xi - p\xi) + (\gamma\epsilon + \epsilon\xi + \gamma\xi + \xi^2 - \gamma\beta - \xi\beta - \epsilon\beta - \gamma p\xi - \epsilon q\xi - p\xi^2) \right] = 0,$$

$$\lambda_1 = -\eta - \xi,$$

$$\lambda_2 = \frac{(\beta - \gamma - 2\xi - \epsilon + p\xi)}{2} + \frac{\sqrt{(\gamma + 2\xi - \beta + \epsilon - p\xi)^2}}{2} - \frac{\sqrt{4 * (\gamma\epsilon + \epsilon\xi + \gamma\xi + \xi^2 - \gamma\beta - \xi\beta - \epsilon\beta - \gamma p\xi - \epsilon q\xi - p\xi^2)}}{2}, \quad (8)$$

$$\lambda_3 = \frac{(\beta - \gamma - 2\xi - \epsilon + p\xi)}{2} - \frac{\sqrt{(\gamma + 2\xi - \beta + \epsilon - p\xi)^2}}{2} - \frac{\sqrt{4 * (\gamma\epsilon + \epsilon\xi + \gamma\xi + \xi^2 - \gamma\beta - \xi\beta - \epsilon\beta - \gamma p\xi - \epsilon q\xi - p\xi^2)}}{2}.$$

Clearly,  $\lambda_1 < 0$ ,  $\lambda_3 < 0$ , and  $\lambda_2 < 0$  if  $R_0 \leq 1$ , which intimates  $\beta(\xi + \epsilon + \gamma) + p\xi(\gamma + \xi) + \epsilon q\xi - (\gamma + \xi)(\epsilon + \xi) < 0$ . The correctness of Theorem 1 can be proved according to stability theory in [36].  $\square$

**Theorem 2.** If  $R_0 \leq 1$ ,  $E_0$  is globally asymptotically stable relative to  $\Psi$ .

*Proof.* Give a Lyapunov function,

$$\begin{aligned} V_1(t) &= \frac{dL}{dt} + \frac{\epsilon - p\xi + q\xi + \xi}{(\xi + \gamma + \epsilon)} \frac{dB}{dt}, \\ &= \left( \beta S - \frac{(\epsilon + \xi)(\xi + \gamma) - p\xi(\xi + \gamma) - \epsilon q\xi}{(\xi + \gamma + \epsilon)} \right) L + \left( \beta S - \frac{(\epsilon + \xi)(\xi + \gamma) - p\xi(\xi + \gamma) - \epsilon q\xi}{(\xi + \gamma + \epsilon)} \right) B. \end{aligned} \quad (10)$$

### 3. Stability of the Virus-Free Equilibrium

Global stability of steady state revealed the basic rule of the spread of the virus. Subsequently, the global stability of the virus-free equilibrium will be derived.

**Theorem 1.** The virus-free equilibrium  $E_0$  is local asymptotically stable if  $R_0 \leq 1$ , but unstable if  $R_0 > 1$ .

*Proof.* We obtained the Jacobian matrix of system (3) at disease-free equilibrium as follows:

$$J_{E_0} = \begin{bmatrix} -\eta - \xi & -\beta - \eta - p\xi & -\beta - \eta - q\xi \\ 0 & \beta - \epsilon + p\xi - \xi & \beta + q\xi \\ 0 & \epsilon & -\gamma - \xi \end{bmatrix}, \quad (7)$$

Accordingly, the characteristic equation is easily obtained by the matrix (7) as

$$V(t) = L + \frac{\epsilon - p\xi + q\xi + \xi}{(\xi + \gamma + \epsilon)} B, \quad (9)$$

Obviously, the Lyapunov function is positive definite. Through direct computing, the differential equation of the function is obtained:



When  $R_0 \leq 1$ , it is calculated that  $\beta(\xi + \gamma + \varepsilon) + p\xi(\xi + \gamma) + \varepsilon q\xi - (\xi + \gamma)(\varepsilon + \xi) < 0$ . It is observed that  $V'(t) \leq 0$ . Furthermore,  $V'(t) = 0$  when and only when  $L = 0$  and  $B = 0$  are satisfied. In addition, when  $L$  tends to be infinite or  $B$  tends to infinity, one can get  $V(t)$  to tend to be infinite. LaSalle's invariance principle [37] is an important basis for proving global stability. According to the theorem, we can see that when  $R_0 \leq 1$ , the global stability of  $E_0$  in  $\Psi$  has been verified. Theorem 2 has been proved.  $\square$

#### 4. Stability of the Virose Equilibrium

Local stability and global stability analysis of endemic equilibrium is the important approach to analyze the propagation of the virus. At this stage, we put forward two theories to analyze the stability of  $E^*$  and gave analysis and proof.

**Theorem 3.** *In the case of  $R_0 > 1$ , the virose equilibrium is locally asymptotically stable.*

*Proof.* We obtained the Jacobian matrix of system (3) at endemic equilibrium as follows:

$$J_{E^*} = \begin{bmatrix} -\beta(L^* + B^*) - \eta - \xi & -\beta S^* - \eta - p\xi & -\beta S^* - \eta - q\xi \\ \beta(L^* + B^*) & \beta S^* - \varepsilon + p\xi - \xi & \beta S^* + q\xi \\ 0 & \varepsilon & -\gamma - \xi \end{bmatrix}, \quad (11)$$

$$n_1 n_2 - n_3 = (\varepsilon + \gamma + \eta + 2\xi)H^2 + (1 + \varepsilon + \gamma + \eta + 2\xi)(A + B)H + H(\gamma + \xi)^2 + H\varepsilon\xi + H(\xi + \eta)^2(\gamma + \xi) + (A + B)^2(\eta + \xi) + (A + B)(\xi + \eta)(\gamma + \xi)(1 + \xi + \eta) + (\xi + \eta)(\gamma + \xi)(\gamma + \eta + 2\xi). \quad (12)$$

By calculation,  $n_1 > 0$ ,  $n_2 > 0$ ,  $n_3 > 0$ , and  $(n_1 n_2 - n_3) > 0$  if  $R_0 > 1$ . On the basis of the Routh–Hurwitz criterion [38], Theorem 3 is proved.

Theorem 1 proves that the virus-free equilibrium is unstable under the condition of  $R_0 > 1$ . Besides that, as a result of  $E_0$  belonging to the boundary of the feasible region

$$\lim_{t \rightarrow \infty} \inf f S(t) > \omega, \lim_{t \rightarrow \infty} \inf f L(t) > \omega, \lim_{t \rightarrow \infty} \inf f B(t) > \omega, \lim_{t \rightarrow \infty} \inf f (1 - S(t) - L(t) - B(t)) > \omega. \quad (14)$$

**Theorem 4.** *The virus equilibrium is globally asymptotically stable under the condition of  $R_0 > 1$ .*

*Proof.* Now we will use a geometric method [41] to illustrate that  $E^*$  is globally stable. From the above analysis, we know

The characteristic equation of  $J_{E^*}$  is  $\lambda^3 + n_1\lambda^2 + n_2\lambda + n_3 = 0$ , where

$$n_1 = \eta + 2\xi + \gamma + H + A + B,$$

$$n_2 = (\varepsilon + \eta + 2\xi + \gamma)H + \eta\gamma + \xi\gamma + \eta\xi + \xi^2 + (\eta + \xi)(A + B),$$

$$n_3 = (\xi\gamma + \xi^2 + \varepsilon\xi + \eta\gamma + \eta\xi + \varepsilon\eta + \gamma\varepsilon)H,$$

$$A = q\xi \frac{\varepsilon}{\gamma + \xi},$$

$$B = \beta S^* \frac{\varepsilon}{\gamma + \xi},$$

$$H = \beta L^* + \beta B^*,$$

$$\beta S^* = \varepsilon + p\xi - A - B,$$

(12)

we have

$\Psi$ , state variables of the system are uniformly persistent [39, 40]. Here, we advance the proposition as follows.  $\square$

**Proposition 1.** *System (3) is consistent and durable under the condition of  $R_0 > 1$ . In other words, there is a positive constant  $\omega$  independent of the initial state of system (3), which satisfies*

that system (3) has a compact attractive set  $U \in \Psi^*$ , and the only viral equilibrium exists in system (3).

Set  $a = (S, L, B)$ , and express the vector field of system (3) by  $f(a)$ . Find the Jacobian determinant, the Jacobian of the general solution  $a(t)$  of system (3), that is,

$$J_{a(t)} = \begin{bmatrix} -\beta(L+B) - \eta - \xi & -\beta S - \eta - p\xi & -\beta S - \eta - q\xi \\ \beta(L+B) & \beta S - \varepsilon + p\xi - \xi & \beta S + q\xi \\ 0 & \varepsilon & -\gamma - \xi \end{bmatrix}. \quad (15)$$

By calculation, we obtain the second additive compound Jacobian matrix [42, 43] as

$$J_{a(t)}^{[2]} = \begin{bmatrix} -\beta(L+B-S) - (\eta + \xi + \varepsilon + p\xi) & \beta S + q'\xi & \beta S + \eta - q\xi \\ \varepsilon & -\beta(L+B) - (\eta + 2\xi + \gamma) & -\beta S - \eta + p\xi \\ 0 & \beta(L+B) & \beta S - (\gamma + \xi + \varepsilon + p\xi) \end{bmatrix}. \quad (16)$$

Now, set the function  $\Gamma(a) = \Gamma(S, L, B)$  as

$$\Gamma(S, L, B) = \begin{bmatrix} q_1 & 0 & 0 \\ 0 & (1 - q_2)\frac{L}{B} & 0 \\ 0 & q_2\frac{L}{B} & \frac{L}{B} \end{bmatrix}, \quad (17)$$

where

$$1 < q_1 < \frac{2\beta\omega^2}{\beta + \xi + 2\eta} + 1, \quad (18)$$

$$q_2 = \begin{cases} 0 & \varepsilon \geq \beta + \eta + p\xi, \\ 1 - \frac{\varepsilon}{\beta + \eta + p\xi} & \varepsilon < \beta + \eta + p\xi. \end{cases} \quad (19)$$

Note that  $\omega$  is the positive constant given in Proposition 1. Then, there are

$$\Gamma_f \Gamma^{-1} = \begin{bmatrix} 0 & 0 & 0 \\ 0 & \frac{\dot{L}}{L} - \frac{\dot{B}}{B} & 0 \\ 0 & 0 & \frac{\dot{L}}{L} - \frac{\dot{B}}{B} \end{bmatrix}. \quad (20)$$

We rewrite the matrix  $B = \Gamma_f \Gamma^{-1} + \Gamma J_{a(t)}^{[2]} \Gamma^{-1}$  used in the geometric method of global stability [41]:

$$B = \begin{bmatrix} B_{11} & B_{12} \\ B_{21} & B_{22} \end{bmatrix}, \quad (21)$$

where

$$B_{11} = [-\beta(L+B-S) - (\eta + 2\xi + \varepsilon - p\xi)],$$

$$B_{12} = \left[ \frac{q_1 B (\beta S + q\xi) - q_2 q_1 B (\beta S + \eta + q\xi)}{(1 - q_2)L} \quad \frac{q_1 (\beta S + \eta + q\xi) B}{L} \right],$$

$$B_{21} = \begin{bmatrix} \frac{\varepsilon(1 - q_2)L}{q_1 B} \\ \frac{\varepsilon q_2 L}{q_1 B} \end{bmatrix},$$

$$B_{22} = \begin{bmatrix} \frac{\dot{L}}{L} - \frac{\dot{B}}{B} - \beta(L+B) - (\eta + 2\xi + \gamma) + q_2(\beta S + \eta + p\xi) & (q_2 - 1)(\beta S + \eta + p\xi) \\ \beta(L+B) + \frac{q_2 \varepsilon}{1 - q_2} - q_2(\beta S + \eta + p\xi) & \frac{\dot{L}}{L} - \frac{\dot{B}}{B} - (\gamma + 2\xi + \varepsilon + \eta) + (1 - q_2)(\beta S + \eta + p\xi) \end{bmatrix}. \quad (22)$$

The vectors in  $R^3$  are denoted by  $y = (\xi, \delta, \psi)$ , where  $|(\xi, \delta, \psi)| = \max\{|\xi|, |\delta| + |\psi|\}$  is selected as the norm of  $R^3$ .

Suppose that the Lozinskii measure about this norm is represented as  $u$ , we can obtain the following estimates [44]:

$$u(B) \leq \sup\{\kappa_1, \kappa_2\} = \sup\{u_1(B_{11}) + |B_{12}|, u_1(B_{22}) + |B_{21}|\}, \quad (23)$$

where

$$\begin{aligned} \kappa_1 &= u_1(B_{11}) + |B_{12}|, \\ \kappa_2 &= u_1(B_{22}) + |B_{21}|. \end{aligned} \quad (24)$$

Accordingly,  $u_1$  represents the Lozinskii measure of the norm of the  $L_1$  vector, and  $|B_{21}|$ ,  $|B_{12}|$  are the matrix norms about  $L_1$  vector norm.

Therefore, we obtain

$$\begin{aligned} \kappa_1 &= -\beta(L+B-S) - (\eta + 2\xi + \varepsilon - p\xi) + \frac{q_1(\beta S + q\xi)B}{L} + \max\left\{\frac{-q_1 q_2 \eta B}{(1-q_2)L}, \frac{q_1 \eta B}{L}\right\}, \\ \kappa_2 &= \frac{\dot{L}}{L} - \frac{\dot{B}}{B} - (\eta + \gamma + 2\xi) + \frac{\varepsilon L}{q_1 B} + \max\{q_2(\beta S + \eta + p\xi), -\varepsilon + 2(1-q_2)(\beta S + \eta + p\xi)\}, \end{aligned} \quad (25)$$

From (18) and (19), we can obtain

$$\kappa_1 = -\beta(L+B-S) - (\eta + 2\xi + \varepsilon - p\xi) + \frac{q_1(\beta S + q\xi)B}{L} + \frac{q_1 \eta B}{L}, \quad (26)$$

$$\kappa_2 \leq \frac{\dot{L}}{L} - \frac{\dot{B}}{B} - (\eta + \gamma + 2\xi) + \eta + p\xi + \frac{\varepsilon L}{q_1 B}. \quad (27)$$

Now rewriting system (3), we have

$$\frac{\dot{L}}{L} = \beta S + \beta S \frac{B}{L} - \varepsilon + p\xi - \xi + q\xi \frac{B}{L}, \quad (28)$$

$$\frac{\dot{B}}{B} = \varepsilon \frac{L}{B} - \gamma - \xi. \quad (29)$$

Adjust the consistent continuous constant  $\omega$  in 4.1 so that there is a constant  $T$  greater than zero in  $K$  that is independent of the initial value  $x(0)$  and satisfies

$$S(t) \geq \omega, L(t) \geq \omega, B(t) \geq \omega \text{ for } t > T. \quad (30)$$

Substitute (28) into (26), and (29) into (27). From (18) and (19), using formula (27), we have, for  $t > T$ ,

$$\begin{aligned} \kappa_1 &= \frac{\dot{L}}{L} + \frac{(q_1-1)(\beta S + q\xi)B}{L} - \beta(L+B) - \xi - \eta + \frac{q_1 \eta B}{L} \\ &\leq \frac{\dot{L}}{L} + \frac{(q_1-1)(\beta S + q\xi)}{\omega} - 2\beta\omega - \xi - \eta + \frac{q_1 \eta}{\omega} \\ &\leq \frac{\dot{L}}{L} - \xi - \eta \\ &\leq \frac{\dot{L}}{L} - \xi, \end{aligned} \quad (31)$$

$$\begin{aligned} \kappa_2 &\leq \frac{\dot{L}}{L} - \frac{\varepsilon L}{B} + \frac{\varepsilon L}{q_1 B} \\ &\leq \frac{\dot{L}}{L} - \frac{(q_1-1)\varepsilon L}{q_1 B}. \end{aligned} \quad (32)$$

Consequently,  $u(B) \leq \dot{L}/L - b$  for  $t > T$  by (23), and (31) and (32), where  $b = \min\{\xi, (q_1-1)\varepsilon L/q_1 B\} > 0$ . For each answer  $x(t, x_0)$  of system (3) satisfying  $x_0 \in K$  and  $t > T$ , there is

$$\frac{1}{t} \int_0^T u(B) ds \leq \frac{1}{t} \int_0^T u(B) ds + \frac{1}{t} \log \frac{L(t)}{L(T)} - b \frac{t-T}{t}, \quad (33)$$

meaning that  $\bar{q} \leq -b/2 < 0$  from (23), proving Theorem 4.  $\square$

## 5. Further Discussion

Combined with the analysis in the previous sections, we first analyze the sensitivity of  $R_0$  to system parameters and give a visualization diagram. Then, we studied the influence of relevant parameters on  $R_0$  and drew a series of visualization graphs.

As described earlier,  $\beta$  denotes the infection rate of uninfected computers, and  $p$  and  $q$  are part of infected newborns in the latent internal computers and breaking-out internal computers classes, respectively. In addition,  $\gamma$  represents the healing rate of disconnected nodes. To better analyze the spread of computer viruses, it is necessary to carry out sensitivity analysis of these system parameters for  $R_0$ . Next, calculate the normalized forward sensitivity index of  $\beta$ ,  $p$ ,  $q$ , and  $\gamma$  [45] as follows, respectively:

$$\begin{aligned} \frac{\partial R_0/R_0}{\partial \beta/\beta} &= \frac{\beta}{R_0} \frac{\partial R_0}{\partial \beta} = \frac{\beta(\xi + \gamma + \varepsilon)}{\beta(\xi + \gamma + \varepsilon) + (\varepsilon + \gamma)p\xi + \varepsilon q\xi} > 0, \\ \frac{\partial R_0/R_0}{\partial p/p} &= \frac{p(\xi + \gamma)}{\beta(\xi + \gamma + \varepsilon) + (\varepsilon + \gamma)p\xi + \varepsilon q\xi} > 0, \\ \frac{\partial R_0/R_0}{\partial q/q} &= \frac{q\xi\varepsilon}{\beta(\xi + \gamma + \varepsilon) + (\varepsilon + \gamma)p\xi + \varepsilon q\xi} > 0, \\ \frac{\partial R_0/R_0}{\partial \gamma/\gamma} &= \frac{-\gamma(\beta\varepsilon + \varepsilon q\xi)}{(\xi + \gamma)[\beta(\xi + \gamma + \varepsilon) + (\varepsilon + \gamma)p\xi + \varepsilon q\xi]} < 0. \end{aligned} \quad (34)$$

From these numerical results, we can draw the following conclusions:

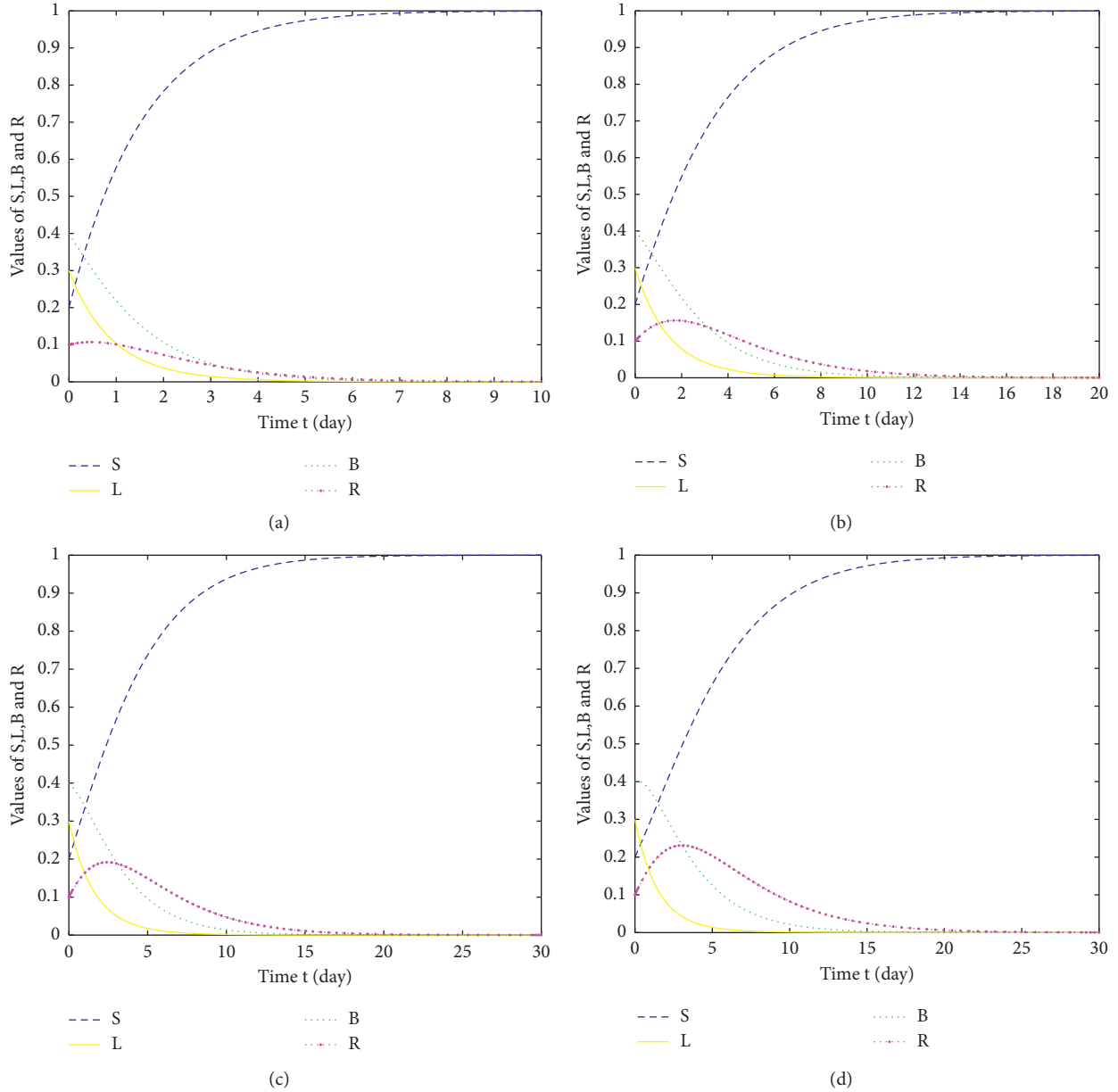


FIGURE 2: Evolution trend chart of system (3) at (a)  $R_0 = 0.3119$ , (b)  $R_0 = 0.5242$ , (c)  $R_0 = 0.6783$ , and (d) at  $R_0 = 0.8333$ .

TABLE 3: The typical  $R_0$  and associated parameter values of system (3).

$R_0$	$\xi$	$\beta$	$\eta$	$p$	$q$	$\gamma$	$\epsilon$	$S(0)$	$L(0)$	$B(0)$
0.3119	0.66	0.01	0.2	0.1	0.1	0.3	0.6	0.2	0.3	0.4
0.5242	0.26	0.01	0.2	0.1	0.1	0.3	0.5	0.2	0.3	0.4
0.6783	0.16	0.01	0.2	0.1	0.1	0.3	0.5	0.2	0.3	0.4
0.8333	0.1	0.01	0.2	0.1	0.1	0.3	0.6	0.2	0.3	0.4

(1) If the infection rate  $\beta$  is reduced, the spread of the virus can be controlled.

(2) If the birth rate of nodes in the vertical direction,  $p, q$ , is reduced, it will help control the spread of the virus.

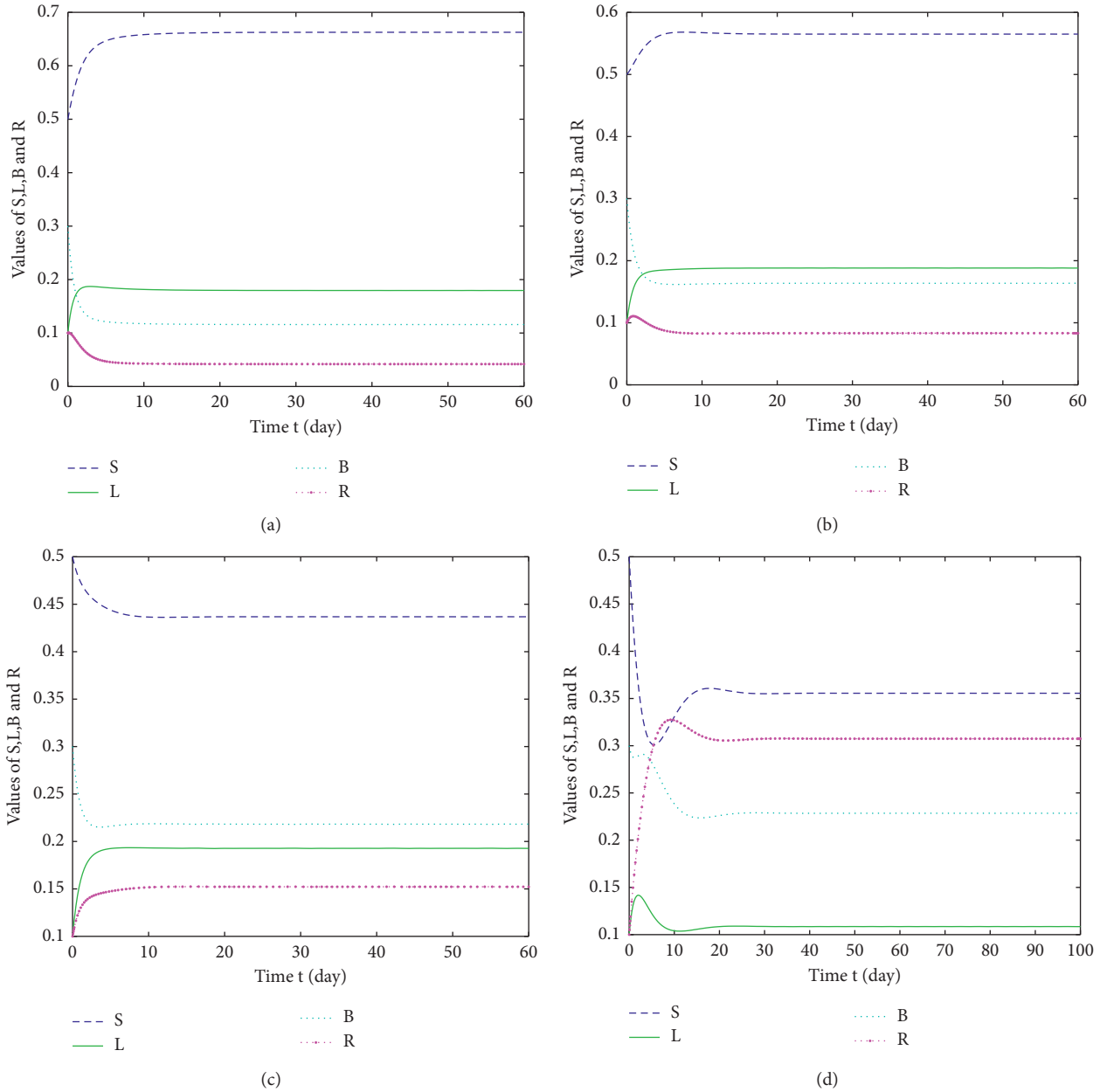


FIGURE 3: Evolution trend chart of system (3) at (a)  $R_0 = 3.9880$ , (b)  $R_0 = 6.1771$ , (c)  $R_0 = 11.2353$ , and (d)  $R_0 = 121.7206$ .

(3) If the cure rate  $\gamma$  is increased, it will help suppress the virus.

## 6. Numerical Experiments

Numerical simulations are an important tool for the quantitative analysis of models. Next, a series of numerical examples were made to visualize all the above theories.

**6.1. Stability Analysis.** For  $R_0 \leq 1$ ,  $E_0$  is globally asymptotically stable according to Theorem 2. Figure 2 shows how

the various types of states in the network evolve in time for  $R_0 = 0.3119, 0.5242, 0.6783$  and  $0.8333$  where the corresponding parameter values are shown in Table 3. From the graph, we can see that if  $R_0 < 1$ , the virus in the network eventually tends to die out.

For  $R_0 > 1$ , after the previous analysis and elaboration, Theorem 4 has been confirmed. Figure 3 shows how the various types of states in the network evolve in time for  $R_0 = 3.9880, 6.1771, 11.2353$ , and  $121.7206$ , where the corresponding parameter values are shown in Table 4. From the graph, we can see that if  $R_0 > 1$ , the virus in the network will always be there and tend to stabilize.

TABLE 4: The typical  $R_0$  and associated parameter values of system (3).

$11F0E0R_0$	$\xi$	$\beta$	$\eta$	$p$	$\epsilon$	$\gamma$	$q$	$S(0)$	$L(0)$	$B(0)$
3.9880	0.63	0.5	0.2	0.7	0.6	0.3	0.6	0.5	0.1	0.3
6.1771	0.39	0.56	0.2	0.5	0.6	0.3	0.6	0.5	0.1	0.3
11.2353	0.23	0.6	0.2	0.5	0.6	0.3	0.6	0.5	0.1	0.3
121.7206	0.023	0.6	0.2	0.5	0.6	0.3	0.68	0.5	0.1	0.3

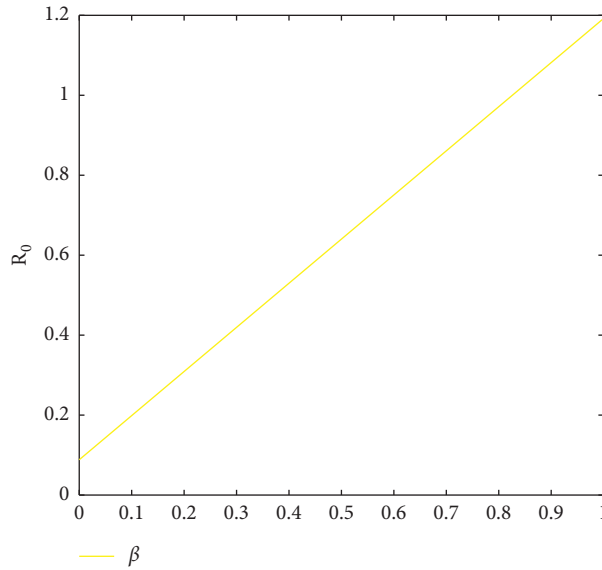


FIGURE 4: Influence of parameter  $\beta$  on  $R_0$ .

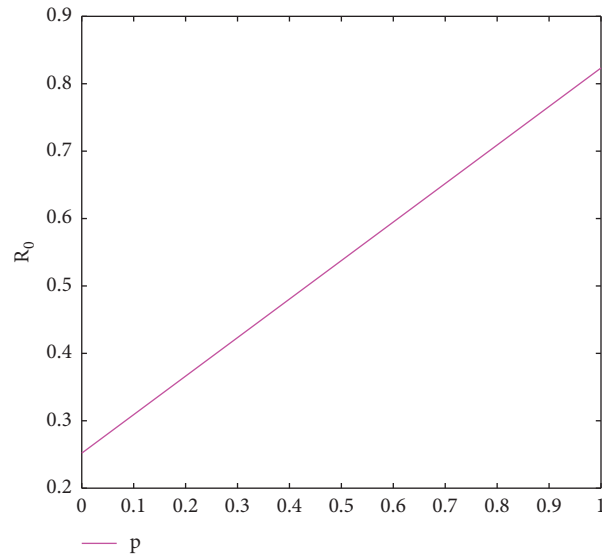


FIGURE 5: Influence of parameter  $p$  on  $R_0$ .

6.2. Influence of Parameters on the Value of  $R_0$ . From the previous subsection, we can see that the basic regeneration number determines whether the virus tends to die

out in the network or not. So analyzing the effect of parameters in the system on the basic regeneration number can help to contain the spread of the virus. It can

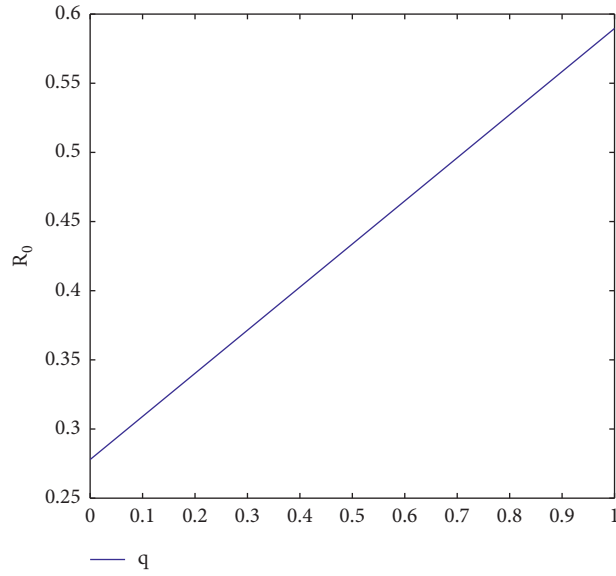


FIGURE 6: Influence of parameter  $q$  on  $R_0$ .

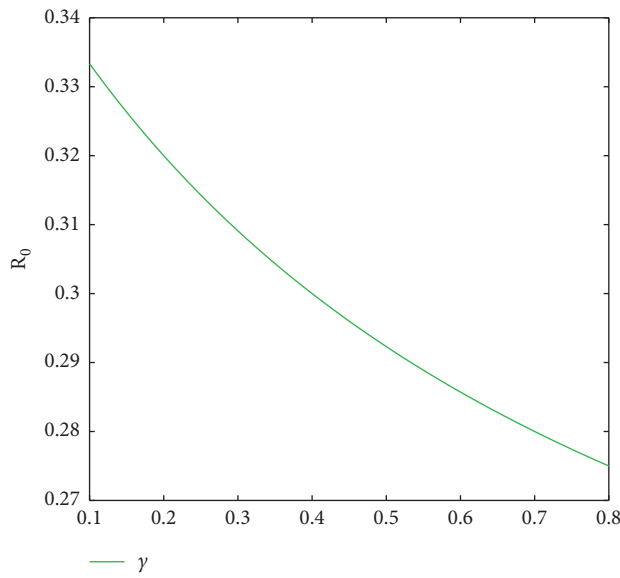


FIGURE 7: Influence of parameter  $\gamma$  on  $R_0$ .

TABLE 5: Simulation parameters.

Figure	$\xi$	$\beta$	$\eta$	$p$	$q$	$\gamma$	$\epsilon$
Figure 4	0.8	*	0.2	0.1	0.1	0.3	0.6
Figure 5	0.8	0.2	0.2	*	0.1	0.3	0.6
Figure 6	0.8	0.2	0.2	0.1	*	0.3	0.6
Figure 7	0.8	0.2	0.1	0.1	0.3	*	0.6

be seen that Figures 4–6 show that increases in  $\beta$ ,  $p$ , and  $q$  produce an equal proportional increase in  $R_0$ , respectively. Figure 7 shows a decline in the size of  $R_0$  as the

parameter  $\gamma$  increases. The parameters are shown in Table 5. These numerical simulations validate the analysis in Section 5.

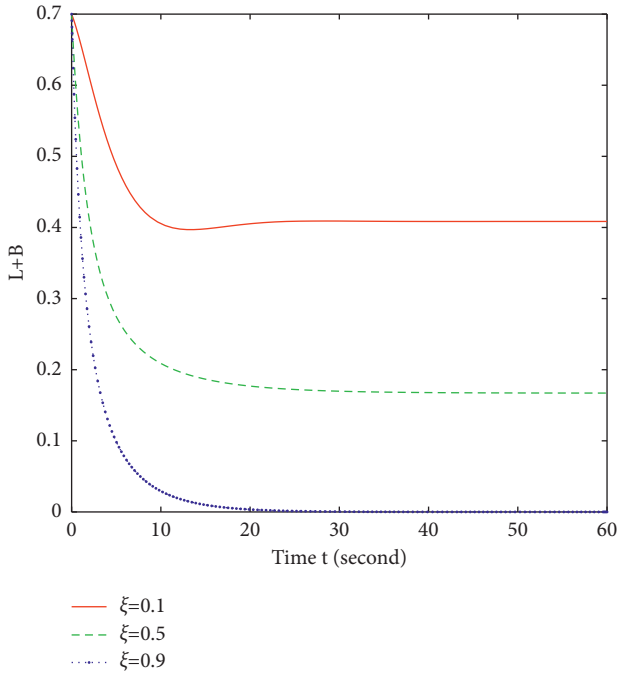


FIGURE 8: Influence of parameter  $\xi$  on  $L + B$ .

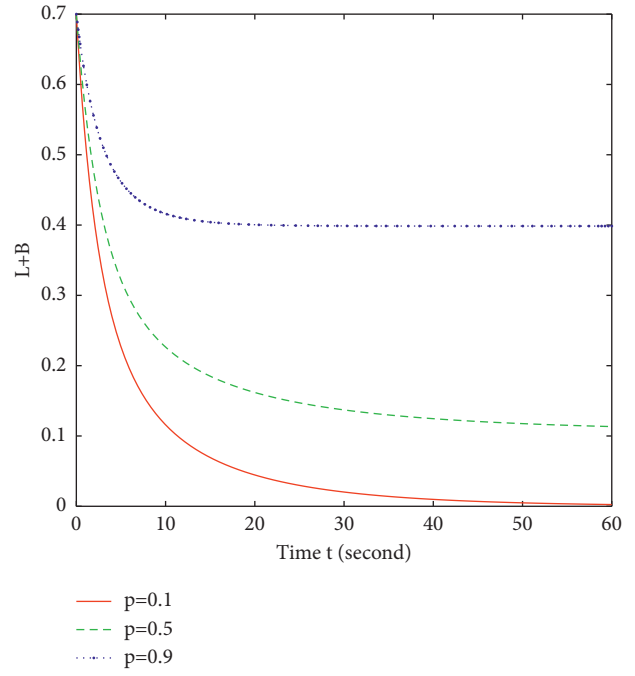


FIGURE 10: Influence of parameter  $p$  on  $L + B$ .

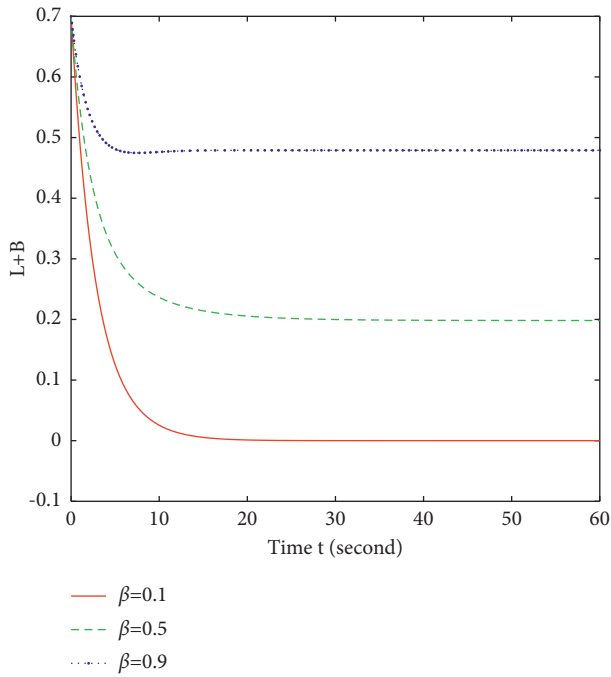


FIGURE 9: Influence of parameter  $\beta$  on  $L + B$ .

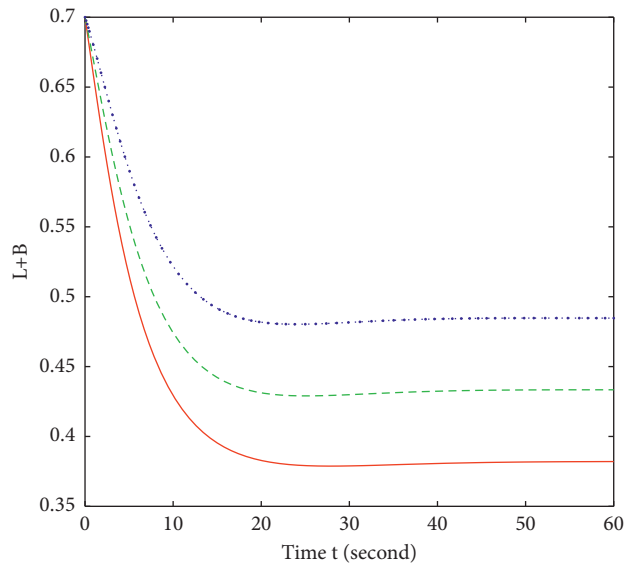


FIGURE 11: Influence of parameter  $q$  on  $L + B$ .

6.3. *Influence of Parameters on the Number of Infected Nodes.* When the basic regeneration number is inevitably greater than one, we take steps to reduce the number of infected

nodes. Analyzing the impact of parameters on infected nodes helps us to select measures to contain the virus. In this subsection, we analyze the parameters that affect the level of



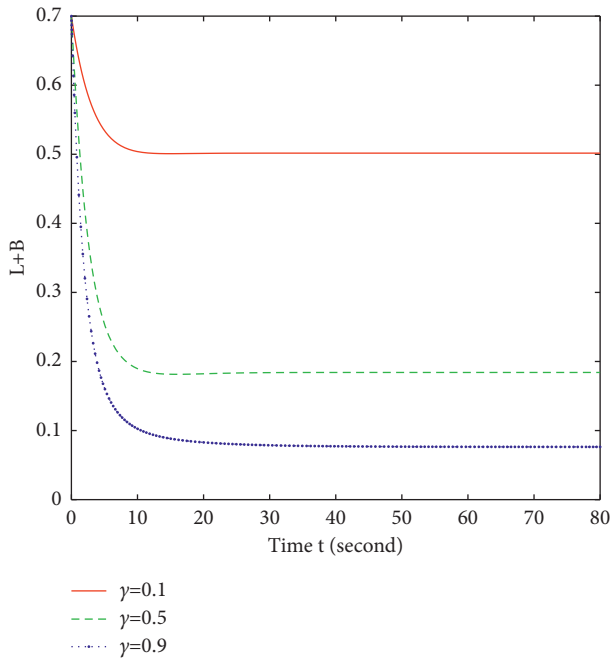


FIGURE 12: Influence of parameter  $\gamma$  on  $L + B$ .

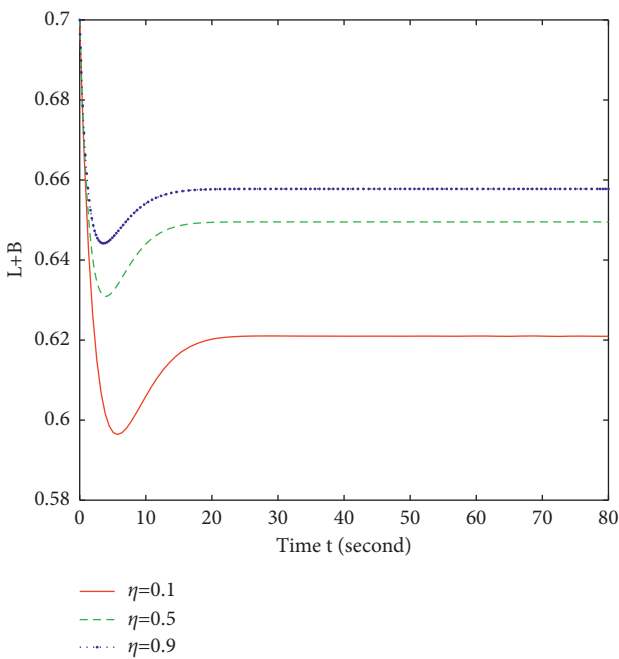


FIGURE 13: Influence of parameter  $\eta$  on  $L + B$ .

stability of the infected computer, and Figures 8–13 show the results of the analysis.

### 7. Conclusion

Considering the impact of the vertical transmission of computer viruses on new uninfected nodes, a novel dynamic model of network virus transmission is put forward, and this model is discussed and analyzed. The conclusions drawn from the analysis of the model are as follows:

- (1) This article studies an SLBRS model in which the virus infection can spread vertically and horizontally
- (2) It is confirmed that this model is asymptotically stable globally
- (3) Numerical simulation verifies the theoretical analysis of model balance
- (4) Perform system parameter sensitivity analysis on  $R_0$
- (5) The parameters affecting the stability level of the infected computer are analyzed

To our minds, the model proposed in this article more truly reflects some of the characteristics of network viruses than previous models. We believe that in the later work, the model can be extended on the complex network, and consider some of the most optimal control strategies.

### Abbreviations

- SEI: Susceptible-exposed-infected
- SEIQRS: Susceptible-exposed-infected-quarantined-recovered-susceptible
- SEIQV: Susceptible-exposed-infected-quarantined-vaccinated
- SEIR: Susceptible-exposed-infected-recovered
- SEIRS: Susceptible-exposed-infected-recovered-susceptible
- SIR: Susceptible-infected-recovered
- SIRS: Susceptible-infected-recovered-susceptible
- SIS: Susceptibility-infection-susceptibility
- SLBRS: Susceptible-latent-breaking-recovered-susceptible
- SLBS: Susceptible-latent-breaking-susceptible.

### Data Availability

Data sharing is not applicable to this article as no datasets were generated.

### Conflicts of Interest

All authors declare that there are no conflicts of interest.

### Authors' Contributions

The authors claim that the research was realized in collaboration with the same responsibility. All authors read and approved the last version of the manuscript.

### Acknowledgments

This work was supported by the National Natural Science Foundation of China (Grant no. 61903056), Major Project of Science and Technology Research Program of Chongqing Education Commission of China (Grant no. KJZDM201900601), Chongqing Research Program of Basic Research and Frontier Technology (Grant nos. cstc2019jcyj-msxmX0681, cstc2021jcyj-msxmX0530, and cstc2021jcyj-msxmX0761), Chongqing Municipal Key Laboratory of Institutions of Higher Education (Grant no. cqjpt-mct-201901), Chongqing Key Laboratory of

Mobile Communications Technology (Grant no. cqupt-mct-202002), and Engineering Research Center of Mobile Communications, Ministry of Education (Grant no. cqupt-mct202006).

## References

- [1] M. Shoaib Arif, A. Raza, M. Rafiq et al., “Numerical simulations for stochastic computer virus propagation model,” *Computers, Materials & Continua*, vol. 62, no. 1, pp. 61–77, 2020.
- [2] X. Han and Q. Tan, “Dynamical behavior of computer virus on internet,” *Applied Mathematics and Computation*, vol. 217, no. 6, pp. 2520–2526, 2010.
- [3] N. Scaife, H. Carter, P. Traynor, and K. R. Butler, “Cryptolock (and drop it): stopping ransomware attacks on user data,” in *Proceedings of the 2016 IEEE 36th International Conference on Distributed Computing Systems (ICDCS)*, pp. 303–312, IEEE, Nara, Japan, June 2016.
- [4] krebsonsecurity, *Parkmobile Breach Exposes License Plate Data, mobile Numbers of 21m Users*, <https://krebsonsecurity.com/2021/04/parkmobile-breach-exposes-license-plate-data-mobile-numbers-of-21m-users/>, accessed April 12, 2021, 2021.
- [5] J. O. Kephart and S. R. White, “Directed-graph epidemiological models of computer viruses,” in *Proceedings of the 1991 IEEE Computer Society Symposium on Research in Security and Privacy*, pp. 71–102, IEEE, Oakland, CA, USA, May 1992.
- [6] B. Xie and M. Liu, “Dynamics stability and optimal control of virus propagation based on the e-mail network,” *IEEE Access*, vol. 9, pp. 32449–32456.
- [7] V. P. Dubey, R. Kumar, and D. Kumar, “A hybrid analytical scheme for the numerical computation of time fractional computer virus propagation model and its stability analysis,” *Chaos, Solitons & Fractals*, vol. 133, Article ID 109626, 2020.
- [8] M. Zhang, K. Liu, K. Liu, L. Chen, and Z. Li, “State feedback impulsive control of computer worm and virus with saturated incidence,” *Mathematical Biosciences and Engineering*, vol. 15, no. 6, pp. 1465–1478, 2018.
- [9] D. Prodanov, “Comments on some analytical and numerical aspects of the sir model,” *Applied Mathematical Modelling*, vol. 95, pp. 236–243, 2021.
- [10] H. El-Saka, A. Arafa, and M. Gouda, “Dynamical analysis of a fractional sirs model on homogenous networks,” *Advances in Difference Equations*, vol. 2019, no. 1, pp. 1–15, 2019.
- [11] B. Li and Q. Bie, “Long-time dynamics of an sirs reaction-diffusion epidemic model,” *Journal of Mathematical Analysis and Applications*, vol. 475, no. 2, pp. 1910–1926, 2019.
- [12] S. P. Rajasekar and M. Pitchaimani, “Ergodic stationary distribution and extinction of a stochastic sirs epidemic model with logistic growth and nonlinear incidence,” *Applied Mathematics and Computation*, vol. 377, Article ID 125143, 2020.
- [13] Q. Liu, D. Jiang, and D. Jiang, “Dynamics of a multigroup sirs epidemic model with random perturbations and varying total population size,” *Communications on Pure and Applied Analysis*, vol. 19, no. 2, pp. 1089–1110, 2020.
- [14] S. Kim, J. H. Byun, and I. H. Jung, “Global stability of an seir epidemic model where empirical distribution of incubation period is approximated by coxian distribution,” *Advances in Difference Equations*, vol. 2019, no. 1, pp. 1–15, 2019.
- [15] S. Han and C. Lei, “Global stability of equilibria of a diffusive seir epidemic model with nonlinear incidence,” *Applied Mathematics Letters*, vol. 98, pp. 114–120, 2019.
- [16] Y. Yang and L. Xu, “Stability of a fractional order seir model with general incidence,” *Applied Mathematics Letters*, vol. 105, Article ID 106303, 2020.
- [17] H. Kang, M. Sun, Y. Yu, X. Fu, and B. Bao, “Spreading dynamics of an seir model with delay on scale-free networks,” *IEEE Transactions on Network Science and Engineering*, vol. 7, no. 1, pp. 489–496, 2018.
- [18] Z. Yin, Y. Yu, and Z. Lu, “Stability analysis of an age-structured seirs model with time delay,” *Mathematics*, vol. 8, no. 3, p. 455, 2020.
- [19] L. Zhang, X. Fan, and Z. Teng, “Global dynamics of a non-autonomous seirs epidemic model with vaccination and nonlinear incidence,” *Mathematical Methods in the Applied Sciences*, vol. 44, no. 11, pp. 9315–9333, 2021.
- [20] P. Song, Y. Lou, and Y. Xiao, “A spatial seirs reaction-diffusion model in heterogeneous environment,” *Journal of Differential Equations*, vol. 267, no. 9, pp. 5084–5114, 2019.
- [21] W. Yang, “Dynamical behaviors and optimal control problem of an seirs epidemic model with interventions,” *Bulletin of the Malaysian Mathematical Sciences Society*, vol. 44, no. 2, pp. 1–16, 2021.
- [22] M. A. Khan, Y. Khan, T. W. Khan, and S. Islam, “Dynamical system of a seiqv epidemic model with nonlinear generalized incidence rate arising in biology,” *International Journal of Biomathematics*, vol. 10, no. 7, Article ID 1750096, 2017.
- [23] N. Ahmed, M. Fatima, D. Baleanu et al., “Numerical analysis of the susceptible exposed infected quarantined and vaccinated (seiqv) reaction-diffusion epidemic model,” *Frontiers in Physics*, vol. 7, p. 220, 2020.
- [24] Z. Zhang and L. Song, “Dynamics of a computer virus propagation model with delays and graded infection rate,” *Advances in Mathematical Physics*, vol. 2017, no. 1, 13 pages, Article ID 4514935, 2017.
- [25] Z. Zhang, S. Kundu, and R. Wei, “A delayed epidemic model for propagation of malicious codes in wireless sensor network,” *Mathematics*, vol. 7, no. 5, p. 396, 2019.
- [26] B. K. Mishra and N. Jha, “Seiqrs model for the transmission of malicious objects in computer network,” *Applied Mathematical Modelling*, vol. 34, no. 3, pp. 710–715, 2010.
- [27] M. Essouifi and A. Achahbar, “A mixed sir-sis model to contain a virus spreading through networks with two degrees,” *International Journal of Modern Physics C*, vol. 28, no. 9, Article ID 1750114, 2017.
- [28] R. K. Upadhyay, S. Kumari, and A. K. Misra, “Modeling the virus dynamics in computer network with sveir model and nonlinear incident rate,” *Journal of Applied Mathematics and Computing*, vol. 54, no. 1, pp. 485–509, 2016.
- [29] F. Yang and Z. Zhang, “Hopf bifurcation analysis of seir-ks computer virus spreading model with two-delay,” *Results in Physics*, vol. 24, no. 1, Article ID 104090, 2021.
- [30] A. Coronel, F. Huancas, I. Hess, E. Lozada, and F. Novoa-Muoz, “Analysis of a Seir-Ks mathematical model for computer virus propagation in a periodic environment,” *Mathematics*, vol. 8, no. 5, p. 20, 2020.
- [31] N. Zdemir, S. Uar, and B. B. S. Erolu, “Dynamical analysis of fractional order model for computer virus propagation with kill signals,” *International Journal of Nonlinear Sciences and Numerical Simulation*, vol. 21, no. 3-4, pp. 239–247, 2020.
- [32] W. Tang, Y.-J. Liu, Y.-L. Chen, Y.-X. Yang, and X.-X. Niu, “Slbrs: network virus propagation model based on safety entropy,” *Applied Soft Computing*, vol. 97, Article ID 106784, 2020.

- [33] X. Yang and L.-X. Yang, "Towards the epidemiological modeling of computer viruses," *Discrete Dynamics in Nature and Society*, vol. 2012, Article ID 259671, 11 pages, 2012.
- [34] M. Yang, Z. Zhang, Q. Li, and G. Zhang, "An sibrs model with vertical transmission of computer virus over the internet," *Discrete Dynamics in Nature and Society*, vol. 2012, Article ID 925648, 17 pages, 2012.
- [35] B. K. Mishra and S. K. Pandey, "Dynamic model of worms with vertical transmission in computer network," *Applied Mathematics and Computation*, vol. 217, no. 21, pp. 8438–8446, 2011.
- [36] J. K. Hale, *Theory of Functional Differential Equation*, Springer, New York, NY, USA, 1977.
- [37] J. P. La Salle, *The Stability of Dynamical Systems*, SIAM, Thailand, 1976.
- [38] R. C. Robinson, *An Introduction to Dynamical Systems*, American Mathematical Society, RI, USA, 2005.
- [39] H. I. Freedman, S. Ruan, and M. Tang, "Uniform persistence and flows near a closed positively invariant set," *Journal of Dynamics and Differential Equations*, vol. 6, no. 4, pp. 583–600, 1994.
- [40] S. Sun, "Global dynamics of a seir model with a varying total population size and vaccination," *International Journal of Mathematics and Analysis*, vol. 6, no. 40, pp. 1985–1995, 2012.
- [41] M. Y. Li and J. S. Muldowney, "A geometric approach to global-stability problems," *SIAM Journal on Mathematical Analysis*, vol. 27, no. 4, pp. 1070–1083, 1996.
- [42] M. Fiedler, "Additive compound matrices and an inequality for eigenvalues of symmetric stochastic matrices," *Czechoslovak Mathematical Journal*, vol. 24, no. 3, pp. 392–402, 1974.
- [43] J. S. Muldowney, "Compound matrices and ordinary differential equations," *Rocky Mountain Journal of Mathematics*, vol. 20, no. 4, pp. 857–872, 1990.
- [44] R. H. Martin Jr., "Logarithmic norms and projections applied to linear differential systems," *Journal of Mathematical Analysis and Applications*, vol. 45, no. 2, pp. 432–454, 1974.
- [45] L. Arriola and J. Hyman, "Forward and adjoint sensitivity analysis with applications in dynamical systems," *Lecture Notes in Linear Algebra and Optimization*, Mathematical and Theoretical Biology Institute, Columbus, OH, USA, 2005.

## Research Article

# A Novel Tripartite Evolutionary Game Model for Misinformation Propagation in Social Networks

Xianyong Li <sup>1</sup>, Qizhi Li <sup>1</sup>, Yajun Du <sup>1</sup>, Yongquan Fan,<sup>1</sup> Xiaoliang Chen,<sup>1</sup> Fashan Shen,<sup>2</sup> and Yunxia Xu<sup>2</sup>

<sup>1</sup>School of Computer and Software Engineering, Xihua University, Chengdu 610039, China

<sup>2</sup>Sichuan Suitang Science and Technology Co., Ltd., Chengdu 610045, China

Correspondence should be addressed to Xianyong Li; [lixy@mail.xhu.edu.cn](mailto:lixy@mail.xhu.edu.cn)

Received 20 November 2021; Accepted 31 December 2021; Published 19 January 2022

Academic Editor: Chenquan Gan

Copyright © 2022 Xianyong Li et al. This is an open access article distributed under the Creative Commons Attribution License, which permits unrestricted use, distribution, and reproduction in any medium, provided the original work is properly cited.

Misinformation has brought great challenges to the government and network media in social networks. To clarify the influences of behaviors of the network media, government, and netizen on misinformation propagation, a large number of influence parameters are proposed for the three participants. Then, a tripartite evolutionary game model for misinformation propagation is constructed. According to the proposed game model, the expected payoffs of three participants are analyzed when they adopt different strategies. The evolutionary stabilities of the game model are also analyzed theoretically. Finally, the impacts of different parameters on expected payoffs of three participants are analyzed experimentally. Meanwhile, coping strategies of three participants under different conditions are given. The experimental results show that the proposed tripartite evolutionary game model can properly describe the influence of network media, government, and netizen on misinformation propagation.

## 1. Introduction

In social networks, misinformation propagation may bring adverse impacts on society or individuals who used the networks. Many researchers have found some effective ways to characterize the law of misinformation propagation and to further control misinformation propagation. To detect misinformation with a limited budget in online social networks, Zhang et al. [1] proposed two algorithms with minimum monitors. On real networks, their methods showed effective performance. To stop misinformation propagating to online social networks, Pham et al. [2] designed a PR-DAG algorithm to maximize misinformation restriction in the networks. Tan et al. [3] introduced an activation increment based on nodes' different statuses. They further proposed a strategy of minimizing activation increments to find the important nodes, which can be used to limit the information propagation. Based on the rumor characteristics in social networks, Liu et al. [4] distinguished users into four compartments and further built a novel rumor spreading model. According to their theoretical

results, one can select proper measures to control rumor propagation in the networks. Shrivastava et al. [5] built a system of differential equations to describe misinformation propagation among groups. They validated their model from theoretical and experimental aspects. Wang et al. [6] studied an energy propagation model of rumors on multiple social networks. They found effective rumor mitigation strategies by various model parameters on the networks. To clarify the relationship between misinformation and debunking information, Jiang et al. [7] proposed a novel RSD (rumor-spreading-debunking) model. Their model obtained the scope, scale, and popularity about rumor spreading. Manouchehri et al. [8] proposed some techniques to generate required samples. They further found top-k nodes to minimize the impact of misinformation in social networks. Wang et al. [9] designed an optimal strategy of community seeds to reduce misinformation propagation and added it into their triggering model. Their method obtained better performance than all baseline models. Zareie and Sakellariou [10] summarized some methods about minimizing misinformation propagation. Therefore, misinformation

propagation and control models can help researchers to design misinformation governance strategy in social networks.

Some scholars have integrated various influence factors into their methods to block misinformation propagation. Aswani et al. [11] investigated misinformation propagation factors by their experience in social media. They found that tweet sentiment, tweet polarity, network attributes, etc., influence misinformation propagation. Glenski et al. [12] investigated large amounts of news in social media. They found that spreading behaviors of trusted news source and suspicious news source are very different, such as diffusion rates, users' annual incomes, and educations. To identify potential misinformation propagators in social networks, Kar et al. [13] screened out eleven related factors from a large number of users and tweets. They further established a combined classification algorithm, which fused bioinspired algorithms with K-means method. Their findings presented that their proposed algorithm is able to identify propagators of the networks. Based on the sociological properties, psychological features, and persuasion theories, Chen et al. [14] studied the impact of persuasion strategies on the process of misinformation post-propagation in social networks. They found that pathos strategies are suitable persuasion strategies for misinformation propagation. Based on the topic of COVID-19 in Twitter, Shahi et al. [15] studied misinformation contents, authors, and diffusion. They found the three parts of influence misinformation propagation in social media. Considering that information propagation leads to the asynchronous process of initial opinion formation, Liu and Rong [16] introduced multiple impact factors including online communication, network topology, propagation rate, and repost rate, into their opinion dynamic model for public opinion misinformation. They found that compulsively deleting comments and timely exposing misinformation benefit the control of negative opinion. On the Internet of battlefield things (IoBT) system, Abuzainab and Saad [17] proposed a mean-field game model with multiclass agents. The experimental results showed that their model effectively suppressed misinformation propagation. Wang et al. [18] summarized the properties of misinformation propagation on published papers with health misinformation. They found that scholars adopted various methods including content analysis, co-citation analysis, and network analysis. Thus, a reasonable selection of parameters can help to establish good misinformation suppression models in social networks.

In recent, more and more researchers have studied the information propagation dynamics with evolutionary game methods. Xiao et al. [19] combined user multidimensional attributes, evolutionary games, and SIR epidemic model. They proposed a new propagation dynamic model with an evolutionary game. Based on their model, they analyzed the multisource information propagation and the complexity of user interaction behaviors. Li et al. [20] combined heterogeneous mean-field and evolutionary games and proposed a hot spot propagation model. They further analyzed the relationships between the users' desire to participate in hot spot and the infection rate of information propagation

model. Wang et al. [21] proposed a tripartite evolutionary game model. They analyzed the equilibrium conditions of stakeholder's behavior strategies. They also studied management strategies and key intervention points of public opinion. Fei et al. [22] proposed an opinion dynamic model by evolutionary game theory. They analyzed the relationships of user behaviors, preferences, and ratings in this game model. To better understand information propagation scope and dynamic characteristics, Yang et al. [23] proposed an information propagation model with an evolutionary game. They further analyzed relationships between two pieces of competitive information. On the live streaming e-commerce networks, Lv et al. [24] proposed an information propagation game model with incentive mechanism. They further analyzed the relationships between rewards and live streaming information propagation based on the game model. Therefore, evolutionary games can better reveal the laws of information propagation in social networks.

In the field of misinformation spreading, Zhang et al. [25] investigated the propagation of conspiracy information and scientific information, respectively. In their experiments, they found that conspiracy information tends to propagate in a multigenerational branching process and science information tends to propagate in a breadth-first manner. To effectively constrain malicious actions in large-scale MANETs, Wang et al. [26] proposed a trust cooperative stimulation model based on the evolutionary game methods. They further found an optimum strategy through their model. Xiao et al. [27] proposed an evolutionary game model to analyze the dynamics of rumor propagation. Their model considered anti-rumor information to find the reasons that users have spread rumors. To deal with the diversity and complexity of data in rumor communication, Xiao et al. [28] proposed a group behavior model for rumor and anti-rumor. Considering the conflict and symbiotic relationships between rumor and anti-rumor, they integrated user-influenced rumor with anti-rumor based on the evolutionary game theory and representation learning methods. Askarizadeh et al. [29] proposed an evolutionary game model to reveal the relationships between rumor propagation and users' decision control. Askarizadeh et al. [30] also proposed a soft rumor control model to avoid rumor spreading. They further analyzed the relationships between rumor and anti-rumor spreaders based on the evolutionary game model. Consequently, evolutionary game models are useful to find misinformation (rumor) propagation and control rules.

Under multiple factors and circumstances, some scholars have analyzed their relationships based on the evolutionary game methods. Zhang et al. [31] introduced a reputation mechanism into evolutionary game theory and solved negative influences caused by malicious users. They further analyzed the relationships between current reputation and instant incentives based on the game model. In backscatter-assisted RF-powered cognitive networks, some secondary transmitters (STs) may choose different transmission services. Gao et al. [32] proposed an evolutionary game to analyze the relationship between the access point and service adaptation of the STs. To reveal the dynamic evolution of intervention policies, Alam et al. [33] combined

some network topologies' social feedbacks, behavioral responses, and viral propagation into one framework. They analyzed the relationships among the game payoff, epidemic dynamics, and individual health statuses in social networks. To investigate the influences of node attitudes on information propagation, Huang et al. [34] used the evolutionary game method to build an information propagation model. They further analyzed relationships between positive and negative attitudes of nodes. Michael et al. [35] analyzed the trust game based on the previous work. They introduced "delays" and "memories" in the process of information propagation. They also found that information explained the trust and trustworthiness among users clearly and reasonably. Considering that "deceitful pricing for acquaintances" has received extensive public attention on e-commerce platforms, Wu et al. [36] proposed a tripartite evolutionary game model concerning consumers, government, and platforms. Their model provided reasonable selection schemes for the three participants. It concludes that the evolution analysis of information propagation need to be combined with the evolutionary game theory, network structures, individual features, etc., in social networks.

However, there are few results fusing misinformation propagation and tripartite evolutionary game methods. This study aims to establish a new tripartite evolutionary game model for misinformation propagation. Three players including network media, government, and netizen are considered in the tripartite evolutionary game model. The mutual influences of the players will be analyzed both theoretically and experimentally.

The rest of the study is arranged as follows. In Section 2, a tripartite evolutionary game model for misinformation propagation is described. The model construction, players' payoffs, and analysis of evolutionary stable strategies are presented in this section. In Section 3, some experiments under different parameters are made. Finally, the results are summarized; and some directions are proposed in the future.

## 2. Tripartite Evolutionary Game Model for Misinformation Propagation

*2.1. Description of the Tripartite Evolutionary Game Model and the Players' Payoffs for Misinformation Propagation.* In social networks, network media, government, and netizen play an important role in the process of misinformation propagation. The three participants reciprocally influence the networks, affecting the trends of misinformation propagation. The tripartite evolutionary game provides an effective way to analyze the impacts of participant behaviors on misinformation propagation. In the game, the three players are network media, government, and netizen, and their strategies are  $(M_1, M_2)$ ,  $(G_1, G_2)$ , and  $(N_1, N_2)$ . Each player only chooses a strategy without knowledge of the actual choices made by the other players. For the network media,  $M_1$  and  $M_2$  represent the strategies of "promoting misinformation propagation" (such as extensive report) and "blocking

misinformation propagation" (such as selective report), respectively. For the government,  $G_1$  and  $G_2$  denote the strategies of "supervision" and "non-supervision," respectively. For the netizen,  $N_1$  and  $N_2$  represent the strategy of "spread" and "non-spread" media information. Therefore, the game strategies are  $(M_1, G_1, N_1)$ ,  $(M_1, G_1, N_2)$ ,  $(M_1, G_2, N_1)$ ,  $(M_1, G_2, N_2)$ ,  $(M_2, G_1, N_1)$ ,  $(M_2, G_1, N_2)$ ,  $(M_2, G_2, N_1)$ , and  $(M_2, G_2, N_2)$ , and their corresponding payoffs are denoted by  $(PF_{M111}, PF_{G111}, PF_{N111})$ ,  $(PF_{M112}, PF_{G112}, PF_{N112})$ ,  $(PF_{M121}, PF_{G121}, PF_{N121})$ ,  $(PF_{M122}, PF_{G122}, PF_{N122})$ ,  $(PF_{M211}, PF_{G211}, PF_{N211})$ ,  $(PF_{M212}, PF_{G212}, PF_{N212})$ ,  $(PF_{M221}, PF_{G221}, PF_{N221})$ , and  $(PF_{M222}, PF_{G222}, PF_{N222})$ , respectively.

To quantitatively analyze the benefits of three players, which are correlated with misinformation propagation under each game strategy in more detail, the descriptions of parameters for the network media, government, and netizen are displayed in Tables 1–3, respectively.

According to the above terminologies and symbols, the payoff matrix of the tripartite evolutionary game is shown in Table 4, and the game tree of the tripartite evolutionary game, shown in Figure 1, is established to intuitively express the game among network media, government, and netizen. In the game tree, the circles in the front three rows represent the game players and the lines drawn from the players represent the strategies made by the players. The top circle represents that the network media select the information about some network misinformation and has two choices: promoting misinformation and blocking misinformation. The circles in the second row represent that the government selects the misinformation from the network media and may choose one of two strategies: supervision and non-supervision. In the third row, the circles represent that the netizen selects the misinformation from the network media and government and may choose to spread or not to spread the information. At the bottom of the game tree, the circles are terminal nodes of the game, which hold the benefits of three players to reach the corresponding terminals when they have chosen different strategies.

In the game process, it assumes that each player seeks to maximize its own benefit. According to the parameters of the network media, government, and netizen, the payoffs of the three players under different strategies are as follows:

$$\begin{aligned}
 PF_{M111} &= IM_0 + IM_1 - CM_1 - FM_1, \\
 PF_{G111} &= IG_0 + IG_1 - CG, \\
 PF_{N111} &= IN_0 - CN - FN_1, \\
 PF_{M112} &= IM_0 + IM_1 - CM_1 - FM_1 - FM_3, \\
 PF_{G112} &= IG_0 + IG_1 - CG + BG_1, \\
 PF_{N112} &= IN_0 + IN_3 - LN, \\
 PF_{M121} &= IM_0 + IM_1 - CM_1 + BM_1, \\
 PF_{G121} &= IG_0 + IG_2 - LG_1, \\
 PF_{N121} &= IN_0 + IN_1 - CN, \\
 PF_{M122} &= IM_0 + IM_1 - CM_1, \\
 PF_{G122} &= IG_0 + IG_2 - LG_1 - FG_1,
 \end{aligned}$$

TABLE 1: Parameters of the network media.

Parameters	Descriptions of the parameters for the network media
$IM_0$	The initial income from the advertisements, netizen resource, etc.
$IM_1$	The income from the increasing advertisements, click rate, new netizen, popularity, etc., of the network media, when network media choose $M_1$
$IM_2$	The profit from the government attention, netizen approval, etc., when the network media choose $M_2$
$CM_1$	The cost from manpower, material resources, etc., of the network media, when the network media choose $M_1$
$CM_2$	The cost from manpower, material resources, etc., of the network media, when the network media choose $M_2$
$BM_1$	The bonus brought from netizen when the network media, government, and netizen choose $M_1$ , $G_2$ , and $N_1$ , respectively
$BM_2$	The bonus brought from netizen when the network media, government, and netizen choose $M_2$ , $G_2$ , and $N_1$ , respectively
$LM$	The loss from the decreasing advertisements, click rate, netizen, popularity, etc., of the network media, when the network media choose $M_2$
$FM_1$	The fine from the government choosing $G_1$ when the network media choose $M_1$
$FM_2$	The fine from the government choosing $G_1$ when the network media choose $M_2$ ( $FM_2 < FM_1$ )
$FM_3$	The fine from the netizen who no longer trusts or follows the network media, when the network media, government, and netizen choose $M_1$ , $G_1$ , and $N_2$ , respectively
$FM_4$	The fine from the netizen who no longer trusts or follows the network media, when the network media, government, and netizen choose $M_2$ , $G_1$ , and $N_2$ , respectively

TABLE 2: Parameters of the government.

Parameters	Descriptions of the parameters for the government
$IG_0$	The initial income from the power of government image, credibility, etc.
$IG_1$	The profit from the increasing power of government image, credibility, etc., and the security and stability of cyberspace, when the government chooses $G_1$
$IG_2$	The profit from the increasing tax of the network media, increasing public service advertisements, etc., when the government chooses $G_2$ ( $IG_2 < IG_1 < IG_0$ )
$CG$	The cost from manpower, material resources, etc., when the government chooses $G_1$
$LG_1$	The loss from the damage of the government image power, credibility, even unstable, and disharmonious cyberspace, when the network media choose $M_1$ and the government chooses $G_2$
$LG_2$	The loss from the damage of the government image power, credibility, even unstable, and disharmonious cyberspace, when the network media choose $M_2$ and the government chooses $G_2$ ( $LG_2 < LG_1$ )
$BG_1$	The bonus from the netizen who trusts the government and chooses non-spread media misinformation, when the network media choose $M_1$ and the government chooses $G_1$
$BG_2$	The bonus from the netizen who trusts the government and chooses non-spread media misinformation, when the network media choose $M_2$ and the government chooses $G_1$ ( $BG_2 < BG_1$ )
$FG_1$	The fine from the netizen who distrusts the government and chooses non-spread media misinformation, when the network media choose $M_1$ and the government chooses $G_2$
$FG_2$	The fine from the netizen who distrusts the government and chooses non-spread media misinformation, when the network media choose $M_2$ and the government chooses $G_2$ ( $FG_2 < FG_1$ )

TABLE 3: Parameters of the netizen.

Parameters	Descriptions of the parameters for the netizen
$IN_0$	The initial income from the netizen who have increasing attention, influence, etc.
$IN_1$	The profit from the increasing attention, influence, etc., when the network media, government, and netizen choose $M_1$ , $G_2$ , and $N_1$ , respectively
$IN_2$	The profit from the increasing attention, influence, etc., when the network media, government, and netizen choose $M_2$ , $G_2$ , and $N_1$ , respectively
$IN_3$	The profit from stable and harmonious cyberspace, etc., when the netizen chooses $N_2$
$CN$	The cost from manpower, material resources, time, etc., when the netizen collects and organizes misinformation, and chooses $N_1$
$LN$	The loss from decreasing attention, followers, etc., when the netizen chooses $N_2$
$FN_1$	The fine from the government when the network media, government, and netizen choose $M_1$ , $G_1$ , and $N_1$ , respectively
$FN_2$	The fine from the government when the network media, government, and netizen choose $M_2$ , $G_1$ , and $N_1$ , respectively.

TABLE 4: Payoff matrix of the tripartite evolutionary game.

Game strategies	Incomes
$(M_1, G_1, N_1)$	$(PF_{M111}, PF_{G111}, PF_{N111})$
$(M_1, G_1, N_2)$	$(PF_{M112}, PF_{G112}, PF_{N112})$
$(M_1, G_2, N_1)$	$(PF_{M121}, PF_{G121}, PF_{N121})$
$(M_1, G_2, N_2)$	$(PF_{M122}, PF_{G122}, PF_{N122})$
$(M_2, G_1, N_1)$	$(PF_{M211}, PF_{G211}, PF_{N211})$
$(M_2, G_1, N_2)$	$(PF_{M212}, PF_{G212}, PF_{N212})$
$(M_2, G_2, N_1)$	$(PF_{M221}, PF_{G221}, PF_{N221})$
$(M_2, G_2, N_2)$	$(PF_{M222}, PF_{G222}, PF_{N222})$

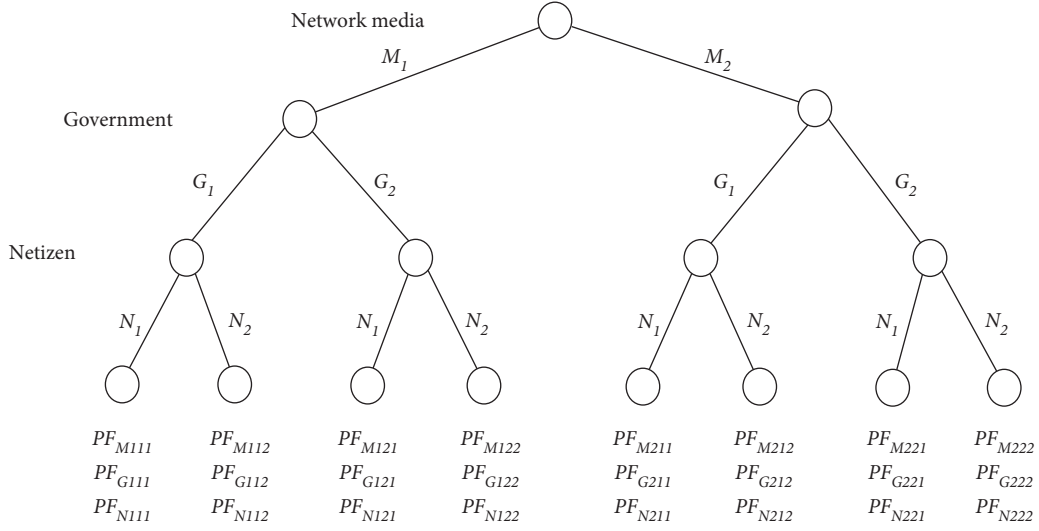


FIGURE 1: Game tree of the tripartite evolutionary game.

$$\begin{aligned}
 PF_{N122} &= IN_0 + IN_3 - LN, \\
 PF_{M211} &= IM_0 + IM_2 - CM_2 - LM - FM_2, \\
 PF_{G211} &= IG_0 + IG_1 - CG, \\
 PF_{N211} &= IN_0 - CN - FN_2, \\
 PF_{M212} &= IM_0 + IM_2 - CM_2 - LM - FM_2 - FM_4, \\
 PF_{G212} &= IG_0 + IG_1 - CG + BG_2, \\
 PF_{N212} &= IN_0 + IN_3 - LN, \\
 PF_{M221} &= IM_0 + IM_2 - CM_2 + BM_2 - LM, \\
 PF_{G221} &= IG_0 + IG_2 - LG_2, \\
 PF_{N221} &= IN_0 + IN_2 - CN, \\
 PF_{M222} &= IM_0 + IM_2 - CM_2 - LM, \\
 PF_{G222} &= IG_0 + IG_2 - LG_2 - FG_2, \\
 PF_{N222} &= IN_0 + IN_3 - CN - LN.
 \end{aligned} \tag{1}$$

Let  $x$ ,  $y$ , and  $z$  be the function of time  $t$ . If the network media, government, and netizen, respectively, choose the strategies  $M_1$ ,  $G_1$ , and  $N_1$ , then their probabilities are correspondingly  $x$ ,  $y$ , and  $z$ ; if the network media, government, and netizen, respectively, choose the strategies  $M_2$ ,  $G_2$ , and  $N_2$ , then their probabilities are correspondingly  $1 - x$ ,  $1 - y$ , and  $1 - z$ . Next, the expected payoffs of the network media, government, and netizen will be analyzed as follows.

If the network media choose the strategy  $M_1$ , the expected payoff of the network media in this case, denoted by  $EM_1$ , is as follows:

$$\begin{aligned}
 EM_1 &= yzPF_{M111} + y(1-z)PF_{M112} + (1-y)zPF_{M121} + (1-y)(1-z)PF_{M122} \\
 &= yz(IM_0 + IM_1 - CM_1 - FM_1) + y(1-z)(IM_0 + IM_1 - CM_1 - FM_1 - FM_3) \\
 &\quad + (1-y)z(IM_0 + IM_1 - CM_1 + BM_1) + (1-y)(1-z)(IM_0 + IM_1 - CM_1), \\
 &= yz(FM_3 - BM_1) - y(FM_1 + FM_3) + zBM_1 + IM_0 + IM_1 - CM_1.
 \end{aligned} \tag{2}$$

If the network media choose the strategy  $M_2$ , the expected payoff of the network media in this case, denoted by  $EM_2$ , is as follows:



$$\begin{aligned}
EM_2 &= yzPF_{M211} + y(1-z)PF_{M212} + (1-y)zPF_{M221} + (1-y)(1-z)PF_{M222} \\
&= yz(IM_0+IM_2 - CM_2 - LM - FM_2) + y(1-z)(IM_0+IM_2 - CM_2 - LM - FM_2 - FM_4) \\
&\quad + (1-y)z(IM_0+IM_2 - CM_2+BM_2 - LM) + (1-y)(1-z)(IM_0+IM_2 - CM_2 - LM) \\
&= yz(FM_4 - BM_2) - y(FM_2+FM_4) + zBM_2+IM_0+IM_2 - CM_2 - LM.
\end{aligned} \tag{3}$$

For the mixed strategy of the network media, the expected payoff of the network media, denoted by EM, is as follows:

$$\begin{aligned}
EM &= xEM_1 + (1-x)EM_2 \\
&= xyzPF_{M111} + xy(1-z)PF_{M112} + x(1-y)zPF_{M121} + x(1-y)(1-z)PF_{M122} \\
&\quad + (1-x)yzPF_{M211} + (1-x)y(1-y)PF_{M212} + (1-x)(1-y)zPF_{M221} + (1-x)(1-y)(1-z)PF_{M222} \\
&= xyz(FM_3 - FM_4 - BM_1+BM_2) - xy(FM_1 - FM_2+FM_3 - FM_4) + xz(BM_1 - BM_2) + yz(FM_4 - BM_2) \\
&\quad + x(IM_1 - IM_2 - CM_1+CM_2 + LM) - y(FM_2+FM_4) + zBM_2+IM_0+IM_2 - CM_2 - LM.
\end{aligned} \tag{4}$$

If the government chooses the strategy  $G_1$ , the expected payoff of the network media in this case, denoted by  $EG_1$ , is as follows:

$$\begin{aligned}
EG_1 &= xzPF_{G111} + x(1-z)PF_{G112} + (1-x)zPF_{G211} + (1-x)(1-z)PF_{G212} \\
&= xz(IG_0+IG_1 - CG) + x(1-z)(IG_0+IG_1 - CG + BG_1) + (1-x)z(IG_0+IG_1 - CG) \\
&\quad + (1-x)(1-z)(IG_0+IG_1 - CG + BG_2) \\
&= -xz(BG_1 - BG_2) + x(BG_1 - BG_2) - z(IG_0+IG_1 - CG + BG_2) + (2IG_0+2IG_1 - 2CG + BG_2).
\end{aligned} \tag{5}$$

If the government chooses the strategy  $G_2$ , the expected payoff of the government in this case, denoted by  $EG_2$ , is as follows:

$$\begin{aligned}
EG_2 &= xzPF_{G121} + x(1-z)PF_{G122} + (1-x)zPF_{G221} + (1-x)(1-z)PF_{G222} \\
&= xz(IG_0 + IG_2 - LG_1) + x(1-z)(IG_0 + IG_2 - LG_1 - FG_1) + (1-x)z(IG_0 + IG_2 - LG_2) \\
&\quad + (1-x)(1-z)(IG_0 + IG_2 - LG_2 - FG_2) \\
&= xz(FG_1 - FG_2) - x(FG_1 - FG_2 + LG_1 - LG_2) + zFG_2 + IG_0 + IG_2 - LG_2 - FG_2.
\end{aligned} \tag{6}$$

For the mixed strategy of the government, the expected payoff of the government, denoted by EG, is as follows:

$$\begin{aligned}
EG &= yEG_1 + (1-y)EG_2 = xyzPF_{G111} + xy(1-z)PF_{G112} + (1-x)yzPF_{G211} + (1-x)y(1-z)PF_{G212} \\
&\quad + x(1-y)zPF_{G121} + x(1-y)(1-z)PF_{G122} + (1-x)(1-y)zPF_{G221} + (1-x)(1-y)(1-z)PF_{G222} \\
&= -xyz(BG_1 - BG_2 + FG_1 - FG_2) + xy(BG_1 - BG_2 + FG_1 - FG_2 + LG_1 - LG_2) + xz(FG_1 - FG_2) \\
&\quad - yz(IG_0 + IG_1 + IG_2 - CG + FG_2) - x(FG_1 - FG_2 + LG_1 - LG_2) \\
&\quad + y(IG_0 + 2IG_1 - IG_2 + BG_2 - 2CG + LG_2 + FG_2) + zFG_2 + IG_0 + IG_2 - LG_2 - FG_2.
\end{aligned} \tag{7}$$

If the netizen chooses the strategy  $N_1$ , the expected payoff of the netizen in this case, denoted by  $EN_1$ , is as follows:

$$\begin{aligned}
EN_1 &= xyPF_{N111} + x(1-y)PF_{N121} + (1-x)yPF_{N211} + (1-x)(1-y)PF_{N221} \\
&= xy(IN_0 - CN - FN_1) + x(1-y)(IN_0 + IN_1 - CN) + (1-x)y(IN_0 - CN - FN_2) + (1-x)(1-y)(IN_0 + IN_2 - CN) \\
&= -xy(IN_1 - IN_2 + FN_1) + x(IN_1 - IN_2) - y(IN_2 + FN_2) + IN_0 + IN_2 - CN.
\end{aligned} \tag{8}$$

If the netizen chooses the strategy  $N_2$ , the expected payoff of the netizen in this case, denoted by  $EN_2$ , is as follows:

$$\begin{aligned}
EN_2 &= xyPF_{N112} + x(1-y)PF_{N122} + (1-x)yPF_{N212} + (1-x)(1-y)PF_{N222} \\
&= xy(IN_0 + IN_3 - LN) + x(1-y)(IN_0 + IN_3 - LN) + (1-x)y(IN_0 + IN_3 - LN) \\
&\quad + (1-x)(1-y)(IN_0 + IN_3 - CN - LN) \\
&= -xyCN + xCN + yCN + IN_0 + IN_3 - CN - LN.
\end{aligned} \tag{9}$$

For the mixed strategy of the netizen, the expected payoff of the netizen, denoted by  $EN$ , is as follows:

$$\begin{aligned}
EN &= zEN_1 + (1-z)EN_2 \\
&= xyzPF_{N111} + x(1-y)zPF_{N121} + (1-x)yzPF_{N211} + (1-x)(1-y)zPF_{N221} + xy(1-z)PF_{N112} \\
&\quad + x(1-y)(1-z)PF_{N122} + (1-x)y(1-z)PF_{N212} + (1-x)(1-y)(1-z)PF_{N222} \\
&= -xyz(IN_1 - IN_2 + FN_1 - CN) - xyCN + xz(IN_1 - IN_2 - CN) - yz(IN_2 + FN_2 + CN) \\
&\quad + xCN + yCN + z(IN_2 - IN_3 + LN) + IN_0 + IN_3 - CN - LN.
\end{aligned} \tag{10}$$

*2.2. Theoretical Analysis of Evolutionary Stable Strategies.* To ensure the harmonious and stable development of the network society, to promote the sustainable development of the network media, and to protect the legitimate rights of the netizen, the network media, government, and

netizen should fulfill their responsibilities to reduce the probabilities of propagating misinformation. By the expected payoffs of the network media, government, and netizen, their evolutionary replication dynamic equations are as follows:

$$\begin{aligned}
f(x) &= \frac{dx}{dt} = x(EM_1 - EM) = x(1-x)(EM_1 - EM_2) \\
&= x(1-x)[yzPF_{M111} + y(1-z)PF_{M112} + (1-y)zPF_{M121} + (1-y)(1-z)PF_{M122} - yzPF_{M211} \\
&\quad - y(1-z)PF_{M212} - (1-y)zPF_{M221} - (1-y)(1-z)PF_{M222}] \\
&= x(1-x)[yz(FM_3 - FM_4 - BM_1 + BM_2) - y(FM_1 - FM_2 + FM_3 - FM_4)] + z(BM_1 - BM_2) \\
&\quad + IM_1 - IM_2 - CM_1 + CM_2 + LM],
\end{aligned} \tag{11}$$

$$\begin{aligned}
g(y) &= \frac{dy}{dt} = y(EG_1 - EG) = y(1-y)(EG_1 - EG_2) \\
&= y(1-y)[xzPF_{G111} + x(1-z)PF_{G112} + (1-x)zPF_{G211} + (1-x)(1-z)PF_{G212} \\
&\quad - xzPF_{G121} - x(1-z)PF_{G122} - (1-x)zPF_{G221} - (1-x)(1-z)PF_{G222}] \\
&= y(1-y)[-xz(BG_1 - BG_2 + FG_1 - FG_2) + x(BG_1 - BG_2 + FG_1 - FG_2 + LG_1 - LG_2) \\
&\quad - z(IG_0 + IG_1 - CG + BG_2 + FG_2) + (IG_0 + 2IG_1 - IG_2 - 2CG + BG_2 + LG_2 + FG_2)],
\end{aligned} \tag{12}$$

$$\begin{aligned}
h(z) &= \frac{dz}{dt} = z(EN_1 - EN) = z(1-z)(EN_1 - EN_2) \\
&= z(1-z)[xyPF_{N111} + x(1-y)PF_{N121} + (1-x)yPF_{N211} + (1-x)(1-y)PF_{N221} - xyPF_{N112} \\
&\quad - x(1-y)PF_{N122} - (1-x)yPF_{N212} - (1-x)(1-y)PF_{N222}] \\
&= z(1-z)[-xy(IN_1 - IN_2 + FN_1 + CN) + x(IN_1 - IN_2 - CN) - y(IN_2 + FN_2 + CN) + IN_2 - IN_3 + LN].
\end{aligned} \tag{13}$$

Then, the tripartite evolutionary stabilities of the replication dynamic equations (11)–(13) can be analyzed by the following Jacobian matrix:

$$J_{(x,y,z)} = \begin{bmatrix} f_x & f_y & f_z \\ g_x & g_y & g_z \\ h_x & h_y & h_z \end{bmatrix}, \tag{14}$$

where the elements of  $J_{(x,y,z)}$  are as follows.

$$\begin{aligned}
f_x &= (1-2x)[yzPF_{M111} + y(1-z)PF_{M112} + (1-y)zPF_{M121} + (1-y)(1-z)PF_{M122} - yzPF_{M211} \\
&\quad - y(1-z)PF_{M212} - (1-y)zPF_{M221} - (1-y)(1-z)PF_{M222}] \\
&= (1-2x)[yz(FM_3 - FM_4 - BM_1 + BM_2) - y(FM_1 - FM_2 + FM_3 - FM_4)] + z(BM_1 - BM_2) + IM_1 \\
&\quad - IM_2 - CM_1 + CM_2 + LM], \\
f_y &= x(1-x)[zPF_{M111} + (1-z)PF_{M112} - zPF_{M121} - (1-z)PF_{M122} - zPF_{M211} - (1-z)PF_{M212} + zPF_{M221} + (1-z)PF_{M222}] \\
&= x(1-x)[z(FM_3 - FM_4 - BM_1 + BM_2) - (FM_1 - FM_2 + FM_3 - FM_4)], \\
f_z &= x(1-x)[yPF_{M111} - yPF_{M112} + (1-y)PF_{M121} - (1-y)PF_{M122} - yPF_{M211} + yPF_{M212} - (1-y)PF_{M221} + (1-y)PF_{M222}] \\
&= x(1-x)[y(FM_3 - FM_4 - BM_1 + BM_2) + (BM_1 - BM_2)], \\
g_x &= y(1-y)[zPF_{G111} + (1-z)PF_{G112} - zPF_{G211} - (1-z)PF_{G212} - zPF_{G121} - (1-z)PF_{G122} + zPF_{G221} + (1-z)PF_{G222}] \\
&= y(1-y)[-z(BG_1 - BG_2 + FG_1 - FG_2) + (BG_1 - BG_2 + FG_1 - FG_2 + LG_1 - LG_2)], \\
g_y &= (1-2y)[xzPF_{G111} + x(1-z)PF_{G112} + (1-x)zPF_{G211} + (1-x)(1-z)PF_{G212} - xzPF_{G121} \\
&\quad - x(1-z)PF_{G122} - (1-x)zPF_{G221} - (1-x)(1-z)PF_{G222}] \\
&= (1-2y)[-xz(BG_1 - BG_2 + FG_1 - FG_2) + x(BG_1 - BG_2 + FG_1 - FG_2 + LG_1 - LG_2) \\
&\quad - z(IG_0 + IG_1 - CG + BG_2 + FG_2) + (IG_0 + 2IG_1 - IG_2 - 2CG + BG_2 + LG_2 + FG_2)], \\
g_z &= y(1-y)[xPF_{G111} - xPF_{G112} + (1-x)PF_{G211} - (1-x)PF_{G212} - xPF_{G121} + xPF_{G122} - (1-x)PF_{G221} + (1-x)PF_{G222}]
\end{aligned}$$

$$\begin{aligned}
&= y(1-y)[-x(BG_1 - BG_2 + FG_1 - FG_2) - (IG_0 + IG_1 - CG + BG_2 + FG_2), \\
h_x &= z(1-z)[yPF_{N111} + (1-y)PF_{N121} - yPF_{N211} - (1-y)PF_{N221} - yPF_{N112} - (1-y)PF_{N122} + yPF_{N212} + (1-y)PF_{N222}] \\
&= z(1-z)[-y(IN_1 - IN_2 + FN_1 + CN) + (IN_1 - IN_2 - CN) - y(IN_2 + FN_2 + CN)], \\
h_y &= z(1-z)[xPF_{N111} - xPF_{N121} + (1-x)PF_{N211} - (1-x)PF_{N221} - xPF_{N112} + xPF_{N122} - (1-x)PF_{N212} + (1-x)PF_{N222}] \\
&= z(1-z)[-x(IN_1 - IN_2 + FN_1 + CN) - (IN_2 + FN_2 + CN)], \\
h_z &= (1-2z)[xyPF_{N111} + x(1-y)PF_{N121} + (1-x)yPF_{N211} + (1-x)(1-y)PF_{N221} \\
&\quad - xyPF_{N112} - x(1-y)PF_{N122} - (1-x)yPF_{N212} - (1-x)(1-y)PF_{N222}] \\
&= (1-2z)[-xy(IN_1 - IN_2 + FN_1 + CN) + x(IN_1 - IN_2 - CN) - y(IN_2 + FN_2 + CN) + IN_2 - IN_3 + LN].
\end{aligned} \tag{15}$$

Let  $f(x) = 0$ ,  $f(y) = 0$ , and  $f(z) = 0$ . Then, it can obtain ten equilibrium points:  $P_1(0, 0, 0)$ ,  $P_2(0, 0, 1)$ ,  $P_3(0, 1, 0)$ ,  $P_4(0, 1, 1)$ ,  $P_5(1, 0, 0)$ ,  $P_6(1, 0, 1)$ ,  $P_7(1, 1, 0)$ ,  $P_8(1, 1, 1)$ ,  $P_9(- (IG_0 + 2IG_1 - IG_2 - 2CG + BG_2 + LG_2 + FG_2)/(BG_1 - BG_2 + FG_1 - FG_2 + LG_1 - LG_2), (IM_1 - IM_2 - CM_1 + CM_2 + LM)/(FM_1 - FM_2 + FM_3 - FM_4), 0)$ , and  $P_{10}((IG_1 - IG_2 + LG_2 - CG)/(LG_2 - LG_1), (BM_1 - BM_2 + IM_1 - IM_2 - CM_1 + CM_2 + LM)/(BM_1 - BM_2 + FM_1 - FM_2), 1)$ .

Let the equilibrium solution domain of the tripartite evolutionary game be  $D = \{(x, y, z) | 0 \leq x \leq 1, 0 \leq y \leq 1, 0 \leq z \leq 1\}$ . Based on the definitions of  $IG_1$  and  $CG$ ,  $IG_1 > CG$  is reasonable and explicable. Because  $IG_0 > IG_2$ ,  $BG_1 > BG_2$ ,  $FG_1 > FG_2$ , and  $LG_1 > LG_2$ , we have  $-(IG_0 + 2IG_1 - IG_2 - 2CG + BG_2 + LG_2 + FG_2)/(BG_1 - BG_2 + FG_1 - FG_2 + LG_1 - LG_2) < 0$ . Then,  $P_9$  is not in  $D$ . Since the loss of the government is always larger than the cost of the

government choosing  $G_1$  when the network media choose  $M_1$  and the government chooses the strategy  $G_2$ , there are  $IG_1 - IG_2 + LG_1 - CG$  and  $(IG_1 - IG_2 + LG_2 - CG)/(LG_2 - LG_1) > 1$ . Then,  $P_{10}$  is not in  $D$ . Hence, for the ten equilibrium points, only  $P_1, P_2, P_3, P_4, P_5, P_6, P_7$ , and  $P_8$  are in  $D$ .

Let  $\text{diag}(a_1, a_2, \dots, a_3)$  be a diagonal matrix. For a matrix  $A$ , let  $\det A$  and  $\text{tr}(A)$  represent the determinant and trace of the matrix, respectively. For each equilibrium point  $P_i(x_i, y_i, z_i)$ , if  $\det J_{(x_i, y_i, z_i)} > 0$  and  $\text{tr} J_{(x_i, y_i, z_i)} < 0$ , the equilibrium point  $P_i(x_i, y_i, z_i)$  is evolutionary stable; if  $\det J_{(x_i, y_i, z_i)} < 0$  or  $\text{tr} J_{(x_i, y_i, z_i)} > 0$ , the equilibrium point  $P_i(x_i, y_i, z_i)$  is not evolutionary stable. Thus, the asymptotic stabilities from  $P_1$  to  $P_8$  are analyzed as follows.

For the equilibrium point  $P_1(0, 0, 0)$ , we have

$$J_{(0,0,0)} = \text{diag}(PF_{M122} - PF_{M222}, PF_{G212} - PF_{G222}, PF_{N221} - PF_{N222}). \tag{16}$$

Then,  $\det J_{(0,0,0)} = (PF_{M122} - PF_{M222})(PF_{G212} - PF_{G222})(PF_{N221} - PF_{N222})$ ,  $\text{tr} J_{(0,0,0)} = PF_{M122} - PF_{M222} + PF_{G212} - PF_{G222} + PF_{N221} - PF_{N222}$ . For  $PF_{M122} - PF_{M222}$ ,  $PF_{G212} - PF_{G222}$ , and  $PF_{N221} - PF_{N222}$ , if they are all positive or negative, then we have  $\det A > 0$  and  $\text{tr} A > 0$ , or  $\det A < 0$  and  $\text{tr} A < 0$ , and so the equilibrium point  $P_1(0, 0, 0)$  is not evolutionary stable; if one of them is positive, and two others are negative, then there exist two cases: (1) when the sum of absolute values of two negative items is larger than the positive one, we have  $\det A > 0$  and  $\text{tr} A > 0$ , and then, the equilibrium point  $P_1(0, 0, 0)$  is evolutionary

stable, and (2) when the sum of absolute values of two negative items is less than the positive one, we have  $\det A > 0$  and  $\text{tr} A > 0$ , and then, the equilibrium point  $P_1(0, 0, 0)$  is not evolutionary stable; if one of them is negative, and two others are positive, we have  $\det A > 0$ , and then, the equilibrium point  $P_1(0, 0, 0)$  is not evolutionary stable.

For the equilibrium points  $P_2(0, 0, 1)$ ,  $P_3(0, 1, 0)$ ,  $P_4(0, 1, 1)$ ,  $P_5(1, 0, 0)$ ,  $P_6(1, 0, 1)$ ,  $P_7(1, 1, 0)$ , and  $P_8(1, 1, 1)$ , we have the following:

$$\begin{aligned}
J_{(0,0,1)} &= \text{diag}(PF_{M121} - PF_{M221}, PF_{G211} - PF_{G221}, PF_{N222} - PF_{N221}), \\
J_{(0,1,0)} &= \text{diag}(PF_{M112} - PF_{M212}, PF_{G222} - PF_{G212}, PF_{N211} - PF_{N212}), \\
J_{(0,1,1)} &= \text{diag}(PF_{M111} - PF_{M211}, PF_{G221} - PF_{G211}, PF_{N212} - PF_{N211}), \\
J_{(1,0,0)} &= \text{diag}(PF_{M222} - PF_{M122}, PF_{G112} - PF_{G122}, PF_{N121} - PF_{N122}),
\end{aligned}$$

$$\begin{aligned}
J_{(1,0,1)} &= \text{diag}(\text{PF}_{M221} - \text{PF}_{M121}, \text{PF}_{G111} - \text{PF}_{G121}, \text{PF}_{N122} - \text{PF}_{N121}), \\
J_{(1,1,0)} &= \text{diag}(\text{PF}_{M212} - \text{PF}_{M112}, \text{PF}_{G122} - \text{PF}_{G112}, \text{PF}_{N112} - \text{PF}_{N111}), \\
J_{(1,1,1)} &= \text{diag}(\text{PF}_{M211} - \text{PF}_{M111}, \text{PF}_{G121} - \text{PF}_{G111}, \text{PF}_{N112} - \text{PF}_{N111}).
\end{aligned} \tag{17}$$

Similar to the above discussion of the equilibrium point  $P_1(0,0,0)$ , the stabilities of the remaining equilibrium points are as follows. For  $[\text{PF}_{M121} - \text{PF}_{M221}, \text{PF}_{G211} - \text{PF}_{G221}, \text{PF}_{N222} - \text{PF}_{N221}]$ ,  $[\text{PF}_{M112} - \text{PF}_{M212}, \text{PF}_{G222} - \text{PF}_{G212}, \text{PF}_{N211} - \text{PF}_{N212}]$ ,  $[\text{PF}_{M111} - \text{PF}_{M211}, \text{PF}_{G221} - \text{PF}_{G211}, \text{PF}_{N212} - \text{PF}_{N211}]$ ,  $[\text{PF}_{M222} - \text{PF}_{M122}, \text{PF}_{G112} - \text{PF}_{G122}, \text{PF}_{N121} - \text{PF}_{N122}]$ ,  $[\text{PF}_{M221} - \text{PF}_{M121}, \text{PF}_{G111} - \text{PF}_{G121}, \text{PF}_{N122} - \text{PF}_{N121}]$ ,  $[\text{PF}_{M212} - \text{PF}_{M112}, \text{PF}_{G122} - \text{PF}_{G112}, \text{PF}_{N112} - \text{PF}_{N111}]$ , and  $[\text{PF}_{M211} - \text{PF}_{M111}, \text{PF}_{G121} - \text{PF}_{G111}, \text{PF}_{N112} - \text{PF}_{N111}]$ , if they (the items in a symbol “[ ]”) are all positive or negative, then the equilibrium points  $P_2(0,0,1)$ ,  $P_3(0,1,0)$ ,  $P_4(0,1,1)$ ,  $P_5(1,0,0)$ ,  $P_6(1,0,1)$ ,  $P_7(1,1,0)$ , and  $P_8(1,1,1)$  are not evolutionary stable; if one of them is positive and two others are negative, then  $P_2(0,0,1)$ ,  $P_3(0,1,0)$ ,  $P_4(0,1,1)$ ,  $P_5(1,0,0)$ ,  $P_6(1,0,1)$ ,  $P_7(1,1,0)$ , and  $P_8(1,1,1)$  are evolutionary stable while the sum of absolute values of two negative items is larger than the positive one and are not evolutionary stable while the sum of absolute values of two negative items is less than the positive one; and if one of them is negative, and two others are positive, then the equilibrium points  $P_2(0,0,1)$ ,  $P_3(0,1,0)$ ,  $P_4(0,1,1)$ ,  $P_5(1,0,0)$ ,  $P_6(1,0,1)$ ,  $P_7(1,1,0)$ , and  $P_8(1,1,1)$  are not evolutionary stable.

### 3. Experiment

To facilitate the quantification of parameters on the tripartite evolutionary game model, we exploit the same value functions and decision (probability) weighting functions [36] to characterize (initial) incomes, costs, profits, bonuses, losses, fines, and decision probabilities. To simplify the following experiments, the (initial) incomes, bonus, and profits are measured by the value function:

$$V(x) = \begin{cases} (x - U_0)^\theta, & x \geq U_0, \\ -\lambda(U_0 - x)^\beta, & x < U_0, \end{cases} \tag{18}$$

where  $\beta = 0.88$ ,  $\theta = 0.88$ ,  $\lambda = 2$ ;  $U_0 \in [-1, 1]$  is the reference point.

The costs, losses, and fines in the game are characterized by the value function:

$$Z(x) = \begin{cases} \delta(x - U_1)^\phi, & x \geq U_1, \\ -(U_1 - x)^\sigma, & x < U_1, \end{cases} \tag{19}$$

where  $\delta = 2$ ,  $\phi = 0.98$ ,  $\sigma = 0.98$ ;  $U_1 \in [0, 1]$  is the reference point.

The decision probabilities choosing the strategies  $M_1$ ,  $G_1$ , and  $N_1$  in the game are calculated by the decision (probability) weighting function:

$$\pi(\epsilon) = \frac{\epsilon^\Gamma}{[\epsilon^\Gamma + (1 - \epsilon)^\Gamma]^{1/\Gamma}}, \tag{20}$$

where  $\Gamma = 0.75$ .

In the following experiments, for the reference point  $U_0$  ( $U_1$ , respectively), we randomly generate 50 data, which satisfied the uniform distribution in  $[-1, 1]$  ( $[0, 1]$ , respectively), and take their average value as the reference point. When one influence parameter is considered, other parameters are set as follows: (1) the decision probabilities are set as 0.5; (2) the values of initial incomes, bonuses, and profits are set as 0; and (3) the values of costs, losses, and fines are set as 0.5.

Next, the expected payoffs of the network media, government, and netizen for misinformation propagation in the tripartite evolutionary game model are discussed based on the decision probabilities, (initial) incomes, profits, bonuses, costs, losses, and fines, respectively. In Figure 2, the expected payoffs of the network media, government, and netizen for misinformation propagation change with the values of decision probabilities, i.e.,  $x$ ,  $y$ , and  $z$  in  $[0, 1]$ , respectively. When we analyze parameter  $x$  (resp.  $y$  or  $z$ ), we generated 50 random numbers  $x$  (resp.  $y$  or  $z$ ), which satisfy the uniform distribution in  $[0, 1]$ , and the rest of the other parameters remain unchanged according to the default settings.

It shows that the expected payoffs EM and EG increase when the probabilities of choosing  $M_1$  and  $G_1$  rise, respectively. However, the expected payoff EN decreases when the probabilities of choosing  $N_1$  increase. These results show that if the decision probabilities of the network media and government that they, respectively, choose the “promoting misinformation” and “supervision” strategies increase, their payoffs rise continuously. On the contrary, the payoff of the netizen drops quickly, while the decision probability of choosing the “spread” strategy increases.

In Figure 3, the expected payoffs of the network media for misinformation propagation change with (initial) incomes, profits, bonuses, costs, losses, and fines, respectively. The values of  $\text{IM}_0$ ,  $\text{IM}_1$ ,  $\text{IM}_2$ ,  $\text{BM}_1$ , and  $\text{BM}_2$  belong to  $[-1, 1]$ . The values of  $\text{CM}_1$ ,  $\text{CM}_2$ ,  $\text{LM}$ ,  $\text{FM}_1$ ,  $\text{FM}_2$ ,  $\text{FM}_3$ , and  $\text{FM}_4$  belong to  $[0, 1]$ . The experimental results show that as the values of  $\text{IM}_0$ ,  $\text{IM}_1$ ,  $\text{IM}_2$ ,  $\text{BM}_1$ , and  $\text{BM}_2$  increase, the expected payoff EM increases; and as the values of  $\text{CM}_1$ ,  $\text{CM}_2$ ,  $\text{LM}$ ,  $\text{FM}_1$ ,  $\text{FM}_2$ ,  $\text{FM}_3$ , and  $\text{FM}_4$  increase, the expected payoff slowly decreases. It also shows that the lower the value of  $\text{IM}_0$  is, the lower the expected payoff is; the lower the values of  $\text{LM}$  and  $\text{CM}_1$  are, the higher the expected payoffs are. This phenomenon means that to increase the expected payoff of network media, it is necessary to increase the initial income. In particular, to improve the expected payoff of network media, when the network media choose  $M_2$ , the network media can increase the advertisements, click rate, netizen, and popularity. When the network media choose

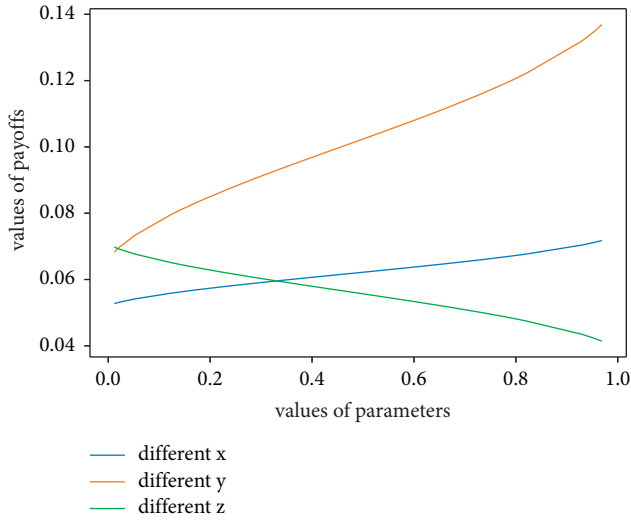


FIGURE 2: Impacts of different decision probabilities on expected payoffs.

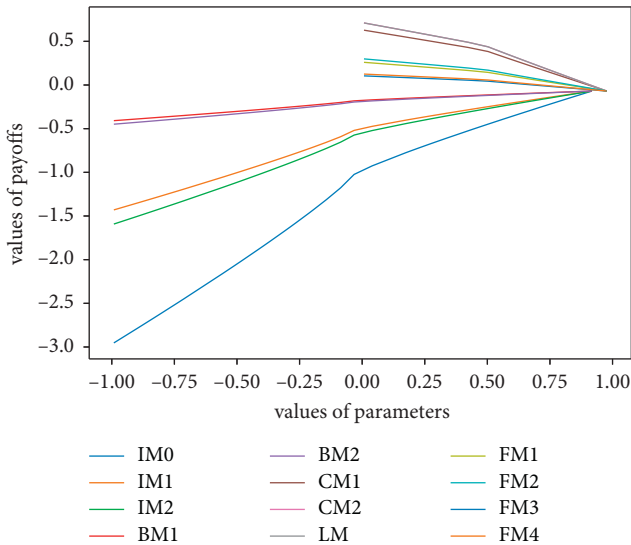


FIGURE 3: Impacts of different parameters on the expected payoffs of the network media.

$M_1$ , the network media can decrease the cost from manpower, material resources, etc.

In Figure 4, the expected payoffs of the government for misinformation propagation change with (initial) incomes, profits, bonuses, costs, losses, and fines, respectively. The values of  $IG_0, IG_1, IG_2, BG_1$ , and  $BG_2$  belong to  $[-1, 1]$ . The values of  $CG, LG_1, LG_2, FG_1$ , and  $FG_2$  belong to  $[0, 1]$ . The experimental results show that as the values of  $IG_0, IG_1, IG_2, BG_1$ , and  $BG_2$  increase, the expected payoffs steadily go up, whereas the values of  $CG, LG_1, LG_2, FG_1$ , and  $FG_2$  increase, expected payoffs continuously decrease. They also show that the lower the value of  $IG_0$  is, the lower the expected payoff is; and the lower the value of  $CG$  is, the higher the expected payoff is. It concludes that if the government intends to increase its expected payoff, when the government chooses  $G_1$ , it can increase the initial income; and if the government

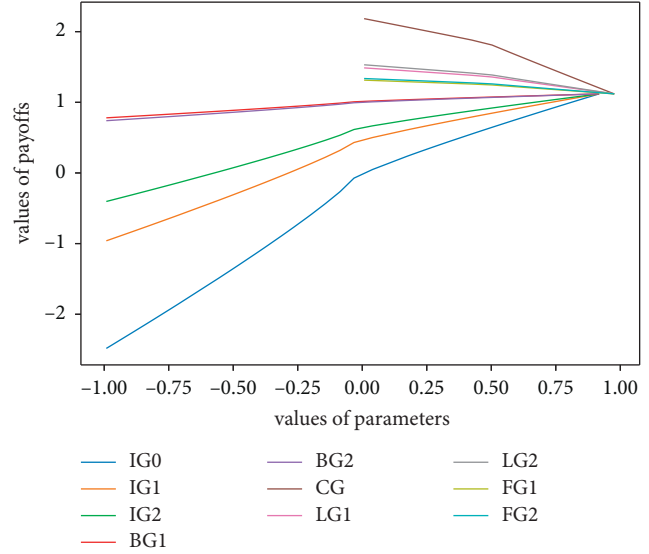


FIGURE 4: Impact of different parameters on the expected payoff of the government.

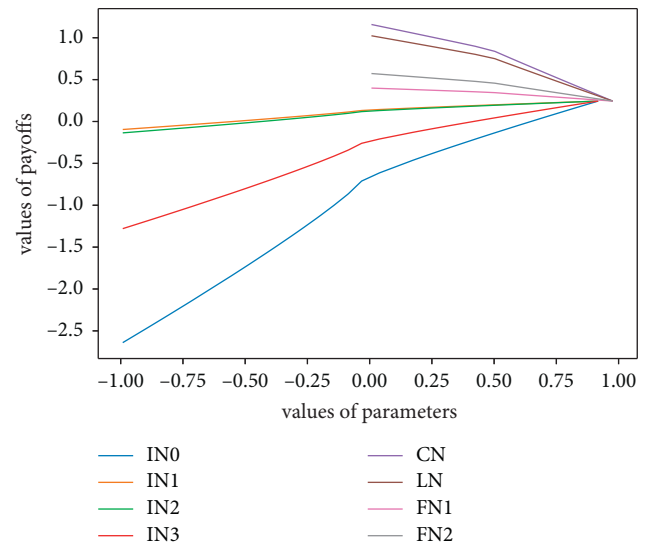


FIGURE 5: Impacts of different parameters on the expected payoffs of the netizen.

chooses  $G_2$ , it can decrease the cost from manpower, material resources, etc.

In Figure 5, the expected payoffs of the netizen for misinformation propagation change with (initial) incomes, profits, costs, losses, and fines, respectively. The values of  $IN_0, IN_1, IN_2$ , and  $IN_3$  belong to  $[-1, 1]$ . The values of  $CN, LN, FN_1$ , and  $FN_2$  belong to  $[0, 1]$ . The experimental results show that as the values of  $IN_0, IN_1, IN_2$ , and  $IN_3$  increase, the expected payoffs increase; and as the values of  $CN, LN, FN_1$ , and  $FN_2$  increase, the expected payoffs quickly reduce. The results also show that the lower the value of  $IN_0$  is, the lower the expected payoff is; the lower the values of  $CN$  and  $LN$  are, the higher the expected payoffs are. This phenomenon means that if the netizen wants to promote the expected payoff of the netizen, the netizen can increase the initial

income. That is, if the netizen expects to increase its expected payoff, when the netizen chooses  $N_1$ , it can decrease the cost from manpower, material resources, etc. When the netizen chooses  $N_2$ , it can increase the attention, followers, etc.

Based on the above discussion, the expected payoffs of the players in the proposed tripartite evolutionary game model for misinformation propagation are influenced by different parameters including (initial) incomes, profits, bonuses, costs, losses, and fines. If one player intends to increase its expected payoff, then it can choose a proper strategy and can select various measures to change the values of different parameters, maximizing the expected payoff of the player.

#### 4. Conclusion

This study established a tripartite evolutionary game model for misinformation propagation. This model considered three players, i.e., network media, government, and netizen. Various parameters, such as (initial) incomes, profits, bonuses, costs, losses, and fines, are proposed for three players. The expected payoffs of the players are derived in detail. By evolutionary replication dynamic equations, the evolutionary stable strategies for the proposed model are proved theoretically. Finally, some experiments are made to find the influences of different parameters on the proposed game model. To increase the expected payoffs of network media, government, and netizen, if the network media, government, and netizen choose “promoting misinformation,” “non-supervision,” and “spread,” respectively, the network media, government, and netizen can decrease manpower, material resources, and so on. If the network media choose “blocking misinformation propagation,” the network media can increase the advertisements, click rate, netizen, and popularity. If the government chooses “supervision,” it can increase the initial income. If the netizen chooses “non-spread,” it can increase the attention, followers, etc. In future, the experiments of the tripartite evolutionary game model on real misinformation dataset and the new evolutionary game model for misinformation propagation are both worthy of study carefully.

#### Data Availability

Data sharing is not applicable to this article as no datasets were generated.

#### Conflicts of Interest

Sichuan Suitang Science and Technology Co., Ltd. was affiliated with this study. The authors declare that there are no conflicts of interest.

#### Authors' Contributions

The authors claim that the research was realized in collaboration with the same responsibility. All authors read and approved the last version of the manuscript.

#### Acknowledgments

This work was partially supported by the National Natural Science Foundation of China (Nos. 61 802 316, 61 872 298, and 61 902 324), Chunhui Plan Cooperation and Research Project, Ministry of Education of China (Nos. Z2015109 and Z2015100), “Young Scholars Reserve Talents” program of Xihua University, Science and Technology Department of Sichuan Province (Nos. 22ZDYF3157 and 2021YFQ0008), Key Scientific Research Fund of Xihua University (No. z1422615), and Innovation Fund of Postgraduate, Xihua University (Nos. YCJJ2021025, YCJJ2021031, and YCJJ2021124), and Opening Project of Intelligent Policing Key Laboratory of Sichuan Province (No. ZNJW2022ZZZD003).

#### References

- [1] H. Zhang, M. A. Alim, X. Li, M. T. Thai, and H. T. Nguyen, “Misinformation in online social networks: detect them all with a limited budget,” *ACM Transactions on Information Systems*, vol. 34, no. 3, p. 18, 2016.
- [2] C. V. Pham, M. T. Thai, H. V. Duong, B. Q. Bui, and H. X. Hoang, “Maximizing misinformation restriction within time and budget constraints,” *Journal of Combinatorial Optimization*, vol. 35, no. 4, pp. 1202–1240, 2018.
- [3] Z. Tan, D. Wu, T. Gao, I. You, and V. Sharma, “AIM: activation increment minimization strategy for preventing bad information diffusion in OSNs,” *Future Generation Computer Systems*, vol. 94, pp. 293–301, 2019.
- [4] W. Liu, X. Wu, W. Yang, X. Zhu, and S. Zhong, “Modeling cyber rumor spreading over mobile social networks: a compartment approach,” *Applied Mathematics and Computation*, vol. 343, no. 4, pp. 214–229, 2019.
- [5] G. Shrivastava, P. Kumar, R. P. Ojha, P. K. Srivastava, S. Mohan, and G. Srivastava, “Defensive modeling of fake news through online social networks,” *IEEE Transactions on Computational Social Systems*, vol. 7, no. 5, pp. 1159–1167, 2020.
- [6] C. Wang, G. Wang, X. Luo, and H. Li, “Modeling rumor propagation and mitigation across multiple social networks,” *Physica A: Statistical Mechanics and its Applications*, vol. 535, Article ID 122240, 2019.
- [7] M. Jiang, Q. Gao, and J. Zhuang, “Reciprocal spreading and debunking processes of online misinformation: a new rumor spreading-debunking model with a case study,” *Physica A: Statistical Mechanics and its Applications*, vol. 565, Article ID 125572, 2021.
- [8] M. A. Manouchehri, M. S. Helfroush, and H. Danyali, “A theoretically guaranteed approach to efficiently block the influence of misinformation in social networks,” *IEEE Transactions on Computational Social Systems*, vol. 8, no. 3, pp. 716–727, 2021.
- [9] C. Wang, Y. Zhang, Q. Shi, Y. Feng, and C. Chen, “Efficient influence spread management via budget allocation at community scale,” *Expert Systems with Applications*, vol. 175, Article ID 114814, 2021.
- [10] A. Zareie and R. Sakellariou, “Minimizing the spread of misinformation in online social networks: a survey,” *Journal of Network and Computer Applications*, vol. 186, Article ID 103094, 2021.
- [11] R. Aswani, A. K. Kar, and P. V. Ilavarasan, “Experience: managing misinformation in social media—insights for

- policymakers from twitter analytics,” *Journal of Data and Information Quality*, vol. 12, no. 1, pp. 1–18, 2020.
- [12] M. Glenski, T. Weninger, and S. Volkova, “Propagation from deceptive news sources who shares, how much, how evenly, and how quickly?” *IEEE Transactions on Computational Social Systems*, vol. 5, no. 4, pp. 1071–1082, 2018.
- [13] A. K. Kar and R. Aswani, “How to differentiate propagators of information and misinformation-Insights from social media analytics based on bio-inspired computing,” *Journal of Information and Optimization Sciences*, vol. 42, no. 6, pp. 1307–1335, 2021.
- [14] S. Chen, L. Xiao, and J. Mao, “Persuasion strategies of misinformation-containing posts in the social media,” *Information Processing and Management*, vol. 58, no. 5, Article ID 102665, 2021.
- [15] G. K. Shahi, A. Dirkson, and T. A. Majchrzak, “An exploratory study of COVID-19 misinformation on Twitter,” *Online Social Networks and Media*, vol. 22, Article ID 100104, 2021.
- [16] M. Liu and L. Rong, “An online multi-dimensional opinion dynamic model with misinformation diffusion in emergency events,” *Journal of Information Science*, 2021.
- [17] N. Abuzainab and W. Saad, “A multiclass mean-field game for thwarting misinformation spread in the internet of battlefield things,” *IEEE Transactions on Communications*, vol. 66, no. 12, pp. 6643–6658, 2018.
- [18] Y. Wang, M. McKee, A. Torbica, and D. Stuckler, “Systematic literature review on the spread of health-related misinformation on social media,” *Social Science and Medicine*, vol. 240, Article ID 112552, 2019.
- [19] Y. Xiao, C. Song, and Y. Liu, “Social hotspot propagation dynamics model based on multidimensional attributes and evolutionary games,” *Communications in Nonlinear Science and Numerical Simulation*, vol. 67, pp. 13–25, 2019.
- [20] Q. Li, C. Song, B. Wu, Y. Xiao, and B. Wang, “Social hotspot propagation dynamics model based on heterogeneous mean field and evolutionary games,” *Physica A: Statistical Mechanics and its Applications*, vol. 508, pp. 324–341, 2018.
- [21] J. Wang, X. Wang, and L. Fu, “Evolutionary game model of public opinion information propagation in online social networks,” *IEEE Access*, vol. 8, Article ID 127732, 2020.
- [22] F. Xiong, X. Wang, S. Pan, H. Yang, H. Wang, and C. Zhang, “Social recommendation with evolutionary opinion dynamics,” *IEEE Transactions on Systems, Man, and Cybernetics: Systems*, vol. 50, no. 10, pp. 3804–3816, 2020.
- [23] X. Yang, Z. Zhu, H. Yu, Y. Zhao, and L. Guo, “Evolutionary Game Dynamics of the Competitive Information Propagation on Social Networks,” *Complexity*, vol. 2019, Article ID 8385426, 11 pages, 2019.
- [24] J. Lv, W. Yao, Y. Wang, Z. Wang, and J. Yu, “A game model for information dissemination in live streaming e-commerce environment,” *International Journal of Communication Systems*, vol. 35, no. 18, 2021.
- [25] Y. Zhang, L. Wang, J. J. H. Zhu, and X. Wang, “Conspiracy vs science: a large-scale analysis of online discussion cascades,” *World Wide Web*, vol. 24, no. 2, pp. 585–606, 2021.
- [26] X. Wang, Y. Wu, Y. Ren, R. Feng, N. Yu, and J. Wan, “An evolutionary game-based trust cooperative stimulation model for large scale MANETs,” *International Journal of Distributed Sensor Networks*, vol. 9, no. 6, Article ID 245017, 2013.
- [27] Y. Xiao, D. Chen, S. Wei, Q. Li, H. Wang, and M. Xu, “Rumor propagation dynamic model based on evolutionary game and anti-rumor,” *Nonlinear Dynamics*, vol. 95, no. 1, pp. 523–539, 2019.
- [28] Y. Xiao, Q. Yang, C. Sang, and Y. Liu, “Rumor diffusion model based on representation learning and anti-rumor,” *IEEE Transactions on Network and Service Management*, vol. 17, no. 3, pp. 1910–1923, 2020.
- [29] M. Askarizadeh, B. T. Ladani, and M. H. Manshaei, “An evolutionary game model for analysis of rumor propagation and control in social networks,” *Physica A: Statistical Mechanics and its Applications*, vol. 523, pp. 21–39, 2019.
- [30] M. Askarizadeh and B. Tork Ladani, “Soft rumor control in social networks: modeling and analysis,” *Engineering Applications of Artificial Intelligence*, vol. 100, Article ID 104198, 2021.
- [31] H. Zhang, Y. Li, Y. Chen, and H. V. Zhao, “Smart evolution for information diffusion over social networks,” *IEEE Transactions on Information Forensics and Security*, vol. 16, pp. 1203–1217, 2021.
- [32] X. Gao, S. Feng, D. Niyato, P. Wang, K. Yang, and Y. C. Liang, “Dynamic access point and service selection in backscatter-assisted RF-powered cognitive networks,” *IEEE Internet of Things Journal*, vol. 6, no. 5, pp. 8270–8283, 2019.
- [33] M. Alam, Y. Ida, and J. Tanimoto, “Abrupt epidemic outbreak could be well tackled by multiple pre-emptive provisions-A game approach considering structured and unstructured populations,” *Chaos, Solitons and Fractals*, vol. 143, Article ID 110584, 2021.
- [34] H. Huang, T. Wang, M. Hu, M. Dong, and L. Lai, “Node attitude aware information dissemination model based on evolutionary game in social networks,” *Mobile Networks and Applications*, vol. 26, no. 1, pp. 114–129, 2021.
- [35] M. L. Manapat and D. G. Rand, “Delayed and inconsistent information and the evolution of trust,” *Dynamic Games and Applications*, vol. 2, no. 4, pp. 401–410, 2012.
- [36] B. Wu, J. Cheng, and Y. Qi, “Tripartite evolutionary game analysis for “Deceive acquaintances” behavior of e-commerce platforms in cooperative supervision,” *Physica A: Statistical Mechanics and its Applications*, vol. 550, Article ID 123892, 2020.



## Research Article

# Lag Secure Consensus for Second-Order Nonlinear Multiagent Systems with Event-Triggered Control Strategy under DoS Attacks

Qi Han <sup>1</sup>, Ao Zhang <sup>1</sup>, Tengfei Weng,<sup>1</sup> Yan Xie,<sup>1</sup> Liping Feng <sup>2</sup>, Guorong Chen,<sup>1</sup> and Yuan Tian<sup>1</sup>

<sup>1</sup>School of Intelligent Technology and Engineering, Chongqing University of Science and Technology, Chongqing 401331, China

<sup>2</sup>Computer Science Department, Xinzhou Teachers University, Xinzhou, Shanxi 034000, China

Correspondence should be addressed to Ao Zhang; [zhangaocq@163.com](mailto:zhangaocq@163.com)

Received 10 November 2021; Accepted 31 December 2021; Published 19 January 2022

Academic Editor: Chenquan Gan

Copyright © 2022 Qi Han et al. This is an open access article distributed under the Creative Commons Attribution License, which permits unrestricted use, distribution, and reproduction in any medium, provided the original work is properly cited.

Compared with previous studies, this paper focuses on the time delay phenomenon in the consensus state between the leader and followers and considers that the DoS attack occurs nonperiodically. First, a new event-triggered mechanism and lag consensus control strategy are proposed. Then, through the Lyapunov stability theory, algebraic knowledge, and graph theory, it is proved that followers and leader can achieve lag consistent under the DoS attack, and the trigger interval is designed to ensure that Zeno behavior does not occur. Finally, the correctness and effectiveness of the proposed theory and method are verified by numerical simulation.

## 1. Introduction

In recent years, distributed cooperative control of multi-agent systems (MASs) has been widely used in various fields, such as smart grid collaborative control [1], distributed optimal cooperation [2], coordinated defense systems [3], and so on. In cooperative control, the consensus has always been a hot topic in the research of multi-agent systems. Many researchers have studied the consensus of MASs from different perspectives [4–6]. The overall goal of leader-follower consensus is to drive the states of all followers in the network to track the state of the leader [7]. However, in the actual communication process, many factors, such as the limitation of communication speed, the limited bandwidth, and the asymmetry of information transmission, may lead to delay in transmitting and receiving information between agents [8]. At present, there are many research results on the consensus of communication delay systems. Reference [9] investigated the consensus problem of continuous-time nonlinear MASs with time-varying communication delay via reliable control. The tracking consensus regulation was studied in [10], where high-order MASs was subjected to Lipschitz nonlinear perturbations.

In order to solve the problem of limited resources to a certain extent, this paper introduces an event trigger mechanism to design a control protocol [11]. The event-trigger mechanism avoids the problem of continuous update of the controller, which not only reduces the amount of data in network transmission but also extends the service life of network components. The event-triggered distributed predictive control (DPC) problem was considered in [12], where multi-agent systems were subject to bounded disturbances. Reference [13] studied the event-triggered containment control problem for a class of networked nonlinear MASs subjected to limited communication resources and proposed a distributed containment output feedback control strategy with an event-triggered communication mechanism.

With the increasingly mature communication technology, the denial-of-service attacks always threaten the normal work of the network systems. The DoS attacks prevent legitimate users from accessing resources properly and even collapse the resources [14]. Therefore, in order to avoid DoS attacks causing damage to the system, some security control protocols have been proposed [15–18]. Reference [19] investigated the secure consensus for second-order MASs with

nonlinear dynamics and event-triggered control strategy under DoS attacks. In [20], a distributed stochastic model predictive controller was designed for a networked control system with stochastic disturbances and denial-of-service (DoS) attacks. Reference [21] investigated the leader-follower robust  $H_\infty$  consensus of heterogeneous multi-agent systems with denial-of-service attacks. Reference [22] studied the secure consensus problem of multiagent systems under switching topologies, and the studied multiagent systems were affected by both denial-of-service (DoS) attacks and external disturbances. The observer-based output feedback control problem was studied in [23] for cyber-physical systems against randomly occurring packet dropout and periodic DoS attacks. The problem of event-triggered distributed state estimation was considered in [24] for linear multiagent systems under DoS attacks. The distributed event-triggered consensus problem of a generally linear multiagent system was considered in [25] with periodic DoS jamming attacks. Reference [26] applied an input-based triggering approach to investigate the secure consensus problem in multiagent systems under DoS attacks. Reference [27] studied secure L-F consensus of linear MASs under a directed communication network with denial-of-service (DoS) attacks. However, there are few studies on the consensus of nonlinear systems under DoS attacks. In practical applications, most systems are nonlinear, so it is necessary to study nonlinear systems and have practical application value. Compared with the above methods, the distributed control algorithm proposed in this paper achieves the lag consensus of MASs under DoS attacks.

The consensus considered in most of the above literatures was completely consistent  $\lim_{t \rightarrow +\infty} \|x_i(t) - x_0(t)\| = 0$ . However, in the real network, there is a time lag between the state of leader (indexed the leader agent as node 0) and followers, where lag consensus can be denoted  $\lim_{t \rightarrow +\infty} \|x_i(t) - x_0(t - \tau)\| = 0$  ( $\tau > 0$  is time delay). In real life, being completely consistent may bring us trouble, and lag consistent can avoid such trouble. For example, many cars are on a road. If they need to reach a certain location at the same time, they may cause a traffic jam. But if they have an appropriate delay on the arrival time, they can pass smoothly and orderly. Reference [28] studied lag consensus of second-order nonlinear MASs. Reference [29] proposed a new distributed controller to solve the prescribed-time cluster lag consensus control for MASs. Reference [30] investigated the problem of cluster lag consensus for first-order MASs which can be formulated as moving agents in a capacity-limited network. Our three contributions in this paper as follows:

- (1) The denial-of-service attacks always threaten the normal work of the network systems. However, there are few studies on the consensus of nonlinear systems under DoS attacks, and the lag consensus in this paper is also rarely studied in this field.
- (2) DoS attacks are periodically initiated using known attack strategies in [16], [23], and [25]. However, in practical applications, we often do not predict how DOS attacks will work. Therefore, this paper

considers that DoS attacks are nonperiodic and the attack strategy is unknown. In addition, the lag secure consensus of the system is studied in this case.

- (3) An event-triggered controller is designed for lag consensus, and the lag secure consensus is studied for second-order nonlinear MASs with event-triggered control strategy under DoS attack. Through the Lyapunov stability method, a sufficient condition is given for ensuring lag secure consensus of multi-agent system.

*Notations.*  $\mathbb{R}^n$  represents the  $n$ -dimensional Euclidean space, the diagonal matrix is represented by  $\text{diag}(\dots)$ .  $\|\cdot\|$  refers to the Euclidean norm.  $\mathbb{N}$  represents a positive integer.  $I_{Nn}$  denotes the  $N \times n$  identity matrix. The Kronecker product is denoted by  $\otimes$ . For two sets  $Y$  and  $Z$ ,  $Y/Z$  means excluding elements belonging to  $Z$  in  $Y$ .

## 2. Problem Formulation

*2.1. Graph Theory.* For a multiagent system consisting of  $N$  followers, the directed graph  $G = (V, E, A)$  represents the communication topology, where  $V = \{v_1, v_2, \dots, v_N\}$  is the agent set,  $E = \{e_{ji} = (v_i, v_j), v_i \neq v_j\}$ ,  $\subseteq V \times V$  represents the edge set, and the adjacency matrix of  $G$  is represented by  $A = (a_{ij})_{N \times N} \in \mathbb{R}^{N \times N}$ .  $(v_i, v_j)$  represents that  $v_j$  can transmit information to  $v_i$ . If  $(v_i, v_j) \in E, \forall v_i, v_j \in V$ , then  $a_{ij} > 0$ , and  $a_{ij} = 0$  otherwise.  $D = \text{diag}(d_1, d_2, \dots, d_N)$  is a diagonal matrix, where  $d_i > 0$  indicates that the leader can transmit information to node  $v_i$ , otherwise  $d_i = 0$ . The Laplace matrix in  $G$  satisfies the following definition:

$$L_{ij} = \begin{cases} \sum_{j \in N, j \neq i} a_{ij}, & i = j, \\ -a_{ij}, & i \neq j. \end{cases} \quad (1)$$

$\bar{G}$  represents the directed graph of the MASs composed of  $N$  followers and a leader. Clearly,  $G$  is a subgraph of  $\bar{G}$ .

*2.2. System Model.* Considering that the MASs in this paper consists of  $N$  followers and a leader, the dynamics of the leader agent is given as

$$\begin{cases} \dot{x}_0(t) = v_0(t), \\ \dot{v}_0(t) = g(t, x_0(t), v_0(t)), \end{cases} \quad (2)$$

where  $x_0(t) \in \mathbb{R}^n$  and  $v_0(t) \in \mathbb{R}^n$  represent the position and velocity of the leader respectively, and  $g(t, x_0(t), v_0(t)) \in \mathbb{R}^n$  is a nonlinear function.

The dynamics of the  $i$ th follower agent can be described as

$$\begin{cases} \dot{x}_i(t) = v_i(t), \\ \dot{v}_i(t) = g(t, x_i(t), v_i(t)) + u_i(t), \end{cases} \quad (3)$$

where  $i = 1, 2, \dots, N$ ,  $x_i(t) \in \mathbb{R}^n$  is the position of the  $i$ th agent, the velocity of the  $i$ th agent can be expressed by  $v_i(t) \in \mathbb{R}^n$ , and  $u_i(t) \in \mathbb{R}^n$  represents the control input of the  $i$ th agent.  $g(t, x_i(t), v_i(t)) = [g_1(t, x_1(t), v_1(t)),$

$g_2(t, x_2(t), v_2(t)), \dots, g_N(t, x_i(t), v_i(t))]^T \in \mathbb{R}^n$  is a nonlinear function.

*Assumption 1.* There exist two nonnegative constants  $\beta_1$  and  $\beta_2$ , so that  $g(t, x_i(t), v_i(t))$  satisfies the following condition:

$$\|g(t, x, v) - g(t, y, w)\| \leq \beta_1 \|x - y\| + \beta_2 \|v - w\|, \quad (4)$$

$$\forall x, y, v, w \in \mathbb{R}^n, t \in [0, \infty).$$

*Assumption 2.* Assume that the graph  $\bar{G}$  is directed and at least one directed spanning tree exists.

**2.3. DoS Attack Model.** The DoS attack [16–19] refers to intentionally attacking network protocols or a large number of illegal users who directly exhaust the resources of the attacked object. In this paper, DoS attacks are assumed to occur nonperiodic based on time series, and their attack energy is limited. The end of an attack requires stopping to add energy. DoS attacks can attack targets in many ways and its attack strategy is unknown. DoS attacks can affect the control channel so that the agent loses control. Let  $\{\tilde{t}_m\}_{m \in \mathbb{N}}$  represents the attack sequence initiated by the denial of service attack at  $\tilde{t}_m$ .  $H_m = [\tilde{t}_m, \tilde{t}_m + \tilde{\Delta}_m]$  represents the  $m$ th DoS time interval, where  $\tilde{\Delta}_m > 0$  is length. Obviously,  $\tilde{t}_{m+1} > \tilde{t}_m + \tilde{\Delta}_m$ . For the given  $t > t_0 \in \mathbb{R}$ , similar to [27], let

$$\prod_a(t_0, t) = \cup H_m \cap [t_0, t], \quad m \in \mathbb{N}, \quad (5)$$

denote the time instants set of communication rejected.  $\prod_s(t_0, t) = [t_0, t] / \prod_a(t_0, t)$  represent the sets of time for communication areas.

$$u_i(t) = -\varepsilon Z_i(t_{k_i}^i) = -\varepsilon \sum_{j=1}^N a_{ij} \left( x_i(t_{k_i}^i) - x_j(t_{k_j}^j) + v_i(t_{k_i}^i) - v_j(t_{k_j}^j) \right) - \varepsilon d_i \left( x_i(t_{k_i}^i) - x_0(t_{k_i}^i - \tau) + v_i(t_{k_i}^i) - v_0(t_{k_i}^i - \tau) \right), \quad t \in [t_{k_i}^i, t_{k_{i+1}}^i), \quad (9)$$

Where the triggering instant of agent  $j$  is represented by  $t_{k_j}$ , and  $\varepsilon > 0$ , and  $\tau$  represent the control gain and a time delay, respectively. When  $d_i > 0$ , it means that the leader can send

*Definition 1* (secure leader-following lag consensus [8]). A control law  $u_i(t)$  can achieve the secure lag consensus for MASs (1) and (2) under DoS attacks if the following conditions are satisfied:

$$\lim_{t \rightarrow \infty} \|x_i(t) - x_0(t - \tau)\| = 0, \quad i = 1, 2, \dots, N, \quad (6)$$

$$\lim_{t \rightarrow \infty} \|v_i(t) - v_0(t - \tau)\| = 0, \quad i = 1, 2, \dots, N.$$

For any initial condition  $x_i(0)$  and  $v_i(0)$ ,  $i = 1, 2, \dots, N$ .

*Definition 2* (attack frequency [27]). For any  $T_2 > T_1 \geq t_0$ , the total number of DoS attacks occurring over  $[T_1, T_2)$  is denoted by  $N_a(T_1, T_2)$ . Thus, the attack frequency is defined as

$$F_a(T_1, T_2) = \frac{N_a(T_1, T_2)}{T_2 - T_1}. \quad (7)$$

*Definition 3* (attack length rate [19]). For any  $t > t_0 > 0$ , the total time interval of DoS attacks occurring over  $[t_0, t)$  is denoted by  $\prod_a(t_0, t)$ . Thus, the attack length rate is defined as

$$r_a = \frac{\prod_a(t_0, t)}{t - t_0}. \quad (8)$$

### 3. Main Result

**3.1. Event-Triggered Control Scheme Design.** Let  $t_0 = t_0^i, t_1^i, \dots, t_{k_i}^i, \dots$  represent the event trigger times for agent  $i$ . An event-triggered control protocol under the DoS attacks was given as follows:

information to agent  $i$ , otherwise  $d_i = 0$ . The last successful update is represented by the subscript  $k_i(t)$ , which is described in [27] as follows:

$$k_i(t) = \begin{cases} -1, & \text{if } \prod_s(0, t) \in \emptyset, \sup \left\{ k_i \in \mathbb{N} \mid t_{k_i}^i \in \prod_s(0, t) \right\}, \\ \text{otherwise.} & \end{cases} \quad (10)$$

Let

$$Z_i(t) = \sum_{j=1}^N a_{ij} \left( x_i(t) - x_j(t) + v_i(t) - v_j(t) \right) + d_i \left( x_i(t) - x_0(t - \tau) + v_i(t) - v_0(t - \tau) \right). \quad (11)$$

The Event-trigger error is defined as

$$\theta_i(t) = Z_i(t_{k_i}^i) - Z_i(t). \quad (12)$$

The Event-trigger function is defined as follows:

$$f_i(t) = \|\theta_i(t)\| - \alpha \|Z_i(t_{k_i}^i)\|, \quad \alpha > 0. \quad (13)$$

The Event-trigger instant sequence of agent  $i$  is expressed as

$$t_{k_i+1}^i = \inf\{t | t > t_{k_i}^i : f_i(t) \geq 0\}. \quad (14)$$

In order to ensure that the agent does not have Zeno behavior, we adopt the following approach proposed in [31] to determine the event time instant of agent  $i$ :

$$\begin{aligned} t_{k_i+1}^i &= t_{k_i}^i + \tilde{\Delta}_{k_i}^i, \\ \tilde{\Delta}_{k_i}^i &= \max\{\tilde{\tau}_{k_i}^i, \tilde{b}_i\}, \end{aligned} \quad (15)$$

where  $\tilde{\Delta}_{k_i}^i$  represents event interval time,  $\tilde{b}_i > 0$ , and  $\tilde{\tau}_{k_i}^i$  is defined as follows:

$$\tilde{\tau}_{k_i}^i = \inf_{t > t_{k_i}^i} \{t - t_{k_i}^i | f_i(t) = 0\} \quad (16)$$

**3.2. Lag Consensus Analysis.** The consensus error is given by

$$\begin{aligned} \hat{x}_i(t) &= x_i(t) - x_0(t - \tau), \\ \hat{v}_i(t) &= v_i(t) - v_0(t - \tau). \end{aligned} \quad (17)$$

Combining with (9) and (12), systems (1) and (2) can be rewritten as

$$\begin{cases} \dot{\hat{x}}_i(t) = \hat{v}_i(t), \\ \dot{\hat{v}}_i(t) = \varepsilon \theta_i(t) - \varepsilon \sum_{j=1}^N a_{ij}(\hat{x}_j(t) + \hat{v}_j(t)), \\ -\varepsilon d_i(\hat{x}_i(t) + \hat{v}_i(t)) + g(t, x_i(t), v_i(t)) - g(t, x_0(t - \tau), v_0(t - \tau)). \end{cases} \quad (18)$$

Le

$$\begin{aligned} \hat{\eta}(t) &= [\hat{x}^T(t), \hat{v}^T(t)]^T, \\ \hat{x}(t) &= [\hat{x}_1(t), \hat{x}_2(t), \dots, \hat{x}_N(t)], \\ \hat{v}(t) &= [\hat{v}_1(t), \hat{v}_2(t), \dots, \hat{v}_N(t)], \\ G(t) &= [G^T(t, \hat{x}_1(t), \hat{v}_1(t)), G^T(t, \hat{x}_2(t), \hat{v}_2(t)), \dots, G^T(t, \hat{x}_N(t), \hat{v}_N(t))]^T, \\ G(t, \hat{x}_i(t), \hat{v}_i(t)) &= g(t, x_i(t), v_i(t)) - g(t, x_0(t - \tau), v_0(t - \tau)). \end{aligned} \quad (19)$$

Rewriting (18) as follows:

$$\dot{\hat{\eta}}(t) = \begin{bmatrix} 0 & I_N \\ -\varepsilon(L + D) & -\varepsilon(L + D) \end{bmatrix} \otimes I_n \hat{\eta}(t) + \begin{bmatrix} 0 \\ \varepsilon \end{bmatrix} \otimes I_n \theta(t) + \begin{bmatrix} 0 \\ G(t) \end{bmatrix}. \quad (20)$$

It is noticed that

$$\|\theta_i(t)\| \leq \alpha \|Z_i(t_{k_i}^i)\| \leq \alpha \|\theta_i(t) + Z_i(t)\| \leq \alpha \|\theta_i(t)\| + \alpha \|Z_i(t)\|. \quad (21)$$

From  $0 \leq \alpha < 1/3$ , we have

$$\begin{aligned} \|\theta_i(t)\| &\leq \frac{\alpha}{1 - \alpha} \|Z_i(t)\| = \frac{\alpha}{1 - \alpha} \left\| \sum_{j=1}^N a_{ij}(x_i(t) - x_j(t) + v_i(t) - v_j(t)) + d_i(x_i(t) - x_0(t - \tau) + v_i(t) - v_0(t - \tau)) \right\| \\ &= \frac{\alpha}{1 - \alpha} \left\| \sum_{j=1}^N a_{ij}(\hat{x}_j(t) + \hat{v}_j(t)) + d_i(\hat{x}_i(t) + \hat{v}_i(t)) \right\|. \end{aligned}$$

Then, we can get

$$\|\theta(t)\| \leq \omega \|\hat{\eta}(t)\|, \quad (23)$$

where  $\omega = \alpha/1 - \alpha\lambda_{\max}(L + D)$ .

**Theorem 1.** *Suppose that Assumption 1 and 2 holds. Let  $\tilde{\gamma}_1 > 0$  and  $\tilde{\gamma}_2 > 0$  satisfy  $\tilde{\gamma}_1 + \tilde{\gamma}_2 = \tilde{\gamma} < 1$ ,  $\omega^2 \leq \tilde{\gamma}_1$  and  $b_i \in (0, 1/h \ln(1 + \sqrt{\tilde{\gamma}_2/N}))$ . Lag secure consensus for MASs can be achieved under the following conditions:*

- (1) *There is a constant  $\tilde{\eta}_* \in (0, \xi_1)$  that makes the attack frequency  $F_a(t_0, t)$  in Definition 2 satisfy the following inequality:*

$$F_a(t_0, t) = \frac{N_a(T_1, T_2)}{t - t_0} \leq \frac{\tilde{\eta}_*}{\ln(\zeta) + (\xi_1 + \xi_2)\tilde{\Delta}_*}. \quad (24)$$

- (2) *The attack length rate  $r_a$  in Definition 3 satisfies the following inequality:*

$$r_a < \frac{\xi_1 - \tilde{\eta}_*}{\xi_1 + \xi_2}. \quad (25)$$

*Proof.* Consider two time sequences  $\{t_{k_i}^i\}_{k_i \in \mathbb{N}}$  and  $\{\tilde{t}_m\}_{m \in \mathbb{N}}$ . The set of attempted updates under DoS attacks is defined as follows:

$$\Psi = \{(i, k_i) \in (V \times \mathbb{N}) | t_{k_i}^i \in \cup_{m \in \mathbb{N}} H_m\}. \quad (26)$$

The agent can recover to a controllable state after the DoS attack, and there must be a time interval  $\tilde{\Delta}_*$ , which satisfies  $\sup_{(i, k_i) \in \Psi} \tilde{\Delta}_{k_i}^i \leq \tilde{\Delta}_*$ . Obviously, after an attack stops, it takes more than  $\tilde{\Delta}_*$  to launch the next attack. The  $m$ th time interval is defined as follows:

$$\phi_m = [\tilde{t}_m, \tilde{t}_m + \tilde{\Delta}_m + \tilde{\Delta}_*]. \quad (27)$$

Two sub-intervals  $\overline{\Pi}_a(t_0, t)$  and  $\overline{\Pi}_s(t_0, t)$  form a time interval  $[t_0, t]$ , that is

$$[t_0, t] = \overline{\Pi}_a(t_0, t) \cup \overline{\Pi}_s(t_0, t), \quad (28)$$

where  $\overline{\Pi}_a(t_0, t) = \cup \phi_m \cap [t_0, t]$  and  $\overline{\Pi}_s(t_0, t) = [t_0, t] \setminus \overline{\Pi}_a(t_0, t)$ .

Under the time interval  $\overline{\Pi}_s(t_0, t)$ , the Lyapunov function is as follows:

$$\begin{aligned} V_S(t) &= \frac{1}{2} \hat{\eta}^T(t) P \hat{\eta}(t) \\ &= \frac{1}{2} \hat{\eta}^T(t) \begin{bmatrix} \varepsilon M \otimes I_n & I_{Nn} \\ I_{Nn} & I_{Nn} \end{bmatrix} \hat{\eta}(t), \end{aligned} \quad (29)$$

where  $M = (L + D) + (L + D)^T > 0$ .

Taking the time derivatives of  $V_S(t)$ , we have

$$\begin{aligned} \dot{V}_S(t) &= \hat{\eta}^T(t) \begin{bmatrix} \varepsilon M \otimes I_n & I_{Nn} \\ I_{Nn} & I_{Nn} \end{bmatrix} \dot{\hat{\eta}}(t) \\ &= \hat{\eta}^T(t) \begin{bmatrix} \varepsilon M \otimes I_n & I_{Nn} \\ I_{Nn} & I_{Nn} \end{bmatrix} \left\{ \left\{ \begin{bmatrix} 0 & I_N \\ -\varepsilon(L + D) & -\varepsilon(L + D) \end{bmatrix} \otimes I_n \right\} \hat{\eta}(t) + \begin{bmatrix} 0 \\ \varepsilon I_N \otimes I_n \end{bmatrix} \theta(t) + \begin{bmatrix} 0 \\ G(t) \end{bmatrix} \right\} \\ &= \hat{\eta}^T(t) \begin{bmatrix} \varepsilon M \otimes I_n & I_{Nn} \\ I_{Nn} & I_{Nn} \end{bmatrix} \times \begin{bmatrix} 0 & I_N \otimes I_n \\ -\varepsilon(L + D) \otimes I_n & -\varepsilon(L + D) \otimes I_n \end{bmatrix} \hat{\eta}(t) + \hat{\eta}^T(t) \begin{bmatrix} \varepsilon I_N \otimes I_n \\ \varepsilon I_N \otimes I_n \end{bmatrix} \theta(t) + \hat{\eta}^T(t) \begin{bmatrix} G(t) \\ G(t) \end{bmatrix} \\ &= \frac{1}{2} \hat{\eta}^T(t) \begin{bmatrix} \varepsilon M & I_N \\ I_N & I_N \end{bmatrix} \left\{ \left\{ \begin{bmatrix} 0 & I_N \\ -\varepsilon(L + D) & -\varepsilon(L + D) \end{bmatrix} \otimes I_n \right\} \hat{\eta}(t) + \frac{1}{2} \hat{\eta}^T(t) \left\{ \begin{bmatrix} 0 & I_N \\ -\varepsilon(L + D) & -\varepsilon(L + D) \end{bmatrix} \otimes I_n \right\} \begin{bmatrix} \varepsilon M & I_N \\ I_N & I_N \end{bmatrix} \hat{\eta}(t) \right. \\ &\quad \left. + \hat{\eta}^T(t) \begin{bmatrix} \varepsilon I_N \otimes I_n \\ \varepsilon I_N \otimes I_n \end{bmatrix} \theta(t) + \hat{\eta}^T(t) \begin{bmatrix} G(t) \\ G(t) \end{bmatrix} \right\} \\ &= \frac{1}{2} \hat{\eta}^T(t) \left\{ \begin{bmatrix} -\varepsilon M & 0 \\ 0 & 2I_N - \varepsilon M \end{bmatrix} \otimes I_n \right\} \hat{\eta}(t) + \hat{\eta}^T(t) \begin{bmatrix} \varepsilon I_N \otimes I_n \\ \varepsilon I_N \otimes I_n \end{bmatrix} \theta(t) + \hat{\eta}^T(t) \begin{bmatrix} G(t) \\ G(t) \end{bmatrix}. \end{aligned} \quad (30)$$

The last term of equality (30) can be written as

$$\begin{aligned}
\tilde{\eta}^T(t) \begin{bmatrix} G(t) \\ G(t) \end{bmatrix} &= \sum_{i=1}^N (\hat{x}_i(t) + \hat{v}_i(t))^T G(t) \leq \sum_{i=1}^N (\|\hat{x}_i(t)\| + \|\hat{v}_i(t)\|) \|G(t)\| \leq \sum_{i=1}^N (\|\hat{x}_i(t)\| + \|\hat{v}_i(t)\|) (\beta_1 \|\hat{x}_i(t)\| + \beta_2 \|\hat{v}_i(t)\|) \leq \sum_{i=1}^N \beta_1 \|\hat{x}_i(t)\|^2 \\
&\quad + \beta_2 \|\hat{v}_i(t)\|^2 + \frac{\beta_1 + \beta_2}{2} (\|\hat{x}_i(t)\|^2 + \|\hat{v}_i(t)\|^2) \\
&= \frac{3\beta_1 + \beta_2}{2} \|\hat{x}_i(t)\|^2 + \frac{\beta_1 + 3\beta_2}{2} \|\hat{v}_i(t)\|^2 \\
&= \frac{3\beta_1 + \beta_2}{2} \hat{x}^T(t) (I_N \otimes I_n) \hat{x}(t) + \frac{\beta_1 + 3\beta_2}{2} \hat{v}^T(t) (I_N \otimes I_n) \hat{v}(t) \\
&= \tilde{\eta}^T(t) \begin{bmatrix} \frac{3\beta_1 + \beta_2}{2} (I_N \otimes I_n) & 0 \\ 0 & \frac{\beta_1 + 3\beta_2}{2} (I_N \otimes I_n) \end{bmatrix} \hat{\eta}(t).
\end{aligned} \tag{31}$$

The second term of equality (30) can be written as

$$\begin{aligned}
\tilde{\eta}^T(t) \begin{bmatrix} \varepsilon I_N \otimes I_n \\ \varepsilon I_N \otimes I_n \end{bmatrix} \theta(t) &= \varepsilon \sum_{i=1}^N (\hat{x}_i(t) + \hat{v}_i(t))^T \theta_i(t) \leq \varepsilon \sum_{i=1}^N (\|\hat{x}_i(t)\| + \|\hat{v}_i(t)\|) \|\theta_i(t)\|, \\
\tilde{\eta}^T(t) \begin{bmatrix} \varepsilon I_N \otimes I_n \\ \varepsilon I_N \otimes I_n \end{bmatrix} \theta(t) &= \varepsilon \sum_{i=1}^N (\hat{x}_i(t) + \hat{v}_i(t))^T \theta_i(t) \leq \varepsilon \sum_{i=1}^N (\|\hat{x}_i(t)\| + \|\hat{v}_i(t)\|) \|\theta_i(t)\|.
\end{aligned} \tag{32}$$

By (22), we have

$$\begin{aligned}
&\leq \varepsilon \sum_{i=1}^N (\|\hat{x}_i(t)\| + \|\hat{v}_i(t)\|) \times \left( \frac{\alpha}{1-\alpha} \left\| \sum_{j=1}^N a_{ij} (\hat{x}_j(t) + \hat{v}_j(t)) + d_i (\hat{x}_i(t) + \hat{v}_i(t)) \right\| \right) \\
&\leq \frac{\varepsilon \alpha}{1-\alpha} (\hat{x}(t) + \hat{v}(t))^T ((L+D) \otimes I_n) (\hat{x}(t) + \hat{v}(t)) \\
&\leq \frac{2\varepsilon \alpha}{1-\alpha} \hat{x}(t)^T ((L+D) \otimes I_n) \hat{x}(t) + \frac{2\varepsilon \alpha}{1-\alpha} \hat{v}(t)^T ((L+D) \otimes I_n) \hat{v}(t) \\
&\leq \tilde{\eta}^T(t) \begin{bmatrix} \frac{2\varepsilon \alpha}{1-\alpha} ((L+D) \otimes I_n) & 0 \\ 0 & \frac{2\varepsilon \alpha}{1-\alpha} ((L+D) \otimes I_n) \end{bmatrix} \hat{\eta}(t).
\end{aligned} \tag{33}$$

Combining (31) and (33), we have

where

$$\dot{V}_S(t) \leq -\frac{1}{2} \tilde{\eta}^T(t) \begin{bmatrix} S & 0 \\ 0 & J \end{bmatrix} \hat{\eta}(t), \tag{34}$$

$$S = \frac{\varepsilon(1-3\alpha)}{1-\alpha} (M \otimes I_n) - (3\beta_1 + \beta_2) (I_N \otimes I_n) J = \frac{\varepsilon(1-3\alpha)}{1-\alpha} (M \otimes I_n) - (2 + \beta_1 + 3\beta_2) (I_N \otimes I_n). \tag{35}$$

Let,  $\varepsilon(1-3\alpha)/1-\alpha = \gamma$ ,  $\beta = \max\{3\beta_1 + \beta_2/2, 2 + \beta_1 + 3\beta_2/2\}$ , we obtain

$$\dot{V}_S(t) \leq -\frac{1}{2}\hat{\eta}^T(t) \begin{bmatrix} \gamma(M \otimes I_n) - 2\beta(I_N \otimes I_n) & 0 \\ 0 & \gamma(M \otimes I_n) - 2\beta(I_N \otimes I_n) \end{bmatrix} \hat{\eta}(t). \quad (36)$$

When  $\gamma > 2\beta/\lambda_{\min}(M)$ , we have  $\gamma(M \otimes I_n) - 2\beta(I_N \otimes I_n) > 0$ .

Then  $\dot{V}_S(t) \leq -\xi_1 V_S(t)$ , where

$$\xi_1 = \frac{2\lambda_{\min}(T)}{\lambda_{\max}(P)},$$

$$T = \begin{bmatrix} \gamma(M \otimes I_n) - 2\beta(I_N \otimes I_n) & 0 \\ 0 & \gamma(M \otimes I_n) - 2\beta(I_N \otimes I_n) \end{bmatrix}. \quad (37)$$

We consider system (2) in  $\bar{\Pi}_a(t_0, t)$ , choose the following Lyapunov function:

$$V_a(t) = \frac{1}{2}\hat{\eta}^T(t)R\hat{\eta}(t), \quad (38)$$

$$\text{where } R = \begin{bmatrix} I_{Nn} & 0 \\ 0 & I_{Nn} \end{bmatrix}.$$

We know that when system (2) under DoS attacks, the controller cannot work, that is,  $u_i(t) = 0$ . Therefore,  $\hat{\eta}(t)$  can be written as

$$\dot{\hat{\eta}}(t) = \begin{bmatrix} 0 & I_{Nn} \\ 0 & 0 \end{bmatrix} \hat{\eta}(t) + \begin{bmatrix} 0 \\ G(t) \end{bmatrix} \quad (39)$$

Differentiating  $V_a(t)$ , we obtain

$$\begin{aligned} V(t) &\leq e^{-\xi_1(t-\tilde{t}_{m-1}-\tilde{\Delta}_{m-1})} V_a(\tilde{t}_{m-1} + \tilde{\Delta}_{m-1}) \leq \zeta e^{-\xi_1(t-\tilde{t}_{m-1}-\tilde{\Delta}_{m-1})} V_b(\tilde{t}_{m-1} + \tilde{\Delta}_{m-1}) \\ &\leq \zeta e^{-\xi_1(t-\tilde{t}_{m-1}-\tilde{\Delta}_{m-1})} \left[ e^{\xi_2(t-\tilde{t}_{m-2}-\tilde{\Delta}_{m-2})} \times V_b(\tilde{t}_{m-2} + \tilde{\Delta}_{m-2}) \right] \leq \zeta^m e^{-\xi_1 \left| \bar{\Pi}_s(t_0, t) \right|} e^{\xi_2 \left| \bar{\Pi}_a(t_0, t) \right|} V_a(t_0). \end{aligned} \quad (43)$$

If  $t \in [\tilde{t}_m, \tilde{t}_m + \tilde{\Delta}_m + \tilde{\Delta}_*]$ , one has

$$V(t) \leq e^{\xi_2(t-\tilde{t}_m)} V_b(\tilde{t}_m) \leq \zeta^{m+1} e^{-\xi_1 \left| \bar{\Pi}_s(t_0, t) \right|} e^{\xi_2 \left| \bar{\Pi}_a(t_0, t) \right|} V_a(t_0) \quad (44)$$

where  $\zeta = \max\{\lambda_{\max}(P)/\lambda_{\min}(R), \lambda_{\max}(R)/\lambda_{\min}(P)\}$ .

By Definition 2, we can obtain

$$N_a(t_0, t) = \begin{cases} m, & t \in [\tilde{t}_{m-1} + \tilde{\Delta}_{m-1}, \tilde{t}_m), \\ m+1, & t \in [\tilde{t}_m, \tilde{t}_m + \tilde{\Delta}_m + \tilde{\Delta}_*). \end{cases} \quad (45)$$

Therefore, for any  $t > t_0$ , combining (43) and (44), we can obtain

$$\dot{V}_a(t) = \hat{\eta}^T(t)R\dot{\hat{\eta}}(t) \quad (40)$$

Substituting (39), we have

$$\begin{aligned} \dot{V}_a(t) &= \hat{\eta}^T(t) \begin{bmatrix} 0 & I_{Nn} \\ 0 & 0 \end{bmatrix} \hat{\eta}(t) + \hat{\eta}^T(t) \begin{bmatrix} 0 \\ G(t) \end{bmatrix} \\ &\leq \hat{\eta}^T(t) \begin{bmatrix} \frac{3\beta_1 + \beta_2}{2} I_{Nn} & I_{Nn} \\ 0 & \frac{\beta_1 + 3\beta_2}{2} I_{Nn} \end{bmatrix} \hat{\eta}(t). \end{aligned} \quad (41)$$

It is defined that

$$K = \begin{bmatrix} (3\beta_1 + \beta_2/2)I_{Nn} & I_{Nn} \\ 0 & (\beta_1 + 3\beta_2/2)I_{Nn} \end{bmatrix},$$

$\xi_2 = 2\lambda_{\min}(K)/\lambda_{\max}(R)$ . Through (41), we can have  $\dot{V}_a(t) \leq \xi_2 V_a(t)$ .

It is defined that  $V(t) = V_{\sigma(t)}(t)$ , where  $\sigma(t) \in \{a, b\}$ . Through the Comparison lemma, we can obtain

$$V(t) \leq \begin{cases} e^{-\xi_1(t-\tilde{t}_{m-1}-\tilde{\Delta}_{m-1})} V_a(\tilde{t}_{m-1} + \tilde{\Delta}_{m-1}), \\ e^{\xi_2(t-\tilde{t}_m)} V_b(\tilde{t}_m). \end{cases} \quad (42)$$

If  $t \in [\tilde{t}_{m-1} + \tilde{\Delta}_{m-1}, \tilde{t}_m)$ , one has

$$V(t) \leq \zeta^{N_a(t_0, t)} e^{-\xi_1 \left| \bar{\Pi}_s(t_0, t) \right|} e^{\xi_2 \left| \bar{\Pi}_a(t_0, t) \right|} V(t_0) \quad (46)$$

Noticing that

$$\left| \bar{\Pi}_s(t_0, t) \right| = t - t_0 - \left| \bar{\Pi}_a(t_0, t) \right|, \quad (47)$$

$$\left| \bar{\Pi}_a(t_0, t) \right| \leq \left| \bar{\Pi}_a(t_0, t) \right| + (1 + N_a(t_0, t))\tilde{\Delta}_*. \quad (48)$$

Then combining (47) and (48), we have

$$\begin{aligned}
& -\xi_1 \left| \overline{\prod}_s(t_0, t) \right| + \xi_2 \left| \overline{\prod}_a(t_0, t) \right| = -\xi_1 \left( t - t_0 - \left| \overline{\prod}_a(t_0, t) \right| \right) + \xi_2 \left| \overline{\prod}_a(t_0, t) \right| = -\xi_1 (t - t_0) + (\xi_1 + \xi_2) \left| \overline{\prod}_a(t_0, t) \right| \leq -\xi_1 (t - t_0) + (\xi_1 + \xi_2) \\
& \left( \left| \overline{\prod}_a(t_0, t) \right| + (1 + N_a(t_0, t)) \tilde{\Delta}_* \right).
\end{aligned} \tag{49}$$

By Definition 3, we have

$$\begin{aligned}
V(t) & \leq \zeta^{N_a(t_0, t)} e^{-\xi_1 (t - t_0) + (\xi_1 + \xi_2) \left( \left| \overline{\prod}_a(t_0, t) \right| + (1 + N_a(t_0, t)) \tilde{\Delta}_* \right)} V(t_0) = e^{N_a(t_0, t) \ln \zeta - \xi_1 (t - t_0) + (\xi_1 + \xi_2) (r_a (t - t_0) + (1 + N_a(t_0, t)) \tilde{\Delta}_*)} V(t_0) \\
& = e^{(\ln \zeta + (\xi_1 + \xi_2) \tilde{\Delta}_*) N_a(t_0, t) - \xi_1 + r_a (\xi_1 + \xi_2) (t - t_0) + (\xi_1 + \xi_2) \tilde{\Delta}_*} V(t_0).
\end{aligned} \tag{50}$$

Combining (24) and (25), the previous inequality can be rewritten as

$$V(t) \leq e^{\tilde{\eta}_* (t - t_0)} e^{(-\xi_1 + r_a (\xi_1 + \xi_2)) (t - t_0)} e^{(\xi_1 + \xi_2) \tilde{\Delta}_*} V(t_0) = e^{(-\tilde{\eta}_* + \xi_1 - r_a (\xi_1 + \xi_2)) (t - t_0)} e^{(\xi_1 + \xi_2) \tilde{\Delta}_*} V(t_0) \leq e^{-\eta_* (t - t_0)} e^{(\xi_1 + \xi_2) \tilde{\Delta}_*} V(t_0), \tag{51}$$

where  $\eta_* = -\tilde{\eta}_* + \xi_1 - r_a (\xi_1 + \xi_2) > 0$ .

Next, we will prove that the proposed control strategy can exclude the Zeno behavior. The Zeno behavior is that in the event trigger control, the control is triggered infinitely in a finite time. The interevent time of the agent is proposed in (15). Let  $W_1(t)$  represent the set of agents with the latest interevent time of  $\tilde{r}_{k_i}^i$  and  $W_2(t)$  represent the set of agents with the latest interevent time of  $\tilde{b}$ . Let  $\tilde{\gamma}_1 + \tilde{\gamma}_2 = \tilde{\gamma} < 1$ , we have

$$\sum_{i \in W_1(t)} \|\theta_i(t)\|^2 \leq \tilde{\gamma}_1 \sum_{i \in W_1(t)} \|\hat{\eta}_i(t)\|^2 \leq \tilde{\gamma}_1 \sum_{i=1}^N \|\hat{\eta}_i(t)\|^2, \tag{52}$$

$$\sum_{i \in W_2(t)} \|\theta_i(t)\|^2 \leq \tilde{\gamma}_2 \sum_{i \in W_2(t)} \|\hat{\eta}_i(t)\|^2 \leq \tilde{\gamma}_2 \sum_{i=1}^N \|\hat{\eta}_i(t)\|^2. \tag{53}$$

For the agent in  $W_1(t)$ ,  $\|\theta(t)\| \leq \omega \|\hat{\eta}(t)\|$  with  $\omega^2 \leq \tilde{\gamma}_1$ . Considering the agent in  $W_2(t)$ , from (53), we have  $\|\theta_i(t)\|^2 \leq \sum_{j=1}^N \tilde{h} \|\hat{\eta}_j(t)\|^2$ , where  $\tilde{h} = \tilde{\gamma}_2 / N$ . For the agent in  $W_2(t)$ ,  $t_{k_i+1}^i = t_{k_i}^i + \tilde{b}_i$  can ensure (53). To prove that the interevent time is greater than 0, we have

$$\frac{d}{dt} \frac{\|\theta_i(t)\|}{\|\hat{\eta}(t)\|} \leq \left( 1 + \frac{\|\theta_i(t)\|}{\|\hat{\eta}(t)\|} \right) \frac{\|\dot{\hat{\eta}}(t)\|}{\|\hat{\eta}(t)\|}. \tag{54}$$

By (39), we have

$$\left\| \frac{\begin{bmatrix} 0 \\ G(t) \end{bmatrix}}{\|\hat{\eta}(t)\|} \right\| \leq \left\| \begin{bmatrix} 0 & 0 \\ 0 & \frac{\beta_1 + 3\beta_2}{2} I_{Nn} \end{bmatrix} \right\|. \tag{55}$$

Combining (20) and (55), we have

$$\frac{d}{dt} \frac{\|\theta_i(t)\|}{\|\hat{\eta}(t)\|} \leq h \left( 1 + \frac{\|\theta_i(t)\|}{\|\hat{\eta}(t)\|} \right), \tag{56}$$

where

$$h = \left\| \begin{bmatrix} 0 & I_{Nn} \\ -\varepsilon(L+D) \otimes I_n & -\varepsilon(L+D) \otimes I_n \end{bmatrix} \right\| + \left\| \begin{bmatrix} 0 \\ \varepsilon \end{bmatrix} \otimes I_n \right\| \sqrt{\tilde{h}} + \left\| \begin{bmatrix} 0 \\ 0 \\ 0 \\ \beta_1 + 3\beta_2/2 I_{Nn} \end{bmatrix} \right\|.$$

Therefore,  $\tilde{B} = 1/h \ln(1 + \sqrt{\tilde{\gamma}_2/N})$  determines the minimum time for  $\|\theta_i(t)\|/\|\hat{\eta}(t)\|$  to evolve from 0 to  $\sqrt{\tilde{h}}$ . Obviously, for the agent in  $W_2(t)$ ,  $\tilde{b}_i \leq \tilde{B}$  can be guaranteed (53). It is concluded that the controller (9) based on event trigger (13) guarantees that (51) holds for all agents, which means  $\lim_{t \rightarrow \infty} V(t) = 0$ . That is, systems (1) and (2) can achieve the desired objectives under DoS attacks.  $\square$

#### 4. Numerical Simulation

This section verifies the correctness and effectiveness of the proposed theory and method by an example. We construct a nonlinear second-order system with four followers and one leader, where the communication topology is shown in Figure 1.

$$\text{By calculation, we have } M = \begin{bmatrix} 4 & -1 & -1 & -1 \\ -1 & 4 & -1 & -1 \\ -1 & -1 & 2 & -1 \\ -1 & -1 & -1 & 6 \end{bmatrix}.$$

The initial values of the leader's position and velocity in system (1) are -7 and 1, respectively. The initial value of the follower is [3, -2, 3, 0.3; 6, -2, 2, 1]. The nonlinear function is  $g(t, x_i(t), v_i(t)) = 0.4 \cos(v_i(t)) + 0.1 \sin(x_i(t))$ .

Let  $\beta_1 = \beta_2 = 0.003$ ,  $\tau = 5s$ ,  $\varepsilon = 3$ , and  $\tilde{\eta}_* = 0.02$ . By calculation, we have  $\xi_1 = 0.043$ ,  $\xi_2 = 0.012$ ,  $\zeta = \max\{\lambda_{\max}(P)/\lambda_{\min}(R), \lambda_{\max}(R)/\lambda_{\min}(P)\} = 2.989$ ,



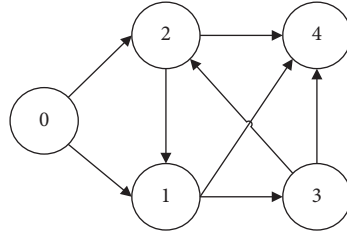


FIGURE 1: A second-order system topology with four followers and one leader is proposed.  $L = \begin{bmatrix} 1 & -1 & 0 & 0 \\ 0 & 1 & -1 & 0 \\ -1 & 0 & 1 & 0 \\ -1 & -1 & -1 & 3 \end{bmatrix}$  is the Laplacian matrix. The adjacency matrix is  $A = \begin{bmatrix} 0 & 1 & 0 & 0 \\ 0 & 0 & 1 & 0 \\ 1 & 0 & 0 & 0 \\ 1 & 1 & 1 & 0 \end{bmatrix}$ .

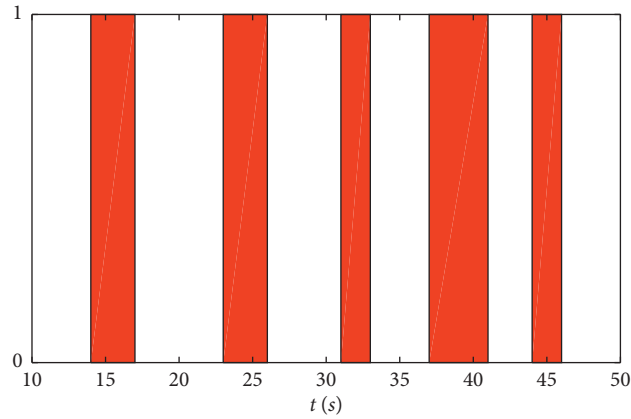


FIGURE 2: Sequence of DoS attacks.

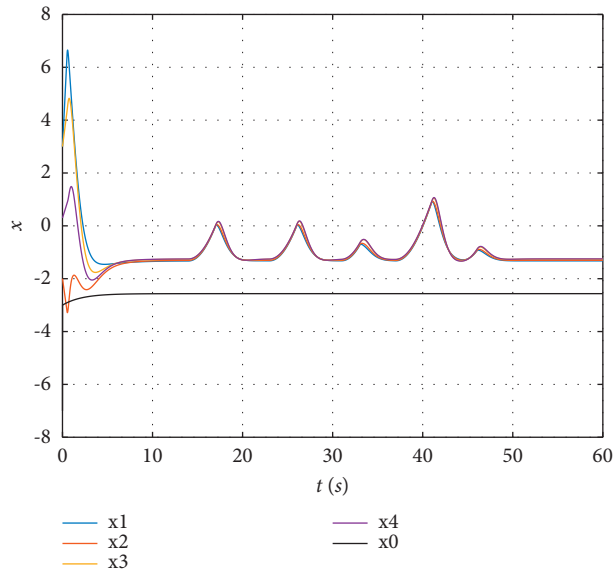


FIGURE 3: The position trajectory of the agent.

$\lambda_{\min}(M) = 0.506$ , and  $\beta = 2.012$ , so that we can get  $\gamma = 8.8$ ,  $r_a = 0.233 < \xi_1 - \bar{\eta}_*/\xi_1 + \xi_2 = 0.420$ , and  $F_a(t_0, t) \leq 0.003$ . Figure 2 shows the sequence of DoS attacks. Figures 3 and 4 show the trajectory of the position and velocity of the five agents, respectively. We can see that there is a delay in the consistent state between the leader and the follower. Therefore, the leader and the follower achieve lag

consensus under the DoS attack. Errors of leader-following lag consensus are shown in Figures 5 and 6. Obviously, the lag error between followers and leader finally tends to 0, indicating that the multiagent system achieves lag consensus. Figures 5 and 6 show that the control protocol designed in this paper can effectively defend against nonperiodic DoS attacks. Figure 7 shows

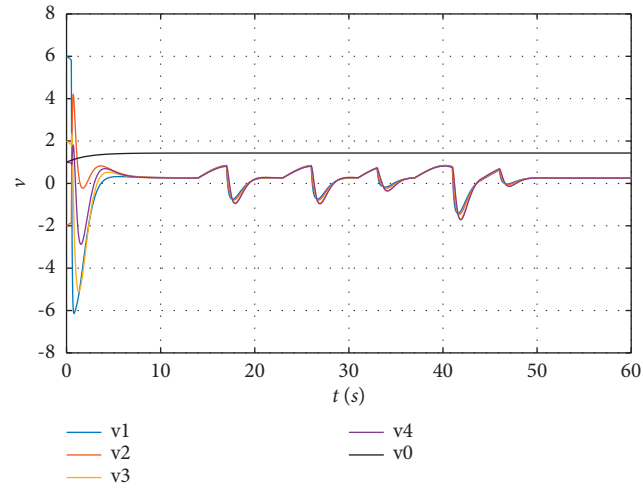


FIGURE 4: Velocity trajectory of agents.

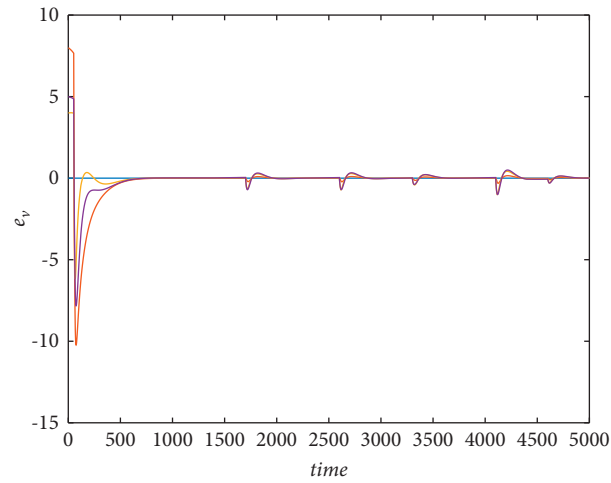


FIGURE 5: Velocity error trajectory of agents.

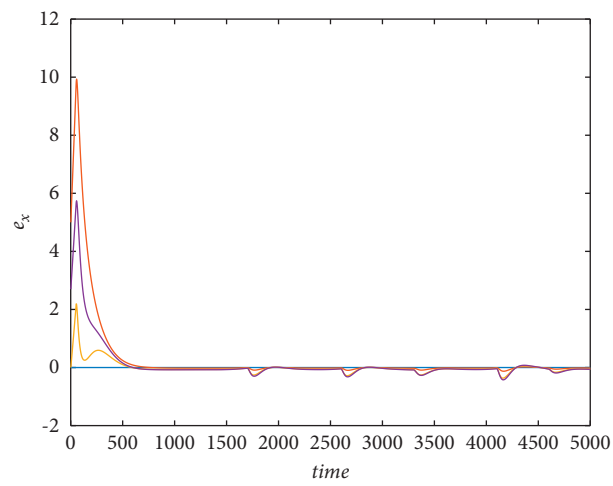


FIGURE 6: Position error trajectory of agents.

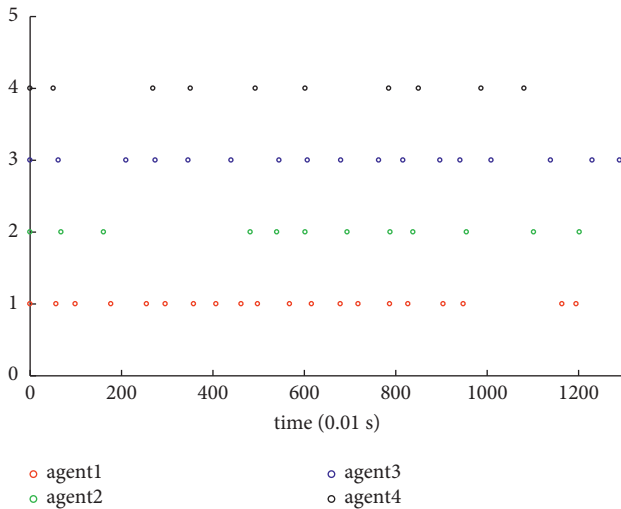


FIGURE 7: Trigger interval.

the event trigger instants for four agents. Obviously, this article can effectively avoid the Zeno behavior by setting the minimum event trigger interval.

## 5. Conclusion

This paper focuses on the time-delay phenomenon in the consensus state of the leader and followers and studies the lag secure consensus problem of MASs under the non-periodic DoS attack.

In order to achieve the lag consensus between a leader and followers, this paper proposes a security control strategy based on event triggering and derives the upper bound of the frequency and length rate of DoS attacks. Without exceeding the upper bound, the MASs can achieve lagging security consensus. In future works, we will study the high-order multiagent system with communication delay and discuss the lag consensus of MASs under DoS attack.

## Data Availability

The data are available from the corresponding author upon request.

## Conflicts of Interest

The authors declare that they have no conflicts of interest.

## Acknowledgments

This work was supported in part by Humanities and Social Sciences Research of Ministry of Education (19YJCZH047), in part by the West Light Foundation of the Chinese Academy of Science, in part by the Scientific and Technological Research Program of Chongqing Municipal Education Commission (KJZD-K201901504 and KJQN201901537), in part by the Research Foundation of The Natural Foundation of Chongqing City (cstc2021jcyj-msxmX0146), and in part

by the Science and Technology Planning Project of Luzhou City (2021-JYJ-92). The authors would like to thank the support of China Scholarship Council.

## References

- [1] B. Li, R. Lu, W. Wang, and K. K. R. Choo, "Distributed host-based collaborative detection for false data injection attacks in smart grid cyber-physical system," *Journal of Parallel and Distributed Computing*, vol. 103, pp. 32–41, 2017.
- [2] Z. Li, Z. Wu, Z. Li, and Z. Ding, "Distributed optimal coordination for heterogeneous linear multiagent systems with event-triggered mechanisms," *IEEE Transactions on Automatic Control*, vol. 65, no. 4, pp. 1763–1770, 2020.
- [3] B. L. Su and Y. X. Duan, "Distributed optimal control of nonlinear time-delay system subject to delayed measurements and communication disruptions," *Journal of Systems Science and Complexity*, vol. 34, no. 4, pp. 1426–1437, 2021.
- [4] W. Zhu, H. Pu, D. Wang, and H. Li, "Event-based consensus of second-order multi-agent systems with discrete time," *Automatica*, vol. 79, pp. 78–83, 2017.
- [5] W. Zhu, D. D. Wang, and Q. H. Zhou, "Leader-following consensus of multi-agent systems via adaptive event-based control," *Journal of Systems Science and Complexity*, vol. 32, no. 3, pp. 114–124, 2019.
- [6] H. Chu, D. Yue, C. Dou, and L. Chu, "Adaptive PI control for consensus of multiagent systems with relative state saturation constraints," *IEEE Transactions on Cybernetics*, vol. 54, no. 1, pp. 1–7, 2019.
- [7] H. Zhang and F. L. Lewis, "Adaptive cooperative tracking control of higher-order nonlinear systems with unknown dynamics," *Automatica*, vol. 48, no. 7, pp. 1432–1439, 2012.
- [8] Y. Y. Xie, Y. Wang, and Z. J. Ma, "Delay consensus of leader-following multi-agent systems," *Acta Physica Sinica*, vol. 63, no. 4, Article ID 040202, 2014.
- [9] K. Subramanian, P. Muthukumar, and Y. H. Joo, "Leader-following consensus of nonlinear multi-agent systems via reliable control with time-varying communication delay," *International Journal of Control, Automation and Systems*, vol. 17, pp. 1–9, 2019.
- [10] X. L. Jiang, G. H. Xia, Z. G. Feng, and Z. Y. Jiang, "Consensus tracking of data-sampled nonlinear multi-agent systems with packet loss and communication delay," *IEEE Transactions on Network Science and Engineering*, vol. 8, no. 1, 2020.
- [11] S. M. Chen, J. J. Guan, Y. L. Gao, and H. C. Yan, "Observer-based Event-Triggered Tracking Consensus of Non-ideal General Linear Multi-Agent Systems," *Journal of the Franklin Institute*, vol. 35617, 2018.
- [12] Y. Zou, X. Su, S. Li, Y. Niu, and D. Li, "Event-triggered distributed predictive control for asynchronous coordination of multi-agent systems," *Automatica*, vol. 99, pp. 92–98, 2019.
- [13] Y. Yang and Y. Qian, "Event-trigger-based recursive sliding-mode dynamic surface containment control with nonlinear gains for nonlinear multi-agent systems," *Information Sciences*, vol. 560, pp. 202–216, 2021.
- [14] M. Cong, X. Mu, and Z. Hu, "Sampled-data-based event-triggered secure bipartite tracking consensus of linear multi-agent systems under DoS attacks," *Journal of the Franklin Institute*, vol. 358, no. 13, pp. 6798–6817, 2021.
- [15] Y. Li, P. Zhang, and L. Ma, "Denial of service attack and defense method on load frequency control system," *Journal of the Franklin Institute*, vol. 356, no. 15, pp. 8625–8645, 2019.

- [16] S. Liu, S. B. Li, and B. G. Xu, "Event-triggered resilient control for cyber physical system under denial-of-service attacks," *International Journal of Control*, vol. 93, no. 8, pp. 1–24, 2018.
- [17] X. Li, C. Wen, J. Wang, C. Chen, and C. Deng, "Resilient leader tracking for networked Lagrangian systems under DoS attacks," *Information Sciences*, vol. 577, no. 6, pp. 622–637, 2021.
- [18] X. Shao and D. Ye, "Neural-network-based adaptive secure control for nonstrict-feedback nonlinear interconnected systems under DoS attacks," *Neurocomputing*, vol. 448, pp. 263–275, 2021.
- [19] T. Dong and Y. Gong, "Leader-following secure consensus for second-order multi-agent systems with nonlinear dynamics and event-triggered control strategy under DoS attack," *Neurocomputing*, vol. 416, pp. 95–102, 2019.
- [20] H. Yang, Y. Li, L. Dai, and Y. Xia, "MPC-based defense strategy for distributed networked control systems under DoS attacks," *Systems & Control Letters*, vol. 128, pp. 9–18, 2019.
- [21] D. Zhang and G. Feng, "A new switched system approach to leader-follower consensus of heterogeneous linear multiagent systems with DoS attack," *IEEE Transactions on Systems, Man, and Cybernetics: Systems*, vol. 51, no. 2, pp. 1–9, 2019.
- [22] S. Du, Y. Wang, L. Dong, and X. Li, "Secure consensus of multiagent systems with DoS attacks via a graph-based approach," *Information Sciences*, vol. 570, pp. 94–104, 2021.
- [23] L. Su and D. Ye, "Observer-based output feedback  $H_\infty$  control for cyber-physical systems under randomly occurring packet dropout and periodic DoS attacks," *ISA Transactions*, vol. 104, 2019.
- [24] Y. C. Sun and G. H. Yang, "Event-triggered distributed state estimation for multiagent systems under DoS attacks," *IEEE Transactions on Cybernetics*, pp. 1–10, 2020.
- [25] Z. H. Cheng, D. Yue, S. L. Hu, H. Gei, and L. Chen, "Distributed event-triggered consensus of multi-agent systems under periodic DoS jamming attacks," *Neurocomputing*, vol. 400, pp. 458–466, 2019.
- [26] Y. Xu, M. Fang, Z. G. Wu, and Y. J. Pan, "Input-based event-triggering consensus of multiagent systems under denial-of-service attacks," *IEEE Transactions on Systems, Man, and Cybernetics: Systems*, vol. 50, pp. 1–10, 2018.
- [27] F. Zhi, G. H. Wen, and G. Q. Hu, "Distributed secure coordinated control for multiagent systems under strategic attacks," *IEEE Transactions on Cybernetics*, vol. 47, no. 5, pp. 1273–1284, 2017.
- [28] Y. Wang and Z. J. Ma, "Lag consensus of the second-order leader-following multi-agent systems with nonlinear dynamics," *Neurocomputing*, vol. 171, pp. 82–88, 2016.
- [29] Y. H. Ren, W. N. Zhou, Z. W. Li, L. Liu, and Y. Q. Sun, "Prescribed-time cluster lag consensus control for second-order non-linear leader-following multiagent systems," *ISA Transactions*, vol. 109, no. 6, 2020.
- [30] Y. Wang, Z. Ma, and G. Chen, "Distributed control of cluster lag consensus for first-order multi-agent systems on QUAD vector fields," *Journal of the Franklin Institute*, vol. 355, no. 15, pp. 7335–7353, 2018.
- [31] Y. Fan, I. Liu, G. Feng, and Y. Wang, "Self-triggered consensus for multi-agent systems with Zeno-free triggers," *IEEE Transactions on Automatic Control*, vol. 60, no. 10, 2015.

## Research Article

# Containing Misinformation Spread: A Collaborative Resource Allocation Strategy for Knowledge Popularization and Expert Education

Linhong Li , Kaifan Huang , and Xiaofan Yang 

*School of Big Data & Software Engineering, Chongqing University, Chongqing, China*

Correspondence should be addressed to Xiaofan Yang; [xfyang1964@cqu.edu.cn](mailto:xfyang1964@cqu.edu.cn)

Received 30 October 2021; Accepted 21 December 2021; Published 13 January 2022

Academic Editor: Wei Wang

Copyright © 2022 Linhong Li et al. This is an open access article distributed under the Creative Commons Attribution License, which permits unrestricted use, distribution, and reproduction in any medium, provided the original work is properly cited.

With the prevalence of online social networks, the potential threat of misinformation has greatly enhanced. Therefore, it is significant to study how to effectively control the spread of misinformation. Publishing the truth to the public is the most effective approach to controlling the spread of misinformation. Knowledge popularization and expert education are two complementary ways to achieve that. It has been proven that if these two ways can be combined to speed up the release of the truth, the impact caused by the spread of misinformation will be dramatically reduced. However, how to reasonably allocate resources to these two ways so as to achieve a better result at a lower cost is still an open challenge. This paper provides a theoretical guidance for designing an effective collaborative resource allocation strategy. First, a novel individual-level misinformation spread model is proposed. It well characterizes the collaborative effect of the two truth-publishing ways on the containment of misinformation spread. On this basis, the expected cost of an arbitrary collaborative strategy is evaluated. Second, an optimal control problem is formulated to find effective strategies, with the expected cost as the performance index function and with the misinformation spread model as the constraint. Third, in order to solve the optimal control problem, an optimality system that specifies the necessary conditions of an optimal solution is derived. By solving the optimality system, a candidate optimal solution can be obtained. Finally, the effectiveness of the obtained candidate optimal solution is verified by a series of numerical experiments.

## 1. Introduction

Misinformation refers to false or inaccurate information, which especially contains a deceptive purpose [1]. The threat level of misinformation is measured in the number of victims. Normally, the more people are cheated, the greater the impacts on the social order. Because online social networks (such as Weibo, Facebook, and Twitter) have wide coverage and fast information circulation [2], once misinformation appears, it will spread quickly on networks and affect a large number of victims, causing a huge impact on our society. For instance, a fake tweet in 2013 claimed that Obama has been injured in an explosion at the White House was viewed more than 100 million times in just a few hours and ultimately caused the stock market to suffer a massive of 130 billion dollars [3]. Therefore, it is of great significance to study how to effectively control the spread of misinformation [4, 5].

The dissemination of the truth is one of the most effective approach to controlling the spread of misinformation [6]. Knowledge popularization and expert education are two complementary ways to achieve that. Knowledge popularization means informing the truth to the public in a simple way so that a large part of citizens can get a basic understanding of the truth. A common way to do it is to post online leaflets. Expert education refers to the indoctrination of the truth in a profound way to a particular group of citizens so that this small set of people can gain a deep acquaintance of the truth. Some common methods include holding guest lectures and sitting series of courses. Generally, knowledge popularization is more suitable for increasing the number of people who can reach the truth than for increasing the speed with which it is accepted, whereas expert education is more about the speed than the quantity [7–9].

*1.1. Motivation.* Given the above discussion, we wonder if the two ways can be combined to speed up the release of the truth. That is for sure. In reality, posting online leaflets and holding expert lectures are not in conflict. However, a challenge is how to reasonably allocate resources to these two ways so as to achieve a better result at a lower cost. This paper calls it the *collaborative resource allocation problem of knowledge popularization and expert education*, also the *collaborative resource allocation (CRA) problem* for short. For convenience, this paper refers to the solution of the CRA problem as the CRA strategy and refers to the optimal solution as the optimal CRA strategy.

To settle the CRA problem is challenging. A reasonable strategy should take into full consideration the collaborative effect of knowledge popularization and expert education. If too many resources are put in knowledge popularization; even if the number of people who knows the truth increases, the accept speed cannot be guaranteed. On the contrary, if too many resources are set in expert education, the truth can be quickly accepted by a small group of people, but the number cannot be promised. In order to design an optimal CRA strategy, it is necessary to deeply understand how the two methods influence each other and then find the balance between them. Unfortunately, as far as we know, there are few theoretical models that evaluate the combined effect of these two truth-publishing methods on collaboratively controlling the spread of misinformation, not to mention the theoretical guidance for designing an effective collaboration strategy.

*1.2. Contributions.* This paper proposes a dynamic resources allocation strategy that combines knowledge popularization and expert education to control the spread of misinformation. Specifically, this paper is committed to solving the CRA problem. The main works are as follows:

- (1) An individual-level misinformation spread model is proposed. This model well describes the comprehensive effect of knowledge popularization and expert education on the collaborative control of misinformation spread. On this basis, the expected cost of any CRA strategy is evaluated, and a continuous-time optimal control model is formulated to find an optimal CRA strategy, with the expected cost as the performance index function.
- (2) In order to solve the optimal control model, an optimality system that specifies the necessary conditions of an optimal solution is derived, and a corresponding numerical iteration algorithm is designed. By solving the optimality system, a candidate optimal solution can be obtained.
- (3) The effectiveness of the obtained candidate optimal solution is verified by a series of numerical experiments. Experimental results show that the candidate optimal solution is significantly better than other comparison schemes. Therefore, the candidate optimal solution can be considered as effective and can be recommended as the optimal CRA strategy.

The remainder of this paper is structured as follows. Section 2 reviews the related work. Section 3 focuses on system modeling and problem formulating. Section 4 discusses solutions. Section 5 shows some numerical experiments. Section 6 closes this paper.

## 2. Related Work

This section reviews related efforts. First, we investigate some common approaches to publishing the truth. Second, we discuss misinformation spread models.

*2.1. Truth-Publishing Approaches.* In the past decade, how to effectively release the truth to the public has received a considerable interest from academic community. Knowledge popularization and expert education are two commonly used truth-publishing approaches. In the way of knowledge popularization, the truth is released to all the people on a social network [6]. Around this topic, the optimization of the truth spread rate is a key challenge. Wen et al. [10] propose a mathematical model that evaluates the effects of different knowledge popularization methods on the control of misinformation spread. Through optimization techniques, Pan et al. [11] study the optimal spread rate of the truth, which achieves a better performance with a lower cost. By using optimal control theory, Wan et al. and Lin et al. [12, 13] focus on the optimization of dynamic misinformation intervention strategies, Liu and Buss [14] investigate efficient misinformation impeding policies, and Chen et al. [15] propose a cost-effective antitumor message-pushing scheme. In the way of expert education, only a small subset of people (usually ones who have great influence on social networks) are selected to publish the truth to their followers and friends. Hence, the main research direction around this topic is to develop a fast, effective algorithm for seeking a proper subset of influence people. See [16–19], for some typical literature.

As far as we know, although the research about knowledge popularization and expert education is rich, there are few theoretical models that evaluate the combined effect of these two truth-publishing methods on the collaborative control of misinformation spread, not to mention the theoretical guidance for designing an effective collaboration strategy.

*2.2. Misinformation Spread Models.* In order to design an effective CRA strategy, it is essential to evaluate the comprehensive effect of knowledge popularization and expert education. To this end, a misinformation spread model is introduced in our work.

Generally, a misinformation spread model refers to a mathematical model that characterizes the process where a piece of misinformation spreads over a social network under (or without) a certain control measure. Although misinformation is broadly a kind of information, there are some differences between the processes of information dissemination and misinformation spread. The biggest difference is that the former emphasizes a unilateral diffusion process,

i.e., information dissemination models seldom consider the situation that people refuse to acquire information (see [14, 20–22], for some examples), whereas the latter emphasizes a competitive process between misinformation and the truth, i.e., misinformation spread models usually account for the situation that some people believe misinformation; meanwhile, some people believe the truth (see [13, 15, 23], for some examples). Therefore, information dissemination models may not be very suitable to characterize the effect of countermeasures on containing misinformation spread. In the rest of this section, we only focus on the discussion of misinformation models.

Common used misinformation spread models can be population level, network level, or individual level. In a population-level model, people on a social network are classified into groups according to their opinions on misinformation. See [12, 24–26]. It is assumed in these models that the social network is homogeneously mixed, i.e., there is no difference between people on the network. As a result, population-level models can only be applied to homogeneous networks. In a network-level model, people on a social network are classified into groups according to their opinions on misinformation as well as the numbers of their friends on the same network. See [27–30]. It is assumed in these models that there is no difference between people with the same number of friends on the network. Hence, network-level models are applied to some special kinds of social networks, e.g., scale-free networks [31]. In an individual-level model, every person on a social network has multiple states that indicate the person's opinion on misinformation. See [11, 14, 15, 32–34]. In these models, it is assumed that every person is a distinct individual. Therefore, individual-level models can be applied to any arbitrary social network.

In this paper, a novel individual-level misinformation spread model is proposed, so as to evaluate the influence of a CRA strategy. It considers the interaction between misinformation and the truth under knowledge popularization and expert education. To our best knowledge, this is the first time to characterize the collaborative effect of the two truth-publishing approaches.

### 3. System Modeling and Problem Formulating

This section discusses how to find an optimal CRA strategy. First, we introduce basic terms and notations and specify the mathematical form of a CRA strategy. Second, we propose a novel individual-level misinformation spread model, which considers the effect of a CRA strategy on controlling misinformation. Third, based on the proposed misinformation spread model, we quantify the expected costs of different CRA strategies so as to find an optimal CRA strategy and formulate a continuous-time optimal control model with the expected cost as the performance index.

**3.1. Basic Terms and Notations.** Suppose that a truth-publishing campaign will last  $\tau$  units of time. In this paper, we focus on the time horizon  $[0, \tau]$ . Consider a social network

of  $N$  individuals. All individuals are denoted by  $v_1, v_2, \dots, v_N$ . In practice, any individual at any given moment will either believe misinformation, believe the truth, or remain neutral. For any time  $t \in [0, \tau]$ , let  $S_i(t) = 0, 1$ , and  $2$  to indicate that the individual  $v_i$  is in the neutral state, misinformation-believing state, and truth-believing state at the time  $t$ , respectively. By definition, the number of victims is  $\sum_{i=1}^N \Gamma[S_i(t) = 1]$ , where  $\Gamma[x] \in \{0, 1\}$ , and when the event  $x$  holds true,  $\Gamma[x] = 1$ , otherwise,  $\Gamma[x] = 0$ .

If misinformation appears and spreads on a social network, a truth-publishing campaign consisting of knowledge popularization and expert education will be carried out on that social network to response. As the previous discussion, in the way of knowledge popularization, the truth can be released to all individuals on the network, while in the way of expert education, the truth can only be released to a set of specific groups on the network. Without loss of generality, it is assumed that the truth can be released to  $M$  specific groups by means of expert education. Denote these groups by  $B_1, B_2, \dots, B_M$ .

At any time  $t \in [0, \tau]$ ,  $u_0(t)$  is denoted as the instantaneous resource investment rate for disseminating the truth in a knowledge popularization way to all individuals;  $u_i(t)$ ,  $i = 1, 2, \dots, M$ , is denoted as the instantaneous resource investment rate for disseminating the truth in an expert education way to group  $B_i$ . Then, a CRA strategy is expressed as a  $(M + 1)$ -dim function  $u(t) = (u_0(t), u_1(t), \dots, u_M(t))$  on time  $t \in [0, \tau]$ .

In practice, a CRA strategy should be as easy to perform as possible, with some upper and lower bounds due to resource constraints. First, to make a CRA strategy easy to perform, assume that the admissible set of CRA strategies consists of all  $(M + 1)$  dimensional piecewise continuous real-valued functions defined on time horizon  $[0, \tau]$ . Such an admissible set is represented by  $PC[0, \tau]^{M+1}$ . Then, there is  $u \in PC[0, \tau]^{M+1}$ . Second, due to the limitation of resource flow, the resource investment rate of each part should not be infinite. Without loss of generality, denote by  $\bar{u}_i$  the upper bound of  $u_i(t)$  at any time  $t$ . Let  $\bar{u} = (\bar{u}_0, \bar{u}_1, \dots, \bar{u}_M)$ ; then, for any time  $t \in [0, \tau]$ , there is  $0 \leq u(t) \leq \bar{u}$ . Therefore, the admissible set of CRA strategies can be expressed as

$$U = \{u \in PC[0, \tau]^{M+1} \mid 0 \leq u(t) \leq \bar{u}, \quad 0 \leq t \leq \tau\}. \quad (1)$$

In this paper, CRA strategies are designed to minimize the impact caused by the spread of misinformation at the lowest possible cost. By definition, the cost of a CRA strategy  $u(t)$  within the time horizon  $[0, \tau]$  is

$$J_1(u) = \int_0^\tau \sum_{i=0}^M u_i(t) dt. \quad (2)$$

Recall that the impact caused by misinformation spread is determined by the number of victims. Given that the cost caused by victim  $v_i$  per unit time is  $\omega_i$ , then, in the time horizon  $[0, \tau]$ , the total cost caused by misinformation is

$$J_2(u) = \int_0^\tau \sum_{i=1}^N \omega_i \Gamma[S_i(t) = 1] dt. \quad (3)$$

For any given time  $t \in [0, \tau]$ , let  $E_i(t) = \Pr[S_i(t) = 0]$ ,  $M_i(t) = \Pr[S_i(t) = 1]$ , and  $T_i(t) = \Pr[S_i(t) = 2]$ . Then, the expected total cost caused by misinformation is

$$J_2(\mathbf{u}) = \int_0^\tau \sum_{i=1}^N \omega_i M_i(t) dt. \quad (4)$$

Combining the above discussions, during the time horizon  $[0, \tau]$ , the expected total cost of a CRA strategy  $\mathbf{u}(t)$  is

$$\begin{aligned} J(\mathbf{u}) &= J_1(\mathbf{u}) + J_2(\mathbf{u}) \\ &= \int_0^\tau \sum_{i=0}^M u_i(t) dt + \int_0^\tau \sum_{i=1}^N \omega_i M_i(t) dt. \end{aligned} \quad (5)$$

### 3.2. Misinformation Spread Model under a CRA Strategy.

With the above terms and notations, we now discuss the control effect of a given CRA strategy on the spread of misinformation. To this end, we need to examine how individual states shift over time under a CRA strategy.

Firstly, let us consider the influence of misinformation spread on individual states. Let  $a_{ij} \in \{0, 1\}$  represent the social relation between the individuals  $v_i$  and  $v_j$ , where  $a_{ij} = 1$  represents that  $v_i$  and  $v_j$  are friends with each other (i.e., they can share ideas to each other); otherwise,  $a_{ij} = 0$ . Suppose that, at any time, a neutral individual will transfer to the misinformation-believing state at an average rate of  $\alpha$  due to the influence of a single misinformation-believing friend. Assume that the influence between friends is linearly cumulative; then, at any time  $t \in [0, \tau]$ , the neutral individual  $v_i$  will transfer to the misinformation-believing state at the average rate of  $\alpha \sum_{j=1}^N a_{ji} \Gamma[S_j(t) = 1]$ .

Secondly, we consider the influence of truth dissemination on individual states. Suppose that, at any time, due to the influence of a single truth-believing friend, each neutral individual and each misinformation-believing individual transfer to the truth-believing state at average rates of  $\beta$  and  $\gamma\beta$ , respectively, where  $0 < \gamma < 1$  is the discount factor which indicates the fact that individuals are difficult to change their cognition of things because of their preconceived ideas. Due to the linear accumulation of friends' influences, at any time  $t \in [0, \tau]$ , the neutral individual  $v_i$  and the misinformation-believing individual  $v_k$  will transfer to the truth-believing state at the average rates of  $\beta \sum_{j=1}^N a_{ji} \Gamma[S_j(t) = 2]$  and  $\gamma\beta \sum_{j=1}^N a_{jk} \Gamma[S_j(t) = 2]$ , respectively.

Finally, we consider the influence of a CRA strategy on individual states. Suppose that if the instantaneous resource investment rate of knowledge popularization is  $u_0$ , each neutral individual and each misinformation-believing individual will transfer to the truth-believing state at average rates of  $f(u_0)$  and  $\gamma f(u_0)$ , respectively. Suppose that if the instantaneous resource investment rate of expert education in group  $B_j$  is  $u_j$ , each

neutral individual and each misinformation-believing individual will transfer to the truth-believing state at average rates of  $g(u_j)$  and  $\gamma g(u_j)$ , respectively. Let  $b_{ij} \in \{0, 1\}$  represent the subordinate relation between the individual  $v_i$  and the group  $B_j$ , where  $b_{ij} = 1$  represents that  $v_i$  belongs to  $B_j$ ; otherwise,  $b_{ij} = 0$ . If the influences of knowledge popularization and expert education on individuals are independent, then, at any time  $t \in [0, \tau]$ , the neutral individual  $v_i$  and the misinformation-believing individual  $v_k$  will transfer to the truth-believing state at the average rates of  $f(u_0(t)) + \sum_{l=1}^M b_{il} g(u_l(t))$  and  $\gamma[f(u_0(t)) + \sum_{l=1}^M b_{kl} g(u_l(t))]$ , respectively.

According to the modeling idea of individual-level epidemic theory [15, 23, 35], the evolution of individual states over time follows a continuous-time Markov chain. At any time  $t \in [0, \tau]$ , the transfer rates among the individual  $v_i$  states are as follows:

- (1) If  $v_i$  is in the neutral state, then  $v_i$  transfers to the misinformation-believing state at the total average rate of

$$r_{01}(t) = \alpha \sum_{j=1}^N a_{ji} \Gamma[S_j(t) = 1]. \quad (6)$$

- (2) If  $v_i$  is in the neutral state, then  $v_i$  transfers to the truth-believing state at the total average rate of

$$r_{02}(t) = \beta \sum_{j=1}^N a_{ji} \Gamma[S_j(t) = 2] + f(u_0(t)) + \sum_{l=1}^M b_{il} g(u_l(t)). \quad (7)$$

- (3) If  $v_i$  is in the misinformation-believing state, then  $v_i$  transfers to the truth-believing state at the total average rate of

$$r_{12}(t) = \gamma \left[ \beta \sum_{j=1}^N a_{ji} \Gamma[S_j(t) = 2] + f(u_0(t)) + \sum_{l=1}^M b_{il} g(u_l(t)) \right]. \quad (8)$$

Because every continuous-time Markov chain admits a Kolmogorov forward equation [36], the expected probability of each individual state will evolve over time with the differential dynamical system:

$$\begin{cases} \dot{E}_i(t) = -\mathbb{E}[r_{01}(t) + r_{02}(t)]E_i(t), \\ \dot{M}_i(t) = -\mathbb{E}[r_{12}(t)]M_i(t) + \mathbb{E}[r_{01}(t)]E_i(t), \\ \dot{T}_i(t) = \mathbb{E}[r_{02}(t)]E_i(t) + \mathbb{E}[r_{12}(t)]M_i(t), \end{cases} \quad (9)$$

where  $\mathbb{E}[\cdot]$  represents mathematical expectation. Because  $E_i(t) + M_i(t) + T_i(t) = 1$ ,  $\forall i$ , the above differential dynamical system can be simplified as



$$\begin{cases} \dot{M}_i(t) = -\gamma \left[ \beta \sum_{j=1}^N a_{ji} T_j(t) + f(u_0(t)) + \sum_{l=1}^M b_{il} g(u_l(t)) \right] \\ M_i(t) + \alpha \sum_{j=1}^N a_{ji} M_j(t) [1 - M_i(t) - T_i(t)], \quad 1 \leq i \leq N, 0 \leq t \leq \tau \\ \dot{T}_i(t) = \left[ \beta \sum_{j=1}^N a_{ji} T_j(t) + f(u_0(t)) + \sum_{l=1}^M b_{il} g(u_l(t)) \right] [1 - M_i(t) - T_i(t)] \\ + \gamma \left[ \beta \sum_{j=1}^N a_{ji} T_j(t) + f(u_0(t)) + \sum_{l=1}^M b_{il} g(u_l(t)) \right] M_i(t), \quad 1 \leq i \leq N, 0 \leq t \leq \tau \end{cases} \quad (10)$$

Because the above dynamic system depicts the evolution of individual states over time, we call it the *individual state evolution model*, or simply the *evolution model* for short. The evolution model is an individual-level misinformation spread model that considers the cooperation of knowledge popularization and expert education to publish the truth. For writing convenience, let  $X(t) = (M_1(t), \dots, M_N(t), T_1(t), \dots, T_N(t))$ , and let  $F(X(t), u(t), t) = 0$  denote the evolution model.

**3.3. Optimal CRA Strategy Model.** Having proposed the evolution model in the previous section, we now need to formulate an optimization problem to design an effective CRA strategy.

Based on previous discussions, we formulate the following optimization problems:

$$\begin{aligned} & \min_{u \in U} J(u) \\ & \text{s.t. } F(X(t), u(t), t) = 0, \quad \forall t \in [0, \tau]. \end{aligned} \quad (11)$$

This is a continuous-time optimal control problem. We call it the optimal CRA strategy model.

## 4. Solution

After having formulated an optimal control model to seek optimal CRA strategies, in this section, we discuss the solutions. First, we derive a set of necessary conditions for an optimal solution. We refer to the collection of all these necessary conditions as the *optimality system*. With the optimality system, we can obtain a solution that is most likely to be the optimal one, which is called the candidate optimal solution. Second, we give an iteration algorithm to numerically obtain a candidate optimal solution.

**4.1. Optimality System.** Firstly, the Hamiltonian function for the optimal CRA strategy model (11) is constructed as follows:

$$H(u, X) = \sum_{i=0}^M u_i + \sum_{i=1}^N \omega_i M_i + \sum_{i=1}^N \lambda_i \left\{ \alpha \sum_{j=1}^N a_{ji} M_j (1 - M_i - T_i) - \gamma \left[ \beta \sum_{j=1}^N a_{ji} T_j + f(u_0) + \sum_{l=1}^M b_{il} g(u_l) \right] M_i \right\} + \sum_{i=1}^N \mu_i \left\{ [1 - (1 - \gamma)M_i - T_i] \times \left[ \beta \sum_{j=1}^N a_{ji} T_j + f(u_0) + \sum_{l=1}^M b_{il} g(u_l) \right] \right\}, \quad (12)$$

where  $P = (\lambda_1, \lambda_2, \dots, \lambda_N, \mu_1, \mu_2, \dots, \mu_N)$  denotes the adjoint function of the Hamiltonian.

Let  $u(t) \in U$  represent an optimal CRA strategy,  $X(t)$  represent the corresponding expected individual state evolution trajectory, and  $P(t)$  represent the corresponding adjoint function. According to Pontryagin's principle [37], the following conclusions must hold true simultaneously.

(1) The optimal CRA strategy  $u(t)$  satisfies

$$u(t) = \arg \min_{u \in U} H(u(t), X(t), t), \quad 0 \leq t \leq \tau. \quad (13)$$

(2) The expected individual state evolution trajectory  $X(t)$  meets

$$\begin{cases} \frac{dM_i(t)}{dt} = + \frac{\partial H(u(t), X(t), t)}{\partial \lambda_i(t)}, & 0 \leq t \leq \tau, \\ \frac{dT_i(t)}{dt} = + \frac{\partial H(u(t), X(t), t)}{\partial \mu_i(t)}, & 0 \leq t \leq \tau, \\ X(0) = X_0, \end{cases} \quad (14)$$

where  $X_0$  is an initial condition.

(3) The adjoint function  $P(t)$  satisfies

$$\begin{cases} \frac{d\lambda_i(t)}{dt} = -\frac{\partial H(u(t), X(t), t)}{\partial M_i(t)}, & 0 \leq t \leq \tau, \\ \frac{d\mu_i(t)}{dt} = -\frac{\partial H(u(t), X(t), t)}{\partial T_i(t)}, & 0 \leq t \leq \tau, \\ P(T) = 0. \end{cases} \quad (15)$$

After direct calculation, we get that the trajectory  $X(t)$  admits the evolution model (10) and the adjoint function  $P(t)$  admits the following dynamic system:

$$\begin{cases} \frac{d\lambda_i(t)}{dt} = -\omega_i + [\gamma\lambda_i(t) + (1-\gamma)\mu_i(t)] \\ \times \left[ f(u_0(t)) + \sum_{l=1}^M b_{il}g(u_l(t)) + \beta \sum_{j=1}^N a_{ji}T_j(t) \right] + \alpha\lambda_i(t) \sum_{j=1}^N a_{ji}M_j(t) \\ - \alpha \sum_{j=1}^N \lambda_j(t)a_{ij} [1 - M_j(t) - T_j(t)], \quad 1 \leq i \leq N, 0 \leq t \leq \tau \\ \frac{d\mu_i(t)}{dt} = \alpha\lambda_i(t) \sum_{j=1}^N a_{ji}M_j(t) + \beta\gamma \sum_{j=1}^N \lambda_j(t)a_{ij}M_j(t) - \beta \sum_{j=1}^N \mu_j(t)a_{ij} [1 - (1-\gamma)M_j(t) - T_j(t)] + \mu_i(t) \\ \left[ f(u_0(t)) + \sum_{l=1}^M b_{il}g(u_l(t)) + \beta \sum_{j=1}^N a_{ji}T_j(t) \right], \quad 1 \leq i \leq N, 0 \leq t \leq \tau \\ P(0) = 0 \end{cases} \quad (16)$$

Combining the above discussions, the optimality system includes equation (13), evolution model (10), and dynamical system (16). By solving the optimality system, a candidate optimal CRA strategy can be obtained. Because of the complexity of optimal control model (11), it is difficult to directly get a real sense of optimal CRA strategy. As a result, the optimality system provides great convenience for problem solving or at least reduces the range of optimal solutions. Even if the candidate optimal CRA strategy we got is not necessarily a real sense of optimal solution, it can be regarded as optimal if it shows a better performance than most other comparison schemes.

**4.2. Numerical Iteration Algorithm.** Because of the complexity of the optimality system, it is very difficult to directly obtain the analytical form of solutions. Therefore, a numerical algorithm is needed. Because solving the optimal

system is essentially solving a two-point boundary value problem [38] and because the forward-backward sweep method (FBSM) [39] is just a practical numerical method to solve that problem, this paper use the FBSM to solve the optimality system. The pseudocode is shown in Algorithm 1.

We need to note that it is difficult to prove the convergence of the FBSM, as the literature [40] explains. However, as described in [41], it can achieve good convergence in most practical cases. Therefore, we can still choose it as the numerical method.

In lines 1, 5, and 7 of Algorithm 1, there are several ordinary differential equations (ODEs) to be solved. Common methods for solving ODEs include the Euler method [42] and the Runge–Kutta method [43]. The Runge–Kutta method has not only been proven more accurate than the Euler method but also has higher time consumption due to its higher complexity. However, practical experience shows that the accuracy difference

**Input:** acceptable iteration length  $K$ , convergence error  $\varepsilon$ , and initial seed  $u^{(0)}(t)$ .  
**Output:** a candidate optimal CRA strategy  $u(t)$ .  
(1)  $u(t) \leftarrow u^{(0)}(t)$ .  $X^{(0)}(t) \leftarrow X(t)$ , by solving Equation (10).  
(2)  $J^{(0)} \leftarrow J(u)$ , by solving Equation (5).  
(3) **for**  $k = 0: 1: K - 1$  **do**  
(4)  $X(t) \leftarrow X^{(k)}(t)$ ,  $u(t) \leftarrow u^{(k)}(t)$ .  
(5)  $P^{(k)}(t) \leftarrow P(t)$ , by solving Equation (16).  
(6)  $u^{(k+1)}(t) \leftarrow u(t)$ , by solving Equation (13).  
(7)  $X^{(k+1)}(t) \leftarrow X(t)$ , by solving Equation (10).  
(8)  $J^{(k+1)} \leftarrow J(u)$ , by solving Equation (5).  
(9) **if**  $|J^{(k+1)} - J^{(k)}| < \varepsilon$  **then**  
(10) **return**  $u^{(k+1)}(t)$ .  
(11) **return**  $u^{(k+1)}(t)$ .

ALGORITHM 1: Forward-backward sweep method.

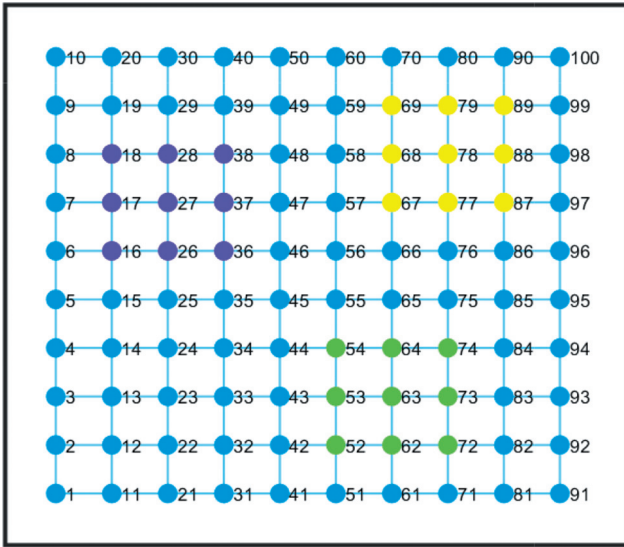


FIGURE 1: The topological structure of  $G_g$ . Nodes of group  $B_1$  are marked in purple; nodes of group  $B_2$  are marked in green; nodes of group  $B_3$  are marked in yellow; nodes that do not belong to any group are marked in blue.

between them is usually negligible as long as the discrete step length on time is small enough. Therefore, the Euler method is used as part of the FBSM in this paper to solve ODEs.

## 5. Numerical Experiments

Having discussed the solution of the optimal CRA strategy model (11), we now give a series of numerical experiments to illustrate obtained candidate optimal strategies.

**5.1. Network Topological Structure.** In order to better show the misinformation spread process and the control effect of a CRA strategy on it, let us consider a 100-node grid social network plotted in Figure 1. Suppose that the truth can be released to three specific groups of individuals in the way of expert education, where (a) group  $B_1$  consists of the individuals  $v_{16}, v_{17}, v_{18}, v_{26}, v_{27}, v_{28}, v_{36}, v_{37}$ , and  $v_{38}$ , (b) group  $B_2$  consists of the individuals  $v_{52}, v_{53}, v_{54}, v_{62}, v_{63}, v_{64}, v_{72}, v_{73}$ ,

and  $v_{74}$ , and (c) group  $B_3$  consists of the individuals  $v_{67}, v_{68}, v_{69}, v_{77}, v_{78}, v_{79}, v_{87}, v_{88}$ , and  $v_{89}$ . Individuals of different groups are marked with different colors in Figure 1. For convenience, we denote this network by  $G_g$ .

Besides, in order to show the influences of arbitrary network topological structures, the following three networks are involved in our experiments. The first one is a 100-node small-world network obtained from [35, 44]. We denote this network by  $G_{sw}$ . The second one is a 100-node scale-free network obtained from [35, 44]. We denote this network by  $G_{sf}$ . The last one is a 100-node Facebook network obtained from [23, 45]. We denote this network by  $G_{fb}$ . In each network, the truth can be released to three random groups of nodes in the way of expert education. The topological structures of these three networks are shown in Figure 2.

### 5.2. Candidate Optimal CRA Strategy

*Experiment 1.* Consider the social network  $G_g$ . Consider a situation, where  $\tau = 3$ ,  $\alpha = 1$ ,  $\beta = 1$ ,  $\gamma = 0.8$ ,  $\omega_i$  is generated within  $[5, 15]$ ,  $\bar{u} = (1, 1.5, 2)$ ,  $f(u) = 0.02\sqrt{u}$ ,  $g(u) = 0.07\sqrt{u}$ , and  $X_0 = [0.2_{1 \times 100}, 0_{1 \times 100}]$ . Denote the obtained candidate optimal CRA strategy by  $u^*(t) = (u_0^*(t), u_1^*(t), u_2^*(t), u_3^*(t))$  and the corresponding individual state evolution trajectory by  $X^*(t) = (M_1^*(t), \dots, M_{100}^*(t), T_1^*(t), \dots, T_{100}^*(t))$ . Define the corresponding expected network state evolution trajectory as  $\bar{X}^*(t) = (\bar{M}^*(t), \bar{T}^*(t))$ , where  $\bar{M}^*(t) = 1/100 \sum_{i=1}^{100} M_i^*(t)$  and  $\bar{T}^*(t) = 1/100 \sum_{i=1}^{100} T_i^*(t)$ .

Results: the obtained candidate optimal CRA strategy  $u^*(t)$  is shown in Figure 3. We can see that the instantaneous resource investment rate of knowledge popularization, i.e.,  $u_0^*(t)$ , first remains at its upper bound till time  $t = 2$ , then gradually decreases to its lower bound, and finally remains at its lower bound. Each component of the instantaneous resource investment rates of expert education, i.e.,  $u_i^*(t)$ ,  $i = 1, 2, 3$ , first remains at its upper bound till time  $t = 1$ , then gradually decreases to its lower bound, and finally remains at its lower bound. Figure 4 shows the corresponding expected network state evolution trajectory. We can see that  $\bar{M}^*(t)$  gradually increases from 0.2 till time  $t = 1$ , then reaches the peak 0.7 at

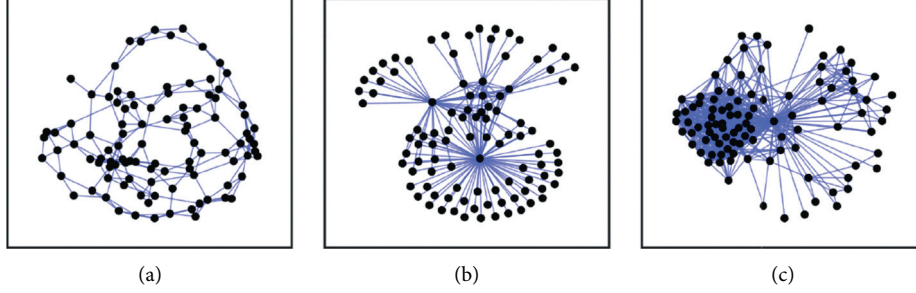


FIGURE 2: The topological structures of (a)  $G_{sw}$ , (b)  $G_{sf}$ , and (c)  $G_{fb}$ . In each of these three networks, the truth can be released to three random groups of nodes in the way of expert education.

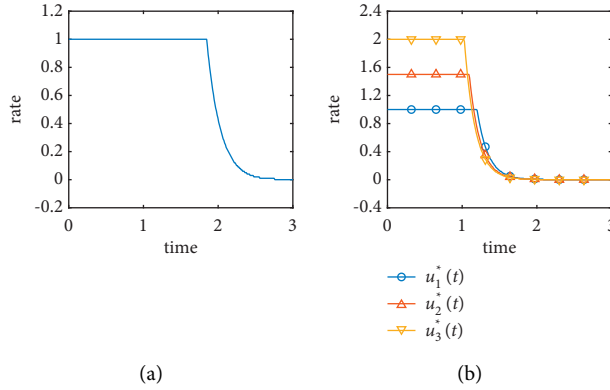


FIGURE 3: The obtained candidate optimal CRA strategy  $u^*(t)$  in Experiment 1: (a) the instantaneous resource investment rate of knowledge popularization, i.e.,  $u_0^*(t)$ , and (b) the instantaneous resource investment rates of expert education in the three groups, i.e.,  $u_1^*(t)$ ,  $u_2^*(t)$ , and  $u_3^*(t)$ .

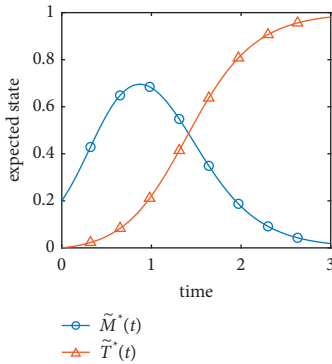


FIGURE 4: The corresponding expected network state evolution trajectory  $\tilde{X}^*(t) = (\tilde{M}^*(t), \tilde{T}^*(t))$  in Experiment 1.

time  $t = 1$ , and gradually decreases to 0. During time  $t \in [0, 3]$ ,  $\tilde{T}^*(t)$  quickly then slowly increases from 0 to 1. Figure 5 shows the distribution of the misinformation-believing state at some moments with respect to the network  $G_f$ . Combining the results in Figure 4, we can see that when the average expected probability of people being in the misinformation-believing state increases, the expected probabilities of people who belong to the three groups  $B_1$ ,  $B_2$ , and  $B_3$  increase more slowly than those of the others. When the average expected probability decreases, the expected probabilities of those people decrease more quickly than the probabilities of the others. Figure 6 shows the distribution of the truth-believing state at some moments with respect to the network  $G_g$  (shown in Figure 1).

Combining the results in Figure 4, we can see that, in terms of the expected probability of being in the truth-believing state, those of people belong to the three groups  $B_1$ ,  $B_2$ , and  $B_3$  increase more quickly than those of the others.

Reasons: at the beginning of the truth-publishing campaign, misinformation has large coverage over the social network, and therefore, the speed of misinformation spreading is remarkable. In this context, the optimal strategy suggests putting the highest amount of resources in publishing the truth, so as to reduce the coverage of misinformation and further contain the speed of misinformation spreading. Knowledge popularization helps all people accept the truth at a low rate, expanding slowly the coverage of the truth. Expert education helps people in the three groups accept the truth at a high rate. Once people in the three groups become believers of the truth, they can quickly influence the individuals around them and further expand the coverage of the truth. When the truth has large coverage over the social network, the optimal strategy suggests reducing the resource investment in releasing the truth, so as to reduce the cost. Under the effect of word-of-mouth, even if the truth is no longer released, it can eventually fill the whole social network.

*Experiment 2.* Given the parameters, where  $\tau = 3$ ,  $\alpha = 1$ ,  $\beta = 1$ ,  $\gamma = 0.8$ ,  $\omega_i$  is generated within  $[5, 15]$ ,  $\bar{u} = (1, 1.5, 2)$ ,  $f(u) = 0.02\sqrt{u}$ ,  $g(u) = 0.07\sqrt{u}$ , and  $X_0 = [0.2_{1 \times 100}, 0_{1 \times 100}]$ , consider the social networks  $G_{sw}$ ,  $G_{sf}$ , and  $G_{fb}$ , respectively.

Results: Figure 7 shows the obtained candidate optimal CRA strategies in Experiment 2. Figure 8 shows the expected network state evolution trajectories in Experiment 2. It is

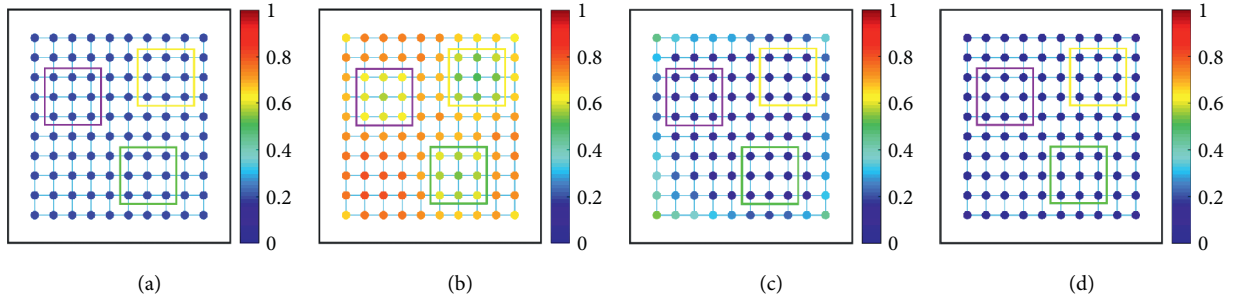


FIGURE 5: The distribution of the misinformation-believing state with respect to the network  $G_g$  (shown in Figure 1) at some moments, where (a)  $t = 0$ , (b)  $t = 1$ , (c)  $t = 2$ , and (d)  $t = 3$ . The three colored boxes indicate the three groups,  $B_1$ ,  $B_2$ , and  $B_3$ . The color of a node represents the expected probability of the corresponding individual being in the misinformation-believing state at the current moment.

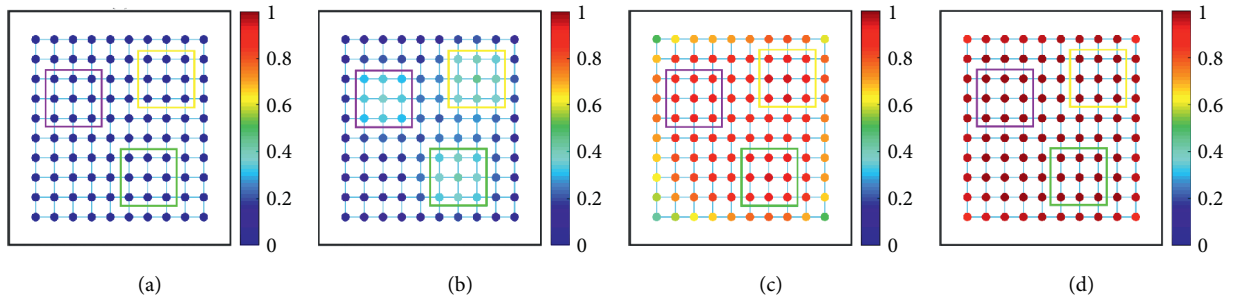


FIGURE 6: The distribution of the truth-believing state with respect to the network  $G_g$  (shown in Figure 1) at some moments, where (a)  $t = 0$ , (b)  $t = 1$ , (c)  $t = 2$ , and (d)  $t = 3$ . The three colored boxes indicate the three groups,  $B_1$ ,  $B_2$ , and  $B_3$ . The color of a node represents the expected probability of the corresponding individual being in the truth-believing state at the current moment.

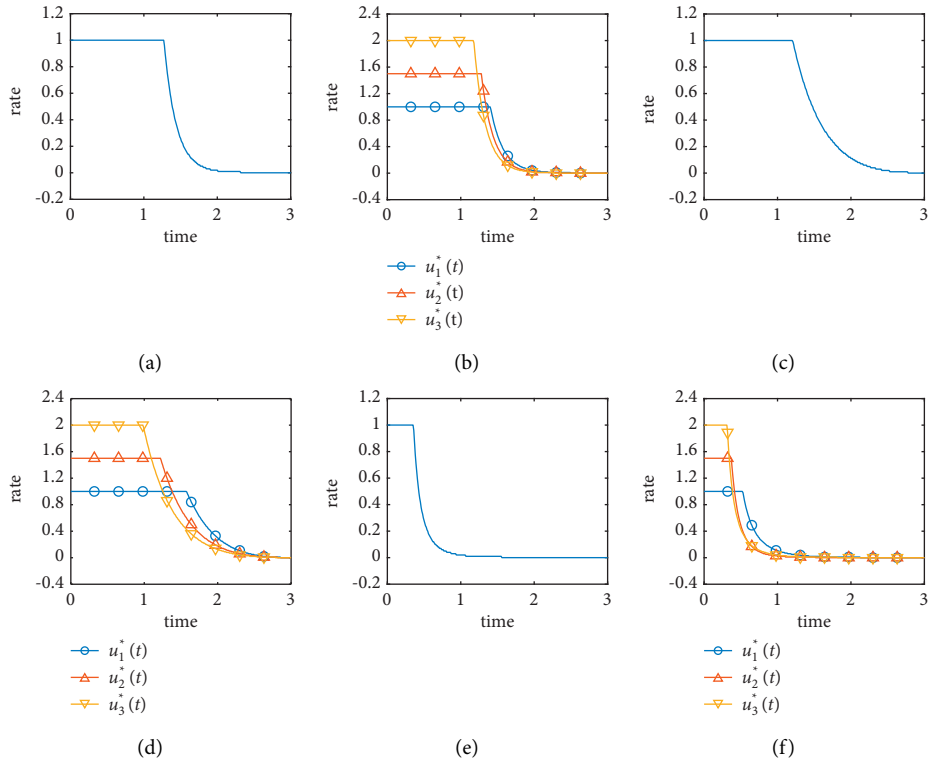


FIGURE 7: The obtained candidate optimal CRA strategies in Experiment 2: (a) and (b) the results of  $G_{sw}$ , (c) and (d) the results of  $G_{sf}$ , and (e) and (f) the results of  $G_{fb}$ .

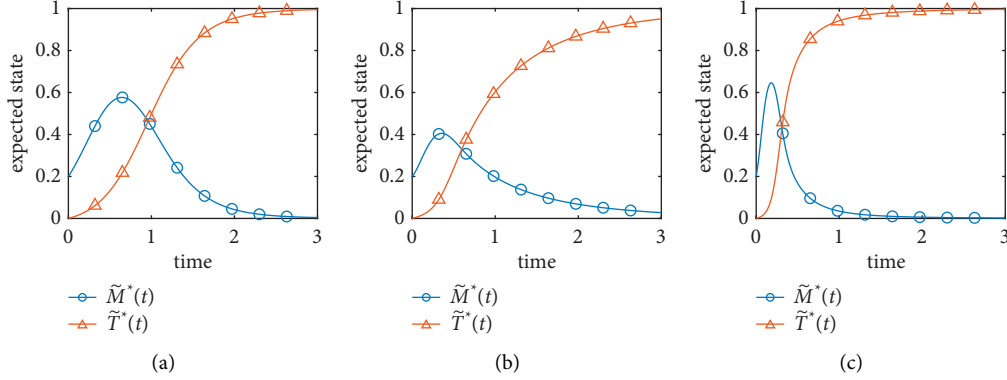


FIGURE 8: The expected network state evolution trajectories in Experiment 2: (a) shows the results of  $G_{sw}$ , (b) the results of  $G_{sf}$ , and (c) the results of  $G_{fb}$ .

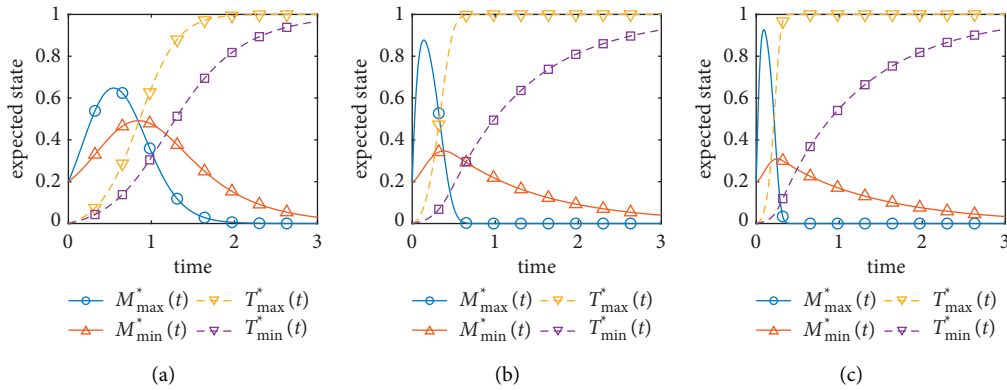


FIGURE 9: Results in Experiment 2: the state evolution trajectories of nodes that have different degrees: (a) the results of  $G_{sw}$ , (b) the results of  $G_{sf}$ , and (c) the results of  $G_{fb}$ . In each figure,  $M_{\max}^*(t)$  denotes the misinformation-believing trajectory of the node that has the highest degree and  $M_{\min}^*(t)$  denotes the misinformation-believing trajectory of the node that has the lowest degree. Besides,  $T_{\max}^*(t)$  and  $T_{\min}^*(t)$  have similar meanings.

seen that results are similar to those of Experiment 1. Therefore, we may be able to conclude that even though network topological structures are different, the obtained candidate optimal CRA strategies should be similar. Furthermore, we examine the state evolution trajectories of nodes that have different degrees, as shown in Figure 9. It is seen that despite of network topological structures, nodes of higher degrees are more sensitive to CRA strategies.

In the above two experiments, the functions  $f$  and  $g$  are set as concave. Next, we examine the cases when they are convex.

*Experiment 3.* Given the parameters, where  $\tau = 3$ ,  $\alpha = 1$ ,  $\beta = 1$ ,  $\gamma = 0.8$ ,  $\omega_i$  is generated within  $[5, 15]$ ,  $\bar{u} = (1, 1.5, 2)$ ,  $f(u) = 0.02u^2$ ,  $g(u) = 0.07u^2$ , and  $X_0 = [0.2_{1 \times 100}, 0_{1 \times 100}]$ , consider the social networks  $G_g$ ,  $G_{sw}$ ,  $G_{sf}$ , and  $G_{fb}$ , respectively.

Results: the obtained candidate optimal CRA strategy  $u^*(t)$  is shown in Figure 10. We can see that all instantaneous resource investment rates first remain at their upper bounds, then drop to their lower bounds, and finally remain at their lower bounds. Figure 11 shows the expected network state evolution trajectories of the four networks. We can see that their results are similar. On each network, the average

probability of the misinformation-believing state, i.e.,  $\tilde{M}^*(t)$ , first increases, then reaches the peak, and finally decreases to 0. The average probability of the truth-believing state, i.e.,  $\tilde{T}^*(t)$ , quickly then slowly increases from 0 to 1 during the whole time horizon.

Reasons: at the beginning of the truth-publishing campaign, misinformation has large coverage over the social network, and therefore, the speed of misinformation spreading is remarkable. In this context, the optimal strategy suggests putting the highest amount of resources in publishing the truth, so as to reduce the coverage of misinformation and further contain the speed of misinformation spreading. When the truth has large coverage over the social network, the optimal strategy suggests reducing the resource investment in releasing the truth, so as to reduce the cost. Under the effect of word-of-mouth, even if the truth is no longer released, it can eventually fill the whole social network.

### 5.3. Effectiveness Verification

*Experiment 4.* Consider network  $G_g$ . Consider a situation, where  $\tau = 3$ ,  $\alpha = 1$ ,  $\beta = 1$ ,  $\gamma = 0.8$ ,  $\omega_i$  is generated within  $[5, 15]$ ,  $\bar{u} = (1, 1.5, 2)$ ,  $f(u) = 0.02\sqrt{u}$ ,  $g(u) = 0.07\sqrt{u}$ , and

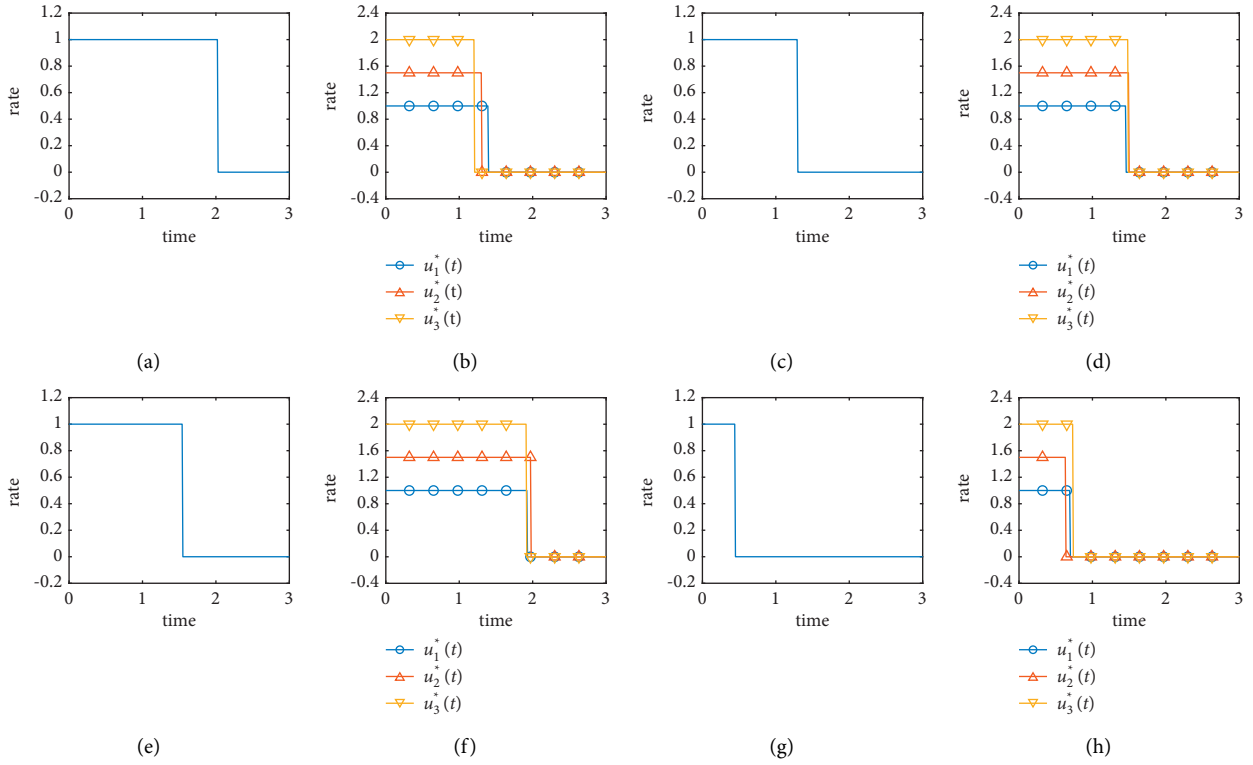


FIGURE 10: The obtained candidate optimal CRA strategies in Experiment 3: (a) and (b) the results of  $G_g$ , (c) and (d) the results of  $G_{sw}$ , (e) and (f) the results of  $G_{sf}$ , and (g) and (h) the results of  $G_{fb}$ .

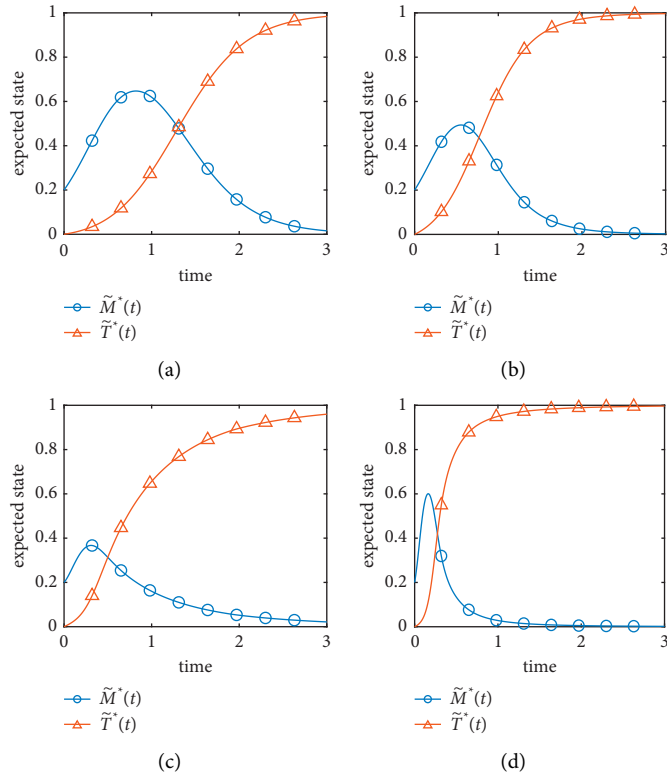


FIGURE 11: The expected network state evolution trajectories in Experiment 3: (a) the results of  $G_g$ , (b) the results of  $G_{sw}$ , (c) the results of  $G_{sf}$ , and (d) the results of  $G_{fb}$ .

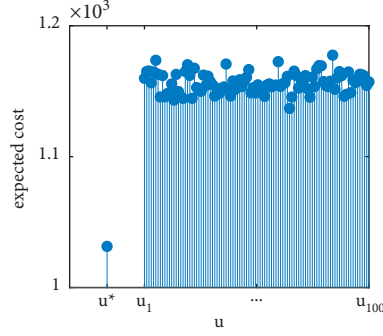


FIGURE 12: Results in Experiment 4: the expected costs under the optimal strategy  $u^*$  and the uniformly random strategies  $u_1, \dots, u_{100}$ .

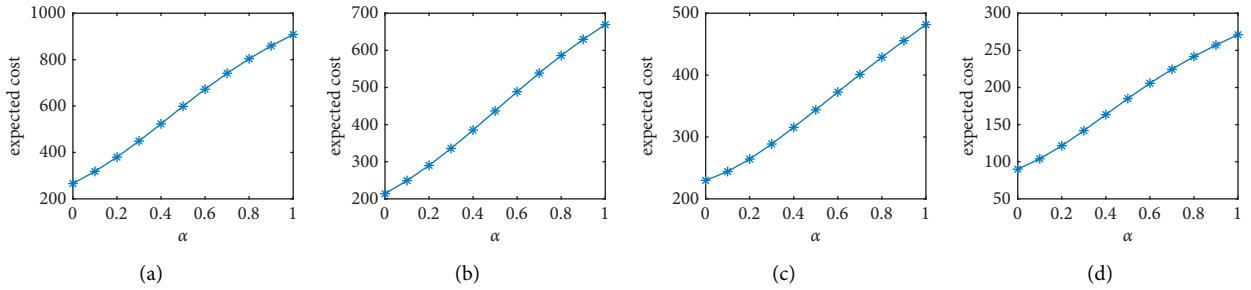


FIGURE 13: Results in Experiment 5: the influences of the misinformation spread rate  $\alpha$  in network: (a)  $G_g$ , (b)  $G_{sw}$ , (c)  $G_{sf}$ , and (d)  $G_{fb}$ .

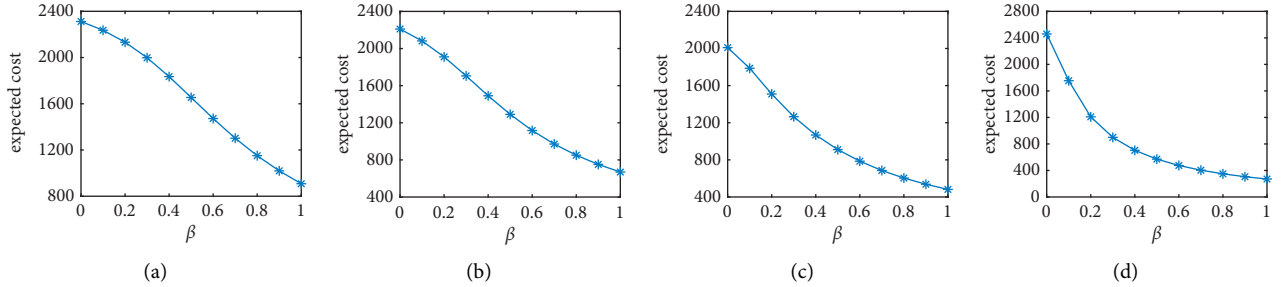


FIGURE 14: Results in Experiment 6: the influences of the truth spread rate  $\beta$  in network: (a)  $G_g$ , (b)  $G_{sw}$ , (c)  $G_{sf}$ , and (d)  $G_{fb}$ .

$X_0 = [0.2_{1 \times 100}, 0_{1 \times 100}]$ . Denote the obtained candidate optimal CRA strategy by  $u^*$ . Generate a hundred uniformly random CRA strategies and denote them by  $u_1, \dots, u_{100}$ .

Figure 12 compares the expected costs under the optimal strategy  $u^*$  and the uniformly random strategies  $u_1, \dots, u_{100}$ . We can see that the optimal strategy is better than the 100 random strategies. To prevent the contingency, we did another 1000 similar experiments and obtained the same conclusion. Hence, we recommend the candidate optimal strategy as an optimal solution.

**5.4. Influences of Crucial Factors.** Finally, let us investigate the influences of some crucial factors in the evolution model (10), including the misinformation spread rate  $\alpha$ , the truth spread rate  $\beta$ , and the discount factor  $\gamma$ .

*Experiment 5.* Given the parameters, where  $\tau = 3$ ,  $\beta = 1$ ,  $\gamma = 0.8$ ,  $\omega_i$  is generated within  $[5, 15]$ ,  $\bar{u} = (1, 1.5, 2)$ ,  $f(u) = 0.02\sqrt{u}$ ,  $g(u) = 0.07\sqrt{u}$ ,  $X_0 = [0.2_{1 \times 100}, 0_{1 \times 100}]$ , and

$\alpha \in \{0, 0.1, \dots, 1\}$ , consider the social networks  $G_g, G_{sw}, G_{sf}$ , and  $G_{fb}$ , respectively.

Figure 13 shows the influence of the misinformation spread rate  $\alpha$ . Even though the four networks have different topological structures, their experiment results are similar. We can see that the minimized expected cost is increasing with the misinformation spread rate. This conclusion suggests that it is important to improve the citizens' ability to distinguish misinformation so that the misinformation spread rate is reduced.

*Experiment 6.* Given the parameters, where  $\tau = 3$ ,  $\alpha = 1$ ,  $\gamma = 0.8$ ,  $\omega_i$  is generated within  $[5, 15]$ ,  $\bar{u} = (1, 1.5, 2)$ ,  $f(u) = 0.02\sqrt{u}$ ,  $g(u) = 0.07\sqrt{u}$ ,  $X_0 = [0.2_{1 \times 100}, 0_{1 \times 100}]$ , and  $\beta \in \{0, 0.1, \dots, 1\}$ , consider the social networks  $G_g, G_{sw}, G_{sf}$ , and  $G_{fb}$ , respectively.

Figure 14 shows the influence of the truth spread rate  $\beta$ . Even though the four networks have different topological structures, their experiment results are similar. We can see that the minimized expected cost is decreasing with the truth



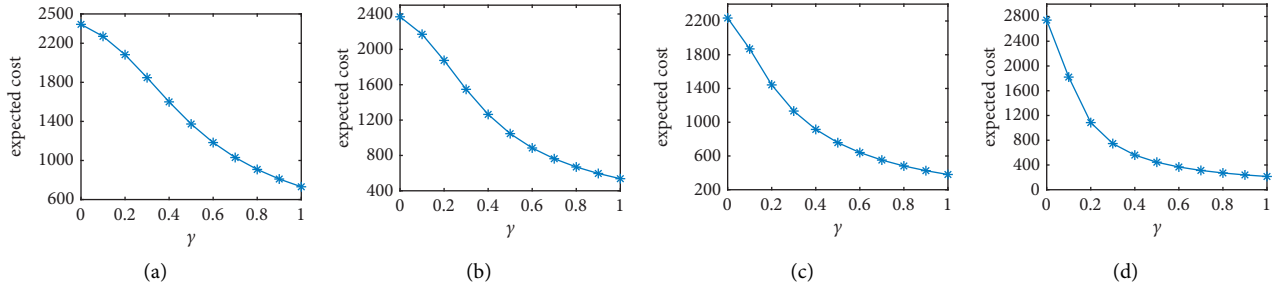


FIGURE 15: Results in Experiment 7: the influences of the discount factor  $\gamma$  in network: (a)  $G_g$ , (b)  $G_{sw}$ , (c)  $G_{sf}$ , and (d)  $G_{fb}$ .

spread rate. This conclusion suggests that it is necessary to make the truth more interesting so that the truth spread rate is enhanced.

*Experiment 7.* Given the parameters, where  $\tau = 3$ ,  $\alpha = 1$ ,  $\beta = 1$ ,  $\omega_i$  is generated within  $[5, 15]$ ,  $\bar{u} = (1, 1.5, 2)$ ,  $f(u) = 0.02\sqrt{u}$ ,  $g(u) = 0.07\sqrt{u}$ ,  $X_0 = [0.2_{1 \times 100}, 0_{1 \times 100}]$ , and  $\beta \in \{0, 0.1, \dots, 1\}$ , consider the networks  $G_g$ ,  $G_{sw}$ ,  $G_{sf}$ , and  $G_{fb}$ , respectively.

Figure 15 shows the influence of the discount factor  $\gamma$ . Even though the four networks have different topological structures, their experiment results are similar. We can see that the minimized expected cost is decreasing with the discount factor. This conclusion suggests that it is necessary to help the truth change people's cognition of things.

## 6. Conclusion

This paper addresses the CRA problem, a problem about how to reasonably allocate resources to knowledge popularization and expert education so as to mitigate the spread of misinformation with a better performance but a lower cost. First, a novel individual-level misinformation spread model is proposed to characterize the collaborative effect of knowledge popularization and expert education on containing the spread of misinformation. Thereafter, based on the proposed misinformation spread model, the CRA problem is reduced to an optimal control problem, and an optimality system for solving it is derived. Finally, with a series of numerical experiments, the obtained solution is verified to be optimal.

Still, there are some problems to be solved in the future. First, in our work, the truth is continuously released to the public, which may not be convenient in practice. Instead, it is more common to release the truth at some given moments. If so, a continuous-time optimal control problem may not be very suitable, and we may formulate an impulsive optimal control problem [46] to seek effective CRA strategies. Second, in our numerical experiments, the values of model parameters are set according to some related literature and our experience. In the future work, they should be determined by practical data.

## Data Availability

All the data used to support the findings of this study are included within the article.

## Conflicts of Interest

The authors declare that there are no conflicts of interest regarding the publication of this paper.

## Acknowledgments

This work was supported by the National Natural Science Foundation of China, under Grant 61572006.

## References

- [1] A. Mian and S. Khan, "Coronavirus: the spread of misinformation," *BMC Medicine*, vol. 18, no. 1, pp. 89–92, 2020.
- [2] J. Kim and M. Hastak, "Social network analysis: characteristics of online social networks after a disaster," *International Journal of Information Management*, vol. 38, no. 1, pp. 86–96, 2018.
- [3] K. Rapoza, "Can 'fake News' Impact the Stock Market?," 2017, <https://www.forbes.com/sites/kenrapoza/2017/02/26/can-fake-news-impact-the-stock-market/?sh=64a67df22fac>.
- [4] S. Tasnim, M. M. Hossain, and H. Mazumder, "Impact of rumors and misinformation on covid-19 in social media," *Journal of preventive medicine and public health*, vol. 53, no. 3, pp. 171–174, 2020.
- [5] W.-Y. S. Chou, A. Oh, and W. M. P. Klein, "Addressing health-related misinformation on social media," *JAMA*, vol. 320, no. 23, pp. 2417–2418, 2018.
- [6] K. Sharma, F. Qian, H. Jiang, N. Ruchansky, M. Zhang, and Y. Liu, "Combating fake news," *ACM Transactions on Intelligent Systems and Technology*, vol. 10, no. 3, pp. 1–42, 2019.
- [7] I. Kishore, "Importance of guest lectures in schools," 2017, <https://www.slideshare.net/IshitaKishore2/importance-of-guest-lectures-in-schools>.
- [8] S. S. Ho, A. D. Leong, J. Looi, and A. S. F. Chuah, "Online, offline, or word-of-mouth? complementary media usage patterns and credibility perceptions of nuclear energy information in southeast asia," *Energy Research & Social Science*, vol. 48, pp. 46–56, 2019.
- [9] B. M. Okdie, R. E. Guadagno, F. J. Bernieri, A. L. Geers, and A. R. McLaren-Vesotski, "Getting to know you: face-to-face versus online interactions," *Computers in Human Behavior*, vol. 27, no. 1, pp. 153–159, 2011.
- [10] S. Wen, J. Jiang, Y. Xiang, S. Yu, W. Zhou, and W. Jia, "To shut them up or to clarify: restraining the spread of rumors in online social networks," *IEEE Transactions on Parallel and Distributed Systems*, vol. 25, no. 12, pp. 3306–3316, 2014.
- [11] C. Pan, L.-X. Yang, X. Yang, Y. Wu, and Y. Y. Tang, "An effective rumor-containing strategy," *Physica A: Statistical Mechanics and Its Applications*, vol. 500, pp. 80–91, 2018.

- [12] P. Wan, X. Wang, X. Wang, L. Wang, Y. Lin, and W. Zhao, "Intervening Coupling Diffusion of Competitive Information in Online Social Networks," *IEEE Transactions on Knowledge and Data Engineering*, vol. 33, no. 6, pp. 2548–2559, 2019.
- [13] Y. Lin, X. Wang, F. Hao et al., "Dynamic Control of Fraud Information Spreading in mobile Social Networks," *IEEE Transactions on Systems, Man, and Cybernetics: Systems*, vol. 51, no. 6, pp. 3725–3738, 2019.
- [14] F. Liu and M. Buss, "Optimal control for heterogeneous node-based information epidemics over social networks," *IEEE Transactions on Control of Network Systems*, vol. 7, no. 3, pp. 1115–1126, 2020.
- [15] J. Chen, L.-X. Yang, X. Yang, and Y. Y. Tang, "Cost-effective anti-rumor message-pushing schemes," *Physica A: Statistical Mechanics and Its Applications*, vol. 540, Article ID 123085, 2020.
- [16] N. P. Nguyen, G. Yan, and M. T. Thai, "Analysis of misinformation containment in online social networks," *Computer Networks*, vol. 57, no. 10, pp. 2133–2146, 2013.
- [17] G. Tong, W. Wu, L. Guo et al., "An efficient randomized algorithm for rumor blocking in online social networks," *IEEE Transactions on Network Science and Engineering*, vol. 7, no. 2, pp. 845–854, 2017.
- [18] G. Tong, W. Wu, and D.-Z. Du, "Distributed rumor blocking with multiple positive cascades," *IEEE Transactions on Computational Social Systems*, vol. 5, no. 2, pp. 468–480, 2018.
- [19] D. Yang, X. Liao, H. Shen, X. Cheng, and G. Chen, "Dynamic node immunization for restraint of harmful information diffusion in social networks," *Physica A: Statistical Mechanics and Its Applications*, vol. 503, pp. 640–649, 2018.
- [20] F. D. Sahneh and C. M. Scoglio, "Optimal Information Dissemination in Epidemic Networks," in *Proceedings of the 2012 IEEE 51st IEEE Conference on Decision and Control (Cdc)*, pp. 1657–1662, IEEE, Maui, HI, USA, December, 2012.
- [21] Q. Xu, Z. Su, K. Zhang, P. Ren, and X. S. Shen, "Epidemic information dissemination in mobile social networks with opportunistic links," *IEEE Transactions on Emerging Topics in Computing*, vol. 3, no. 3, pp. 399–409, 2015.
- [22] P.-Y. Chen, S.-M. Cheng, and K.-C. Chen, "Optimal control of epidemic information dissemination over networks," *IEEE Transactions on Cybernetics*, vol. 44, no. 12, pp. 2316–2328, 2014.
- [23] D.-W. Huang, L.-X. Yang, P. Li, X. Yang, and Y. Y. Tang, "Developing cost-effective rumor-refuting strategy through game-theoretic approach," *IEEE Systems Journal*, vol. 15, no. 4, pp. 5034–5045, 2020.
- [24] F. Jin, W. Wang, L. Zhao et al., "Misinformation propagation in the age of twitter," *Computer*, vol. 47, no. 12, pp. 90–94, 2014.
- [25] W. Liu, X. Wu, W. Yang, X. Zhu, and S. Zhong, "Modeling cyber rumor spreading over mobile social networks: a compartment approach," *Applied Mathematics and Computation*, vol. 343, pp. 214–229, 2019.
- [26] X. Wang, X. Wang, F. Hao, G. Min, and L. Wang, "Efficient coupling diffusion of positive and negative information in online social networks," *IEEE Transactions on Network and Service Management*, vol. 16, no. 3, pp. 1226–1239, 2019.
- [27] Z. He, Z. Cai, J. Yu, X. Wang, Y. Sun, and Y. Li, "Cost-efficient strategies for restraining rumor spreading in mobile social networks," *IEEE Transactions on Vehicular Technology*, vol. 66, no. 3, pp. 2789–2800, 2016.
- [28] Y. Moreno, M. Nekovee, and A. F. Pacheco, "Dynamics of rumor spreading in complex networks," *Physical review. E*, *Statistical, nonlinear, and soft matter physics*, vol. 69, no. 6, Article ID 066130, 2004.
- [29] Z. Tan, J. Ning, Y. Liu, X. Wang, G. Yang, and W. Yang, "ECRModel: an elastic collision-based rumor-propagation model in online social networks," *IEEE Access*, vol. 4, pp. 6105–6120, 2016.
- [30] F. Ding, T. Lin, S. Yao, and L. Huo, "Dynamical analysis of rumor spreading model with incubation mechanism and activity of nodes," *IEEE Access*, vol. 7, Article ID 152493, 2019.
- [31] A.-L. Barabási and E. Bonabeau, "Scale-free networks," *Scientific American*, vol. 288, no. 5, pp. 60–69, 2003.
- [32] L.-X. Yang, T. Zhang, X. Yang, Y. Wu, and Y. Yan Tang, "Effectiveness analysis of a mixed rumor-quelling strategy," *Journal of the Franklin Institute*, vol. 355, no. 16, pp. 8079–8105, 2018.
- [33] L.-X. Yang, P. Li, X. Yang, Y. Wu, and Y. Y. Tang, "On the competition of two conflicting messages," *Nonlinear Dynamics*, vol. 91, no. 3, pp. 1853–1869, 2018.
- [34] J. Zhao, L.-X. Yang, X. Zhong, X. Yang, Y. Wu, and Y. Y. Tang, "Minimizing the impact of a rumor via isolation and conversion," *Physica A: Statistical Mechanics and Its Applications*, vol. 526, Article ID 120867, 2019.
- [35] L.-X. Yang, P. Li, X. Yang, Y. Xiang, and Y. Y. Tang, "Simultaneous benefit maximization of conflicting opinions: modeling and analysis," *IEEE Systems Journal*, vol. 14, no. 2, pp. 1623–1634, 2020.
- [36] W. J. Stewart, *Probability, Markov Chains, Queues, and Simulation*, Princeton university press, Princeton, NJ, USA, 2009.
- [37] E. Donald, *Pontryagin's minimum principle and state inequality constrains*, pp. 227–239, Dover Publications, New York, USA, 2nd ed edition, 2004.
- [38] H. B. Keller, *Numerical Methods for Two-point Boundary-Value Problems*, Courier Dover Publications, New York, USA, 2018.
- [39] S. Lenhart and J. Workman, "Forward-backward Sweep Method," in *Optimal Control Applied to Biological Models*, pp. 49–56, CRC Press, Boca Raton, USA, 2nd ed. edition, 2007.
- [40] M. McAsey, L. Mou, and W. Han, "Convergence of the forward-backward sweep method in optimal control," *Computational Optimization and Applications*, vol. 53, no. 1, pp. 207–226, 2012.
- [41] S. Lenhart and J. T. Workman, *Optimal Control Applied to Biological Models*, CRC Press, Boca Raton, USA, 2007.
- [42] J. Hoffman and S. Frankel, "The First-Order Euler Method," in *Numerical Methods for Engineers and Scientists*, pp. 352–370, CRC Press, Boca Raton, USA, 2nd ed. edition, 2001.
- [43] J. Butcher, "Runge-kutta Methods," in *Numerical Methods for Ordinary Differential Equations*, pp. 97–108, Wiley, Hoboken, USA, 2nd ed. edition, 2008.
- [44] H. Peng, K. Huang, L.-X. Yang, X. Yang, and Y. Y. Tang, "Dynamic maintenance strategy for word-of-mouth marketing," *IEEE Access*, vol. 8, Article ID 126496, 2020.
- [45] K. Huang, L.-X. Yang, X. Yang, and Y. Y. Tang, "Effective multiplatform advertising policy," *IEEE Transactions on Systems, Man, and Cybernetics: Systems*, pp. 1–11, 2021.
- [46] A. Blaquière, "Impulsive optimal control with finite or infinite time horizon," *Journal of Optimization Theory and Applications*, vol. 46, no. 4, pp. 431–439, 1985.

## Research Article

# Spread of Misinformation in Social Networks: Analysis Based on Weibo Tweets

Han Luo <sup>1</sup>, Meng Cai <sup>1</sup> and Ying Cui <sup>2</sup>

<sup>1</sup>School of Humanities and Social Sciences, Xi'an Jiaotong University, Xi'an 710049, China

<sup>2</sup>School of Mechano-Electronic Engineering, Xidian University, Xi'an 710071, China

Correspondence should be addressed to Meng Cai; [mengcai@mail.xjtu.edu.cn](mailto:mengcai@mail.xjtu.edu.cn)

Received 28 August 2021; Revised 19 November 2021; Accepted 26 November 2021; Published 16 December 2021

Academic Editor: Chenquan Gan

Copyright © 2021 Han Luo et al. This is an open access article distributed under the Creative Commons Attribution License, which permits unrestricted use, distribution, and reproduction in any medium, provided the original work is properly cited.

Social networks are filled with a large amount of misinformation, which often misleads the public to make wrong decisions, stimulates negative public emotions, and poses serious threats to public safety and social order. The spread of misinformation in social networks has also become a widespread concern among scholars. In the study, we took the misinformation spread on social media as the research object and compared it with true information to better understand the characteristics of the spread of misinformation in social networks. This study adopts a deep learning method to perform content analysis and emotion analysis on misinformation dataset and true information dataset and adopts an analytic network process to analyze the differences between misinformation and true information in terms of network diffusion characteristics. The research findings reveal that the spread of misinformation on social media is influenced by content features and different emotions and consequently produces different changes. The related research findings enrich the existing research and make a certain contribution to the governance of misinformation and the maintenance of network order.

## 1. Introduction

Misinformation is an objective social phenomenon that appears in the social operation environment. It usually refers to the information that is widely circulated intentionally or unintentionally without a factual basis and confirmation or clarification [1]. It has been a concern not only in the social sciences such as sociology and journalism [2] but also in computer science and other research fields [3]. With the development of Internet technology and social media platforms, the misinformation spread by word-of-mouth is rapidly spread through social media platforms and has the characteristics of fission diffusion, fast propagation speed, a wide range of influence, and deep impact. A large amount of false information and the spread of rumors and misleading information on social media platforms not only cause public concern and pose a threat to the public's physical and psychological health but also bring serious challenges to the governance and stability of social order [4].

The destructive nature of misinformation has also made the concept of "information epidemic" known to the

public. "Information epidemic" refers to a series of physical and psychological reactions formed by the public when they are faced with misinformation because it is difficult to identify the veracity of the information, and the spread of misinformation infiltrates into everyone's life [5]. For example, during the COVID-19 outbreak, the World Health Organization considered fighting against the "information epidemic" as an important part of its work [6]. With the influence of social media, the "information epidemic" expanded in scope and magnified the threat posed by misinformation. For example, when faced with misinformation, the uncertainty of the future and the lack of access to information will increase the psychological pressure of the public, causing anxiety and panic among the public [7]. At this time, under the influence of rumors and misleading information, the public is very likely to be trapped by the group, amplifying mass panic, triggering collective social crisis, and even leading to various social tragedies [8]. It has been shown that the harm caused by misinformation spread on social media is more serious due to the characteristics of social media such

as fast propagation speed, a wide range of influence, and deep impact. On this basis, it is urgent to understand the propagation process of misinformation on social media and to govern misinformation [9].

In addition, with the convenience of communication and the timeliness of information dissemination, social media often becomes an important communication channel for two-way information exchange. On the one hand, considering the influence of “information cocoon,” weak ties can provide us with more diverse information, based on which social media becomes a better choice for people to communicate. With the help of social media, we can get in touch with people from different regions and industries more easily, and communicate more frequently with people who different from us. Therefore, the public can also learn about relevant situations and specific information about different events in different regions from social media [10]. On the other hand, influenced by the interaction and fusion of massive true information and misinformation on social media platforms, the public is often prone to emotional fluctuations and tends to publish their views and emotions on social media platforms and receive different responses depending on the type, progress, and content of events [11]. At the same time, social networks formed on social media will spread public opinions or emotions and form new communication networks [12].

In recent years, the spread of misinformation on social media platforms has caused public concern, not only because misinformation can easily confuse people, causing them to make wrong decisions, resulting in economic and material losses, but also because misinformation can have an impact on health, medical, and other fields, spreading wrong treatments which even further damages the public’s physical and mental health. At the same time, unconstrained misinformation will lead to social disorder and the prevalence of negative emotions, ultimately causing a huge impact on society. Therefore, it is especially important to understand the spread process and diffusion characteristics of misinformation on social media platforms [13]. Considering this, the study is based on large-scale social media datasets, takes true information and misinformation as the research objects, and conducts correlation analysis on the content and emotion of true information and misinformation for their dissemination. In addition, we use the social network analysis method to further compare the network structure of true information and misinformation in the process of dissemination, expecting to reveal the evolution law of false information to realize the public opinion governance of misinformation and reduce the negative impact brought by misinformation.

The results for the rest of this article are as follows. In the second part, we introduce relevant studies. In the third part, we present the methodology used in the study. In the fourth part, we show the analysis results and discussions, mainly involving the analysis of the content and emotions spread by true information and misinformation on social media. In the fifth part, we present the conclusion of the research and further put forward future ideas for the research.

## 2. Related Research

*2.1. Misinformation in Social Network.* Unverified or unclarified messages are very common on social media, and studies have attempted to conceptualize unverified messages from different perspectives. Common names include “misinformation,” “disinformation,” “fake news,” and “rumor” [14]. Among them, misinformation, disinformation, and fake news all emphasize the false nature of information and describe the object of information that has been falsified. The difference lies in the fact that misinformation often appears in a random form with unknown intention and motivation, and is often used by researchers to describe false information in a broad sense [15]. Disinformation is usually the deliberate tampering of correct information to obtain benefits or advantages and then spread [16]. Similar to disinformation, fake news is used to disseminate false information and stories in the guise of reliable sources for economic or political gain [17]. Rumor is quite different from the previous three concepts. Although a rumor is also unconfirmed information, it need not always be false information, as it can also be correct information in some cases, and the dissemination motivations and intentions of rumor are often unknown [18].

The spread of misinformation on social media has always been an important research topic. But before we can understand why misinformation can spread on social media, we need to have a clearer understanding of the misinformation. One of the reasons why misinformation is concerned as important by researchers lies in the misleading nature of misinformation. Misinformation often misleads the public to make decisions, causes them to form corresponding actions, and generates emotional and psychological fluctuations [19]. At this time, the public forms an adaptive response under the stimulus and influence of misinformation, and tends to interact with the outside world, and then magnifies the scope and degree of the influence of misinformation [20]. On the one hand, misinformation, as an adaptive form of stimulus-response, has a warning function, indicating that the public’s emotions are dictated by external forces in a tense situation. On the other hand, misinformation also reflects the psychological state behind public emotions in the social environment. For example, when a social crisis occurs, the public is more susceptible to the influence of other public emotions under the misdirection of misinformation, forming a large-scale emotion cluster phenomenon, which will then impact the social order and easily cause a negative effect on society [21].

In addition, some studies have analyzed factors that influence the spread of misinformation on social media. Studies have pointed out that true information and misinformation are often mixed and difficult to identify, and misperception of misinformation as true information is the main reason for the public to share and spread misinformation on social media [22]. Social media users tend to support the spread of unverified information on social media but generally do not spread information that has been proven to be false. The problem is that social media users often lack the ability to recognize misinformation before

sharing it [23]. Studies have been conducted to explain the public's deficiency in misinformation recognition on this basis, with related studies mainly focusing on political, psychological, and media literacy perspectives. For example, from the political perspective, it has been argued that the public's political orientation affects the human brain's processing of information, and an identity-based model of political orientation has been proposed to explain how political orientation causes the public to form information bias and thus choose to trust false information [24]. Other studies have combined web browsing data and online survey data to analyze how people share fake news in political elections. The study found that the public's behavioral preferences have a significant impact on the trust in misinformation and that the public is more willing to believe stories about politicians they support, even if the stories are false and full of implausible elements [25]. In the field of psychology, some studies measured the accuracy of respondents' perception of misinformation by conducting the Cognitive Reflection Test (CRT) for the respondents, and it was found that the better the respondents performed in the CRT test, the more likely they were to detect misinformation and the more accurate they were. The findings of the study prove the importance of psychological factors. When the public is more inclined to use analytical thinking rather than lazy thinking when identifying information, they are more likely to recognize the difference between true and false information [26]. Studies have also paired Twitter data with public accounts during elections to analyze the process of spreading fake news, and they found that psychologically conservative people are more likely to be exposed to fake news and less able to spot it. Related studies have confirmed the influence of psychological factors on the identification of misinformation [27]. In the field of media literacy, some scholars believe that the public's general trust in the misinformation spread on social media mainly stems from the lack of digital media literacy. The study has used survey data from the US and India during elections to assess the effectiveness of media literacy campaign interventions, and the findings confirm that digital media literacy plays an important role in the identification of misinformation [28]. Some scholars have conducted empirical studies to evaluate whether individuals with higher media literacy are more capable of identifying fake news and compared different media literacy aspects such as information literacy and news literacy. The results verified the effectiveness of information literacy, which can effectively enhance the public's ability to identify misinformation [29]. These studies also provide references for us to understand the spread of misinformation on social media from multiple perspectives, and help us further understand the reasons why Internet users share and spread misinformation on social media.

*2.2. Misinformation and Content Analysis.* Social media has become an important mode for the public to communicate and obtain relevant information by virtue of its unlimited access. However, due to the lack of online supervision and user anonymity, the line between true information and

misinformation is not always easy to distinguish, which makes the public often face the risk of being misled when accessing relevant information. And, the unique echo chamber design of social media platforms allows people with a common need for information to gather together. Although this facilitates communication among people in the same situation and increases the possibility that the public will have access to the true information they need, it also amplifies the negative impact of misinformation [30]. Moreover, the interaction and fusion of true information and misinformation on social media platforms have also attracted many scholars to study the dissemination of misinformation and conduct quantitative research on it. For example, some scholars extracted Ebola-related tweets from social media and coded them by using professionals with knowledge background to evaluate the proportion of the extracted tweets that contained specific content. It was found that ten percent of the relevant tweets contained misinformation [31]. Another study conducted a content analysis on the misinformation about COVID-19 and found that only thirty-eight percent of the misinformation about COVID-19 on social media platforms was completely fabricated, and most of the misinformation was formed by distorting and falsifying the true information [32]. The relevant findings confirm the current situation of integration and fusion of misinformation and true information on social media, which can help us understand the evolution and diffusion pattern of misinformation on social media.

In addition to using content analysis to distinguish true information from misinformation, relevant studies have also focused on the characteristics of the spread of misinformation on social media, especially how misinformation spreads relative to true information [33]. For example, by examining the differential distribution of large-scale true information and misinformation on social media platforms, a study found that misinformation had the characteristics of faster propagation speed, longer propagation path, and wider propagation range than true information. Moreover, the information content of misinformation was often more novel than true information, so it was more likely to be shared by the public on social media. It was also found that the content of misinformation was more likely to stimulate emotions such as fear, surprise, and disgust than the emotions such as anticipation, sadness, and joy evoked by true information [34]. Some studies also pointed out that the misinformation can be spread more quickly when the content of misinformation was related to major public crisis events. For example, during COVID-19 in 2019, the amount of misinformation exploded and spread worldwide in a very short spread. According to relevant agencies, during the spread of the epidemic, about 46,000 instances of epidemic-related misinformation were spread on social media every day and spread rapidly with retweets from Internet users [35]. In addition to these studies, some scholars have also tried to understand the sources and evolutionary patterns of misinformation by means of content analysis. Based on the analysis of massive amounts of Twitter data, it was found that most of the misinformation on social media was generated by general accounts, but the content often contained

links to websites that lacked credible sources. It was also found that the spread of misinformation on social media was a dynamic process in which the content undergoes dynamic changes, i.e., it was constantly modified by network users to spread at the next step in the process of spreading [36].

The content analysis method based on misinformation is important. On the one hand, misinformation content conveys bias and misunderstanding which may affect the public's trust in experts, institutions, and governments, leading to the spread of unnecessary fear and suspicion. For example, studies have pointed out that the majority of the public relies on online comments to evaluate and judge enterprises and institutions, and maintains their trust in relevant institutions under the influence of online comments. However, online comments containing misinformation can exacerbate public prejudice and misunderstanding [37]. On the other hand, misinformation can also reverse the public's behavioral response to natural disasters, accidents, public health, and social security emergencies. For example, studies have pointed out that with the development of the Internet, social media has become an important channel for the public to seek health information. However, the authenticity of health information will significantly affect the treatment of patients and threaten their lives [38]. Therefore, the content analysis method is used to analyze the misinformation on social media to understand the content characteristics of the misinformation. It is not only beneficial to identify misinformation on social media, but it also can contribute to the governance of misinformation and the maintenance of network security.

*2.3. Misinformation and Emotion Analysis.* The spread of misinformation on social media implies different emotions of the public, and the emotions also change with the spread of misinformation. On the one hand, in addition to the influence of specific social conditions, the psychological state is an important factor in the production of misinformation, which is formed as an additional product of public events under the adaptive condition of public emotions [39]. On the other hand, emotions also play an important role in spreading misinformation on social media. It is because they can meet some psychological needs of the public that misinformation keeps forming and spreading on social media. Related studies point out that the spread of misinformation is inseparable from emotions, and misinformation can spread rapidly when a group falls into negative emotions such as anxiety [40]. Therefore, it is particularly important to analyze the misinformation on social media based on emotion analysis.

Among the research on misinformation using the emotion analysis method, exploring the influencing factors of emotion changes in misinformation is an important object of research. For example, some researchers explored the factors influencing the emotional dynamics in misinformation by quantitatively analyzing the emotional behaviors of Internet users on social media. Studies have found that misinformation contains far more negative emotions

than other kinds of information, while factors such as user engagement, number of comments, and time of discussion all had an impact on the change of emotions in misinformation. Generally, the more active the users are, the more comments they make, the longer the discussion takes, and the more dominant negative emotions become [41]. Studies have also been conducted to study misinformation active on social media during public crises as the research object and to identify emotions of Internet users in relation to comments under the misinformation. It was found that both the gender of Internet users and the subject category of the content had an impact on the change in emotions [42]. Some studies conducted sentiment analysis on popular misinformation on social media based on content analysis methods and found that as the content, form, and linguistics of misinformation changed, so did the public's sentiment. In general, the more conflicting the content of the misinformation, the more attractive the font (e.g., colorful fonts are more attractive than regular fonts), and the more exaggerated and extreme the use of language, the more intense the change in public sentiment would be [43].

In addition to analyzing the influencing factors of emotions, it is also an important topic to understand the evolution pattern of emotions triggered by misinformation on social media. On the one hand, social media exists as a disseminator of misinformation, and when the public has emotional fluctuations under the influence of misinformation, social media often magnifies the impact of emotions and makes emotions spread rapidly in social networks. On the other hand, the spread of emotions on social media often exists in some regular form. By analyzing a certain amount of text data, we can try to reveal the evolution law of emotions on social media. For example, a study combined with network science to analyze the sentiment of misinformation about the political election in Twitter, and found that posts with negative sentiments last longer than those with positive or neutral sentiments. At the same time, misinformation about the election winners had a broader diffusion network in the social media, and more positive sentiments representing likes and support among them [44]. Some studies used big data-driven approaches to conduct sentiment analysis on the "viral" spread of false and true information about natural disasters on social media based on massive data. The study found that tweets with negative emotions spread faster than tweets with positive or neutral emotions. It was also found that emotions had an opposite effect on the "viral" spread of true and false information on social media [45]. Based on data from social media chat platforms, some studies have also attempted to map the trends in public sentiments over time related to misinformation. The study not only confirmed that the proportion of negative emotions triggered by misinformation was more than positive emotions but also found that negative emotions were affected by event information in an inverted U-shaped curve over time. When event information was further revealed, when handling measures and coping methods were introduced or falsified information appears, the proportion of negative emotions caused by misinformation would decrease and the negative emotions brought by misinformation would be weakened [46].

To sum up, the active misinformation on social media brings mainly negative emotions, which not only affects the public's psychology and behavior and increases the difficulty of network public opinion governance but also has an impact on the stability of social order and the maintenance of social security. Therefore, combining with network analysis methods, and analyzing the law of spreading emotions of misinformation in social networks is not only beneficial to provide suggestions for emotion management when online public opinions occur but also to better achieve guidance and prevention and control of online public opinions, and thus eliminate the negative effects brought about by the changes in group emotions.

### 3. Research Methods

This paper selects misinformation as the research object and compares the network structure of misinformation and true information on social media to better reveal the diffusion and evolution law of misinformation on social media, and provides a reference for the public opinion management of misinformation. The frame structure diagram of the study is shown in Figure 1. Firstly, we obtained misinformation, true information, and the corresponding public opinion datasets on social media, and completed the data pretreatment. Secondly, we combined deep learning methods to conduct content analysis and emotion analysis on misinformation and true information data and tried to compare the diffusion patterns of misinformation and true information on social media using network analysis methods. Finally, we drew a correlation graph to show the disturbance of misinformation and true information on the network structure and revealed the evolution pattern of misinformation and true information in the network.

*3.1. Network Analysis Method.* As a research method for analyzing interpersonal relationships, the network analysis method has been widely used in various disciplines. One of the most typical and well-known network analysis methods belongs to the social network analysis method, which is a combination of methods and tools for studying interpersonal relationships, interactions, and communication, and has been adopted by a large number of researchers and research fields [47]. In the social network analysis method, we describe the relationships between people in the social network through the concepts of nodes and edges. Nodes which are defined as individuals or groups are connected in a certain direction by the edge representing the relationship to form a social network graph [48]. With the social network analysis method, we can understand the sparse relationship between participants in social networks. At the same time, we are able to analyze the importance of the location of participants in the social network by measuring network centrality and identifying important and isolated participants in the network [49]. In short, the social network analysis method is able to analyze not only the breadth (scope) but also the depth of the relationship between participants, providing support for exploring the interpersonal interaction and the degree of communication.

With the development of network technology, the online social network formed on the basis of social media has become an important part of interpersonal activities. Compared with traditional social networks, online social networks are characterized by higher participation, larger network scale, faster changes in network structure, and wider network influence [50]. At the same time, the online social network has a rapid growth rate, and has penetrated people's daily lives, and provides everyone with a convenient way to communicate. Unlike traditional social network analysis methods, online social network analysis methods mainly focus on the flow and dissemination of information on social media and have become an important research method in the field of machine learning, data mining, and complex network systems with the support of massive social media data [51, 52]. In the analysis process of online social network analysis methods, on the one hand, social media users act as individual nodes of the network, and the forwarding of information among users constitutes a propagation relationship, and the network structure is shown by visual methods. On the other hand, relevant information continues to evolve and spread in social networks through user interactions such as comments, favorites, and reposts. Through the online social network analysis method, we can not only analyze the structure of communication and interaction among network users but also explore the propagation evolution pattern of a certain event with the support of social media data. Therefore, we use the network analysis method to analyze the propagation pattern of misinformation on social media.

In this paper, we used the network users involved in the spread of misinformation as nodes and the forwarding relationship between users as edges to map out the network structure of misinformation. In addition, in combination with the content analysis method and emotion analysis method, we analyzed the network diffusion characteristics of misinformation, such as the number of reposts, favorites, and comments of misinformation, and then explored the evolution pattern of misinformation in social networks. At the same time, considering that only misinformation was not enough to investigate the evolution of misinformation on social media, we also selected the corresponding true information as the comparison object. Through the comparison of the spread of misinformation and true information on social media, we can gain an insight into the evolutionary diffusion characteristics of misinformation on social media.

*3.2. Content Analysis Method.* In this paper, we used the content analysis method to analyze the data and summarize the topics of misinformation and true information. Firstly, after data preprocessing, to reduce noise interference and the need for further filtering the data in this paper, we used the TF-IDF method to extract text keywords based on the importance of the words. According to the frequency of words in the text and corpus, we extracted 20 keywords most important in the text using the TF-IDF method based on the weighted processing.

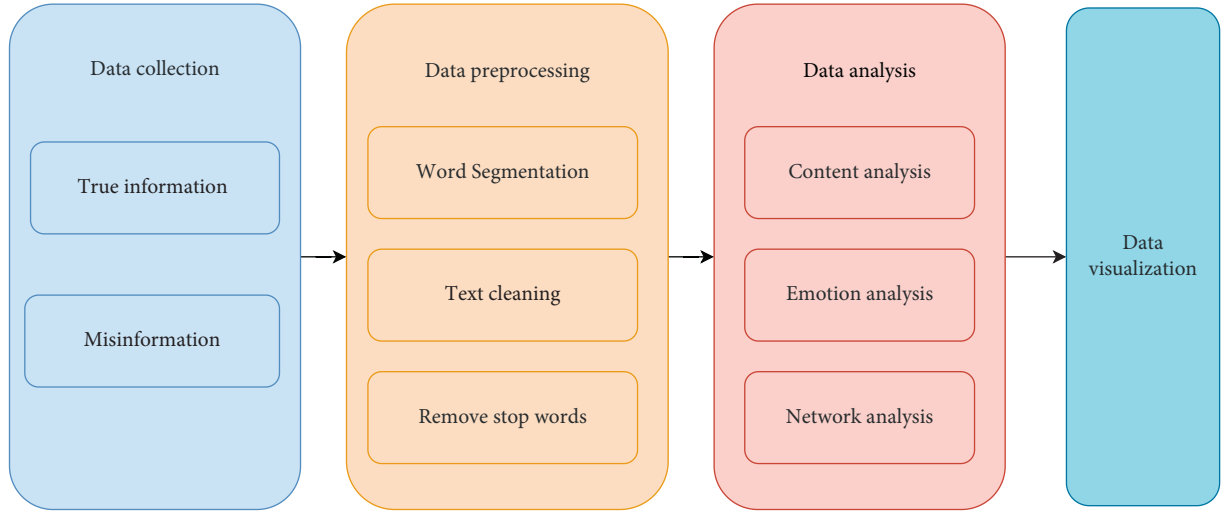


FIGURE 1: Research frame diagram.

Secondly, we need to extract semantic features according to the meaning of words in the language environment and the relationship with other words and then transform semantic features into feature vectors. In general, discrete representation and distributed representation are commonly used for word representation in the computer. The difference is that the former represents each word as a long vector, while the latter represents each word as a dense continuous vector of fixed length. Compared with the former, the latter can not only save the vector space but also better represent the relationship between words. Therefore, in existing studies, distributed representation has often been adopted by researchers to represent word vectors [53]. In this study, we used the Word2vec method introduced by Google to convert text data into word vectors and mapped text content into vector space to calculate the similarity between words [54]. The Word2vec model is mainly composed of the Continuous Bag-of-Words model, which predicts the current word based on the upper and lower words, and the Continuous Skip-gram model, which predicts the context word based on the current word. In the analysis of large sample datasets, the effectiveness of the CBOW model in text analysis has been confirmed by previous studies. Compared with the Skip-gram model, the CBOW model has greater advantages in analysis efficiency and analysis speed [55]. Therefore, we used the CBOW model to complete the training of word vectors and convert text data into word vectors.

Finally, we analyzed the topics of misinformation and true information based on the K-means clustering method. By using the K-means method, the study divided the processed sample set into K categories and tried to minimize the distance between samples in each category and maximize the distance between categories, which in turn could be achieved based on setting the clustering category as  $\omega_1, \omega_2, \omega_3, \dots, \omega_k$ . The calculation process of the least square error is shown in equation (1). The minimum squared error is denoted by  $\beta$ , and the different clustering categories are denoted by  $\omega_n$ . The documents and mean vectors in the clustering category are represented by  $w$  and  $\varphi_n$ , respectively.

$$\beta = \sum_{n=1}^k \sum_{w \in \omega_n} \|w - \varphi_n\|^2. \quad (1)$$

As a common unsupervised clustering method, K-means mainly achieves the classification of different categories through similarity, where K and means, respectively, represent the number of clustering categories and the mean value of clustering vectors. A common method used to measure the size of K is the Elbow method, and the distance is measured by the cosine distance or Euclidean distance formula [56]. Using the Elbow method, we selected different K values to cluster the sample set and calculated the square sum of the error between the document vector and the clustering mean vector, based on which the curve of the sum of the square error is plotted. By observing the comprehensive curve of the square error, we could find that the square error varies with the value of K. Accordingly, we could infer the appropriate value size of K, and then classify the misinformation and true information topics into K categories.

**3.3. Sentiment Analysis Methods.** With the expansion of social network corpora built on social media platforms, sentiment analysis has become an important research field in natural language processing and text mining. Sentiment identification and analysis of comments, opinions, and other texts in the social network corpus through sentiment analysis not only provide data support for our understanding of the dissemination pattern of information on social media and the change of public sentiment but also enable further explanation of the behavior logic behind social networks of Internet users [57]. At present, common sentiment analysis methods are mainly divided into two categories. One is by building sentiment dictionaries and combining semantics to compare the similarity between the text keywords in the sample data and the sentiment words in the dictionary and then calculating the sentiment intensity of the text keywords to assign the corresponding sentiment



labels to the text [58]. The other is to use machine learning methods such as SVM, Naive Bayes, or deep learning methods based on neural networks to conduct bias analysis of sentiments in a supervised way and assign corresponding sentiment labels to texts [59]. However, in the sentiment analysis based on the sentence types of social media platforms, the approach based on sentiment dictionaries often has an impact on the final sentiment classification results due to the neglect of context. Therefore, machine learning and deep learning methods are often used in sentiment analysis of social network data. However, taking sentiment analysis as an example, SVM, CRF, and other machine learning methods excessively rely on manual labeling data and have limitations in processing natural data in the original form. Deep learning methods combine simple but nonlinear modules to learn complex functions and the self-learning feature of deep learning greatly improves its application ability in the field of natural language and shows better effect in sentiment analysis [60, 61].

In sentiment analysis of sentence-level objects, long- and short-term memory models that can learn word vectors of different lengths have shown better performance in sentiment classification and have been widely used by researchers [62]. As a result of the further development of the recurrent neural network, the LSTM model retains the flexibility of recurrent neural networks in learning contextual information of text sequences and addresses the difficulty of traditional recurrent neural networks in storing information for long periods of time. Similarly, the LSTM model remains structurally consistent with recurrent neural networks, but the internal structure is composed of the cell circulation state  $C$ , input gate  $I$ , forgetting gate  $F$ , output gate  $O$ , and hidden state output  $\theta$ , which differs from that of the recurrent neural network. Among them, the final output of the model is completed by tan transformation of the current state. The calculation process is shown in Equation 2, where  $\theta_T$  represents the output of the hidden state at time  $T$ , and  $O_T$  and  $C_T$ , respectively, represent the state of the model output gate cell unit at time  $T$ .

$$\theta_T = O_T * \tan\theta(C_T). \quad (2)$$

The output gate of the model determines what should be output by calculating the sigmoid layer, and the calculation process is shown in equation (3), where  $O_T$  denotes the state of the output gate at the moment of  $T$ ,  $\theta_{T-1}$  denotes the output state at the previous moment,  $\varphi_T$  denotes the input state of the information at the current moment,  $\omega_O$  and  $b_O$  denote the weight and deviation of the output gate, and the activation function is denoted by  $\sigma$ .

$$O_T = \sigma(\omega_O\theta_{T-1} + \omega_O\varphi_T + b_O). \quad (3)$$

As an important stage of model operation, the cell renewal is an intermediate stage in which input information passes through the input gate, the forgetting gate, and finally enters the output gate. The cell state update is updated as shown in equation (4),  $C_T$ ,  $F_T$ , and  $I_T$  denote the state of the cell unit, the forgetting gate, and the output gate at the moment of  $T$ , respectively, and the weights and deviations are denoted by  $\omega_C$  and  $b_C$ .

$$C_T = F_T * C_{T-1} + I_T * \tan\theta(\omega_C\theta_{T-1} + \omega_C\varphi_T + b_C). \quad (4)$$

The forgetting gate determines what information should be discarded and the calculation process is shown in equation (5), where  $\sigma$  denotes the activation function,  $\omega_F$  and  $b_F$  denote the weights and biases of the forgetting gate, respectively.

$$F_T = \sigma(\omega_F\theta_{T-1} + \omega_F\varphi_T + b_F). \quad (5)$$

The main work of the input gate in the model structure is to decide which information should be input, as shown in equation (6). In this case, the weight and deviation of the input gate are denoted by  $\omega_I$  and  $b_I$ , respectively.

$$I_T = \sigma(\omega_I\theta_{T-1} + \omega_I\varphi_T + b_I). \quad (6)$$

Although the LSTM model performs well in processing the input context sequence in this paper, the model also has some shortcomings in that it cannot consider the direction of input and can only process text sequence context in one direction. Therefore, we adopted a bidirectional long- and short-term memory model, which can process text sequences from left to right and from right to left by two parallel long- and short-term memory models. Compared with the long- and short-term memory model, the bidirectional long- and short-term memory model can obtain past and future information and concatenate the hidden states in the backward and backward directions, and output contextual information through the same output layer. It not only improves the scope of text processing but also improves the efficiency of text processing. The calculation process of the final output  $Z$  of the model is shown in the following equation:

$$Z_T = \omega_Z\theta_T + b_Z. \quad (7)$$

In this paper, we used the training and test sets from the NLP&CC dataset, and the emotion labels in the dataset were “like,” “surprise,” “disgust,” “sadness,” “happiness,” “anger,” and “fear,” respectively [63, 64]. In our study, we used a bidirectional LSTM model to assign emotion labels to text data. The test accuracy of the model met our research needs and was expressed as 0.71. Meanwhile, to further improve the accuracy and efficiency of the model emotion, we randomly grabbed 200,000 Weibo tweets for pre-training. Based on the pre-training, we implemented the analysis of both misinformation and true information datasets. Finally, we assigned emotion tags to each Weibo tweet in the misinformation dataset and the true information dataset to study the pattern of emotional evolution in social networks.

## 4. Results and Discussion

**4.1. Data Collection and Preprocessing.** In this paper, we chose the large open-source dataset of the Sina Weibo platform as our analysis object [65]. As one of the most popular social media platforms in China, Sina Weibo has about 530 million active users and has established a huge online social network, which also provides rich data sources to investigate the spread of misinformation in social

networks. Datasets are open-source datasets from 2015 and 2016, mainly composed of misinformation and true information datasets. We obtained the relevant content and forwarding information of each original microblog in the dataset and constructed the dissemination network of misinformation and true information on social media. Among them, the misinformation in the microblog dataset came from the information that has been falsified by the Sina Community Management Center. At the same time, the dataset also collected a similar amount of true information for comparative studies. True information and misinformation were present at the same time, which attracted extensive public attention and the content had been proved to be true. The details of the misinformation dataset and the true information dataset are shown in Table 1.

Table 1 shows the statistics of the dataset. Among them, there were 2351 true information tweets and 1717154 retweets. The original Weibo tweets were retweeted 52,158 times at most and 12 times at least, with an average of 730 retweets. The number of misinformation tweets was 2313, and the number of retweets was 2093056. The original Weibo tweets were retweeted 59,319 times at most, 11 times at least, and 905 times on average.

*4.2. Network Structure of Misinformation.* Through the microblog ID and forwarding relationship in the dataset, we can understand the diffusion of true information and misinformation in the social network. Meanwhile, based on the Mid of microblog, we obtained the secondary and tertiary forwarding information of some true information and misinformation in the process of forwarding, so as to construct the dissemination network of true information and misinformation on social media. Based on this, we used the Fruchterman Reingold layout to draw the graph of the forwarding network. The spread graph of true information and misinformation on social media is shown in Figure 2.

In Figure 2, we can observe the network built by true information and misinformation on social media. Considering the limitation of space, we randomly selected and showed the spread of some true information and misinformation on social media. Among them, Figure 2(a) shows the forwarding network built by true information and misinformation on social media, with the purple node representing misinformation events and network users who forward misinformation, and the green node representing true information events and network users who forward true information. Figures 2(b) and 2(c) show the network diffusion structures of misinformation and true information, respectively.

Firstly, in the network graph composed of misinformation and true information, the network structure of true information or misinformation is sparse, the number of edges is much smaller than the number of nodes, and there are many isolated nodes. This may be related to the nature of the content of the dataset. The dataset we adopted consists of different misinformation events and true information events, and the connection between the events is not very close. Although there are crossover relationships between

some events, most of them are differentiated and exist in an isolated form during the forwarding process. Combined with text materials, most of the related events in the original data collected were related to the topic. For example, when referring to food safety events, users often enumerate previous similar events for comparative analysis, which was also an important reason for the network connection between different events. Secondly, in the dataset adopted in this paper, although the number of events of misinformation is smaller than that of true information, the forwarding relationship of misinformation is much more than that of true information. It can also be intuitively observed from Figure 2 that the network graph of misinformation is denser and the nodes are more closely connected to each other than the network graph of true information. Compared with true information, misinformation has more advantages in both the scope and depth of diffusion and is more likely to attract the attention of the public and be spread by the public in social networks. Combined with text materials, misinformation in social networks often exists with exaggerated titles and contents, which are more likely to be noticed and retweeted by the public. This also tentatively confirms the conclusion of existing studies that misinformation is more likely to be disseminated on social media than true information.

*4.3. Topic Categories of Misinformation and True Information.* Based on the obtained dataset of misinformation and true information, we divided the data into seven categories by using the clustering method and determined the topic tag and interpretation content of each category in conjunction with the information content. However, considering the information content embedded in the event microblog was not always easy to distinguish, there are often situations involving multiple topics. Therefore, researchers extracted the top keywords of each topic and matched the extracted keywords with the text information of the event microblog. If the text information of the event microblog conforms to multiple keywords, the Weibo tweet would be given the corresponding topic tag, while the microblog that did not match the keyword would be given the corresponding topic tag according to the content by manual annotation. The topic categories for true information and misinformation are shown in Table 2.

It can be observed from Table 2 that the distribution of the number of microblogs is in an unbalanced state among the seven topics divided into true information and misinformation. Firstly, both true information and misinformation microblog posts are distributed in the largest number in the field of food and product safety. Food and product safety involves everyone's daily life, so it is most likely to breed misinformation and true information. Existing studies have also revealed the causes of misinformation and true information related to food and product safety from multiple perspectives such as education level, gender, age, and media reports [66].

Secondly, true information and misinformation are distributed in public safety and crime topics only second to

TABLE 1: Descriptive analysis of the dataset.

Descriptive analysis	True information	Misinformation
Tweets (i.e., original posts by Sina Weibo users)	2351	2313
Retweets (i.e., reposted messages by Sina Weibo users)	1717264	2093056
Maximum forwarding relationship	52158	59319
Minimum forwarding relationship	12	11
Average forwarding relationship	730	905

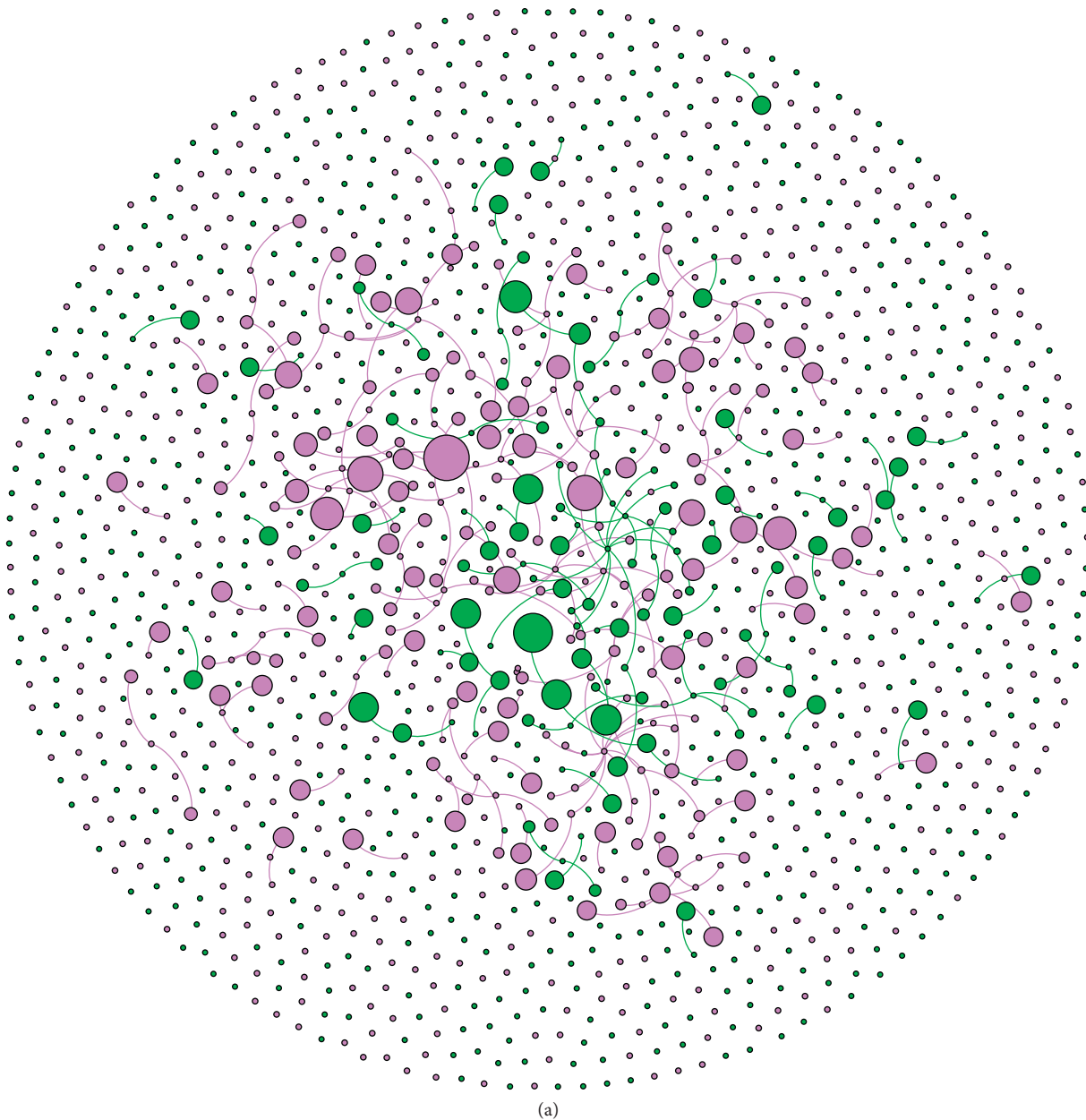
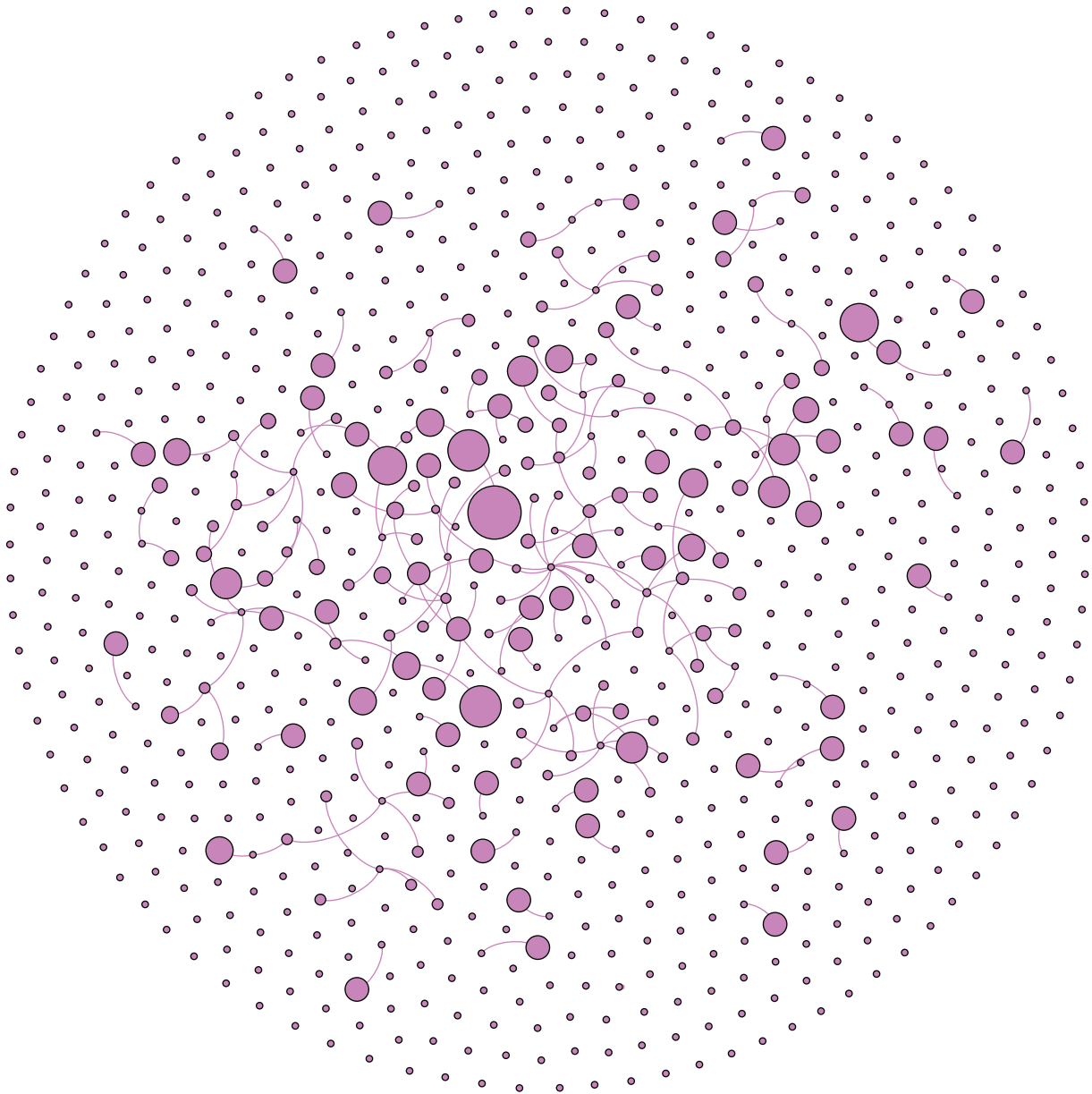


FIGURE 2: Continued.



(b)

FIGURE 2: Continued.

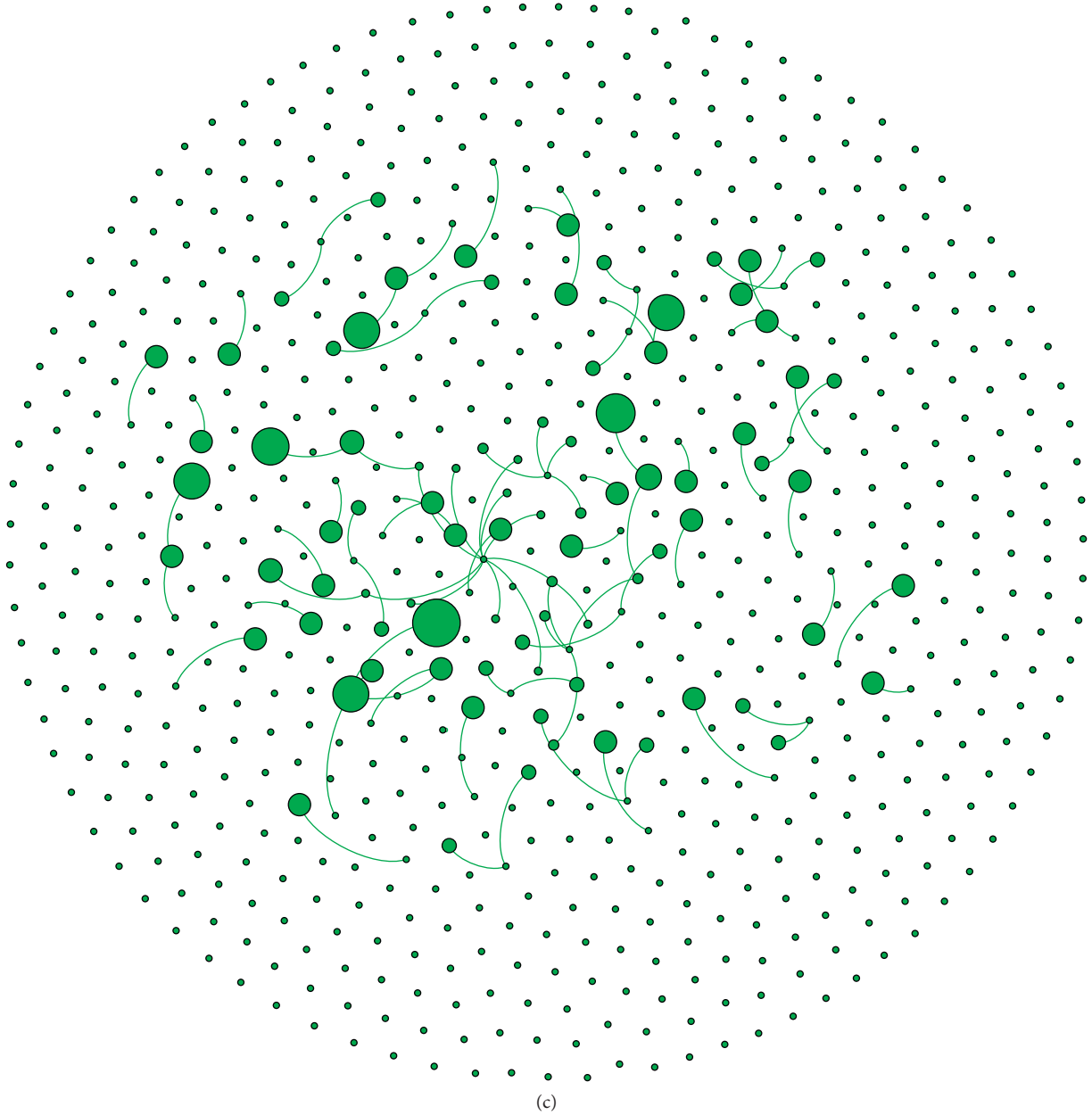


FIGURE 2: An illustration of the forwarding network. In the figure, the node represents the microblog ID and the edge represents the forwarding relationship between the microblogs. (a) True information and misinformation. (b) Misinformation. (c) True information.

TABLE 2: Topic categories of true information and misinformation.

Topic type	Topic content	True information	Misinformation
Public security	Information related to public safety and social security incidents	145	259
Food and product	Related to the safety of the diet or certain type of product	1618	1430
Politics	Information related to political events, politicians, or major policies	74	87
Celebrity	Celebrity information such as anecdotes	26	9
Crime	Information related to criminal events and people	269	358
Disaster	Information related to natural disasters or accidents	79	49
Social events	Involving a strong social response, biased towards folk tales	78	84

food and product safety areas. The difference between the public safety theme and the crime theme lies in that the former has a wider scope, involving national security, social

security, and personal security, while the latter is mainly for acts that violate the law generated by individuals or small groups. The reason why the two topics rank high in terms of

the number of topic distribution is not only because such incidents are most likely to trigger public anger, sympathy, and other emotions but also because related events are easy to be favored and extensively reported by the media. Therefore, both true information and misinformation have a large number of microblogs in public safety and crime topics.

The political topic mainly involves information about political events, politicians, and major policies. On the one hand, the public tends to pay more attention to politics and is keen on discussing and paying attention to events and information related to politics. On the other hand, it is also because the major policies issued by the government often affect every field of society and everyone's life. However, there are also some individuals or groups who misinterpret policies for personal gain, allowing misinformation to spread.

The disaster topic mainly involves natural disasters and accidents that cause economic and property losses to the public and threaten the safety of the public. When natural disasters or accidents occur, social media, as a convenient way of communication, becomes an important platform for the public to share disaster information and seek help. Therefore, there often is a wide public discussion under related topics. However, social media's weak falsification capabilities have also led to the widespread dissemination of misinformation about events such as natural disasters and accidents. For example, disaster-related information is often distorted on social media by exaggerating the number of people, distorting the real situation of events, conspiracy theories, and other ways.

Social events and celebrity topics are more targeted, with the former mainly targeting events that arouse social responses and discussions and concerns about the public, and the latter mainly responding to celebrities and other celebrity-related events. However, these two types of events tend to cover only some groups; for example, the former is more geographically differentiated, the latter is more distinguished by demographic attributes such as fans. The distribution of true information and misinformation is less compared to other topics.

*4.4. Diffusion Characteristics of Misinformation and True Information.* To further compare the evolution pattern of misinformation and true information in social networks and understand the diffusion characteristics of misinformation and true information, we tracked the forwarding relationship of each original microblog and measured the diffusion characteristics of datasets of misinformation events and true information events by using the three indicators: the number of retweets, number of comments, and number of favorites of microblog. The number of retweets mainly refers to the accumulation of the diffusion index of posts in social networks constructed by social media, which measures the diffusion degree of microblog posts. The number of comments refers to the accumulation of user interaction index for posts in the social network, which measures user engagement of microblog posts. The number of favorites

mainly refers to the accumulation of the number of times that posts are collected by users in social networks and measures the user acceptance and recognition degree of microblog posts. The three indicators involve several diffusion characteristics, such as the diffusion range, diffusion participation, user acceptance, etc., which can give us a more comprehensive understanding of the diffusion patterns of misinformation and true information in social networks. Table 3 shows the difference between true information and misinformation in the number of retweets, favorites, and comments on the microblog.

It can be observed from Table 3 that each true information event is forwarded about 924 times (SD 2706.101). Among them, a maximum of one true information was forwarded 81,776 times, and at least one true information was forwarded 30 times. From the point of view of the number of favorites, the average of each true information was about 648 times (SD 1961.269), true information was saved 40,873 times at most, and at least one was not saved. In terms of the number of comments, there were about 387 comments (SD 1061.163) on average for each true information event on Weibo, with a maximum number of 26,275 comments and a minimum number of no comments. Skewness and kurtosis represent the asymmetry and steepness of variables, respectively. Through the observation of skewness and kurtosis, we found that the number of retweets, favorites, and comments of true information was all rightward and steeper, with a sharp peak. Among them, the rightward deviation and peak degree of the forwarding number was the deepest.

Based on the data in Table 3, we also found that each misinformation was forwarded about 2138 times (SD 6299.091), with the maximum number of forwards being 103682 and the minimum number of forwards being 88. In terms of the number of favorites, each misinformation was saved 521 times (SD 2308.874) on average, with the maximum number of favorites being 48889 times and the minimum number of favorites being 0 times. In terms of the number of comments, there were about 540 comments (SD 2261.956) for each misinformation on average, with the maximum number of comments being 38,103, and the minimum number of comments being 0. In terms of skewness and kurtosis, the number of forwards, favorites, and comments of misinformation all showed rightward deviation and peak state. Among them, the spikes of the number of collections were the most obvious, and the right skew of the number of comments was deeper.

At the same time, we also took the independent sample *T*-test to further compare the difference in diffusion characteristics between true information and the misinformation. The results showed that there were significant differences between true information and misinformation in the number of retweets, favorites, and comments ( $P < 0.01$ ), and the mean value of the number of retweets and comments of misinformation was greater than the mean value of the true information, which means that the spread feature of misinformation would have been easier to be spread on social media had it been further verified. Compared with the true information, the public was more inclined to interact

TABLE 3: Diffusion characteristics of true information and misinformation.

	Retweets		Favorites		Comments	
	<i>T</i>	<i>M</i>	<i>T</i>	<i>M</i>	<i>T</i>	<i>M</i>
Mean	923.78	2138.09	648.23	521.28	386.97	540.36
Std. deviation	2706.101	6299.091	1961.269	2308.874	1061.163	2261.956
Maximum	81776	103682	40873	48889	26275	38103
Minimum	30	88	0	0	0	0
Skewness	17.022	7.913	8.716	10.581	10.751	11.033
Kurtosis	421.234	86.120	113.224	153.908	188.846	145.921
<i>T</i> value	-9.750**		16.139**		-1.816**	

Note. \*\* $P < 0.01$ , *T* denotes true information, and *M* denotes misinformation.

and communicate around the misinformation in the social network, and it was more likely to forward and spread the misinformation, which makes the misinformation spread rapidly in the social network. At the same time, we also found that the number of true information events was greater than that of misinformation, which means that despite the rapid spread of misinformation on social media, people had higher levels of recognition and support for true information. Combined with text materials, this was related to the content characteristics of true information. True information usually contained more knowledge and had more detailed arguments, and was more likely to be collected by network users. As for misinformation, on the one hand, it often attracted users' attention through exaggerated titles, and then was retweeted by Internet users. On the other hand, with the help of misleading and controversial content, users often argued with each other, resulting in a large number of comments under misinformation posts. However, as misinformation can be easily proved to be forged and the polarizing debate also made users tend not to collect posts, the number of misinformation collected was smaller than that of true information.

In addition, we used the General Linear Model (GLM) to examine the differences in diffusion characteristics between different categories of topics in true information and misinformation based on setting the number of original Weibo users' followers as the control variable. GLM allows for multivariate analysis of variance and is often used to compare differences in means between two or more variables. First of all, we established the model according to the research needs and decided the model to be a univariate or multivariate analysis of variance. The difference between the two lies in the number of dependent variables. Secondly, we estimated the model through the test and got the value of the model test. And, we used statistical inference to calculate significance and values. Finally, after obtaining significant values, the meaning of the relationship needed to be explained. GLM statistics showed a significant interaction between information veracity and topic category ( $F = 2.264$ , Wilks' Lambda = 0.991,  $P < 0.01$ ). The marginal estimates and confidence intervals on the number of retweets for true information and misinformation on different topic categories are shown in Figure 3. The marginal estimates and confidence intervals on the number of favorites are shown in Figure 4. The marginal estimates and confidence intervals for the number of comments are shown in Figure 5. At the same

time, to further conform to the normal distribution hypothesis, we carried out the logarithmic transformation on the number of retweets, the number of favorites, and the number of comments.

Combining marginal estimates and significance tests, we analyzed the diffusion characteristics of true information and misinformation in each topic category. For the topic categories of public security and politics, the estimated mean value showed that the diffusion index of misinformation in retweets and comments was higher than those of true information, and the diffusion index in favorites was lower than that of true information. However, there was a significant difference between misinformation and true information only for favorites. For the topic category of food and product, the diffusion index of misinformation in retweets and comments was also higher than that of true information, and smaller than that of true information in favorites, and there was a significant difference between misinformation and true information in all the three aspects. For the topic category of celebrity, there was no significant difference between misinformation and true information in the number of retweets, favorites, and comments, which may be related to the small sample size of the topic category of celebrity. For the topic category of crime, there was a significant difference between misinformation and true information in the number of retweets and favorites, and in the diffusion index of retweets, misinformation was larger than true information. In the diffusion index of the favorites, misinformation was less than true information. For the topic category of disaster, misinformation was larger than true information in the diffusion indexes of retweets and favorites, and there was a significant difference, which may be related to the occurrence of disaster information often accompanied by information of first aid measures. As for the topic category of social events, contrary to the previous topic categories, the diffusion index of misinformation was smaller than that of true information in both retweets and favorites, and there was a significant difference, which may be related to the fact that the true information of social events was easier to be identified, and it was more likely to arouse the emotions of Internet users.

To sum up, we further confirmed that in social networks, misinformation spread faster than true information in most cases, and was more likely to be forwarded and spread by network users. In terms of user participation represented by comments, misinformation was also in an advantageous

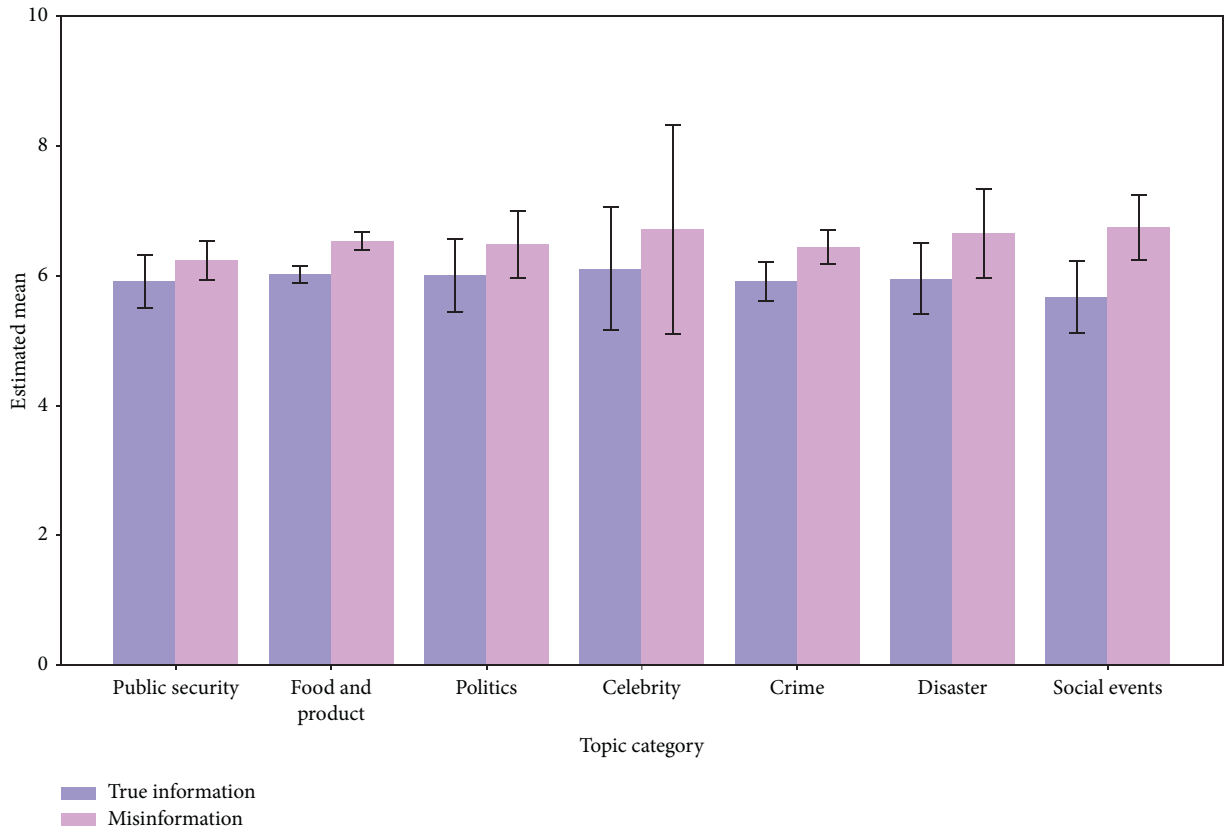


FIGURE 3: Estimated diffusion characteristics of true information and misinformation based on the topic category by the number of retweets.

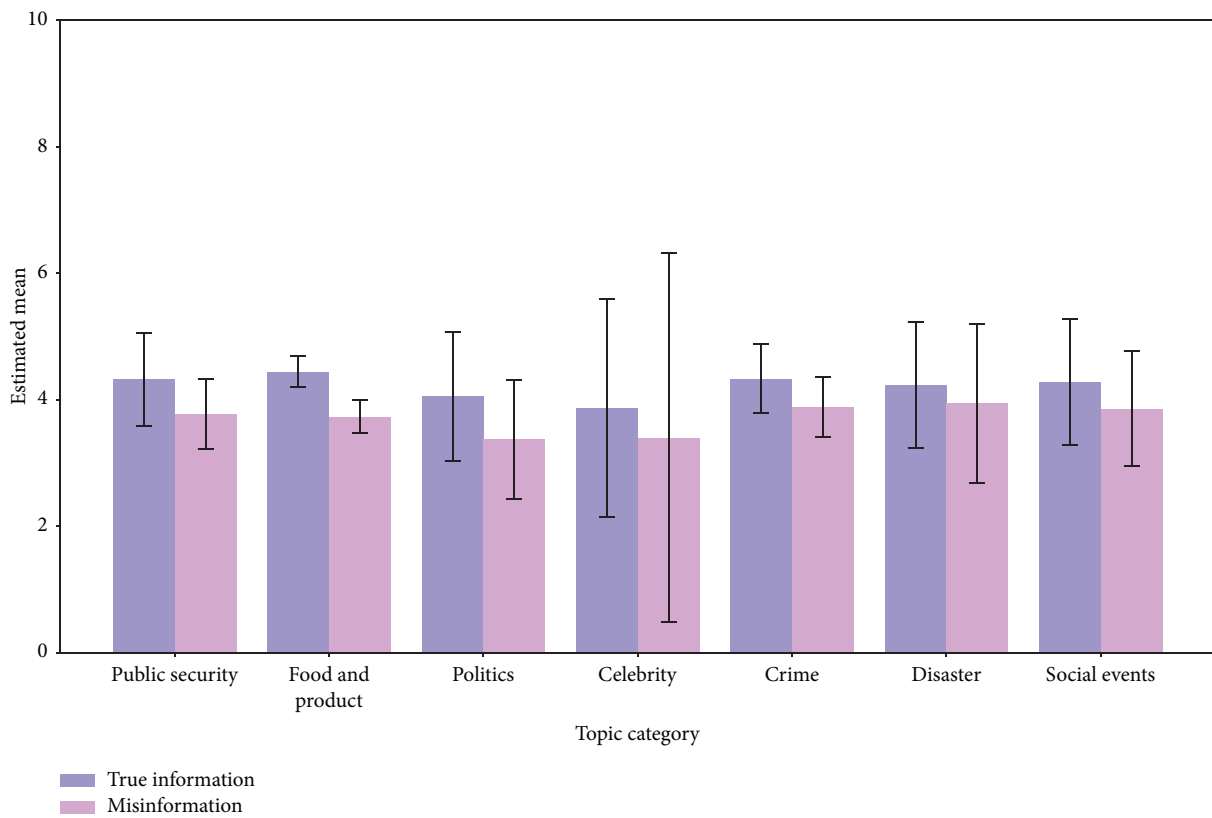


FIGURE 4: Estimated diffusion characteristics of true information and misinformation based on the topic category by the number of favorites.



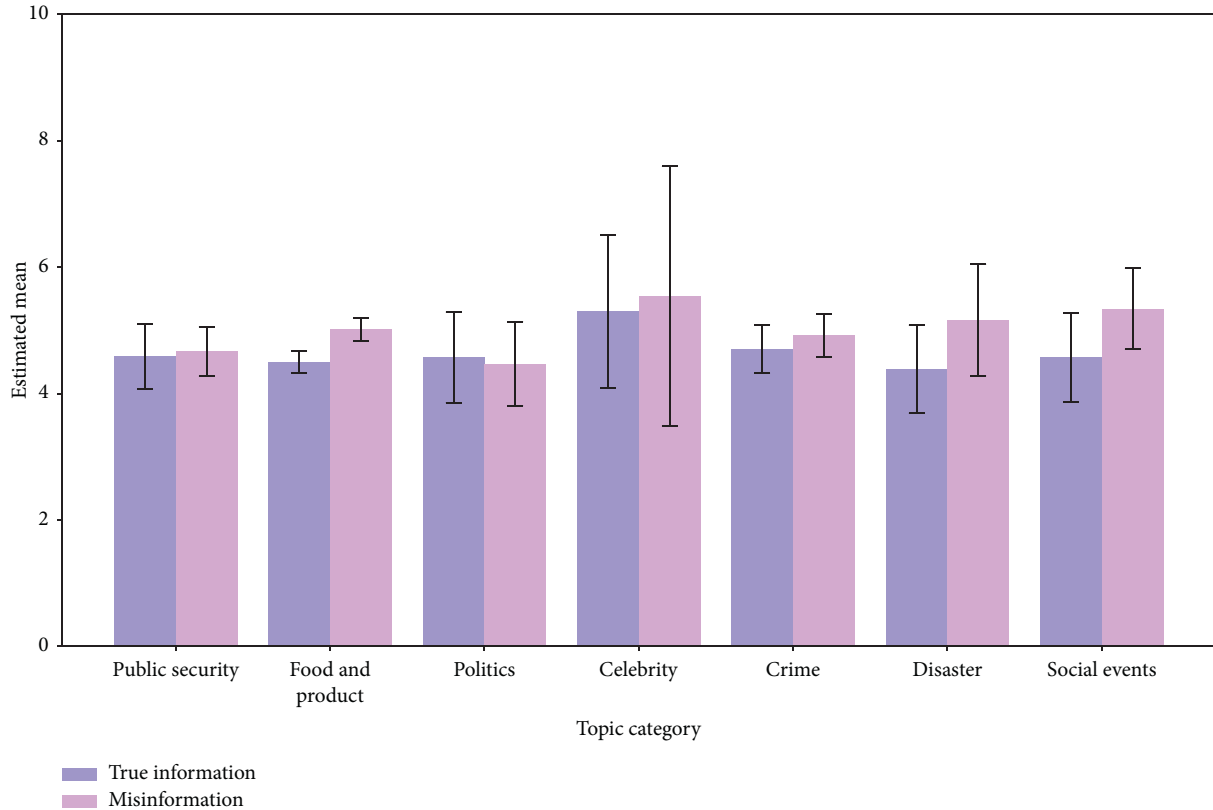


FIGURE 5: Estimated diffusion characteristics of true information and misinformation based on the topic category by the number of comments.

position compared with true information. However, in terms of the number of favorites, misinformation was generally less than true information, and true information was more likely to be recognized by the public for its more detailed content characteristics, and thus showed an advantage in terms of the number of favorites.

**4.5. Emotion Changes of Misinformation in Topic Classification.** After assigning emotion labels corresponding to misinformation and true information events, we first used the Chi-square test to analyze whether there was a significant difference in emotion distribution between misinformation and true information. The results confirmed the existence of significant differences in the distribution of information veracity across emotions (Pearson Chi-Square = 17.705,  $P < 0.01$ ). Second, we compared specific differences in the distribution of emotions between misinformation and true information. The details are shown in Table 4.

It can be observed from Table 4 that “like” emotion dominates both true information and misinformation, which was also the reason why both true information and misinformation can get many retweets. Combined with text materials, both true information and misinformation contained information that the public wanted to obtain, such as diet collocation, health knowledge, anecdotes, etc., which attracted the interest of the public. Therefore, in the distribution of emotions between true information and

TABLE 4: Distribution of information veracity in different emotions.

Emotion type	Information veracity	
	True information	Misinformation
Like	1715	1729
Disgust	300	277
Surprise	31	21
Happiness	29	56
Fear	24	23
Sadness	241	203
Anger	11	4

misinformation, the “like” emotion became the dominant emotion.

Secondly, in contrast, in addition to the emotion of “like,” negative emotions dominated by “disgust” and “sadness” occupied the mainstream in both misinformation and true information, and the number was much larger than other emotion types. The analysis of textual materials showed that the public tended to form emotions of “disgust” and “sadness” in the face of disasters, crimes, and other kinds of news. This finding was also in line with our expectations that when faced with natural disasters, accidents, or other similar events, in reality, we are more likely to form “disgust” and “sadness” emotions under the influence of factors such as compassion and sense of justice.

At the same time, we also divided true information and misinformation into different topic categories and compared

the distribution of true information and misinformation on emotions under different topic categories. The specific distribution information of information veracity on emotion under different topic categories is shown in Table 5.

Based on the observation in Table 5, we found that there was a relationship between misinformation and true information in terms of the content type and sentiment type. In the topics of public security, the most common expressions of emotion in true information and misinformation were the emotions of like, disgust, and sadness. Among them, the emotion of like came from the emergency management measures embodied in information and timely response to events; the emotion of disgust came from the harm brought about by public safety events to the country, society, and individuals; and the emotion of sadness mainly came from sympathy for victims. In the topic category of food and product, emotions in true information and misinformation were most reflected as like and disgust. Combined with the text materials, the emotion of like lied in the knowledge of food safety and products contained in the microblog information, and the emotion of disgust lied in the conflict and hatred of fake and shoddy food and products. In the topic category of politics, like and disgust were often reflected in true information, while like and happy were usually reflected in misinformation. In combination with the text materials, the emotion of like was reflected in the information that satisfies the public's curiosity about the political field, the emotion of disgust was reflected in the dissatisfaction with some political events and policies, and the emotion of happiness was often reflected in the support for political figures and the approval of some policies. In the topic category of celebrity, the emotions of like and disgust became the mainstream in true information and misinformation. The emotion of like came from the public's love for some stars and celebrities, while the emotion of disgust also came from the public's resistance to some stars and celebrities. In the topic category of crime, emotions were mainly embodied in two types of emotions: like and disgust. As the most direct source of information, the public's emotion of like is more obvious when they see images of criminals being arrested and punished in media reports, while the emotion of disgust was mainly from the resistance to the crime. In the topic category of disaster, the emotions of like and sadness were often reflected. Among them, the emotion of like came from the solidarity and common support of the public in the face of disaster, while the emotion of sadness was mainly reflected in the loss of personnel and property. In the topic category of social events, like and disgust often occupied the dominant position. Among them, the emotion of like came from the public's curiosity about strange and usual stories, while the emotion of disgust came from the fact that some social events often contained contents that go against the social conscience.

In addition, we also verified whether there was a significant difference in the effect of subject category on emotion between true information and misinformation. The results showed that compared with true information (Pearson Chi-Square = 38.707,  $P > 0.05$ ), the topic category

of misinformation had a more significant impact on the emotion types (Pearson Chi-Square = 178.625,  $P < 0.01$ ), and there were significant differences in the emotional distribution of different topics in misinformation. Therefore, it is important to divide misinformation into different topics and understand the emotional distribution of misinformation from different topic categories for us to better understand the diffusion pattern of misinformation in social networks.

*4.6. Emotion Analysis of Network Diffusion Characteristics of Misinformation.* Related studies have confirmed that emotion plays an important role in the spread of misinformation. On the one hand, under the influence of emotion, the public will interact and communicate with each other about different events, which will cause heated discussions. On the other hand, information is also embedded with public emotions in the process of information sharing and spreading, and the spread of misinformation in social networks is often promoted by different emotions. Therefore, this paper compares the network diffusion characteristics of misinformation and true information through emotion analysis to further reveal the network diffusion pattern of misinformation. Combined with the available data, to further determine the specific correlation of each topic in different emotions, we used Pearson's Point Biserial correlation coefficient to analyze the correlation between information veracity and the corresponding network diffusion characteristics. Among them, the direction of correlation represents whether it had a dominant position in network diffusion. Positive correlation meant that misinformation was more likely to be retweeted, favored, and commented by network users in social networks than true information, and negative correlation meant that true information was more likely to be retweeted, favored, and commented by network users in social networks than misinformation. The stronger the correlation, the closer the relationship between information veracity and network diffusion. The correlation between information veracity and the number of retweets is shown in Figure 6. The correlation between information veracity and the number of favorites is shown in Figure 7. The correlation between information veracity and the number of comments is shown in Figure 8.

From the perspective of topics, in the topic of public security, misinformation containing like and sadness was more likely to be retweeted by Internet users, while misinformation containing disgust and fear was more difficult to be retweeted by Internet users. Among them, the information containing the emotion of like had statistical significance in the correlation between veracity and the number of retweets ( $P = 0.073 < 0.1$ ). In terms of the number of favorites, misinformation with sadness was more likely to be collected by Internet users, while misinformation with like, disgust, and fear was less likely to be collected by Internet users. Among them, the information containing the emotion of disgust had statistical significance in the correlation between veracity and the number of favorites ( $P = 0.066 < 0.1$ ). In terms of the number of comments, misinformation with emotions of like and sadness was more likely to be

TABLE 5: Distribution of topic types of information veracity in different emotions.

Topic type	Emotion type						
	Like	Disgust	Surprise	Happiness	Fear	Sadness	Anger
<i>True information</i>							
Public security	107	16	2	1	4	15	0
Food and product	1144	218	27	20	18	185	6
Politics	56	11	0	1	0	5	1
Celebrity	20	4	0	0	0	2	0
Crime	215	30	1	6	1	14	2
Disaster	61	6	1	0	1	10	0
Social events	54	14	0	1	0	9	0
<i>Misinformation</i>							
Public security	207	25	0	1	1	24	1
Food and product	1035	194	16	29	16	137	3
Politics	58	6	0	19	1	3	0
Celebrity	7	2	0	0	0	0	0
Crime	292	32	3	5	4	22	0
Disaster	36	5	2	1	0	5	0
Social events	70	11	0	1	1	11	0



FIGURE 6: Correlation between information veracity and retweets' volume.

commented on by Internet users, while misinformation with emotions of fear and disgust was more difficult to be commented on by Internet users.

In the topic of food and product, the veracity of information under different emotional types was positively

correlated with the number of retweets, and misinformation was more likely to be retweeted in social networks. Among them, the information containing the emotions of like ( $P = 0.000 < 0.001$ ), disgust ( $P = 0.001 < 0.01$ ), and sadness ( $P = 0.02 < 0.05$ ) had statistical significance in the

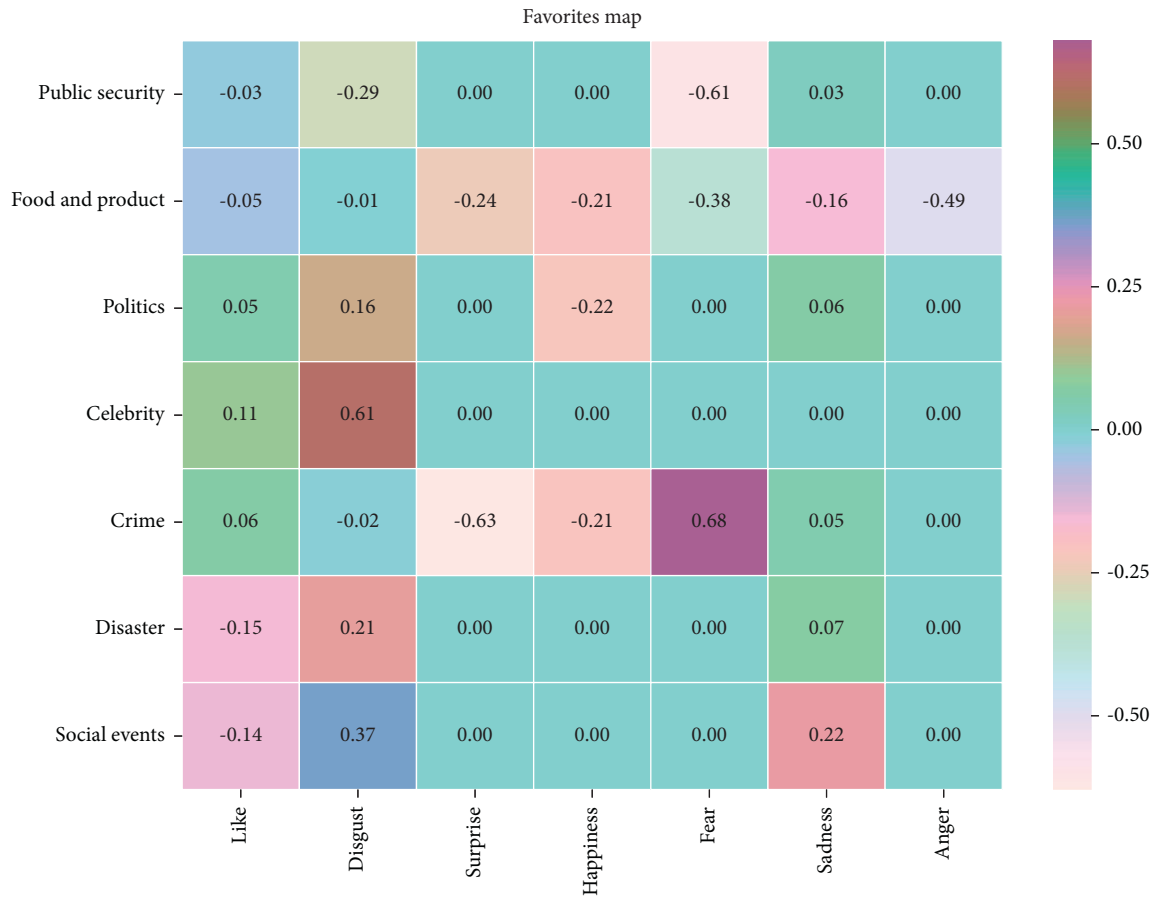


FIGURE 7: Correlation between information veracity and favorites' volume.

correlation between veracity and the number of retweets. In terms of the number of favorites, the veracity of information under different emotional types was negatively correlated with the number of favorites, and true information was more likely to be collected by network users. Among them, the information containing the emotions of like ( $P = 0.024 < 0.05$ ), fear ( $P = 0.03 < 0.05$ ), and sadness ( $P = 0.004 < 0.01$ ) had statistical significance in the correlation between veracity and the number of favorites. In terms of the number of comments, the veracity of information under different emotional types was positively correlated with Internet users, and misinformation was more likely to be commented on by Internet users. Among them, the information containing the emotions of like ( $P = 0.000 < 0.001$ ) and disgust ( $P = 0.04 < 0.05$ ) had statistical significance in the correlation between veracity and the number of comments.

In the topic of politics, misinformation in the emotions of like, disgust, and sadness was more likely to be retweeted by Internet users, while true information with happy emotion was more likely to be retweeted by Internet users. Among them, the information containing the emotions of like ( $P = 0.09 < 0.1$ ) and disgust ( $P = 0.082 < 0.1$ ) had statistical significance in the correlation between veracity and the number of retweets. In terms of the number of favorites, misinformation with the emotions of like, disgust, and sadness were more likely to be collected by Internet users,

while true information with happy emotion was more likely to be collected by Internet users. In terms of the number of comments, misinformation with like, disgust, happiness, and sadness was more likely to elicit comments from Internet users.

In the topic of celebrity, misinformation containing the emotion of like was more difficult to be retweeted by Internet users, and misinformation in the emotion of disgust was more likely to be retweeted by Internet users. In the number of favorites, misinformation in the emotions of like and disgust was easier to be collected by Internet users. In terms of the number of comments, the misinformation in the emotion of like was less likely to be commented by users, while the misinformation in the emotion of disgust was more likely to be discussed by users.

In the topic of crime, misinformation containing emotions of like, disgust, happiness, fear, and sadness was more easily retweeted by Internet users, while misinformation under the emotion of surprise was more difficult to be retweeted by Internet users. Among them, the information containing the emotion of like ( $P = 0.023 < 0.1$ ) had statistical significance in the correlation between veracity and the number of retweets. In terms of the number of favorites, misinformation under the emotions of like, fear, and sadness was more likely to be collected by Internet users, while misinformation under the emotions of disgust, surprise, happiness, and sadness was more difficult to be

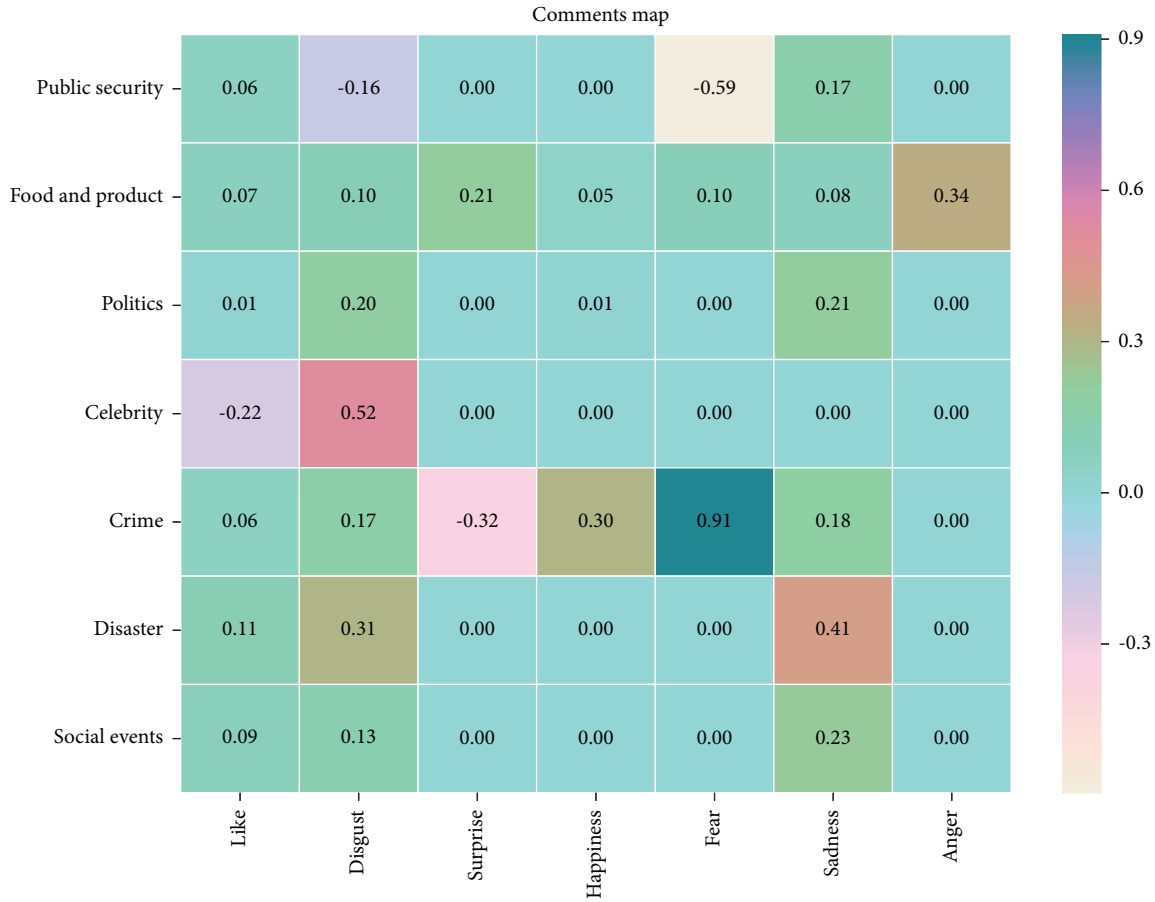


FIGURE 8: Correlation between information veracity and comments' volume.

collected by Internet users. In terms of the number of comments, the misinformation containing emotions of like, disgust, happiness, fear, and sadness was more likely to be commented on by Internet users, while the misinformation containing the emotions of surprise was more difficult to be discussed and communicated by Internet users.

Among the topics of disaster and social events, misinformation containing the emotions of like, disgust, and sadness was more likely to be retweeted by Internet users. In terms of the number of favorites, misinformation containing the emotion of like was more difficult to be collected by network users, and misinformation containing the emotions of disgust and sadness was more likely to be collected by network users. Among the topic of social events, information containing the emotion of disgust ( $P = 0.078 < 0.1$ ) had statistical significance in the correlation between veracity and the number of favorites. In terms of the number of comments, misinformation containing the emotions of like, disgust, and sadness was more likely to be discussed and communicated by Internet users.

From the perspective of emotion, in the topic category under the like emotion, misinformation under the topic of celebrity was more difficult to be retweeted by Internet users, and misinformation under the rest of the topic categories was more likely to be retweeted by Internet users than true information. Among them, the information containing the

topics of public security ( $P = 0.073 < 0.1$ ), food and product ( $P = 0.000 < 0.001$ ), politics ( $P = 0.09 < 0.1$ ), and crime ( $P = 0.023 < 0.05$ ) had statistical significance in the correlation between veracity and the number of retweets. In terms of the number of favorites, true information under the topics of public security, food and product, disaster, and social events were more likely to be collected by network users. Misinformation under the topics of politics, celebrity, and crime was more likely to be collected by Internet users. Among them, the information containing the topic of food and product ( $P = 0.024 < 0.05$ ) had statistical significance in the correlation between veracity and the number of favorites. In terms of the number of comments, misinformation under the topic of celebrity was more difficult to be discussed by online users, and misinformation under the remaining topic categories was more likely to be discussed by online users than true information. Among them, the information containing the topic of food and product ( $P = 0.000 < 0.001$ ) had statistical significance in the correlation between veracity and the number of comments.

In the topic category under disgust emotion, true information under the topic of public security was more likely to be retweeted by Internet users than misinformation. Misinformation under the other types of topic categories was more likely to be retweeted by network users. Among them, information containing the topics of food and product

( $P = 0.001 < 0.05$ ) and politics ( $P = 0.082 < 0.1$ ) had statistical significance in the correlation between veracity and the number of retweets. In terms of the number of favorites, true information under the topics of food and product, public security, and crime were more likely to be collected by Internet users, while misinformation under the topics of politics, celebrity, disaster, and social events was more likely to be collected by Internet users. Among them, information containing the topics of public security ( $P = 0.066 < 0.1$ ) and social events ( $P = 0.078 < 0.1$ ) had statistical significance in the correlation between veracity and the number of favorites. In terms of the number of comments, misinformation under the topic categories of food and product, politics, celebrity, crime, disaster, and social events was more likely to be discussed by Internet users. Compared with misinformation, true information containing the topic of public security is more likely to be commented on by network users. Among them, the information containing the topic of food and product ( $P = 0.04 < 0.05$ ) had statistical significance in the correlation between veracity and the number of comments.

In the topic category under surprise emotion, misinformation under the topic of food and product was more likely to be retweeted by Internet users. In the topic category of crime, true information was more likely to be retweeted by network users than misinformation. In terms of the number of favorites, true information under the topics of food and product, and crime was more likely to be collected by Internet users. In terms of the number of comments, misinformation under the topic of food and product was more likely to be discussed by Internet users. In the topic category of crime, true information was more likely to be discussed by Internet users than misinformation.

In the topic category under happiness emotion, misinformation under the topics of food and product, and crime was more likely to be retweeted in social networks. In the topic category of politics, true information was more likely to be retweeted on the network than misinformation. In terms of the number of favorites, true information under the topics of food and product, politics, and crime was more likely to be collected by Internet users. In terms of the number of comments, misinformation under the topics of food and product, politics, and crime was more likely to be discussed by Internet users.

In the topic category under fear emotion, misinformation in the topic categories of food and product, and crime was more likely to be retweeted in social networks than true information. In the topic category of public security, true information was more likely to be retweeted over the network than misinformation. In terms of the number of favorites, true information under the topics of public security and food and product was more likely to be collected by Internet users, while misinformation under crime was more likely to be collected by Internet users. Among them, the information containing the topic of food and product ( $P = 0.03 < 0.05$ ) had statistical significance in the correlation between veracity and the number of favorites. In terms of the number of comments, misinformation was more likely to arouse users' discussion in social networks in the topic categories of food and product, and crime. In the topic

category of public security, true information was more likely to be discussed by users on the network.

In the topic category under sadness, except for the topic category of celebrity where there was no significant correlation, misinformation in the rest of the topic categories was more likely to be retweeted on the network than true information. Among them, information containing the topic of food and product ( $P = 0.02 < 0.05$ ) had statistical significance in the correlation between veracity and the number of retweets. In terms of the number of favorites, true information under the topic of food and product was more likely to be collected by network users, while misinformation under the topics of public security, politics, crime, disaster, and social events was more likely to be collected by network users. Among them, information containing the topic of food and product ( $P = 0.004 < 0.01$ ) had statistical significance in the correlation between veracity and the number of favorites. In terms of the number of comments, except for the topic of celebrity where there was no obvious correlation, misinformation under other topics was more likely to be discussed by users on the Internet than true information.

In the topic category under anger, misinformation in the topic of food and product was more likely to be retweeted and commented on the network than true information. True information on the topic of food and product was more likely to be collected by Internet users. There was no significant correlation among the rest of the topic categories.

To sum up, by comparing the correlation between information veracity and network diffusion characteristics of each topic under different emotions, we can further provide corresponding suggestions for public opinion governance and prevention assessment of misinformation. When misinformation spreads in social networks, its threat can be effectively reduced by guiding the discussion content and emotions, and the governance goal of maintaining network order and social stability can be achieved.

## 5. Conclusions

As an important channel of information dissemination, social media has not only become an important platform for the communication of true information but has also contributed to the spread of misinformation in social networks. On the one hand, the spread of misinformation on social media misleads the public and prompts them to make wrong decisions. On the other hand, it also brings about great threats to the public's physical and mental health and economic properties. Therefore, it is important to understand the diffusion characteristics of misinformation on social media. It can not only provide reference and basis for the governance of misinformation in social media but also maintain the order of network security. And, it is also possible to prevent and control misinformation in advance by understanding the diffusion rules of misinformation, to reduce the spread of misinformation on social media more effectively, and thereby reduce the harm caused by misinformation from the source. In this paper, we took the misinformation spread on social media as the research object, used the deep learning method to analyze the content

characteristics and emotional characteristics of misinformation, and combined it with the network analysis method to make a targeted analysis of the network diffusion characteristics of misinformation in the social network. In addition, the study also introduced corresponding true information for comparative study on the basis of the analysis of misinformation to further reveal the propagation law of misinformation in social networks.

Related studies have found different characteristics of misinformation and true information dissemination in social networks. In content analysis, there were differences in the network distribution and diffusion characteristics of misinformation and true information of different topics. In emotion analysis, we also found that emotion was an important factor influencing the spread of misinformation, and the process of spread of misinformation in social networks showed different changes due to the influence of different emotions. On the one hand, these findings supplement the research content with misinformation as the object and broaden the research boundary of misinformation. On the other hand, they also provide a reference for the public opinion management of misinformation. By guiding the public to discuss different topics and contents, and guiding the public to generate corresponding emotions, it helps to achieve the management of misinformation, reduce the harm caused by misinformation, and maintain the stability of social order. In addition, with the help of the distribution of topics and emotions of misinformation on social media, we also have a deeper understanding of the propagation rules of misinformation on social media. And, it also makes a deeper analysis of the evolution characteristics of misinformation on social media and the driving factors of the social network to misinformation. This provides a basis for us to further explore the propagation mechanism of misinformation on social media. Meanwhile, in the future, we will further deepen the research based on this paper and adopt different datasets and methods to better reveal the propagation pattern of misinformation in social networks.

### Data Availability

The data used to support the findings of this study are available from the corresponding author upon request.

### Conflicts of Interest

The authors declare that they have no conflicts of interest.

### Acknowledgments

This research was funded by the National Natural Science Foundation of China under Grant no. 71501153, the Innovation Capability Support Project of Shaanxi Province of China under Grant no. 2021KRM135, the Research Fund of Grand Theory and Practical Problem in Philosophy and Social Science of Shaanxi Province of China under Grant no. 2021ND0221, the Research Fund of the Education Department of Shaanxi Province of China under Grant no.

20JG020, and the Natural Science Foundation of Shaanxi Province of China under Grant no. 2019JM-572.

### References

- [1] S. O. S e, "Algorithmic detection of misinformation and disinformation: gricean perspectives," *Journal of Documentation*, vol. 74, no. 2, pp. 309–332, 2017.
- [2] L. Guo and Y. Zhang, "Information flow within and across online media platforms: an agenda-setting analysis of rumor diffusion on news websites, Weibo, and WeChat in China," *Journalism Studies*, vol. 21, no. 15, pp. 2176–2195, 2020.
- [3] L. Li, H. Xia, R. Zhang, and Y. Li, "DDSEIR: a dynamic rumor spreading model in online social networks," in *Proceedings of the International Conference on Wireless Algorithms, Systems, and Applications*, pp. 596–604, Springer, Honolulu, HI, USA, June 2019.
- [4] D. M. J. Lazer, M. A. Baum, Y. Benkler et al., "The science of fake news," *Science*, vol. 359, no. 6380, pp. 1094–1096, 2018.
- [5] T. Caulfield, "Pseudoscience and COVID-19 - we've had enough already," *Nature*, 2020.
- [6] J. Zarocostas, "How to fight an infodemic," *The Lancet*, vol. 395, no. 10225, p. 676, 2020.
- [7] K. M. Malecki, J. A. Keating, and N. Safdar, "Crisis communication and public perception of COVID-19 risk in the era of social media," *Clinical Infectious Diseases*, vol. 72, no. 4, pp. 697–702, 2021.
- [8] C. M. Pulido, B. Villarejo-Carballido, G. Redondo-Sama, and A. G omez, "COVID-19 infodemic: more retweets for science-based information on coronavirus than for false information," *International Sociology*, vol. 35, no. 4, pp. 377–392, 2020.
- [9] C. Huimin, J. Sichen, L. Wei et al., "Quantitative analysis on the communication of COVID-19 related social media rumors," *Journal of Computer Research and Development*, vol. 58, no. 7, pp. 1366–1384, 2021.
- [10] M. S. Granovetter, "The strength of weak ties," *American Journal of Sociology*, vol. 78, no. 6, pp. 1360–1380, 1973.
- [11] L. Zhang, L. Xu, and W. Zhang, "Social media as amplification station: factors that influence the speed of online public response to health emergencies," *Asian Journal of Communication*, vol. 27, no. 3, pp. 322–338, 2017.
- [12] G. Pennycook and D. G. Rand, "Fighting misinformation on social media using crowdsourced judgments of news source quality," *Proceedings of the National Academy of Sciences*, vol. 116, no. 7, pp. 2521–2526, 2019.
- [13] A. Ghenai and Y. Mejova, "Fake cures: user-centric modeling of health misinformation in social media," *Proceedings of the ACM on human-computer interaction*, vol. 2, pp. 1–20, 2018.
- [14] J. Shin, L. Jian, K. Driscoll, and F. Bar, "The diffusion of misinformation on social media: temporal pattern, message, and source," *Computers in Human Behavior*, vol. 83, pp. 278–287, 2018.
- [15] S. Lewandowsky, U. K. Ecker, C. M. Seifert, N. Schwarz, and J. Cook, "Misinformation and its correction: continued influence and successful debiasing," *Psychological Science in the Public Interest*, vol. 13, no. 3, pp. 106–131, 2012.
- [16] R. Faris, H. Roberts, B. Etling, N. Bourassa, E. Zuckerman, and Y. Benkler, "Partisanship, propaganda, and disinformation: online media and the 2016 US presidential election," *Berkman Klein Center Research Publication*, vol. 6, 2017.
- [17] C. J. Vargo, L. Guo, and M. A. Amazeen, "The agenda-setting power of fake news: a big data analysis of the online media landscape from 2014 to 2016," *New Media & Society*, vol. 20, no. 5, pp. 2028–2049, 2018.

- [18] A. Rojecki and S. Meraz, "Rumors and factitious informational blends: the role of the web in speculative politics," *New Media & Society*, vol. 18, no. 1, pp. 25–43, 2016.
- [19] S. Zannettou, M. Sirivianos, J. Blackburn, and N. Kourtellis, "The web of false information: rumors, fake news, hoaxes, clickbait, and various other shenanigans," *Journal of Data and Information Quality (JDIQ)*, vol. 11, no. 3, pp. 1–37, 2019.
- [20] T. Xiaorui, W. Danchen, and D. Anbang, "Research on dissemination mechanism of public crisis information under the influence of psychological stress," *Library and Information Service*, vol. 58, no. 02, pp. 59–65, 2014.
- [21] M. T. Thai, W. Wu, and H. Xiong, *Big Data in Complex and Social Networks*, CRC Press, Boca Raton, FL, United States, 2016.
- [22] G. Pennycook, Z. Epstein, M. Mosleh, A. A. Arechar, D. Eckles, and D. G. Rand, "Shifting attention to accuracy can reduce misinformation online," *Nature*, vol. 592, no. 7855, pp. 590–595, 2021.
- [23] A. Zubiaga, M. Liakata, R. Procter, G. Wong Sak Hoi, and P. Tolmie, "Analysing how people orient to and spread rumors in social media by looking at conversational threads," *PloS one*, vol. 11, no. 3, Article ID e0150989, 2016.
- [24] J. J. Van Bavel and A. Pereira, "The partisan brain: an identity-based model of political belief," *Trends in Cognitive Sciences*, vol. 22, no. 3, pp. 213–224, 2018.
- [25] H. Allcott and M. Gentzkow, "Social media and fake news in the 2016 election," *The Journal of Economic Perspectives*, vol. 31, no. 2, pp. 211–236, 2017.
- [26] G. Pennycook and D. G. Rand, "Lazy, not biased: susceptibility to partisan fake news is better explained by lack of reasoning than by motivated reasoning," *Cognition*, vol. 188, pp. 39–50, 2019.
- [27] N. Grinberg, K. Joseph, L. Friedland, B. Swire-Thompson, and D. Lazer, "Fake news on Twitter during the 2016 US presidential election," *Science*, vol. 363, no. 6425, pp. 374–378, 2019.
- [28] A. M. Guess, M. Lerner, B. Lyons et al., "A digital media literacy intervention increases discernment between mainstream and false news in the United States and India," *Proceedings of the National Academy of Sciences*, vol. 117, no. 27, pp. 15536–15545, 2020.
- [29] S. M. Jones-Jang, T. Mortensen, and J. Liu, "Does media literacy help identification of fake news? Information literacy helps, but other literacies don't," *American Behavioral Scientist*, vol. 65, no. 2, pp. 371–388, 2021.
- [30] Y. Zhao, J. Da, and J. Yan, "Detecting health misinformation in online health communities: incorporating behavioral features into machine learning based approaches," *Information Processing & Management*, vol. 58, no. 1, Article ID 102390, 2021.
- [31] T. K. Sell, D. Hosangadi, and M. Trotochaud, "Misinformation and the US Ebola communication crisis: analyzing the veracity and content of social media messages related to a fear-inducing infectious disease outbreak," *BMC Public Health*, vol. 20, no. 1, pp. 1–10, 2020.
- [32] J. S. Brennen, F. Simon, P. N. Howard, and R. K. Nielsen, "Types, sources, and claims of COVID-19 misinformation," 2020, <https://reutersinstitute.politics.ox.ac.uk/types-sources-and-claims-covid-19-misinformation>.
- [33] L. Chen, X. Wang, and T.-Q. Peng, "Nature and diffusion of gynecologic cancer-related misinformation on social media: analysis of tweets," *Journal of Medical Internet Research*, vol. 20, no. 10, Article ID e11515, 2018.
- [34] S. Vosoughi, D. Roy, and S. Aral, "The spread of true and false news online," *Science*, vol. 359, no. 6380, pp. 1146–1151, 2018.
- [35] E. Hollowood and A. Mostrous, "Fake news in the time of C-19," 2020, <https://members.tortoisemediacom/2020/03/23/the-infodemic-fake-news-coronavirus/content.html>.
- [36] S. M. Jang, T. Geng, J.-Y. Q. Li et al., "A computational approach for examining the roots and spreading patterns of fake news: evolution tree analysis," *Computers in Human Behavior*, vol. 84, pp. 103–113, 2018.
- [37] H. Ahmed, "Detecting opinion spam and fake news using n-gram analysis and semantic similarity," 2017, <https://dspace.library.uvic.ca/handle/1828/8796>.
- [38] Y. Zhao and J. Zhang, "Consumer health information seeking in social media: a literature review," *Health Information and Libraries Journal*, vol. 34, no. 4, pp. 268–283, 2017.
- [39] R. Ma, "Spread of SARS and war-related rumors through new media in China," *Communication Quarterly*, vol. 56, no. 4, pp. 376–391, 2008.
- [40] O. Oh, M. Agrawal, and H. R. Rao, "Community intelligence and social media services: a rumor theoretic analysis of tweets during social crises," *MIS Quarterly*, vol. 37, pp. 407–426, 2013.
- [41] F. Zollo, P. K. Novak, M. Del Vicario et al., "Emotional dynamics in the age of misinformation," *PloS one*, vol. 10, no. 9, Article ID e0138740, 2015.
- [42] K. Klimiuk, A. Czoska, K. Biernacka, and Ł. Balwicki, "Vaccine misinformation on social media—topic-based content and sentiment analysis of Polish vaccine-deniers' comments on Facebook," *Human Vaccines & Immunotherapeutics*, vol. 17, no. 7, pp. 2026–2035, 2021.
- [43] Y. Leng, Y. Zhai, S. Sun et al., "Analysis of misinformation during the COVID-19 outbreak in china: cultural, social and political ntanglements," 2020, <https://arxiv.org/abs/2005.10414>.
- [44] E. Kušen and M. Strembeck, "Politics, sentiments, and misinformation: an analysis of the Twitter discussion on the 2016 austrian presidential elections," *Online Social Networks and Media*, vol. 5, pp. 37–50, 2018.
- [45] K. K. King and B. Wang, "Diffusion of real versus misinformation during a crisis event: a big data-driven approach," *International Journal of Information Management*, Article ID 102390, 2021.
- [46] L. H. X. Ng and J. Y. Loke, "Analyzing public opinion and misinformation in a COVID-19 telegram group chat," *IEEE Internet Computing*, vol. 25, no. 2, pp. 84–91, 2020.
- [47] M. Saqr and A. Alamro, "The role of social network analysis as a learning analytics tool in online problem based learning," *BMC Medical Education*, vol. 19, no. 1, pp. 1–11, 2019.
- [48] S. P. Borgatti, A. Mehra, D. J. Brass, and G. Labianca, "Network analysis in the social sciences," *Science*, vol. 323, no. 5916, pp. 892–895, 2009.
- [49] L. F. Bringmann, T. Elmer, S. Epskamp et al., "What do centrality measures measure in psychological networks?" *Journal of Abnormal Psychology*, vol. 128, no. 8, pp. 892–903, 2019.
- [50] D. Camacho, Á. Panizo-Lledot, G. Bello-Orgaz, A. Gonzalez-Pardo, and E. Cambria, "The four dimensions of social network analysis: an overview of research methods, applications, and software tools," *Information Fusion*, vol. 63, pp. 88–120, 2020.
- [51] P. Wang, B. Xu, Y. Wu, and X. Zhou, "Link prediction in social networks: the state-of-the-art," *Science China Information Sciences*, vol. 58, no. 1, pp. 1–38, 2015.



- [52] R. Pastor-Satorras, C. Castellano, P. Van Mieghem, and A. Vespignani, "Epidemic processes in complex networks," *Reviews of Modern Physics*, vol. 87, no. 3, pp. 925–979, 2015.
- [53] M. Liu, B. Lang, Z. Gu, and A. Zeeshan, "Measuring similarity of academic articles with semantic profile and joint word embedding," *Tsinghua Science and Technology*, vol. 22, no. 6, pp. 619–632, 2017.
- [54] T. Mikolov, K. Chen, G. Corrado, and J. Dean, "Efficient estimation of word representations in vector space," 2013, <https://arxiv.org/abs/1301.3781>.
- [55] B. Liu, "Text sentiment analysis based on CBOW model and deep learning in big data environment," *Journal of Ambient Intelligence and Humanized Computing*, vol. 11, no. 2, pp. 451–458, 2020.
- [56] T. M. Kodinariya and P. R. Makwana, "Review on determining number of cluster in K-means clustering," *International Journal*, vol. 1, no. 6, pp. 90–95, 2013.
- [57] N. K. Nguyen, A.-C. Le, and H. T. Pham, *Deep Bi-directional Long Short-Term Memory Neural Networks for Sentiment Analysis of Social Data, International Symposium on Integrated Uncertainty in Knowledge Modelling and Decision Making*, Springer, New York, NY, USA, 2016.
- [58] V. Loia and S. Senatore, "A fuzzy-oriented sentic analysis to capture the human emotion in Web-based content," *Knowledge-Based Systems*, vol. 58, pp. 75–85, 2014.
- [59] S. Poria, H. Peng, A. Hussain, N. Howard, and E. Cambria, "Ensemble application of convolutional neural networks and multiple kernel learning for multimodal sentiment analysis," *Neurocomputing*, vol. 261, pp. 217–230, 2017.
- [60] F. Luo, C. Li, and Z. Cao, "Affective-feature-based sentiment analysis using SVM classifier," in *Proceedings of the 2016 IEEE 20th International Conference on Computer Supported Cooperative Work in Design (CSCWD)*, pp. 276–281, IEEE, Nanchang, China, May 2016.
- [61] Y. LeCun, Y. Bengio, and G. Hinton, "Deep learning," *Nature*, vol. 521, no. 7553, pp. 436–444, 2015.
- [62] G. Xu, D. Zhou, and J. Liu, "Social network spam detection based on ALBERT and combination of Bi-LSTM with self-attention," *Security and Communication Networks*, vol. 2021, Article ID 5567991, 11 pages, 2021.
- [63] Y. Lai, L. Zhang, D. Han, R. Zhou, and G. Wang, "Fine-grained emotion classification of Chinese microblogs based on graph convolution networks," *World Wide Web*, vol. 23, no. 5, pp. 2771–2787, 2020.
- [64] K. Cheng, Y. Yue, and Z. Song, "Sentiment classification based on Part-of-Speech and self-attention mechanism," *IEEE Access*, vol. 8, pp. 16387–16396, 2020.
- [65] J. Ma, W. Gao, P. Mitra et al., "Detecting rumors from microblogs with recurrent neural networks," in *Proceedings of the Twenty-Fifth International Joint Conference on Artificial Intelligence*, pp. 3818–3824, AAAI Press, New York, NY, USA, July 2016.
- [66] P. Liu and L. Ma, "Food scandals, media exposure, and citizens' safety concerns: a multilevel analysis across Chinese cities," *Food Policy*, vol. 63, pp. 102–111, 2016.

## Research Article

# Controlling Virus Spread Using an Intermittent Quarantine Strategy on Multiplex Networks

Xingguo Li,<sup>1</sup> Xiaoping Luo,<sup>2</sup> and Yiwu Wang<sup>3</sup> 

<sup>1</sup>College of Computer Science, Sichuan University, Chengdu 610065, China

<sup>2</sup>Chengdu Polytechnic, Chengdu 610041, China

<sup>3</sup>Chengdu Medical College, Chengdu 610081, China

Correspondence should be addressed to Yiwu Wang; [one15@cmc.edu.cn](mailto:one15@cmc.edu.cn)

Received 29 April 2021; Revised 19 August 2021; Accepted 19 October 2021; Published 24 November 2021

Academic Editor: AnMin Fu

Copyright © 2021 Xingguo Li et al. This is an open access article distributed under the Creative Commons Attribution License, which permits unrestricted use, distribution, and reproduction in any medium, provided the original work is properly cited.

Virus spreading on the Internet will negatively affect cybersecurity. An intermittent quarantine immunization strategy to control virus spreading when containing information diffusion is proposed herein. In this model, information and virus spread on different subnetworks and interact with each other. We further develop a heterogeneous mean-field approach with time delays to investigate this model and use Monte Carlo simulations to systematically investigate the spreading dynamics. For a relatively short intermittent period, the optimal information transmission probability of the virus will be significantly suppressed. However, when the intermittent period is extremely long; increasing the probability of information transmission can control the virus spreading as well as suppress the increase in the intermittent period. Finally, it is shown that the average degree of the two subnetworks does not qualitatively affect the spreading dynamics.

## 1. Introduction

Computer viruses are spreading widely on the Internet, thereby significantly affecting the cyberspace security [1–4]. For instance, the WannaCry virus, one of the most influential viruses since Panda Burned Incense, has affected more than 100 countries and regions. Researchers from different fields, including computer science, network science, physics, and mathematics, have attempted to eliminate the spread of the virus [5–11]. In this study, we focused on network science to address this problem, in which the ultimate aim is to develop effective measures to control virus spreading using mathematical modeling and network theory.

Network science researchers have developed many effective models to investigate the spread of viruses on the Internet. Data analyses revealed that the topology of the Internet exhibits the heavy-tail degree distribution [12–14]; hence, PastorCSatorras and Vespignani proposed a mathematical susceptible-infected-susceptible (SIS) model on scale-free complex networks [5, 15]. They used a heterogeneous mean-field theory to describe the dynamics and

revealed that a few hubs resulted in vanishingly low values of infection transmission probability that triggered virus spreading on the Internet. Based on this finding, we can design an effective approach to control virus spread. Target immunization [15–19] is one of the most popular strategies, which involve the immunization of hubs to suppress viruses significantly. To implement the target immunization strategy, the topology of the Internet must be determined, which limits its applications. Therefore, researchers proposed the acquaintance immunization strategy [20–23], which necessitates only information regarding local network structures. The progress in state-of-the-art network immunization has been reported in a recent review [24].

Computer users typically communicate with their friends through social networks [25–28]. Hence, the information spread by a virus will diffuse in the social network when the virus is spreading on the Internet. Therefore, researchers have developed models to describe the dynamics of virus-information spread. Scholars typically use epidemic spreading models to model the spread of viruses, such as SIS and susceptible-infected-removed (SIR) models. Therefore,

we herein present some of the advancements in the field of epidemic-information spreading dynamics that can be used to investigate the spread of virus information. Funk et al. [29] assume that an epidemic is spread on homogeneous networks, whereas information regarding the epidemic is also spread within the same network. Using a mean-field approach, they discovered that information spreading can significantly suppress the spread of an epidemic but cannot alter the outbreak threshold. Granell et al. [30, 31] used the unaware-aware-unaware (UAU)-SIS model, which assumes UAU information spreading dynamics on social networks and SIS epidemic spreading dynamics on face-to-face contact networks. They used a discrete Markovian approach to describe the interacting dynamics and revealed that the epidemic outbreak threshold was determined by the topologies of social networks, contact networks, and dynamic information spreading parameters. Subsequently, researchers investigated the effects of network topologies and interacting mechanisms on spreading dynamics [32–37]. Wang et al. [38–40] used an asymmetrical interacting SIR-SIRV model and discovered that the interlayer degree correlation facilitated the control of epidemic spread.

To immunize virus spreading on the Internet, different strategies can be adopted, e.g., barring Internet access, implementing patches, and turning on the firewall. Additionally, advanced information-epidemic spreading dynamics can be adopted to describe more realistic scenarios. Zhao et al. [41] developed a virus-information spreading model to design an optimal allocation strategy for patches. Once a virus spreads on the Internet, the simplest approach to stop the spreading is to bar Internet access until the virus is eliminated [42–44]. Because mathematical studies pertaining to information spreading dynamics are scarce, we herein propose a mathematical model to describe an interaction model based on multiplex networks. We assume that information regarding the virus spreads in the social network, i.e., the virus spreads on the Internet and then performs extensive numerical simulations to determine the optimal intervention strength.

## 2. Model Descriptions

In this section, an interacting spreading dynamics model based on the intermittent quarantine immunization strategy on multiplex networks with  $N_A = N_B = N$  nodes is described. The multiplex networks comprise two subnetworks, denoted as  $A$  and  $B$ , and each subnetwork represents a communication platform. Each node in two subnetworks is matched one-to-one, which implies that a node exists in different communication platforms. The two subnetworks were constructed based on an uncorrelated configuration model with degree distributions  $P_A(k_A)$  and  $P_B(k_B)$ , separately. When the network size is  $N \rightarrow \infty$ , no inter- and interlayer degree correlations exist in the multiplex subnetwork (as shown in Figure 1(a)).

Assume that subnetworks  $A$  and  $B$  represent the social and virus networks, respectively. Information is typically spread on social network  $A$ , whereas virus spreads on subnetwork  $B$ . To describe information spreading, we used

the classic SIR epidemiological model [45–47], in which each node can be susceptible, informed, or recovered at a specified time. At each time step, each informed node first transmits the information to every susceptible neighbor with probability  $\beta_A$  and then recovers with probability  $\gamma_A$ . It is noteworthy that the susceptible node in subnetwork  $A$  is informed once its counterpart in subnetwork  $B$  becomes infected. Hence, virus spread promotes information spreading (as shown in Figure 1(b)).

For virus spreading on subnetwork  $B$ , we used a generalized SIR model. The virus spreading dynamics is the same as the information spreading dynamics on subnetwork  $A$  but with different infection and recovery probabilities, i.e.,  $\beta_B$  and  $\gamma_B$ , respectively. We assume that the susceptible node in subnetwork  $B$  adopts an intermittent quarantine strategy to control virus spread. Specifically, the susceptible node  $i_B$  in subnetwork  $B$  will be quarantined for a period  $t_b$  if its corresponding node  $i_A$  in subnetwork  $A$  is in the informed state. After period  $t_b$ , the susceptible node  $i_B$  is reconnected its neighbors, i.e., the intermittent quarantine strategy is induced (as shown in Figure 1(c)). From the above descriptions, we know the state of the node  $i_A$  depends on the information spreading and thus further determines the adoption intermittent quarantine strategy for the node  $i_A$ . Hence, virus spreading on subnetwork  $B$  is suppressed. According to the above descriptions, the differences between the information diffusion and virus spreading are listed as follows: (i) different dynamical parameters, i.e., transmission and recovery probabilities, and (ii) an addition intermittent quarantine state is induced in the virus spreading.

We randomly selected one node as the virus seed in subnetwork  $B$ ; subsequently, we set its counterpart in subnetwork  $A$  as the information seed. The remaining nodes were set in a susceptible state. The effective information transmission and virus transmission probabilities are expressed as  $\lambda_A = \beta_A/\gamma_A$  and  $\lambda_B = \beta_B/\gamma_B$ , respectively. The interacting spreading dynamics terminate once no node is available in the informed or infected state. In Table 1, we illustrate the definitions of the parameters in our model.

## 3. Results

The results of this study are presented in this section.

*3.1. Theoretical Analysis.* To analyze the results of this study quantitatively, we used a heterogeneous mean-field approach with time delays. We denote  $S_{k_A}^A(t)$ ,  $I_{k_A}^A(t)$ , and  $R_{k_A}^A(t)$  as the fractions of the susceptible, informed, and recovered nodes with degree  $k_A$  in subnetwork  $A$  at time  $t$ , respectively. Similarly, we denote  $S_{k_B}^B(t)$ ,  $I_{k_B}^B(t)$ ,  $R_{k_B}^B(t)$ , and  $V_{k_B}^B(t)$  to represent the fraction of nodes in the susceptible, infected, recovered, and vaccinated states with degree  $k_B$  in subnetwork  $B$  at time  $t$ , respectively. Once the parameters above are obtained, the fraction of nodes in each state can be determined using the degree distributions of the two networks, denoted as  $P_A(k_A)$  and  $P_B(k_B)$ , separately. For instance, the fraction of nodes in the susceptible state in subnetwork  $A$  is  $S_A(t) = \sum_{k_A} S_{k_A}^A(t)P_A(k_A)$ .

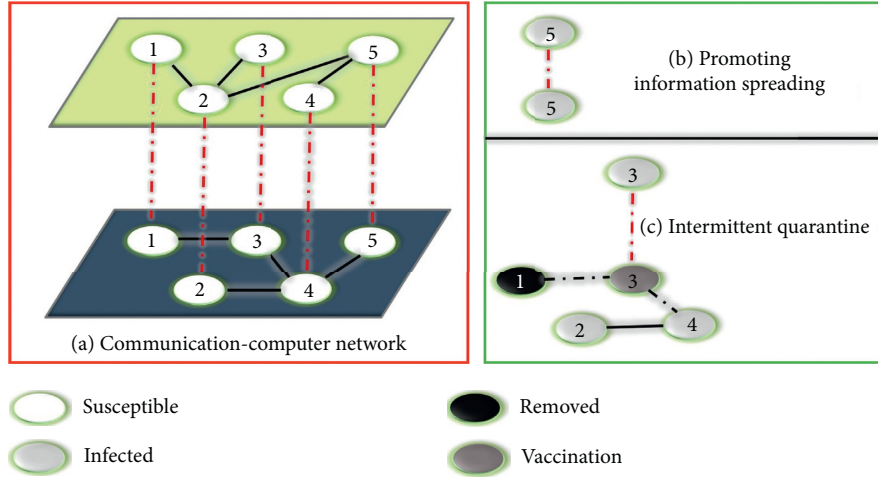


FIGURE 1: Illustration of information-virus spreading on communication-computer networks. (a) Communication-computer multiplex network. (b) Virus spreading promotes the information spreading. (c) Information spreading induces the intermittent quarantine.

TABLE 1: Definitions of parameters and abbreviations.

Parameters/abbreviations	Definitions
$\beta_A$	Information transmission rate
$\beta_B$	Virus transmission rate
$\gamma_A$	Information recovery rate
$\gamma_B$	Virus recovery rate
$t_B$	Intermittent quarantine period
$\langle k_A \rangle$	Average degree of subnetwork A
$\langle k_B \rangle$	Average degree of subnetwork B
$\Theta_A(t)$	The probability of a node connects to an infected neighbor in network A
$\Theta_B(t)$	The probability of a node connects to an infected neighbor in network B
$S_{k_A}^A(t)$	A node with degree $k_A$ in network A is in the susceptible state
$S_{k_B}^B(t)$	A node with degree $k_B$ in network B is in the susceptible state
$I_{k_A}^A(t)$	A node with degree $k_A$ in network A is in the informed state
$I_{k_B}^B(t)$	A node with degree $k_B$ in network B is in the infected state
$R_{k_A}^A(t)$	A node with degree $k_A$ in network A is in the recovered state
$R_{k_B}^B(t)$	A node with degree $k_B$ in network B is in the recovered state

Inspired by [38, 39], we developed a heterogeneous mean-field approach to investigate virus-information spreading dynamics. For the information spreading dynamics on subnetwork A, a susceptible node (e.g., node  $i_A$ ) becomes infected via one of two approaches. (i) Node  $i_A$  can receive the information from its infected neighbors with probability  $s_{k_A}^A(t)\beta_A k_A \Theta_A(t)$ , where  $\Theta_A(t)$  is the probability that node  $i_A$  is connected to an infected neighbor. For uncorrelated networks,  $\Theta_A(t)$  is expressed as

$$\Theta_A(t) = \frac{\sum_{k'_A} (k'_A - 1) P_A(k'_A) \rho_{k'_A}^A(t)}{\langle k_A \rangle}, \quad (1)$$

where  $\langle k_A \rangle = \sum_{k_A} k_A P_A(k_A)$  is the average degree of subnetwork A. (ii) Node  $i_A$  receives the infection once its corresponding node  $i_B$  becomes infected, and the infection probability is  $s_{k_A}^A(t)\beta_B \Theta_B(t) \sum_{k_B} k_B P_B(k_B)$ , where  $\Theta_B(t)$  is

the probability that a susceptible node is connected to an infected neighbor in subnetwork B.  $\Theta_B(t)$  is expressed as

$$\Theta_B(t) = \frac{\sum_{k'_B} (k'_B - 1) P_B(k'_B) \rho_{k'_B}^B(t)}{\langle k_B \rangle}, \quad (2)$$

where  $\langle k_B \rangle = \sum_{k_B} k_B P_B(k_B)$  is the average degree of subnetwork B. Combining the two approaches above, the evolution of  $S_{k_A}^A(t)$  can be expressed as follows:

$$\frac{dS_{k_A}^A(t)}{dt} = -S_{k_A}^A(t) \left[ \beta_A k_A \Theta_A(t) + \beta_B \Theta_B(t) \sum_{k_B} k_B P_B(k_B) \right]. \quad (3)$$

Once the susceptible node is infected by the information, it is regarded as infected. Hence, the evolution of  $I_{k_A}(t)$  is expressed as

$$\frac{dI_{k_A}^A(t)}{dt} = s_{k_A}^A(t) \left[ \beta_A k_A \Theta_A(t) + \beta_B \Theta_B(t) \sum_{k_B} k_B P_B(k_B) \right] - \gamma_A I_{k_A}^A(t), \quad (4)$$

where  $\gamma_A I_{k_A}^A(t)$  is the fraction of nodes recovered from the infected state. Therefore, the evolution of  $R_{k_A}(t)$  is expressed as

$$\frac{dR_{k_A}^A(t)}{dt} = \gamma_A I_{k_A}^A(t). \quad (5)$$

For virus spreading on subnetwork  $B$ , the situation becomes more complex. A susceptible node  $i_B$  may be quarantined for a period  $t_b$  if its corresponding node  $i_A$  becomes the infected state. Mathematically, we use a new state  $V$  to represent the quarantined nodes. We use  $V_{k_B}(t)$  to denote the fraction of nodes with degree  $k_B$  in the quarantined state. The fraction of nodes becomes a quarantined state with probability  $p\beta_A \Theta_A(t) \sum_{k_A} S_{k_A}^A(t) k_A P_A(k_A)$ . Hence, for a randomly selected susceptible node, it becomes an infected state with probability  $S_{k_B}^B(t) \beta_B k_B \Theta_B(t)$ . The evolution of  $S_{k_A}^A(t)$  is expressed as

$$\frac{dS_{k_B}^B(t)}{dt} = -S_{k_B}^B(t) \beta_B k_B \Theta_B(t) - p\beta_A \Theta_A(t) \sum_{k_A} S_{k_A}^A(t) k_A P_A(k_A). \quad (6)$$

The evolution of  $V_{k_B}^B(t)$  is

$$\frac{dV_{k_B}^B(t)}{dt} = p\beta_A \Theta_A(t) \sum_{k_A} S_{k_A}^A(t) k_A P_A(k_A). \quad (7)$$

The evolution of  $I_{k_B}(t)$  occurs in one of two processes: (i) the susceptible nodes become infected by their infected neighbors with probability  $S_{k_B}^B(t) \beta_B k_B \Theta_B(t)$  and (ii) the quarantined node experiences more time steps than  $t_b$  and is infected by neighbors with probability  $\sum_{t'=t_b} V_{k_B}^B(t-t') \beta_B k_B \Theta_B(t)$ . Therefore, the evolution of  $I_{k_B}^B(t)$  is expressed as

$$\begin{aligned} \frac{d\rho_{k_B}^B(t)}{dt} &= S_{k_B}^B(t) \beta_B k_B \Theta_B(t) \\ &+ \sum_{t'=t_b} V_{k_B}^B(t-t') \beta_B k_B \Theta_B(t) - \gamma_B I_{k_B}^B(t). \end{aligned} \quad (8)$$

The evolution of  $R_{k_B}(t)$  is

$$\frac{dR_{k_B}^B(t)}{dt} = \gamma_B I_{k_B}^B(t). \quad (9)$$

**3.2. Numerical Simulations.** We performed extensive Monte Carlo simulations on uncorrelated configuration networks using the method proposed in [48]. Specifically, we generated an uncorrelated configuration network as follows. (i) The network size was determined based on the average degree and degree distributions of the two subnetworks. We set the network sizes of subnetworks  $A$  and  $B$  as

$N_A = N_B = 10^4$ . The degree distributions of the two networks were set based on a power law as  $P_A(k_A) = \xi_A k_A^{-\gamma_A}$  and  $P_B(k_B) = \xi_B k_B^{-\gamma_B}$ , respectively, where  $\gamma_A$  and  $\gamma_B$  are the degree exponents of the two subnetworks, separately:  $\xi_A = \sum_{k_A} k_A^{-\gamma_A}$  and  $\xi_B = \sum_{k_B} k_B^{-\gamma_B}$ . In the numerical simulations, we set  $\gamma_D^A = \gamma_D^B = 3.0$ , and the recovery probability  $\gamma_A = \gamma_B = 0.1$ . The multiplex networks are denoted as SFCSF multiplex networks. (ii) Degree sequences were generated for each subnetwork based on the degree distributions, and stubs were assigned for each node. (iii) For each, two stubs were selected randomly, and an edge was built until no stubs remained in the subnetwork. (iv) For each node in the two subnetworks, we performed one-to-one matching randomly.

We first investigated the final information spreading size  $R_A$  and the virus spreading size  $R_B$  for a specified quarantine value for period  $t_b$ , as shown in Figure 2. For a specified value of  $\lambda_B$ ,  $R_A$  increased monotonically with  $\lambda_A$  (see Figure 2(a)) because the nodes in subnetwork  $A$  had a higher probability of accessing the information. In addition,  $R_A$  increased with  $\lambda_B$  because the spread of the virus promoted information spreading, as shown in Figures 2(a) and 2(b). In general, the virus spreading size  $R_B$  increased with  $\lambda_B$  for a specified  $\lambda_A$ . However, we discovered an optimal information transmission probability for which the virus spreading suppressed significantly, as illustrated in Figures 2(c) and 2(d). Specifically,  $R_B$  first decreased with  $\lambda_A$  because information was obtained by more nodes, and the quarantine strategy was adopted. However, as  $\lambda_A$  increased, more nodes adopted the quarantine strategy for period  $t_b$ . If  $t_b$  (i.e., the virus spreading terminal time) is sufficiently large, those nodes will be protected from being infected by the virus. Otherwise, the quarantined nodes will participate in virus spreading. Therefore,  $R_B$  increases with  $\lambda_A$ . It is noteworthy that when  $\lambda_A$  is sufficiently large, many nodes are quarantined, and only a fraction of quarantined nodes will participate in virus spreading when their quarantine period is completed. Hence,  $R_B$  decreases with  $\lambda_A$ .

We further investigated the effects of the quarantine period on the virus-information spreading dynamics, as shown in Figure 3. For the case of  $t_b = 40$  (see Figures 3(a)–3(d)), i.e., when the quarantine period was relatively small, a similar phenomenon to that shown in Figure 2 was observed. For a large value of  $t_b$ , i.e., when  $t_b = 90$  (as shown in Figures 3(e)–3(h)), a different phenomenon was observed, and the optimal information disappeared. Specifically,  $R_A$  increased monotonically with  $\lambda_A$  or  $\lambda_B$ , whereas  $R_B$  decreases monotonically. When  $t_b$  was extremely large, the quarantined nodes did not participate in the virus spreading dynamics when they completed their quarantine period. Hence, we conclude that increasing the information transmission probability can contain virus spreading for a long quarantine period.

Next, we investigate whether an optimal quarantine period can significantly suppress virus spreading. Hence, we

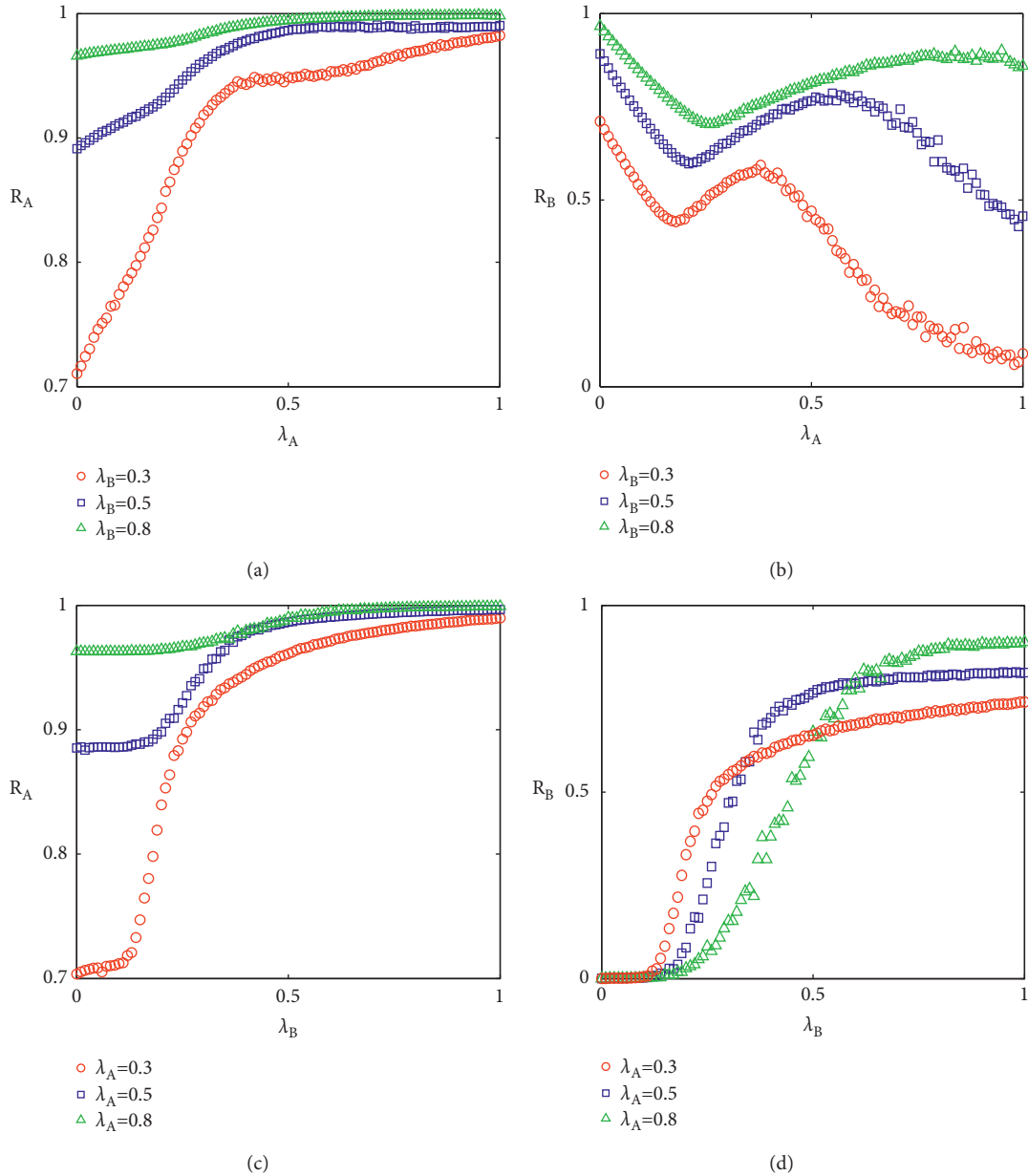


FIGURE 2: Virus-information spreading dynamics on SFCSF networks. (a) Final information outbreak size  $R_A$  and (b) epidemic outbreak size  $R_B$  vs. information transmission probability  $\lambda_B$  under different epidemic transmission probabilities  $\lambda_A = 0.3, 0.5,$  and  $0.8$ . (c)  $R_A$  and (d)  $R_B$  vs.  $\lambda_B$  under  $\lambda_A = 0.3, 0.5,$  and  $0.8$ . We set the intermittent breaking period as  $t_b = 60$ , and average degree of two subnetworks are  $\langle k_A \rangle = \langle k_B \rangle = 8$ .

systematically investigated the spread of virus information for different values of  $\lambda_A$  and  $\lambda_B$ , as shown in Figure 4. We discovered that  $R_A$  decreased with  $t_b$ , regardless of the values of  $\lambda_A$  and  $\lambda_B$ . In terms of virus spreading,  $R_B$  decreased monotonically with  $t_b$  because the larger value of  $t_b$  resulted in fewer nodes participating in virus spreading when they complete their quarantine period.

Finally, we investigated the effects of the average degree of the multiplex networks on virus-information spreading, as shown in Figure 5). It is noteworthy that varying the values of  $\langle k_A \rangle$  and  $\langle k_B \rangle$  do not qualitatively affect the phenomena presented in Figure 2. In other words, an optimal information transmission probability exists at which the spread of virus will be significantly suppressed.

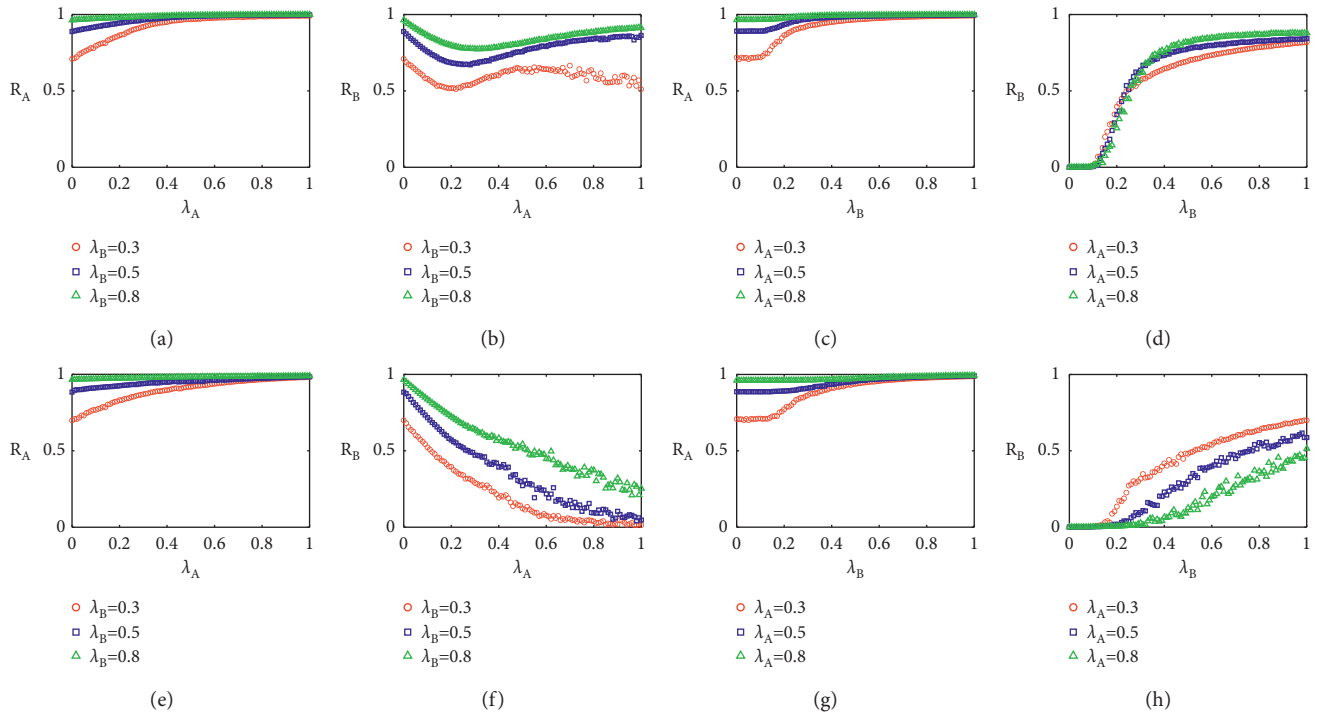


FIGURE 3: Virus-information spreading dynamics on SFCSF networks. (a) Final information outbreak size  $R_A$  and (b) epidemic outbreak size  $R_B$  vs. information transmission probability  $\lambda_A$  under different epidemic transmission probabilities  $\lambda_B = 0.3, 0.5$ , and  $0.8$  when  $t_b = 40$ . (c)  $R_A$  and (d)  $R_B$  vs.  $\lambda_B$  under  $\lambda_A = 0.3, 0.5$ , and  $0.8$  when  $t_b = 40$ . (e)  $R_A$  and (f)  $R_B$  as a function of  $\lambda_A$  under  $\lambda_B = 0.3, 0.5$ , and  $0.8$  when  $t_b = 90$ . (g)  $R_A$  and (h)  $R_B$  vs.  $\lambda_B$  under  $\lambda_A = 0.3, 0.5$ , and  $0.8$  when  $t_b = 90$ . Average degree of two subnetworks are  $\langle k_A \rangle = \langle k_B \rangle = 8$ .

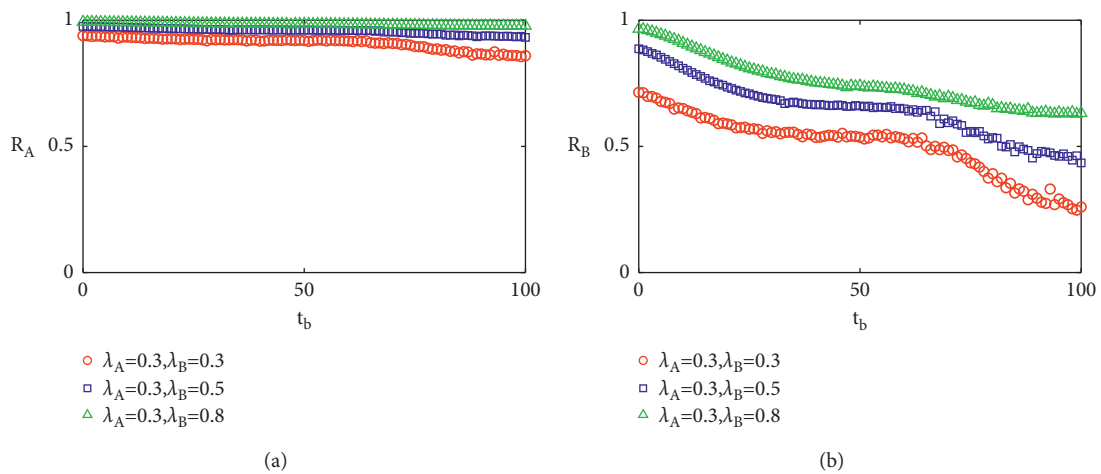


FIGURE 4: Continued.

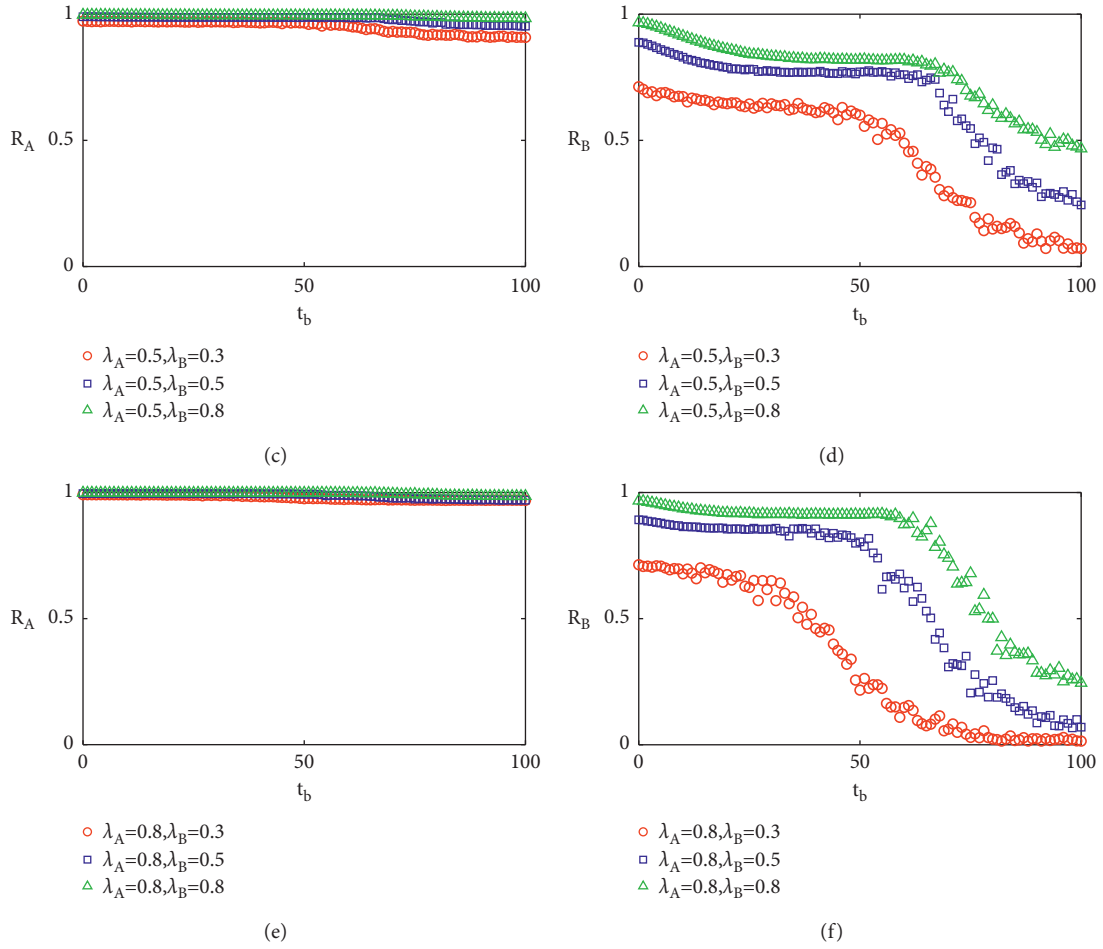


FIGURE 4: Virus-information spreading dynamics on SFCSF networks. Average degrees are  $\langle k_A \rangle = 8$  and  $\langle k_B \rangle = 8$ . We set the intermittent breaking period as  $t_b = 40$ .

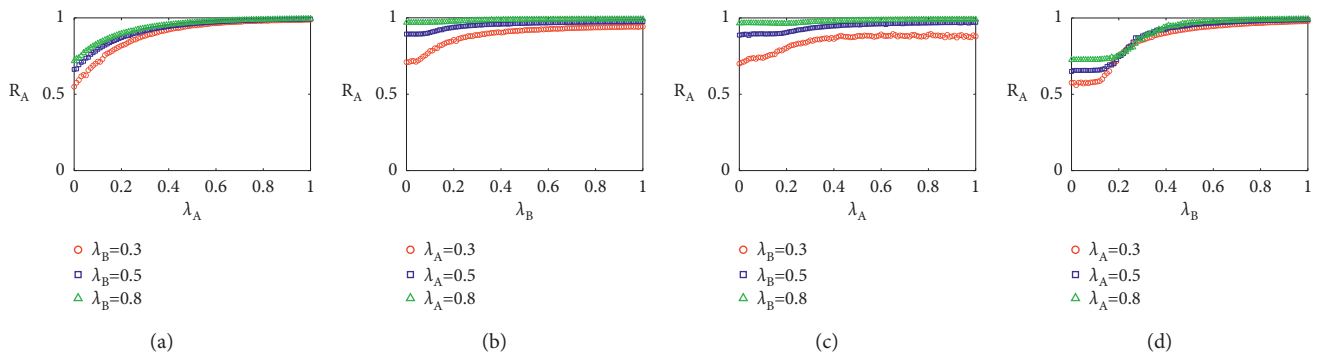


FIGURE 5: Continued.



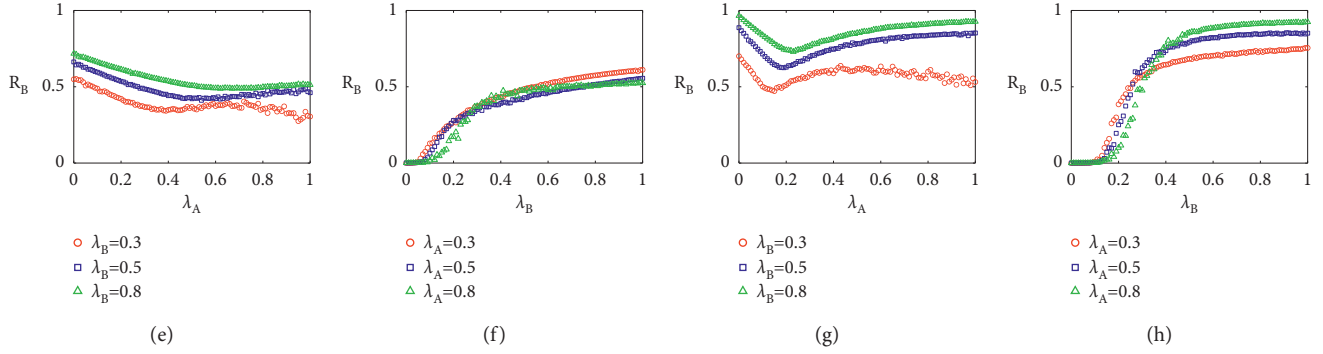


FIGURE 5: Virus-information spreading dynamics on SFCSF networks.  $R_A$  vs.  $\lambda_A$  under different epidemic transmission probabilities  $\lambda_B = 0.3, 0.5,$  and  $0.8$  (a) and different information transmission probabilities  $\lambda_A = 0.3, 0.5,$  and  $0.8$  (b).  $R_B$  vs.  $\lambda_A$  under different  $\lambda_B = 0.3, 0.5,$  and  $0.8$  (e) and different  $\lambda_A = 0.3, 0.5,$  and  $0.8$  (f). In (a), (b), (e), and (f), the average degrees are  $\langle k_A \rangle = 8$  and  $\langle k_B \rangle = 15$ .  $R_A$  vs.  $\lambda_A$  under different  $\lambda_B = 0.3, 0.5,$  and  $0.8$  (c) and different  $\lambda_A = 0.3, 0.5,$  and  $0.8$  (d).  $R_B$  vs.  $\lambda_A$  under different  $\lambda_B = 0.3, 0.5,$  and  $0.8$  (g) and different  $\lambda_A = 0.3, 0.5,$  and  $0.8$  (h). In (c), (d), (g), and (h), average degrees are  $\langle k_A \rangle = 15$  and  $\langle k_B \rangle = 8$ .

## 4. Conclusions

Controlling the spread of virus on the Internet is vital to cyberspace security. The spread of virus on the Internet triggers information spreading on social networks. Hence, we proposed an interacting virus-information spreading dynamics model for multiplex networks, in which a node receiving information is intermittently quarantined for a specified period. The spreading dynamics were described using a time-delay heterogeneous mean-field approach. By performing Monte Carlo simulations, we investigated the spreading dynamics of SFCSF networks and identified two situations. For relatively small intermittent periods, virus spreading suppressed significantly at the optimal information transmission probability. For large intermittent periods, i.e., the intermittent period was larger than the virus spreading time. Therefore, increasing the information diffusion probability will likely facilitate the control of viruses. Furthermore, we discovered that increasing the intermittent period suppressed virus spreading. Finally, we changed the average degrees of the two subnetworks and discovered that the above mentioned phenomena were not qualitatively affected.

## Data Availability

The data used to support the findings of this study are available from the corresponding author upon request.

## Conflicts of Interest

The authors declare that they have no conflicts of interest.

## References

- [1] M. Garetto, W. Gong, and D. Towsley, "Ieee infocom," vol. 3, pp. 1869–1879, in *Proceedings of the Twenty-second Annual Joint Conference of the IEEE Computer and Communications Societies (IEEE Cat. No. 03CH37428)*, vol. 3, pp. 1869–1879, IEEE, USA, October 2003.
- [2] S. Peng, S. Yu, and A. Yang, "Smartphone malware and its propagation modeling: a survey," *IEEE Communications Surveys & Tutorials*, vol. 16, p. 925, 2013.
- [3] L. Feng, X. Liao, Q. Han, and H. Li, "Dynamical analysis and control strategies on malware propagation model," *Applied Mathematical Modelling*, vol. 37, no. 16–17, pp. 8225–8236, 2013.
- [4] Z. Chuanyi Ji and C. Ji, "Spatial-temporal modeling of malware propagation in networks," *IEEE Transactions on Neural Networks*, vol. 16, no. 5, pp. 1291–1303, 2005.
- [5] R. Pastor-Satorras and A. Vespignani, "Epidemic dynamics and endemic states in complex networks," *Physical Review*, vol. 63, Article ID 066117, 2001.
- [6] R. Pastor-Satorras, C. Castellano, P. Van Mieghem, and A. Vespignani, "Epidemic processes in complex networks," *Reviews of Modern Physics*, vol. 87, no. 3, pp. 925–979, 2015.
- [7] W. Wang, M. Tang, H. E. Stanley, and L. A. Braunstein, "Unification of theoretical approaches for epidemic spreading on complex networks," *Reports on Progress in Physics*, vol. 80, Article ID 036603, 2017.
- [8] A. Bose and K. G. Shin, "Agent-based modeling of malware dynamics in heterogeneous environments," *Security and Communication Networks*, vol. 6, no. 12, pp. 1576–1589, 2013.
- [9] H. Guo, H. K. Cheng, and K. Kelley, "Impact of network structure on malware propagation: a growth curve perspective," *Journal of Management Information Systems*, vol. 33, no. 1, pp. 296–325, 2016.
- [10] X. Zhang, D. Saha, and H.-H. Chen, "GLOBECOM'05," in *Proceedings of the IEEE Global Telecommunications Conference*, vol. 3, p. 5, IEEE, Houston, TX, USA, November 2005.
- [11] K. K. Ramachandran and B. Sikdar, "Dynamics of malware spread in decentralized peer-to-peer networks," *IEEE Transactions on Dependable and Secure Computing*, vol. 8, p. 617, 2010.
- [12] A.-L. Barabási and R. Albert, "Emergence of scaling in random networks," *Science*, vol. 286, p. 509, 1999.
- [13] R. Albert and A.-L. Barabási, "Statistical mechanics of complex networks," *Reviews of Modern Physics*, vol. 74, no. 1, pp. 47–97, 2002.
- [14] R. Albert, H. Jeong, and A.-L. Barabási, "Diameter of the worldwide web," *Nature*, vol. 401, no. 6749, pp. 130–131, 1999.
- [15] R. Pastor-Satorras and A. Vespignani, "Immunization of complex networks," *Physical Review*, vol. 65, Article ID 035108, 2002.

- [16] Q. Wu and X. Fu, "Immunization and epidemic threshold of an SIS model in complex networks," *Physica A: Statistical Mechanics and Its Applications*, vol. 444, pp. 576–581, 2016.
- [17] W. Wang, M. Tang, H.-F. Zhang, H. Gao, Y. Do, and Z.-H. Liu, "Epidemic spreading on complex networks with general degree and weight distributions," *Physical Review*, vol. 90, Article ID 042803, 2014.
- [18] F. Nian and X. Wang, "Efficient immunization strategies on complex networks," *Journal of Theoretical Biology*, vol. 264, no. 1, pp. 77–83, 2010.
- [19] B. Mirzasoleiman, M. Babaei, and M. Jalili, "Immunizing complex networks with limited budget," *EPL (Europhysics Letters)*, vol. 98, Article ID 38004, 2012.
- [20] Z. Wang, D.-W. Zhao, L. Wang, G.-Q. Sun, and Z. Jin, "Immunity of multiplex networks via acquaintance vaccination," *EPL (Europhysics Letters)*, vol. 112, Article ID 48002, 2015.
- [21] L. Chen and D. Wang, "An improved acquaintance immunization strategy for complex network," *Journal of Theoretical Biology*, vol. 385, pp. 58–65, 2015.
- [22] Z. Wang, Y. Moreno, S. Boccaletti, and M. Perc, "Vaccination and epidemics in networked populations-an introduction," *Chaos, Solitons & Fractals*, vol. 103, pp. 177–183, 2017.
- [23] S. F. Rosenblatt, J. A. Smith, G. R. Gauthier, and L. Hébert-Dufresne, "Immunization strategies in networks with missing data," *PLoS Computational Biology*, vol. 16, Article ID e1007897, 2020.
- [24] Z. Wang, C. T. Bauch, S. Bhattacharyya et al., "Statistical physics of vaccination," *Physics Reports*, vol. 664, pp. 1–113, 2016.
- [25] S. Boccaletti, G. Bianconi, R. Criado et al., "The structure and dynamics of multilayer networks," *Physics Reports*, vol. 544, no. 1, pp. 1–122, 2014.
- [26] J. Gao, S. V. Buldyrev, H. E. Stanley, and S. Havlin, "Networks formed from interdependent networks," *Nature Physics*, vol. 8, no. 1, pp. 40–48, 2012.
- [27] M. De Domenico, C. Granell, M. A. Porter, and A. Arenas, "The physics of spreading processes in multilayer networks," *Nature Physics*, vol. 12, no. 10, pp. 901–906, 2016.
- [28] M. Kivela, A. Arenas, M. Barthelemy, J. P. Gleeson, Y. Moreno, and M. A. Porter, "Multilayer networks," *Journal of Complex Networks*, vol. 2, no. 3, pp. 203–271, 2014.
- [29] S. Funk, E. Gilad, C. Watkins, and V. A. A. Jansen, "The spread of awareness and its impact on epidemic outbreaks," *Proceedings of the National Academy of Sciences*, vol. 106, no. 16, pp. 6872–6877, 2009.
- [30] C. Granell, S. Gómez, and A. Arenas, "Dynamical interplay between awareness and epidemic spreading in multiplex networks," *Physical Review Letters*, vol. 111, Article ID 128701, 2013.
- [31] C. Granell, S. Gómez, and A. Arenas, "Competing spreading processes on multiplex networks: awareness and epidemics," *Physical Review*, vol. 90, Article ID 012808, 2014.
- [32] J.-Q. Kan and H.-F. Zhang, "Effects of awareness diffusion and self-initiated awareness behavior on epidemic spreading - an approach based on multiplex networks," *Communications in Nonlinear Science and Numerical Simulation*, vol. 44, pp. 193–203, 2017.
- [33] X.-X. Zhan, C. Liu, G. Zhou et al., "Coupling dynamics of epidemic spreading and information diffusion on complex networks," *Applied Mathematics and Computation*, vol. 332, pp. 437–448, 2018.
- [34] Q. Guo, X. Jiang, Y. Lei, M. Li, Y. Ma, and Z. Zheng, "Two-stage effects of awareness cascade on epidemic spreading in multiplex networks," *Physical Review*, vol. 91, Article ID 012822, 2015.
- [35] E. Massaro and F. Bagnoli, "Epidemic spreading and risk perception in multiplex networks: a self-organized percolation method," *Physical Review*, vol. 90, Article ID 052817, 2014.
- [36] A. Lima, M. De Domenico, V. Pejovic, and M. Musolesi, "Disease containment strategies based on mobility and information dissemination," *Scientific Reports*, vol. 5, p. 1, 2015.
- [37] C. Zheng, C. Xia, Q. Guo, and M. Dehmer, "Interplay between SIR-based disease spreading and awareness diffusion on multiplex networks," *Journal of Parallel and Distributed Computing*, vol. 115, pp. 20–28, 2018.
- [38] W. Wang, M. Tang, H. Yang, Y. Younghae Do, Y.-C. Lai, and G. Lee, "Asymmetrically interacting spreading dynamics on complex layered networks," *Scientific Reports*, vol. 4, no. 1, p. 5097, 2014.
- [39] W. Wang, Q.-H. Liu, S.-M. Cai, M. Tang, L. A. Braunstein, and H. E. Stanley, "Suppressing disease spreading by using information diffusion on multiplex networks," *Scientific Reports*, vol. 6, no. 1, p. 29259, 2016.
- [40] Q.-H. Liu, W. Wang, M. Tang, and H.-F. Zhang, "Impacts of complex behavioral responses on asymmetric interacting spreading dynamics in multiplex networks," *Scientific Reports*, vol. 6, 2016.
- [41] D. Zhao, L. Wang, Z. Wang, and G. Xiao, "Virus propagation and patch distribution in multiplex networks: modeling, analysis and optimal allocation," *IEEE Transactions on Information Forensics and Security*, vol. 14, pp. 1755–1767, 2018.
- [42] L.-X. Yang, K. Huang, X. Yang, Y. Zhang, Y. Xiang, and Y. Tang, *IEEE Transactions on Network Science and Engineering*, 2020.
- [43] Y. Zhang, X. Xiao, L.-X. Yang, Y. Xiang, and S. Zhong, "Secure and efficient outsourcing of PCA-based face recognition," *IEEE Transactions on Information Forensics and Security*, vol. 15, pp. 1683–1695, 2019.
- [44] K. Huang, P. Li, L.-X. Yang, X. Yang, and Y. Y. Tang, "Seeking best-balanced patch-injecting strategies through optimal control approach," *Security and Communication Networks*, vol. 2019, Article ID 2315627, 2019.
- [45] M. E. Newman, "Spread of epidemic disease on networks," *Physical Review*, vol. 66, Article ID 016128, 2002.
- [46] Y. Moreno, R. Pastor-Satorras, and A. Vespignani, "Epidemic outbreaks in complex heterogeneous networks," *The European Physical Journal B*, vol. 26, no. 4, pp. 521–529, 2002.
- [47] M. Á. Serrano, and M. Boguñá, "Percolation and epidemic thresholds in clustered networks," *Physical Review Letters*, vol. 97, Article ID 088701, 2006.
- [48] M. Catanzaro, M. Boguñá, and R. Pastor-Satorras, "Diffusion-annihilation processes in complex networks," *Physical Review*, vol. 71, Article ID 027103, 2005.